DEVELOPMENT AND APPLICATIONS OF NEW SLIDING MODE CONTROL APPROACHES

PAN YA-JUN

NATIONAL UNIVERSITY OF SINGAPORE

2003

Founded 1905

DEVELOPMENT AND APPLICATIONS OF NEW SLIDING MODE CONTROL APPROACHES

BY

PAN YA-JUN

(M.Eng. Zhejiang Univ.)

A THESIS SUBMITTED

FOR THE DEGREE OF DOCTOR OF PHILOSOPHY

DEPARTMENT OF ELECTRICAL AND COMPUTER ENGINEERING

NATIONAL UNIVERSITY OF SINGAPORE

2003

Acknowledgments

I would like to express my most sincere appreciation to my supervisors A/Prof Xu Jian-Xin and Prof Lee Tong-Heng for their supervision and support. Without their consistent guidance and invaluable encouragement, it is simply impossible to finish this thesis. For A/Prof Xu Jian-Xin, his impressive academic achievements in the research areas of Learning Control and Variable Structure Control attracted me to do the research work in Sliding Mode Control. During my way on pursuing Ph.D., A/Prof Xu Jian-Xin and Prof Lee Tong-Heng gave me many stimulating advices and consistent encouragement, which heartened me and enabled me overcoming all the difficulties in my research.

I would also like to thank Dr. Wang Qing-Guo, Dr. Panda Sanjib-Kumar, Dr. Loh Ai-Poh, Dr. Ge Shu-Zhi Sam, Dr. Chen Ben-Mei at National University of Singapore who provided me kind encouragement and constructive suggestions for my research. Thanks to my laboratory-mates Cao Wenjun, Tan Ying, Zhang Jin, Xu Jing, Zhang Hengwei, Yan Rui, Zheng Qing, Peng Ying, Chen Jianping and many other research scholars and research fellows who have made their contributions in various ways to my research work.

Thanks are given to National University of Singapore, Control and Simulation Laboratory of the Department of Electrical and Computer Engineering, for the financial support and research facilities provided throughout my research work.

Finally, I would like to express my deepest gratitude to my husband Li Shan-Chun for his love, understandings, support and encouragement. I also want to thank my parents for their love, support and encouragement during my life.

Contents

Summary

As one of the robust control strategies, Variable Structure Control (VSC) or Sliding Mode Control (SMC) has been widely applied in dealing with norm-bounded system uncertainties for nonlinear uncertain systems. In SMC, the controller is designed such that the uncertain system can reach the desired sliding surface in finite time and can remain on the surface for all the subsequent time. The main contributions of this thesis are to develop new sliding mode control schemes for different control objects. Consequently, the proposed approaches widen the application range to real systems, such as servomechanisms and robotic manipulators, and achieve better control system performance under various control environments.

In the first part of the thesis, five different sliding mode control schemes are proposed.

(1) A sliding mode controller with the closed-loop filtering architecture is proposed for a class of nonlinear systems. In the new control approach, the equivalent control profile, which will drive the system to move along the pre-specified switching surface, is acquired by incorporating two first order filters in a closed-loop manner. As a result of the closed-loop filtering and according to the internal model principle, the switching control gain can be significantly scaled down and as a result chattering can be reduced.

(2) Two main robust control strategies, sliding mode control and nonlinear H^∞ control, are integrated to function in a complementary manner for tracking control tasks. The new control method is designed for a class of nonlinear uncertain systems with two cascaded subsystems. Through solving a Hamilton-Jacobien inequality, the nonlinear H^∞ control law for the first subsystem well defines a nonlinear switching surface. By virtue of nonlinear H^∞ control, the resulting sliding manifold in the sliding phase possesses the desired L_2 gain property and to certain extend the

optimality. Associated with the new switching surface, the SMC is applied to the second subsystem to accomplish the tracking task, and ensure the L_2 gain robustness in the reaching phase.

(3) An integral sliding mode control is analyzed and designed under the framework of Lyapunov technology. A nonlinear integral-type sliding surface is used to yield a sliding manifold specified in the entire state space and two types of unmatched system uncertainties are considered and their effects to the sliding manifold are explored. In the sequel a nonlinear nominal control scheme is proposed to improve the performance of the sliding manifold.

(4) A new adaptive variable structure control (VSC) scheme is proposed for nonlinear systems without a prior knowledge of control directions. By incorporating a Nussbaum-type function, the new adaptive VSC law can ensure asymptotic convergence of the tracking error in the existence of non-parametric uncertainties.

(5) A new fractional interpolation based smoothing scheme is proposed for variable structure control. Compared with the conventional fractional interpolation scheme, the new scheme achieves the designated tracking precision bound with an adequate and yet moderate gain. Compared with the well known saturation scheme, the new scheme achieves a smoother control profile, and possesses one extra degree of freedom in adjusting the equivalent control gain while retaining the same precision bound. In the new scheme, the equivalent gain nearby the vicinity of the equilibrium can be adjusted to vary from the saturation type to the signum type.

In the second part of the thesis, the issues on the applications of sliding mode control to multi-link robotic manipulators, permanent magnet synchronous motors (PMSM), DC servo motors and parameter identification are further considered.

(1) In the first application, a gain shaped sliding mode control scheme is successfully applied for the tracking control tasks of multi-link robotic manipulators. Two

classes of low-pass filters are introduced to work concurrently for the purpose of acquiring equivalent control, reducing the switching gain effectively and in the sequel reducing chattering.

(2) In the second application, a modular control approach with a gain shaped sliding mode observer is applied to PMSM speed control to minimize the torque pulsations. By virtue of incorporating internal model, the ILC module in the proposed control scheme achieves the desirable feedforward compensation for all torque harmonics with unknown magnitudes. A novel torque estimation module using gain shaped sliding mode observer is further developed to facilitate the implementation of torque learning control.

(3) In the third application, via describing function techniques, sliding mode control of DC servo mechanisms is analyzed in the presence of unmodeled dynamics. Based on the analysis of the limit cycle problem, the fractional interpolation based smoothing scheme is then proposed to eliminate the limit cycle, and maintain a reasonable tracking precision bound.

(4) Furthermore, an identification scheme suitable for *time-varying* parameters is developed based on variable structure system theory and sliding mode. The new closed-loop identification scheme addresses several key issues in system identification simultaneously: unstable process, highly nonlinear and uncertain dynamics, fast time-varying parameters and rational nonlinear in the parametric space.

List of Tables

List of Figures

Notations

Symbol	Meaning or Operation
$\forall$	for all
$\exists$	there exists
$\triangleq$	definition
$\in$	in the set
$\subset$	subset of
$\rightarrow$	tend to
$\Rightarrow$	imply
$\cap$	intersection of sets
$\cup$	union of sets
$\lambda_{min}(\star)$	the minimum eigenvalue of a matrix
$\lambda_{max}(\star)$	the maximum eigenvalue of a matrix
$\text{sign}(\star)$	signum function
$\mid \star \mid$	absolute value of a number
$\| \star \|$	Euclidean norm of vecotr or its induced matrix norm
I	an identity matrix
A^T	the transpose of A
$\mathcal{R}^n$	the space of n-tuples of real numbers
$\mathcal{R}^{n\times m}$	the space of $n \times m$ real matrices
$L_p[0,\infty)$	the space of p-th power integrable functions on $[0,\infty)$
$L_\infty[0,\infty)$	the space of uniformly bounded functions on $[0,\infty)$
$D_{\mathbf{x}} f(\mathbf{x},\mathbf{y})$	the partial derivative of a scalar function f to a vector $\mathbf{x}$
$C(\mathcal{D})$	the space of continuous functions on $\mathcal{D}$
$C^n(\mathcal{D})$	the space of $n \in \mathcal{Z}_+$ times continuously differentiable functions on $\mathcal{D}$

Chapter 1

Introduction

1.1 Backgrounds and Motivations

Variable Structure Control (VSC) or Sliding Mode Control (SMC) was proposed in the early 1950s (Utkin, 1965), (Emelyanov, 1967), (Itkis, 1976), (Utkin, 1977), (Utkin, 1978). Over the past several decades, increasing attention has been drawn to VSC or SMC and hitherto, significant approaches have been developed world-widely (Young, 1977), (Young *et al.*, 1977), (Young, 1978), (Slotine, 1984), (Fu and Liao, 1990), (Utkin, 1992), (Slotine and Li, 1991), (Sira-Ramirez, 1993), (Xu and Hashimoto, 1993), (Zinober, 1994), (Young and Ozguner, 1997), (Man and Yu, 1997), (Yu and Man, 1998), (Bartolini *et al.*, 1998), (Wu and Yu, 1999), (Young *et al.*, 1999), (Edwards *et al.*, 2000). SMC is one of the well-known robust control design methods which only require the upper bounds of the parametric uncertainties and disturbances. Due to the simplicity and superb robustness of SMC, numerous successful applications have been carried out to a wide variety of engineering systems, such as electric drives, robotic manipulators, etc (Slotine and Sastry, 1983), (Young, 1993), (Man *et al.*, 1994), (Park and Lee, 1996), (Lin and

Chiu, 1998), (Xu and Cao, 2000).

In terms of Filippov's work (Filippov, 1964), (Filippov, 1988), in which the author derived a formal justification which is one possible technique for determining the system motion in a sliding mode, the properties and the definition of the sliding mode have been well presented in detail in (Utkin, 1978) and (Utkin, 1992). A standard SMC controller is designed in two stages. One is the sliding manifold or switching surface. The essential feature of the sliding mode control is the choice of a switching surface of the state space according to the desired dynamical specifications of the closed-loop system. The plant dynamics restricted to this surface or manifold represent the controlled system's behavior. The other is the discontinuous control law which is designed to steer the trajectories onto the sliding manifold in finite time and to keep the subsequent motion on it. In the ideal case, the resulting motion is called sliding mode. The main advantages of the sliding mode control are:

1) The resulting systems have their insensitivities or robustness against a large class of perturbations or model uncertainties, which enter the system in the same channel as control inputs;

2) SMC needs less information in comparison with classical control techniques.

Thus the prescribed specifications would be met through these two designing stages in SMC.

In SMC, switching control using signum function is one of the best control strategies to handle the worst case control environment: where system perturbations can be structured, unstructured, deterministic, stochastic or persistent, and only the upper bounds of system perturbations are available. However, the discontinuous control law with high gain will incur chattering in a real implementation. The actuators have to cope with the high frequency bang-bang type of control actions that could produce premature wear, or even breaking. This main disadvantage,

called chattering, is generally perceived as an oscillation about the sliding manifold which may excite the unmodeled high frequency dynamics of the plant and is harmful to actuation mechanism. The chattering can be reduced or even suppressed by using techniques such as nonlinear gains, dynamics extensions and higher order sliding mode control (Zinober, 1994), (Bartolini and Pydynowski, 1996), (Fridman and Levant, 1996).

In order to avoid the chattering problem and to meet the system specifications perfectly, one of the most imperative tasks in SMC is the acquisition of the equivalent control profile. Originally, the equivalent control methodology (Utkin, 1978), (Utkin, 1992), has been introduced as a regulation technique to analyze the sliding motion for systems affine in the control. It has been shown in Utkin's work that the equivalent control can be obtained using a first-order low-pass filter provided that the following two conditions are satisfied: the system is in the sliding mode and the first-order filter possesses an infinite bandwidth. The concept of the equivalent control is described as follows. While in sliding mode the dynamics of the sliding surface $\sigma = 0$ can be written as $\dot{\sigma} = 0$. By solving the above equation *formally* for the control input u from system dynamics, one obtains an expression for u called the *equivalent control*, u_{eq}, which can be interpreted as the continuous control law that would maintain $\dot{\sigma} = 0$ if the dynamics were exactly known. The *method of equivalent control* is a means of determining the system motion restricted to the sliding surface $\sigma = 0$. The traditional discontinuous control switches in sliding mode so as to imitate the equivalent control in the average which can be broadly defined as the continuous control which would lead to the invariance conditions for the sliding motion. According to the equivalent control methodology, the slow component can be extracted by passing the discontinuous control through a low pass filter whose time constant is sufficiently large to filter out the high frequency switching terms, yet sufficiently small not to eliminate any slow component. How-

ever, it is in an open-loop manner and we cannot use the filtered output equivalent control signal as the feedforward term directly. Thus the high switching control still cannot be replaced by the average continuous control which is called the equivalent control profile.

Usually there are two methods which continuously approximate the discontinuous action of the SMC controller to avoid the chattering problem. In (Zinober, 1994), it was proposed that the signum function $sign(\sigma)$ be replaced by the following fractional interpolation $\frac{\sigma}{|\sigma| + \delta}$, where δ is a positive constant. It provides very smooth control action. The main drawback of the method is that the tracking precision bound cannot be determined and ensured by the selection of δ. Since $\frac{|\sigma|}{|\sigma| + \delta} < 1 \ \forall \delta$, the equivalent switching gain will be lower than the necessary level and may cause large tracking error. This is due to the inadequate control gain which is further provoked by the fact that the switching gain is almost the same size as the upperbound of the system lumped disturbance. Another well adopted smoothing scheme is to replace the signum function with a saturation function, e.g. $sat(\cdot)$ (Slotine, 1984), (Slotine and Li, 1991). Note that the equivalent switching gain outside the saturation bound is at the necessary level, hence the tracking precision is guaranteed. This is the main reason why $sat(\cdot)$ is so popular. However it is less smooth compared with the fractional interpolation method, as the saturation function is only piecewise smooth. Moreover, once the precision bound is fixed, inside the precision bound it is in fact a fixed proportional control with the switching gain which cannot be further adjusted.

In literature, numerous schemes have been proposed to improve the tracking performance and to reduce the chattering problem. Passive smoothing schemes such as the introduction of boundary layer make compromise between the tracking accuracy and the alleviation of chattering, since the reduction of switching gain leads to the reduction of feedback effect (Slotine, 1984) , (Hashimoto *et al.*, 1987). By virtue

of internal model principle, in order to retain good tracking performance with much lower control gain, one has to incorporate the "internal model" in feedforward loop, i.e. provide the equivalent control signals. Adaptive control and learning control combined with SMC are two main strategies to produce "internal model" as in (Liao *et al.*, 1990), (Yoo and Chung, 1992), (Fu, 1992), (Xu and Hashimoto, 1993), (Chen and Papavassilopoulos, 1994), (Xu *et al.*, 1996), (Xu and Qu, 1998), (Xu *et al.*, 1998*a*), (Chien and Fu, 1999), (Bartolini *et al.*, 1999), (Bartolini and Ferrara, 1999), (Xu and Cao, 2001*a*). Note that an adaptive-type VSC requires that the system be in the parameterization form. In many cases, due to the existence of nonlinearities or lack of information, the systems can not be presented in the parameterization form. To tackle this case, a sliding sector technique is used in (Yeung and Chen, 1988), (Shyu *et al.*, 1992), (Xu *et al.*, 1996), (Furuta and Pan, 2000*b*) such that the conventional sliding surface is relaxed to a sliding sector and consequently, the system state moves in the sector without serious chattering. The main restriction of learning control combined with SMC is that it can only handle periodic control environment.

Many other attempts have been devoted to estimate the system uncertainties and disturbance and to reduce the chattering. In (Chan, 1996), a new approach is introduced to determine a system perturbation signal from the dynamics of the sliding mode, in which perturbation feedforward compensation cancels the effects of system uncertainties and external disturbances and thus chattering is reduced. Chattering elimination using filter design is presented in (Kachroo and Tomizuka, 1996) by virtue of the internal model principle. (Bartolini and Pydynowski, 1996) and (Bartolini *et al.*, 1998) generate a second-order sliding motion which uses the first derivative of the control signal instead of the actual control to eliminate chattering. (Chung, 1999) applies the circle criterion to eliminate the chattering phenomenon by a wider class of nonlinearities, which include the saturation or sigmoid function

as special cases.

Another very important issue on sliding mode controller design is how to incorporate or integrate SMC with other control techniques in dealing with different control environments or obtaining different control objects. In literature, SMC has been integrated with many other control strategies in a complementary manner, e.g. with adaptive control (Lee *et al.*, 2000), (Yu, 1999), with learning control (Xu and Cao, 2001*b*), with neural network approach (Karakasoglu and Sundareshan, 1995), (Sundareshan and Askew, 1997), etc.

As sliding mode control, nonlinear H^∞ control is also another well recognized robust control strategy (Basar and Berhard, 1990), (Ball *et al.*, 1993), (Shen and Tamura, 1995). It is well known that SMC can handle matched $L_\infty[0,\infty)$ type system disturbance where the upper-bound knowledge is available (Utkin, 1992). In dealing with $L_2[0,\infty)$ type unmatched disturbance without the upper-bound knowledge, the robust strategy - nonlinear H^∞ control - can be applied.

For a class of cascaded nonlinear systems which consist of a null space dynamics and range space dynamics, a common practice in SMC is to design a switching surface according to the null space dynamics, which must ensure a stable sliding manifold when the system is in sliding mode (Edwards and Spurgeon, 1998). For known Linear Time-Invariant (LTI) systems, such design turns to be pole-placement (Zinober, 1994), (Chang and Chen, 2000) or Linear Quadratic Regulator (LQR) (Young and Ozguner, 1997). For known nonlinear systems, nonlinear optimal design can be applied. In (Xu and Zhang, 2002), a nonlinear sliding mode with inverse optimality can be constructed according to (Krstic and Tsiotras, 1999). For dealing with the tracking control tasks of the null space nonlinear dynamics in which unmatched uncertainties exist, the quasi-optimal VSC scheme is no longer applicable. If there exist uncertaities in the null space nonlinear dynamics, switch-

ing surface design becomes extremely difficult. The challenge lies in that we need a systematic design which captures the inherent relationship between the switching surface and the sliding manifold, in the sequel yields a stable sliding manifold. Note that both the switching surface and the sliding manifold may be highly nonlinear in nature. Nonlinear H^∞ control offers such a systematic design, which can allow even in the presence of unmatched uncertainties of $L_2[0,\infty)$ type, and achieves a desired L_2 gain. The L_2 gain of a nonlinear system has been known to be an useful measure for stabilization and performance, e.g. the finite gain stability and H^∞ disturbance attenuation (Van der Schaft, 1991), (Van der Schaft, 1992).

It is common knowledge that many existing systems are highly coupled and cannot be decomposed into cascaded form with a null space dynamics and a range space dynamics. In this case, we should find a corresponding control approach in SMC for the highly coupled system to deal with the matched and unmatched uncertainties. The concept of integral sliding mode control (ISMC) has been proposed and defined in (Utkin and Shi, 1996). An integral sliding mode controller is constructed by incorporating an integral term in the switching surface. The main feature of the ISMC is that, when in sliding mode, the sliding manifold spans the entire state space. The main advantage of the ISMC, in the sequel, is the ability to directly design and specify the sliding manifold in the entire state space. This is achieved through the integral term, which provides a direct means for us to shape the sliding manifold based on the knowledge of the system nominal part (Chern *et al.*, 1996), (Wang *et al.*, 1996), (Ackermann and Utkin, 1998). An immediate consequence is that we can easily design a nonlinear ISMC to stabilize the sliding manifold in the ideal closed-loop.

Most of the existing VSC or SMC schemes are proposed to deal with the control task when the control directions are known *a priori*. It is a challenging problem to design controller for tracking control task without prior knowledge of control directions.

Up to now, there are mainly two approaches to address this problem. One approach is to incorporate the technique of Nussbaum-type gains into the control design (Nussbaum, 1983), and later extend to adaptive control systems (Ryan, 1991), (Ye and Jiang, 1998). Note that those adaptive control schemes were developed to deal with parametric uncertainties. Another approach is to directly estimate unknown parameters involved in the control directions (Mudgett and Morse, 1985), (Brogliato and Lozano, 1992), (Brogliato and Lozano, 1994), (Kaloust and Qu, 1995). It will be interesting to integrate a Nussbaum-type function with VSC law in the existence of non-parametric uncertainties.

As typical nonlinear control systems (Sinha, 1998), the fields of robotic manipulators and motor control are such broad research areas that many nonlinear control techniques can be applied to address the different control problems. Robotic manipulators have been widely used in different industries and highly motivated industrial automation. Numerous control approaches have been developed for robotic manipulators: Sliding mode control approach (Chern and Wu, 1992), (Chan, 1995), (Pandian and Hanmandlu, 1995), (Tzafestas *et al.*, 1996), (Habibi, 1999); Adaptive control approach (Sadegh and Horowitz, 1990); Adaptive robust control approach (Liao *et al.*, 1990), (Fu, 1992), (Yao *et al.*, 1994), (Parra-Vega and Arimoto, 1995), (Tsaprounis and Aspragathos, 1999), (Zhihong *et al.*, 1999), (Ioannou, 2002); Learning control approach (Oh *et al.*, 1988), (Kuc *et al.*, 1992), (Xu *et al.*, 2000*c*). Among these approaches, the main disadvantage of the adaptive controller for robotic manipulators is the lack of robustness to norm-bounded disturbances. The adaptive robust control approach is still feedback dominant and is not able to generate the desired equivalent control signal although it enhances the robustness to certain extent.

The learning control approach is confined to periodic control circumstances. SMC, as one of the most robust control approaches, makes the robotic control system

insensitive to parametric uncertainties and norm-bounded disturbances. On the other hand, as aforementioned, the control performance is limited either due to its high gain chattering nature or due to the introduction of smoothing technique approach as the trade-off. Thus it will be helpful to apply the gain shaped SMC scheme to robotic manipulators based on the conception of the equivalent control.

Permanent magnet synchronous motors (PMSMs) are used widely for high performance servo applications that require torque smoothness. One of the major disadvantages of the PMSM drive is the produced torque ripple. There are several sources that contribute to torque ripples in the PMSM such as: flux harmonics, cogging, phase angle and peak current unbalancing, current offset and current lag. The presence of flux harmonics results in instantaneous torque that pulsates sinusoidally with rotor position.

In order to minimize the torque pulsations, many techniques have been proposed in the past two decades as in (Low *et al.*, 1990), (Hung and Ding, 1993), (Marchand and Razek, 1993), (Favre *et al.*, 1993), (Low *et al.*, 1994), (Hanselman, 1994), (Jahns and Soong, 1996) and (Chung *et al.*, 1998). Among these approaches, feedforward and feedback control techniques are two major design concepts that have been explored. For the feedforward control, they have generalized the harmonic injection approach by employing numerical optimization techniques to calculate current wave shapes for eliminating all ripples and cogging torque components up to an arbitrarily high harmonic order. However, harmonic injection techniques are based on open loop cancelation concepts. The effectiveness of these algorithms in practical applications, including sensitivity to motor parameter variations, is a justifiable concern. Alternative approach applying the feedback control techniques is proposed to achieve the desired pulsating torque minimization. Various estimation and observer techniques for torque and flux have been proposed to generate the necessary feedback signals for suppressing the pulsating torque components.

However, imperfect knowledge of the motor as well as motor parameter variations limits the application of such schemes. The concept of system modularization has been broadly applied to hardware construction of engineering systems ranging from personal computers to aeroplanes. It greatly facilitates design, development, diagnosis, maintenence and upgrading of a particular module according to the relatively independent functionality. In the proposed approach to minimize the torque pulsations, we apply the same concept to a PMSM speed control system which is the integration of a number of control algorithms and supporting hardware components. Hence, in the PMSM control system, several independent modules can perform their individual functionalities to achieve the same target with minimizing pulsations.

SMC with switching mechanism has superior robustness to matched system uncertainties. However, such a SMC may lose its robustness when unmodeled system dynamics exists, as the discontinuous switching will lead to limit cycles. Limit cycles occur mainly in two circumstances: either in the presence of a sampling delay or an unmodeled dynamics of relative degree above two. In particular when the unmodeled part has a relative degree of two or above, limit cycles are inevitable even with a perfect switching mechanism. Most SMC designs for servomechanism ignore two kinds of dynamic factors in the motor stator circuit and sensor devices (encoder and tachogenerator). They present at least two first order low pass filters cascaded to the mechanical part of the servomechanism. In practice when the sampling frequency is limited, a common way to eliminate chattering is to incorporate a smoothing control scheme to reduce the gain around the equilibrium. In the proposed work, the new fractional interpolation based smoothing scheme is proposed to eliminate the limit cycle in DC servo mechanisms. The describing function method, an extended version of the frequency response method for linear systems (Slotine and Li, 1991), (Chung and Lin, 1998), is used to analyze and

predict the limit cycle approximately.

System identification has been a quite matured field in recent years (Ljung, 1987), (Soderstrom, 1989), (Robert, 1999), (Bontayeb, 2000), *et al*. Numerous results are now available when addressing fundamental issues in system identification: closed-loop approaches, e.g. (Van den Hof and Schrama, 1995), (Hjalmarsson *et al.*, 1996), (Ljung and Forssell, 1999); methods with forgetting factor for slowly time varying parameters (Bittanti and Campi, 1994), (Lindoff and Holst, 1996), (De Mathelin and Lozano, 1999), (Dimogianopoulos and Lozano, 2001); algorithms based on the system dynamics for the system nonlinear in the parametric space (Xu and Hashimoto, 1996), (Robert, 1999). Most identification methods are effective in dealing with one of the fundamental issues. It would be a challenging task where all above three key issues are involved simultaneously, and in addition the parameters may be of fast time varying. In (Xu and Hashimoto, 1993) and (Xu and Hashimoto, 1996), a VSS-theory based parameter identification scheme has been proposed for the system rational nonlinear in the parametric space when the unknown parameters are constants. For the system with unknown fast time varying parameters, the acquisition of the unknown parameters should be in an instantaneous manner while the past measurement cannot be applied. One of the advantages of closed-loop identification, such as the VSS-based scheme, is that it enhances the PE condition. Moreover, the generation of sliding mode allows us to approximate the derivative signals of the system states, and in the sequel simplifies the system dynamics into a structure linear in parameters. Hence, it will be interesting to extend this VSS-theory based scheme to the time varying cases.

All these issues mentioned above are very often encountered in control system design, especially in sliding mode control research area. In this thesis, the focus of the research is to solve or attack these problems by developing new sliding mode control schemes, integrating sliding mode control scheme with other control

strategies and applying sliding mode control schemes to real system such as servo mechanisms and robotic manipulators.

1.2 Contributions

In this thesis, our research is focused on developing new sliding mode control approaches both for theoretical and applications problems. The proposed new sliding mode control schemes aim at the same target, which is to improve the system tracking performance in the existence of matched or unmatched system uncertainties. The main contributions of this thesis lie in the following aspects. In order to acquire the equivalent control profile, the sliding mode controller with the closed-loop filtering architecture is proposed by incorporating two first order filters for a class of nonlinear systems. For the tracking control tasks of a class of nonlinear uncertain systems with two cascaded subsystems, the sliding mode control and nonlinear H^∞ control are integrated to function in a complementary manner, where the nonlinear H^∞ control law for the first subsystem well defines a nonlinear switching surface. When the nonlinear system cannot be seperated into two cascaded subsystems, an integral sliding mode control is analyzed and designed under the framework of Lyapunov technology, in which two types of unmatched system uncertainties are considered and their effects to the sliding manifold are explored. Without a prior knowledge of control directions, a new adaptive variable structure control scheme is proposed for tracking control of nonlinear systems. Furthermore, to eliminate chattering phenomena, a new fractional interpolation based smoothing scheme is proposed for variable structure control. New sliding mode control approaches are also developed to realize other control objectives such as disturbance estimation, modular approach (integrated with iterative learning control), time-varying parameter identification and are applied to the real systems such as multi-link robotic

manipulators, permanent magnet synchronous motors (PMSM), DC servo motors, etc.

In detail, the contributions of this thesis are as follows:

1. In Chapter 2, a new sliding mode control (SMC) approach is proposed for tracking control tasks of a class of nonlinear systems (Xu *et al.*, 2000*e*), (Xu *et al.*, 2002*g*). The new control approach directly addresses the most important issue in the sliding mode control – the acquisition of the equivalent control profile that will drive the system to move along the pre-specified switching surface. In order to realize the equivalent control acquisition, in the proposed SMC approach two first order filters are incorporated. In the sliding motion, one filter is to capture the "average" profile of the switching quantity which by virtue of the equivalent control theory is in proportion to the desired control input. Meanwhile, another filter will scale down the gain of the switching control. We show that the two filters have to work concurrently in the closed-loop. As a result of the closed-loop filtering and according to the internal model principle, the switching control gain can be significantly scaled down while the existence of the sliding mode is still guaranteed. Another advantage of the proposed SMC is that the frequency domain consideration can be easily incorporated as there are extra degrees of freedom in the filter design.

2. In Chapter 3, sliding mode control and nonlinear H^∞ control are integrated to function in a complementary manner for tracking control tasks (Xu *et al.*, 2002*d*), (Xu *et al.*, 2002*e*). The SMC handles matched $L_\infty[0,\infty)$ type system uncertainties with known bounding functions. H^∞ control deals with unmatched disturbances of $L_2[0,\infty)$ type where the upper-bound knowledge is not available. The new control method is designed for a class of nonlinear uncertain systems with two cascaded subsystems. Nonlinear H^∞ control is

applied to the first subsystem in the presence of unmatched disturbances. Through solving a Hamilton-Jacobi inequality, the nonlinear H^∞ control law for the first subsystem well defines a nonlinear switching surface. By virtue of the nonlinear H^∞ control, the resulting sliding manifold in the sliding phase possesses the desired L_2 gain property and to certain extend the optimality. Associated with the new switching surface, the SMC is applied to the second subsystem to accomplish the tracking task, and ensures the L_2 gain robustness in the reaching phase.

3. In Chapter 4, the integral sliding mode control is analyzed and designed under the framework of Lyapunov technology (Xu *et al.*, 2002*b*), (Xu *et al.*, 2003*c*). A nonlinear integral-type sliding surface is used to yield a sliding manifold specified in the entire state space. Two types of unmatched system uncertainties are considered and their effects to the sliding manifold are explored. In the sequel a nonlinear nominal control scheme is proposed to improve the performance of the sliding manifold.

4. In Chapter 5, a new adaptive VSC scheme is proposed for nonlinear systems without prior knowledge of control directions (Xu *et al.*, 2002*a*), (Xu *et al.*, 2003*b*). By incorporating a Nussbaum-type function, the new adaptive VSC law can ensure the asymptotic convergence of the tracking error in the existence of non-parametric uncertainties.

5. In Chapter 6, a new fractional interpolation based smoothing scheme is proposed for variable structure control (Xu *et al.*, 2003*d*), (Xu *et al.*, 2002*c*). Compared with the conventional fractional interpolation scheme, the new scheme achieves the designated tracking precision bound with an adequate and yet moderate gain. Compared with the well known saturation scheme, the new scheme achieves a smoother control profile, and possesses one extra degree of freedom in adjusting the equivalent control gain while retaining the

same precision bound.

6. In Chapter 7, a newly developed gain shaped sliding mode control scheme is applied for tracking control tasks of multi-link robotic manipulators (Xu *et al.*, 2000*d*), (Xu *et al.*, 2001*b*). In the new scheme, filtering techniques also play a key role in acquiring the equivalent control signals and shaping the switching control gain automatically. Once the system enters the sliding motion, two classes of low-pass filters are introduced to work concurrently for the purpose of acquiring the equivalent control, reducing the switching gain effectively and in the sequel chattering is reduced. The passivity property of the robotic manipulators holds for the torque and the velocity is used to ensure the convergence in case of uncertainty surging.

7. In Chapter 8, a modular control approach is applied to PMSM speed control (Xu *et al.*, 2000*b*), (Xu *et al.*, 2001*a*). Based on the functioning of individual module, the modular approach enables the powerful intelligent and robust control modules to easily replace any existing module which does not perform well, meanwhile to retain other existing modules which are still effective. We first conduct property analysis for the existing function modules in a conventional PMSM control system: PI speed control module, reference current generating module and PI current control module. Next, we show that the conventional PMSM controller is not able to reject the torque pulsation which is the main hurdle when PMSM is used as a high performance servo. By virtue of internal model, to nullify the torque pulsation it is imperative to incorporate an internal model in the feed-through path. This is achieved by replacing the reference current generating module with an iterative learning control (ILC) module. The ILC module records the cyclic torque and reference current signals over one entire cycle, and then uses those signals to update the reference current for the next cycle. As a consequence, the

torque pulsation can be reduced significantly. In order to estimate the torque ripples which may exceed certain bandwidth of a torque transducer, a novel torque estimation module using gain shaped sliding mode observer is further developed to facilitate the implementation of torque learning control.

8. In Chapter 9, sliding mode control of DC servo mechanisms is analyzed in the presence of unmodeled dynamics via describing function techniques (Xu *et al.*, 2003*a*), (Xu *et al.*, 2002*f*). It is first shown that, a conventional sliding mode controller with signum function will inevitably generate a limit cycle where a second or higher order unmodeled dynamics exists. The fractional interpolation based smoothing scheme is then proposed to eliminate the limit cycle, and maintain a reasonable tracking precision bound. In particular, a DC servo motor with unmodeled stator and sensor dynamics is taken into consideration. Both theoretical analysis and simulation results verify the effectiveness of the proposed new fractional interpolation control scheme.

9. In Chapter 10, based on variable structure system theory and sliding mode, we develop an identification scheme suitable for time-varying parameters (Xu *et al.*, 2003*e*), (Xu *et al.*, 2002*h*). The new identification scheme, working in closed-loop, addresses several key issues in system identification simultaneously: unstable process, highly nonlinear and uncertain dynamics, fast time varying parameters and rational nonlinear in the parametric space. Other important issues associated with identification, such as the persistent excitation property and insensitivity to measurement noise, are also discussed.

1.3 Thesis Outline

The thesis is organized as follows.

Chapter 2 proposes a new sliding mode control scheme with closed-loop filtering architecture to acquire the equivalent control profile for a class of nonlinear systems.

Chapter 3 presents a new nonlinear H^∞ sliding mode control for a class of nonlinear cascaded systems with L_2 and L_∞ type uncertainties.

Chapter 4 develops an integral sliding mode control based on the Lyapunov's direct method.

Chapter 5 proposes a new adaptive VSC scheme for nonlinear systems without a prior knowledge of control directions.

Chapter 6 presents a new fractional interpolation based smoothing scheme for variable structure control which achieves the designated tracking precision bound with an adequate and yet moderate gain.

Chapter 7 applies a new gain shaped sliding mode control scheme for the tracking task of the multi-link robotic manipulators.

Chapter 8 develops a modular control approach for the speed control of PMSM, in which a gain shaped sliding mode disturbance estimator is incorporated with iterative learning control (ILC) to achieve pulsating torque minimization in the PMSM.

Chapter 9 applies the new fractional interpolation smoothing sliding mode control scheme proposed in Chapter 5 to eliminate the limit cycles of the DC servo mechanisms in the presence of unmodeled dynamics.

Chapter 10 develops a new VSS-based closed-loop identification scheme for time-varying parameters.

Chapter 11 summarizes the work of this thesis and makes recommendations on future research issues.

Appendix A presents a brief introduction to the mathematical definitions used in the thesis.

Appendices B lists the author's publications.

Chapter 2

Sliding Mode Control with Closed-Loop Filtering Architecture for a Class of Nonlinear Systems

2.1 Introduction

Over the past two decades, increasing attention has been drawn to sliding mode control schemes which warrant the system robustness in the presence of norm-bounded system uncertainties or disturbances (Utkin, 1992), (Zinober, 1994), (Young and Ozguner, 1999), (Yu and Xu, 2000), (Man and Yu, 2002). The sliding mode control theory has been widely and successfully applied in many real systems such as robotics, servo mechanisms, power systems, circuits systems, etc (Ozguner and Yurkovich, 1987), (Habibi and Richards, 1992), (Fujimoto and Kawamura, 1995), (Barbosa *et al.*, 1999), (Carrasco *et al.*, 1997), (Giral *et al.*, 1997). In order to

perform perfect tracking, from the viewpoint of internal model principle (Byrnes and Isidori, 2000), the acquisition of the equivalent control signals is imperative in the sliding mode control. However, the existence of system perturbations prevents the possibility of direct acquisition of the equivalent control.

It has been shown in (Utkin, 1992) that equivalent control can be obtained using a first-order filter provided the following two conditions are satisfied: 1) system in sliding mode; and 2) infinite bandwidth of the first-order filter. Note that the second condition is needed only when equivalent control signals possess infinite bandwidth. In most practical circumstances, however, it is not necessary to consider such extreme cases as requiring infinite bandwidth. Most control tasks and control processes (actuators) are predominated by frequency band much lower than Nyquist frequency. It is also well known from sampling theorem that none of control strategies can work near Nyquist frequency. The sliding mode control, as one of the typical nonlinear control strategies implemented using digital techniques, cannot be exempted from this general rule. As a consequence, for most practical control problems, it is sufficient to consider a finite band of frequency components in equivalent control.

Inherently associating with the equivalent control, another important issue constantly being addressed in the sliding mode control is how to avert the use of high gain such as signum function. Passive smoothing schemes such as the introduction of boundary layer make compromise between the tracking accuracy and the alleviation of chattering, since the reduction of switching gain leads to the reduction of feedback effect (Shyu *et al.*, 1992), (Kachroo and Tomizuka, 1996), (Xu *et al.*, 1997). By virtue of internal model principle, in order to retain good tracking performance with much lower control gain, one has to incorporate the "internal model" in the closed-loop, i.e. provide equivalent control signals. Adaptive control and learning control combined with SMC are two main strategies to produce "internal model"

as in (Xu *et al.*, 1998*a*), (Chien and Fu, 1999), (Xu and Cao, 2001*b*). However, learning control can only handle periodic control environment and adaptive control can only handle constant parametric uncertainties.

In this chapter, a sliding mode controller with closed-loop filtering architecture is proposed for tracking control tasks. Based upon the reasonable assumption that actual frequency band in equivalent control is lower than the sampling frequency, a first order filter ($LPF1$) is employed to acquire equivalent control signals from the switching control signals by "averaging" operation. Nevertheless this filter alone cannot fully extract the equivalent control signals if its output is to be fed back to the process as the feedforward compensation. To facilitate the acquisition of equivalent control and reduce the switching gain, a second filter ($LPF2$) is incorporated to shape the switching gain directly. Two filters have to work concurrently in the closed-loop:

1) the output of the first filter will approach the equivalent control only when the switching control gain is kept decreasing; and

2) the switching gain can be reduced to a minimum level only when the equivalent control signal can be acquired and fed back.

As a result of the closed-loop filtering and according to the internal model principle, the switching control gain can be significantly scaled down while the existence of the sliding mode is still guaranteed. In order to maintain the sliding motion, two sufficient conditions have been derived in the design of $LPF1$ and $LPF2$. By making use of extra degrees of freedom in the filter design, it is possible to incorporate frequency domain system knowledge, hence to improve control performance.

Three control phases are taken into consideration. During the reaching phase, it is mandatory to use high gain so as to ensure the global attractiveness of the switching surface and finite reaching time. In the sliding motion phase, two filters $LPF1$ and $LPF2$ are activated simultaneously to produce the equivalent control profile and

automatically reduce the switching gain. In this chapter we further show another important property of the SMC with closed-loop filtering: the control system is able to re-enter the sliding motion in finite time once the system is knocked away from the sliding surface due to any unexpected disturbance surge. In this phase, the control gain originally being scheduled low by $LPF2$ will automatically scale up, and $LPF1$ can quickly capture the desired control signals, in the sequel the sliding motion can be recovered.

The chapter is organized as follows. In Section 2.2, problem formulation, the concept of equivalent control and the new SMC scheme with closed-loop filtering are presented. In Section 2.3, the convergence analysis is presented. Section 2.4 shows that the sliding motion can be recovered in finite time against disturbance surging. In Section 2.5, an illustrative example, which is a synchronization problem between two Van de Pol circuits, is presented which demonstrates the effectiveness of the proposed scheme. Finally, Section 2.6 gives the conclusions.

2.2 Equivalent Control and SMC with Closed-Loop Filtering

A: Problem Formulation

Consider the nth order nonlinear system

$$\begin{cases} \dot{x}_i(t) = x_{i+1}(t), \quad i = 1, 2, \cdots, n-1 \\ \dot{x}_n(t) = f(\mathbf{x}, t) + b(\mathbf{x}, t)\left[u(\mathbf{x}, t) + \eta(\mathbf{x}, t)\right] \end{cases} \tag{2.1}$$

where $t \in \mathcal{R}^+$, $\mathbf{x} = [x_1, x_2, \cdots x_n]^T$ is the measurable state, $f(\mathbf{x}, t)$, $b(\mathbf{x}, t) \neq 0$ are known functions with respect to the arguments, $u(\mathbf{x}, t)$ is the system control input, $\eta(\mathbf{x}, t)$ is a disturbance. In addition, $f(\mathbf{x}, t)$, $b(\mathbf{x}, t)$ and $\eta(\mathbf{x}, t)$ are assumed to be continuously differentiable, $\forall\, (\mathbf{x}, t) \in \mathcal{R}^n \times \mathcal{R}^+$, $\mathcal{R}^+ \triangleq [0, \infty)$.

The system is required to track the trajectory $\mathbf{x}_d$ described by

$$\begin{cases} \dot{x}_{id} = x_{(i+1)d}, \quad i = 1, 2, \cdots, n-1 \\ \dot{x}_{nd} = \psi(\mathbf{x}_d(t), r(t), t) \end{cases} \tag{2.2}$$

where $\mathbf{x}_d = [x_{1d}, x_{2d}, \cdots, x_{nd}]^T$, $\psi \in C^1[0, \infty)$ with respect to all arguments and $r(t)$ is a reference input. The tracking errors are defined as $e_1 = x_1 - x_{1d}$, $e_i = \dot{e}_{i-1}$, $i = 2, 3, \cdots, n$.

In order for a low pass filter to capture the equivalent control profile, it is necessary to limit the bandwidth of the system disturbance, which is equivalent to imposing an upper limit on the variation of $\eta(\mathbf{x}, t)$.

Assumption 2.1. *$\eta(\mathbf{x}, t)$ and its derivative are upperbounded by $|\eta(\mathbf{x}, t)| \leq \beta_0$ and $|\dot{\eta}(\mathbf{x}, t)| \leq \beta_d$, where β_0 and β_d are known constants.*

Assumption 2.2. *$b(\mathbf{x}, t)$ is positive definite which is bounded by known positive constants $\underline{b}$ and $\bar{b}$, i.e., $0 < \underline{b} \leq b(\cdot) \leq \bar{b}$, and its derivative is upperbounded by a known constant as $\dot{b}(\cdot) \leq \bar{b}_d$.*

B: Concept of Equivalent Control

Choose a switching surface $\sigma = \sigma(\mathbf{e}, t)$, a $C^1(\mathcal{R}^n \times \mathcal{R}^+)$ function, where $\mathbf{e} = [e_1, e_2, \cdots e_n]^T$ and $D_{e_n}\sigma \neq 0$ is a constant $\forall(\mathbf{e}, t) \in \mathcal{R}^n \times \mathcal{R}^+$. The condition for a system to remain in sliding mode can be jointly described by $(\sigma = 0) \cap (\dot{\sigma} = 0)$. By solving the equation $\dot{\sigma} = 0$ for the control input, we obtain the equivalent control, u_{eq}, which can be interpreted as the continuous control law that would maintain $\dot{\sigma} = 0$.

$$\begin{aligned} \dot{\sigma} &= D_t\sigma + \sum_{i=1}^{n-1}(D_{e_i}\sigma)e_{i+1} + (D_{e_n}\sigma)\dot{e}_n \\ &= D_t\sigma + \sum_{i=1}^{n-1}(D_{e_i}\sigma)e_{i+1} + (D_{e_n}\sigma)\{f(\mathbf{x}, t) + b(\mathbf{x}, t)\,[u(\mathbf{x}, t) + \eta(\mathbf{x}, t)] - \dot{x}_{nd}\} \\ &= \left[D_t\sigma + \sum_{i=1}^{n-1}(D_{e_i}\sigma)e_{i+1} + (D_{e_n}\sigma)(f(\mathbf{x}, t) - \dot{x}_{nd})\right] + (D_{e_n}\sigma)\{b(\mathbf{x}, t)\,[u(\mathbf{x}, t) + \eta(\mathbf{x}, t)]\} \end{aligned}$$

$$= \quad \theta(\mathbf{x}, \mathbf{x}_d, t) + \rho(\mathbf{x}, \mathbf{x}_d, t)\left[u(\mathbf{x}, t) + \eta(\mathbf{x}, t)\right] = 0, \tag{2.3}$$

where $\theta(\mathbf{x}, \mathbf{x}_d, t) = D_t\sigma + \sum_{i=1}^{n-1}(D_{e_i}\sigma)e_{i+1} + (D_{e_n}\sigma)(f(\mathbf{x}, t) - \dot{x}_{nd})$ and $\rho(\mathbf{x}, \mathbf{x}_d, t) = (D_{e_n}\sigma)b(\mathbf{x}, t)$, where $|\rho|_{min} = |(D_{e_n}\sigma)|\underline{b}$ and $(D_{e_n}\sigma)$ is a constant. Let u_c denote the feedforward compensation term which is to deal with the system nominal part in (2.3), i.e. $\dot{\sigma} = \theta + \rho u_c$. A possible way is to design the nominal control signal u_c as a nonlinear optimal control with such a criterion as $J = \int_0^\infty \left[q(x) + u^2\right] dt$, subject to the solvability of the HJB equation. Nonlinear suboptimal control can also be considered (Xu and Zhang, 2000). One can also choose $u_c = -\rho^{-1}\theta$ to cancel out the nominal part as the simplest way. Then from (2.3), u_{eq} can be expressed as

$$u_{eq} \quad = \quad u_c(\mathbf{x}, t) - \eta(\mathbf{x}, t). \tag{2.4}$$

Obviously u_{eq} is not directly achievable due to the existence of unknown $\eta(\mathbf{x}, t)$. In most SMC designs, a high gain switching control is used to deal with $\eta(\mathbf{x}, t)$.

C: SMC with Closed-Loop Filtering Architecture

The new SMC with closed-loop filtering is

$$u = u_c + k_s(t)u_s + u_v \tag{2.5}$$

where u_s is a switching quantity defined as

$$u_s \quad = \quad -sign(\sigma\rho).$$

The continuous term u_v is generated by a first-order low-pass filter (denoted as LPF1)

$$\tau_1\dot{u}_v + u_v = \gamma_1 u_s, \tag{2.6}$$

where τ_1 and γ_1 are positive constants. LPF1 is activated at the time $t = t_r$ with zero initial condition $u_v(t_r) = 0$.

The switching gain k_s is chosen as below

$$k_s(t) = \begin{cases} \beta_0 + \beta_k & 0 \leq t \leq t_r \\ k(t) & t > t_r, \end{cases} \tag{2.7}$$

where $\beta_k > 0$, t_r is the reaching time and $k(t)$ is the output of another first order filter $LPF2$ shown below

$$\tau_2 \dot{k} + k = \gamma_2 g(\sigma) \tag{2.8}$$

$$g(\sigma) = k_g |\sigma|^q, \tag{2.9}$$

where $\tau_2 \geq \tau_1$, $\gamma_2 > 0$, $p > 0$ and $k_g > 0$ are all constants. The initial condition of LPF2 is $k(t_r) = \beta_0 + \beta_k$ where $\beta_k > 0$ is a constant. Note that $g(\sigma)$ is an even function of the switching surface σ, and $g(\sigma) = 0$ only when $\sigma = 0$.

The Schematic diagram of the proposed control system is shown in $Fig.2.1$.

Remark 2.1. *Choosing $k_s(t) = \beta_0 + \beta_k$ and without using u_v, the reaching condition of the sliding mode is guaranteed by the switching control $k_s u_s$. In most SMC, even after entering the sliding mode, the gain k_s is kept invariant and chattering occurs inevitably. The purpose of introducing LPF1 and LPF2 is to extract equivalent control and hence scale down the switching gain $k_s(t)$.*

2.3 Convergence Analysis

It is worthwhile to point out that the variable structure control system exhibits distinct behavior in the reaching and sliding phases. Therefore it is possible and necessary to design different control schemes better catering to the two phases respectively. During the reaching phase, it is desirable to use a high gain to ensure the global attractiveness of the switching surface.

A. Convergence Analysis in Reaching Phase

In this phase, $k_s(t) = \beta_0 + \beta_k$, $u_v = 0$, $\forall t \in [0, t_r]$, equation (2.5) becomes $u = u_c + k_s u_s$. The Lyapunov candidate is chosen as $V = \frac{1}{2}\sigma^2 > 0$. The derivative of V becomes

$$\dot{V} = \sigma\dot{\sigma} = \sigma\rho(k_s u_s + \eta) \leq -k_s|\sigma\rho| + |\beta_0\sigma\rho| = -\beta_k|\sigma\rho|.$$

Thus the system is convergent during the reaching phase. The reaching time can be calculated as $t_r \leq \frac{|\sigma(0)|}{\beta_k|\rho|_{min}}$ where $\sigma(0) = \sigma(\mathbf{e}(0), 0)$. In this work we choose the maximum value $t_r = \frac{|\sigma(0)|}{\beta_k|\rho|_{min}}$.

B. Existence Conditions of the Sliding Motion

In this subsection we will derive the sufficient conditions for maintaining the sliding mode when using the proposed controller. These are summarized in the following theorem. The properties and the definition of the sliding mode have been presented in detail in (Utkin, 1992) and (Utkin, 1978) in terms of Filippov's work (Filippov, 1960) and (Filippov, 1988). In the sliding mode control, the system states are attracted to the switching surface $\sigma = 0$ in a finite period. Once the system reaches $\sigma = 0$, it cannot leave it, *i.e.* the velocity along the normal direction to the switching surface is zero. Thus we have $\dot{\sigma} = 0$. When introducing the two filters, the switching gain is scaled down in $LPF2$ when σ is sufficiently small in order to facilitate the acquisition of the equivalent control by $LPF1$. In the following theorem we will prove that the system will retain the sliding motion when the two filters start working.

Theorem 2.1. *If the parameters of the two low-pass filters, τ_1, γ_1, and τ_2, are chosen to satisfy the following conditions*

$$\begin{cases} \tau_2 \geq \tau_1, \\ \gamma_1 \geq 2(2\beta_0 + \beta_d\tau_1), \\ \beta_k \geq \alpha\beta_0 \qquad \alpha > 1, \end{cases} \tag{2.10}$$

then the sliding motion is maintained for all $t \in [t_r, \infty)$.

In the subsequent proof, we need to use the following property.

Property 2.1. *Consider the integration*

$$e^{-\int_{t_r}^{t} p(\tau)d\tau} \int_{t_r}^{t} h(\tau) d(e^{-\int_{t_r}^{\tau} p(s)ds})$$

where $p(\cdot) > 0$ *can be arbitrarily large. Assume that* $h(t)$ *has an constant upper bound* $h_{max} \geq |h(t)|$*, then*

$$\begin{aligned} \left| e^{-\int_{t_r}^{t} p(\tau)d\tau} \int_{t_r}^{t} h(\tau) d(e^{-\int_{t_r}^{\tau} p(s)ds}) \right| &\leq e^{-\int_{t_r}^{t} p(\tau)d\tau} h_{max} e^{-\int_{t_r}^{\tau} p(s)ds} \Big|_{t_r}^{t} \\ &= h_{max} \left(1 - e^{-\int_{t_r}^{t} p(\tau)d\tau}\right) \leq h_{max}. \end{aligned} \tag{2.11}$$

Proof: By virtue of the high gain used in the reaching phase, the switching surface is reached in $t = t_r$. When $t \geq t_r$, both filters $LPF1$ and $LPF2$ start working concurrently, and in particular the switching gain k will be shaped by $LPF2$. The key issue, in such circumstance, is to prove that the sliding mode retains after t_r. The proof consists of three parts. First we show the ideal conditions under which $LFP1$ is able to approximate the disturbance, in the sense of equivalent control. Since these conditions with equivalent control are practically not implementable, we look for alternative conditions, which are related to the design parameters of $LPF1$ and $LPF2$, such that the sliding mode holds at least for a sufficiently small interval $[t_r, t_r + \triangle_1]$. Then we show that the sliding mode can be maintained over the subsequent intervals $[t_r + \triangle_1, t_r + \triangle_1 + \triangle_2]$, $\cdots$, where $\triangle_i$ is not infinitesimal. Hence the sliding mode exists over $[t_r, \infty)$

Part A

We first look into the approximation property of $LPF1$ to the disturbance η. Substituting the control law (2.5), with $u_c = -\rho^{-1}\theta$, into the σ dynamics (2.3) leads to the closed-loop σ dynamics

$$\dot{\sigma} = \rho(ku_s + u_v + \eta). \tag{2.12}$$

Substituting the above relation into the dynamics of $LPF1$ (2.6), the following equation holds ($t \geq t_r$)

$$\tau_1 \dot{u}_v + u_v = \frac{\gamma_1}{k}\left(\frac{\dot{\sigma}}{\rho} - u_v - \eta\right), \quad \Rightarrow \dot{u}_v + \left(\frac{\gamma_1 + k}{\tau_1 k}\right) u_v = \frac{\gamma_1 \dot{\sigma}}{\tau_1 k \rho} - \frac{\gamma_1 \eta}{\tau_1 k},$$

where $u_v(t_r) = 0$. Define $p(t) = \dfrac{\gamma_1 + k}{\tau_1 k}$, the solution of u_v is

$$\begin{aligned} u_v &= e^{-\int_{t_r}^{t} p(\tau)d\tau} \int_{t_r}^{t} \left(\frac{\gamma_1 \dot{\sigma}}{\tau_1 k \rho} - \frac{\gamma_1 \eta}{\tau_1 k}\right) e^{\int_{t_r}^{\tau} p(s)ds} d\tau \\ &= e^{-\int_{t_r}^{t} p(\tau)d\tau} \int_{t_r}^{t} \frac{\gamma_1 \dot{\sigma}}{\tau_1 k \rho} e^{\int_{t_r}^{\tau} p(s)ds} d\tau - e^{-\int_{t_r}^{t} p(\tau)d\tau} \int_{t_r}^{t} \frac{\gamma_1 \eta}{\tau_1 k} e^{\int_{t_r}^{\tau} p(s)ds} d\tau \\ &= u_{v1} + u_{v2}, \end{aligned}$$

where $u_{v1} \triangleq e^{-\int_{t_r}^{t} p(\tau)d\tau} \int_{t_r}^{t} \dfrac{\gamma_1 \dot{\sigma}}{\tau_1 k \rho} e^{\int_{t_r}^{\tau} p(s)ds} d\tau$ and $u_{v2} \triangleq -e^{-\int_{t_r}^{t} p(\tau)d\tau} \int_{t_r}^{t} \dfrac{\gamma_1 \eta}{\tau_1 k} e^{\int_{t_r}^{\tau} p(s)ds} d\tau$. Calculating u_{v1} and u_{v2} using integral by part, and noticing the fact $\sigma(t_r) = 0$, we have

$$\begin{aligned} u_{v1} &= e^{-\int_{t_r}^{t} p(\tau)d\tau} \int_{t_r}^{t} \frac{\gamma_1 \dot{\sigma}}{\tau_1 k \rho} e^{\int_{t_r}^{\tau} p(s)ds} d\tau \\ &= e^{-\int_{t_r}^{t} p(\tau)d\tau} \left[\left(\frac{\gamma_1 \sigma}{\tau_1 k \rho} e^{\int_{t_r}^{\tau} p(s)ds}\right) |_{t_r}^{t} - \int_{t_r}^{t} \sigma \left(\frac{\gamma_1}{\tau_1 k \rho} e^{\int_{t_r}^{\tau} p(s)ds}\right)' d\tau\right] \\ &= \frac{\gamma_1 \sigma}{\tau_1 k \rho} - \frac{\gamma_1 \sigma(t_r)}{\tau_1 k(t_r)\rho(t_r)} e^{-\int_{t_r}^{t} p(\tau)d\tau} \\ &\quad - e^{-\int_{t_r}^{t} p(\tau)d\tau} \int_{t_r}^{t} \sigma \left[\left(\frac{\gamma_1}{\tau_1 k \rho}\right)' + \frac{\gamma_1 p}{\tau_1 k \rho}\right] e^{\int_{t_r}^{\tau} p(s)ds} d\tau \\ &= \frac{\gamma_1 \sigma}{\tau_1 k \rho} - e^{-\int_{t_r}^{t} p(\tau)d\tau} \int_{t_r}^{t} \sigma \left[\left(\frac{\gamma_1}{\tau_1 k \rho}\right)' + \frac{\gamma_1 p}{\tau_1 k \rho}\right] p^{-1} d\left(e^{\int_{t_r}^{\tau} p(s)ds}\right) \\ &= \frac{\gamma_1 \sigma}{\tau_1 k \rho} - e^{-\int_{t_r}^{t} p(\tau)d\tau} \int_{t_r}^{t} \left[\frac{-\gamma_1 \dot{k} \sigma}{k\rho(\gamma_1 + k)} + \frac{-\gamma_1 \dot{\rho} \sigma}{(\gamma_1 + k)\rho^2} + \frac{\gamma_1 \sigma}{\tau_1 \rho k}\right] d\left(e^{\int_{t_r}^{\tau} p(s)ds}\right) \end{aligned} \tag{2.13}$$

and

$$\begin{aligned} u_{v2} &= -e^{-\int_{t_r}^{t} p(\tau)d\tau} \int_{t_r}^{t} \frac{\gamma_1 \eta}{\tau_1 k} e^{\int_{t_r}^{\tau} p(s)ds} d\tau \\ &= -e^{-\int_{t_r}^{t} p(\tau)d\tau} \left[\left(\frac{\eta \gamma_1}{\gamma_1 + k} e^{\int_{t_r}^{\tau} p(s)ds}\right) |_{t_r}^{t} - \int_{t_r}^{t} e^{\int_{t_r}^{\tau} p(s)ds} \left(\frac{\eta \gamma_1}{\gamma_1 + k}\right)' d\tau\right] \end{aligned}$$

$$
\begin{aligned}
&= -\frac{\eta\gamma_1}{\gamma_1+k} + \frac{\eta(t_r)\gamma_1}{\gamma_1+k(t_r)} e^{-\int_{t_r}^{t} p(\tau)d\tau} \\
&\quad + e^{-\int_{t_r}^{t} p(\tau)d\tau} \int_{t_r}^{t} e^{\int_{t_r}^{\tau} p(s)ds} \frac{(\gamma_1+k)\gamma_1\dot{\eta} - \eta\gamma_1\dot{k}}{(\gamma_1+k)^2} d\tau \\
&= -\frac{\eta\gamma_1}{\gamma_1+k} + \frac{\eta(t_r)\gamma_1}{\gamma_1+k(t_r)} e^{-\int_{t_r}^{t} p(\tau)d\tau} \\
&\quad + e^{-\int_{t_r}^{t} p(\tau)d\tau} \int_{t_r}^{t} \frac{\left[(\gamma_1+k)\gamma_1\dot{\eta} - \eta\gamma_1\dot{k}\right]\tau_1 k}{(\gamma_1+k)^3} d\left(e^{\int_{t_r}^{\tau} p(s)ds}\right). \qquad (2.14)
\end{aligned}
$$

From the equation (2.8) of $LPF2$, we have

$$
\dot{k} = -\frac{1}{\tau_2}k + \frac{k_g\gamma_2}{\tau_2}|\sigma|^q. \qquad (2.15)
$$

Using (2.13), (2.14) and substituting $\dot{k}$ in (2.15), we have

$$
\begin{aligned}
u_v + \eta &= \frac{\gamma_1\sigma}{\tau_1 k\rho} + \frac{k\eta}{\gamma_1+k} + \frac{\eta(t_r)\gamma_1}{\gamma_1+k(t_r)} e^{-\int_{t_r}^{t} p(\tau)d\tau} \\
&\quad - e^{-\int_{t_r}^{t} p(\tau)d\tau} \int_{t_r}^{t} \left[\frac{-\gamma_1\dot{k}\sigma}{k\rho(\gamma_1+k)} + \frac{-\gamma_1\dot{\rho}\sigma}{(\gamma_1+k)\rho^2} + \frac{\gamma_1\sigma}{\tau_1\rho k}\right] d\left(e^{\int_{t_r}^{\tau} p(s)ds}\right) \\
&\quad + e^{-\int_{t_r}^{t} p(\tau)d\tau} \int_{t_r}^{t} \frac{\left[(\gamma_1+k)\gamma_1\dot{\eta} - \eta\gamma_1\dot{k}\right]\tau_1 k}{(\gamma_1+k)^3} d\left(e^{\int_{t_r}^{\tau} p(s)ds}\right) \\
&= \frac{\gamma_1\sigma}{\tau_1 k\rho} + \frac{k\eta}{\gamma_1+k} + \frac{\eta(t_r)\gamma_1}{\gamma_1+k(t_r)} e^{-\int_{t_r}^{t} p(\tau)d\tau} \\
&\quad - e^{-\int_{t_r}^{t} p(\tau)d\tau} \int_{t_r}^{t} \left[\frac{\gamma_1\sigma}{\tau_2\rho(\gamma_1+k)} - \frac{\gamma_1\sigma|\sigma|^q k_g\gamma_2}{k\rho\tau_2(\gamma_1+k)} - \frac{\gamma_1\dot{\rho}\sigma}{(\gamma_1+k)\rho^2} + \frac{\gamma_1\sigma}{\tau_1\rho k}\right] \\
&\quad d\left(e^{\int_{t_r}^{\tau} p(s)ds}\right) \\
&\quad + e^{-\int_{t_r}^{t} p(\tau)d\tau} \int_{t_r}^{t} \left[\frac{\tau_1 k\gamma_1\dot{\eta}}{(\gamma_1+k)^2} + \frac{\eta\gamma_1\tau_1 k^2}{\tau_2(\gamma_1+k)^3} - \frac{\gamma_1\eta k_g\gamma_2|\sigma|^q\tau_1 k}{\tau_2(\gamma_1+k)^3}\right] \\
&\quad d\left(e^{\int_{t_r}^{\tau} p(s)ds}\right) \qquad (2.16)
\end{aligned}
$$

Now let us show that $|u_v + \eta| \to 0$ if the following conditions are satisfied $\forall t \geq t_r$,

$$
|\sigma| \to 0, \quad k \to 0, \quad \frac{|\sigma|}{k} \to 0. \qquad (2.17)
$$

Let $\sigma(t) \to 0$ and $\dfrac{|\sigma|}{k} \to 0$ $\forall t \geq t_r$, and use Property (2.11), (2.16) renders to

$$
\begin{aligned}
u_v + \eta &= \frac{k\eta}{\gamma_1+k} + \frac{\eta(t_r)\gamma_1}{\gamma_1+k(t_r)} e^{-\int_{t_r}^{t} p(\tau)d\tau} \\
&\quad + e^{-\int_{t_r}^{t} p(\tau)d\tau} \int_{t_r}^{t} \left[\frac{\tau_1 k\gamma_1\dot{\eta}}{(\gamma_1+k)^2} + \frac{\eta\gamma_1\tau_1 k^2}{\tau_2(\gamma_1+k)^3}\right] d\left(e^{\int_{t_r}^{\tau} p(s)ds}\right). \qquad (2.18)
\end{aligned}
$$

Furthermore, let $k \to 0$ and use Property (2.11), then $\frac{k\eta}{\gamma_1 + k} \to 0$, $e^{-\int_{t_r}^{t} p(\tau)d\tau} \to 0$ because of a very large $p(\tau)$ and $\frac{\tau_1 k \gamma_1 \dot{\eta}}{(\gamma_1 + k)^2} + \frac{\eta \gamma_1 \tau_1 k^2}{\tau_2(\gamma_1 + k)^3} \to 0$. Note that conditions (2.17) are similar to the conditions for deriving equivalent control [22]. Clearly, shaping the gain k is necessary in order to capture the disturbance. However, $k(t)$ tends to 0 when $t \to \infty$. Thus the estimate of disturbance by $LPF1$ will converge asymptotically to the disturbance.

Part B

The preceding part did not provide the assurance for the existence of the sliding mode. In this part, we investigate the system behavior for a sufficiently small interval right after t_r, and demonstrate that the system state cannot move away from the switching surface in the interval.

Suppose that $\sigma(t)$ is in anyway moving away from $\sigma(t) = 0$, $\forall t \in [t_r, t_r + \triangle_1]$. In such circumstance, there will be no switching and the system trajectory is continuous, so is $\sigma(t)$. Therefore, for a given sufficiently small ε_0, there exists a sufficiently small $\triangle_1$, such that $\sigma(t_r) = 0$, $\sigma(t)$ monotonically increases and reaches the maximum $|\sigma(t_r + \triangle_1)| = \varepsilon_0$. Likewise, with the given ε_0, from the continuity of $k(t)$ $\forall t \in [t_r, t_r + \triangle_1]$, there exists a sufficiently small $\triangle_1$, such that $k_{max} \leq k_{min}(1 + \varepsilon_0)$, where k_{max} and k_{min} are defined as the maximum and minimum values of $k(t)$ in the time interval $t \in [t_r, t_r + \triangle_1]$. Choose $\triangle_1$ which meets both requirements.

Taking the absolute values on both sides of (2.16), taking the upper bounds on the right hand side and using Property (2.11), we have $\forall t \in [t_r, t_r + \triangle_1]$

$$\begin{aligned} |u_v + \eta| \quad \leq \quad & \frac{\gamma_1 \varepsilon_0}{k_{min}\tau_1|\rho|_{min}} + \frac{\beta_0 k}{\gamma_1 + k_{min}} + \frac{\beta_0 \gamma_1}{\gamma_1 + k(t_r)} e^{-\int_{t_r}^{t} p(\tau)d\tau} \\ & + \frac{\gamma_1 \varepsilon_0}{\tau_2|\rho|_{min}(\gamma_1 + k_{min})} + \frac{\gamma_1 \varepsilon_0^{q+1} k_g \gamma_2}{k_{min}|\rho|_{min}\tau_2(\gamma_1 + k_{min})} + \frac{\gamma_1 |(D_{e_n}\sigma)|\bar{b}_d \varepsilon_0}{(\gamma_1 + k_{min})|\rho|_{min}^2} \\ & + \frac{\gamma_1 \varepsilon_0}{k_{min}\tau_1|\rho|_{min}} + \frac{k_{max}\beta_d \gamma_1 \tau_1}{(\gamma_1 + k_{min})^2} + \frac{k_{max}^2 \beta_0 \gamma_1 \tau_1}{\tau_2(\gamma_1 + k_{min})^3} + \frac{k_{max}\beta_0 \gamma_1 \tau_1 k_g \gamma_2 \varepsilon_0^q}{\tau_2(\gamma_1 + k_{min})^3}. \end{aligned} \tag{2.19}$$

Now we are in a position to derive the sliding mode in $[t_r, t_r + \triangle_1]$. Note that $k(t)$ tends to 0 when $t \to \infty$, i.e., $k(t)$ is finite when $t < \infty$. From the closed-loop σ dynamics (2.12) and the switching control law $u_s = -sign(\sigma\rho)$, the derivative of V is

$$\dot{V} \leq -|\sigma\rho|(k - |u_v + \eta|) = -k|\sigma\rho|(1 - \frac{|u_v + \eta|}{k}). \tag{2.20}$$

Hence, if $\frac{|u_v + \eta|}{k} < 1$ can be ensured $\forall t \in [t_r, t_r + \triangle_1]$, the sliding mode is retained. Now let us prove that $\frac{|u_v + \eta|}{k} < 1$ holds $\forall t \in [t_r, t_r + \triangle_1]$.

Note that

$$k(t) = e^{-\frac{t-t_r}{\tau_2}} k(t_r) + \frac{\gamma_2}{\tau_2} \int_{t_r}^{t} g(\sigma) e^{-\frac{t-\tau}{\tau_2}} d\tau \geq e^{-\frac{t-t_r}{\tau_2}} k(t_r). \tag{2.21}$$

From (2.19) and (2.21), we can derive

$$\begin{aligned} \frac{|u_v + \eta|}{k} \leq & \frac{\gamma_1 \varepsilon_0}{k_{min}^2 \tau_1 |\rho|_{min}} + \frac{\beta_0}{\gamma_1 + k_{min}} + \frac{\beta_0 \gamma_1}{(\gamma_1 + k(t_r))k(t_r)} e^{-\int_{t_r}^{t} \frac{\gamma_1}{\tau_1 k} d\tau} e^{-\frac{\tau_2 - \tau_1}{\tau_1 \tau_2}(t - t_r)} \\ & + \frac{\gamma_1 \varepsilon_0}{k_{min} \tau_2 |\rho|_{min} (\gamma_1 + k_{min})} + \frac{\gamma_1 \varepsilon_0^{q+1} k_g \gamma_2}{k_{min}^2 |\rho|_{min} \tau_2 (\gamma_1 + k_{min})} \\ & + \frac{\gamma_1 |(D_{e_n}\sigma)| \bar{b}_d \varepsilon_0}{k_{min}(\gamma_1 + k_{min})|\rho|_{min}^2} + \frac{\gamma_1 \varepsilon_0}{k_{min}^2 \tau_1 |\rho|_{min}} + \frac{k_{max} \beta_d \gamma_1 \tau_1}{k_{min}(\gamma_1 + k_{min})^2} \\ & + \frac{k_{max}^2 \beta_0 \gamma_1 \tau_1}{k_{min} \tau_2 (\gamma_1 + k_{min})^3} + \frac{k_{max} \beta_0 \gamma_1 \tau_1 k_g \gamma_2 \varepsilon_0^q}{k_{min} \tau_2 (\gamma_1 + k_{min})^3}. \end{aligned} \tag{2.22}$$

For all terms related to ε_0 in (2.22), choose a small constant $\varepsilon_1 < \frac{\alpha - 1}{4(1 + \alpha)}$. There exists a sufficiently small $\triangle_1$, in the sequel ε_0 is sufficiently small such that the following condition is satisfied

$$\begin{aligned} & \frac{\gamma_1 \varepsilon_0}{k_{min}^2 \tau_1 |\rho|_{min}} + \frac{\gamma_1 \varepsilon_0}{\tau_2 |k_{min} \rho|_{min} (\gamma_1 + k_{min})} + \frac{\gamma_1 \varepsilon_0^{q+1} k_g \gamma_2}{k_{min}^2 |\rho|_{min} \tau_2 (\gamma_1 + k_{min})} \\ & + \frac{\gamma_1 |(D_{e_n}\sigma)| \bar{b}_d \varepsilon_0}{k_{min}(\gamma_1 + k_{min})|\rho|_{min}^2} + \frac{\gamma_1 \varepsilon_0}{k_{min}^2 \tau_1 |\rho|_{min}} + \frac{k_{max} \beta_0 \gamma_1 \tau_1 k_g \gamma_2 \varepsilon_0^q}{k_{min} \tau_2 (\gamma_1 + k_{min})^3} \leq \varepsilon_1 < \frac{\alpha - 1}{4(1 + \alpha)}. \end{aligned}$$

Using (2.23) and choosing $\tau_2 \geq \tau_1$, (2.22) becomes

$$\begin{aligned} \frac{|u_v + \eta|}{k} \leq & \varepsilon_1 + \frac{\beta_0}{\gamma_1 + k_{min}} + \frac{\beta_0 \gamma_1}{(\gamma_1 + k(t_r))k(t_r)} \\ & + \frac{(1 + \varepsilon_0)\beta_d \gamma_1 \tau_1}{(\gamma_1 + k_{min})^2} + \frac{k_{min}(1 + \varepsilon_0)^2 \beta_0 \gamma_1 \tau_1}{\tau_2 (\gamma_1 + k_{min})^3} \end{aligned}$$

$$\begin{aligned} &\leq \quad \varepsilon_1 + \varepsilon_2 + \frac{\beta_0}{\gamma_1 + k_{min}} + \frac{\beta_0 \gamma_1}{(\gamma_1 + k(t_r))k(t_r)} \\ &\quad + \frac{\beta_d \gamma_1 \tau_1}{(\gamma_1 + k_{min})^2} + \frac{k_{min}\beta_0 \gamma_1 \tau_1}{\tau_2(\gamma_1 + k_{min})^3}. \end{aligned} \tag{2.23}$$

where, analogous to (2.23), ε_0 can be made sufficiently small so that

$$\frac{\beta_d \gamma_1 \tau_1 \varepsilon_0}{(\gamma_1 + k_{min})^2} + \frac{k_{min}(2\varepsilon_0 + \varepsilon_0^2)\beta_0 \gamma_1 \tau_1}{\tau_2(\gamma_1 + k_{min})^3} \leq \varepsilon_2 < \frac{\alpha - 1}{4(1+\alpha)}.$$

Since $k(t_r) = \beta_0 + \beta_k > (1+\alpha)\beta_0$ and $\gamma_1 \geq 2(2\beta_0 + \beta_d \tau_1)$, from (2.23) we can further derive

$$\begin{aligned} \frac{|u_v + \eta|}{k} &\leq \varepsilon_1 + \varepsilon_2 + \frac{\beta_0}{\gamma_1 + k_{min}} + \frac{\beta_0}{k(t_r)} + \frac{\beta_0}{\gamma_1 + k_{min}} + \frac{\tau_1 \beta_d}{\gamma_1 + k_{min}} \\ &= \varepsilon_1 + \varepsilon_2 + \frac{\beta_0}{k(t_r)} + \frac{2\beta_0 + \tau_1 \beta_d}{\gamma_1 + k_{min}} \\ &< \frac{\alpha - 1}{4(1+\alpha)} + \frac{\alpha - 1}{4(1+\alpha)} + \frac{1}{1+\alpha} + \frac{\gamma_1/2}{\gamma_1 + k_{min}} \\ &= \frac{1}{2} + \frac{\gamma_1}{2(\gamma_1 + k_{min})} < 1 - \varepsilon_3, \end{aligned}$$

where $\varepsilon_3 \in \left(0, \frac{k_{min}}{2(\gamma_1 + k_{min})}\right)$. Hence, from (2.20) we have $\dot{V} < -k\varepsilon_3 |\sigma\rho|$, where $k(t) \neq 0$. Thus the sliding mode does exist, that is, $(\sigma = 0) \cap (\dot{\sigma} = 0)$ for $t \in [t_r, t_r + \triangle_1]$.

Part C

Now let us investigate the system behavior in the interval $[t_r + \triangle_1, \infty)$. Suppose that the system diverges in the interval $[t_r + \triangle_1, t_r + \triangle_1 + \triangle_2]$. Because of the existence of the sliding mode in the sub-interval $[t_r, t_r + \triangle_1]$ as proven in *Part B*, at time $t_1 = t_r + \triangle_1$, we have

$$\begin{aligned} \dot{\sigma}(t_1) &= \rho\left[u_v(\mathbf{x}, t_1) + \eta(t_1) - k(t_1) sign(\sigma(t_1))\right] = 0, \\ \Rightarrow u_v(\mathbf{x}, t_1) &= k(t_1) sign(\sigma(t_1)) - \eta(t_1). \end{aligned} \tag{2.24}$$

Here we consider that $sign(\sigma(t_1)) \neq 0$ when $\sigma(t_1) = 0$ because there is no definition for the $sign(\sigma)$ function at the point $\sigma = 0$. Analogous to preceding discussions, let $\triangle_2$ be sufficiently small, such that $\sigma(t)$ increases monotonically and reach the

maximum at $t_r + \triangle_1 + \triangle_2$. For simplicity, assume $\rho = (D_{e_n}\sigma)b(\mathbf{x},t) > 0$ and $\sigma(t) > 0$. In the following, we will prove that sliding mode exists $\forall t \in [t_1, t_1 + \triangle_2]$.

At time $t \in (t_1, t_1 + \triangle_2]$, $LPF1$ and $LPF2$ can be written as

$$\tau_1 \dot{u}_v + u_v = -\gamma_1 sign(\sigma\rho) = -\gamma_1, \qquad \tau_2 \dot{k}(t) + k(t) = \gamma_2 g(\sigma)$$

$$\begin{aligned} u_v &= e^{-\frac{t-t_1}{\tau_1}} u_v(\mathbf{x}, t_1) - \frac{1}{\tau_1}\int_{t_1}^{t} e^{-\frac{t-\tau}{\tau 1}}\gamma_1 d\tau \\ &= e^{-\frac{t-t_1}{\tau_1}}(u_v(\mathbf{x}, t_1) + \gamma_1) - \gamma_1 \qquad (2.25) \\ k(t) &= e^{-\frac{t-t_1}{\tau_2}} k(t_1) + \frac{\gamma_2}{\tau_2}\int_{t_1}^{t} g(\sigma) e^{-\frac{t-\tau}{\tau_2}} d\tau. \qquad (2.26) \end{aligned}$$

Using (2.24), (2.31) and (2.32), the derivative of V becomes ($\forall t > t_1$)

$$\begin{aligned} \dot{V} &= \sigma\dot{\sigma} = \sigma\rho(ku_s + u_v + \eta) = \sigma\rho\left[-k(t) + u_v(\mathbf{x}, t) + \eta(t)\right] \\ &= \sigma\rho\left[-e^{-\frac{t-t_1}{\tau_2}} k(t_1) - e^{-\frac{t}{\tau_2}}\frac{\gamma_2}{\tau_2}\int_{t_1}^{t} k_g|\sigma|^q e^{\frac{\tau}{\tau_2}} d\tau \right. \\ &\quad \left. + e^{-\frac{t-t_1}{\tau_1}}(u_v(\mathbf{x}, t_1) + \gamma_1) - \gamma_1 + \eta(t)\right] \\ &\leq \sigma\rho\left[-e^{-\frac{t-t_1}{\tau_2}} k(t_1) + e^{-\frac{t-t_1}{\tau_1}}(u_v(\mathbf{x}, t_1) + \gamma_1) - \gamma_1 + \eta(t)\right] \\ &= \sigma\rho\left[-e^{-\frac{t-t_1}{\tau_2}} k(t_1) + e^{-\frac{t-t_1}{\tau_1}}(k(t_1)sign(\sigma(t_1)) - \eta(t_1) + \gamma_1) - \gamma_1 + \eta(t)\right] \\ &= -\sigma\rho\left[e^{-\frac{t-t_1}{\tau_2}} - e^{-\frac{t-t_1}{\tau_1}} sign(\sigma(t_1))\right] k(t_1) \\ &\quad -\sigma\rho\left[(1 - e^{-\frac{t-t_1}{\tau_1}})\gamma_1 - \eta(t) + e^{-\frac{t-t_1}{\tau_1}}\eta(t_1)\right]. \qquad (2.27) \end{aligned}$$

Because $\eta(t_1) = \eta(t) - (t - t_1)\dot{\eta}(\zeta)$, where $\zeta \in [t_1, t_1 + \triangle_2]$, (2.27) becomes

$$\begin{aligned} \dot{V} &\leq -\sigma\rho\left[e^{-\frac{t-t_1}{\tau_2}} - e^{-\frac{t-t_1}{\tau_1}} sign(\sigma(t_1))\right] k(t_1) \\ &\quad -\sigma\rho\left[(1 - e^{-\frac{t-t_1}{\tau_1}})\gamma_1 - \eta(t)(1 - e^{-\frac{t-t_1}{\tau_1}}) - (t - t_1)\dot{\eta}(\zeta)e^{-\frac{t-t_1}{\tau_1}}\right] \\ &\leq -\sigma\rho\left[e^{-\frac{t-t_1}{\tau_2}} - e^{-\frac{t-t_1}{\tau_1}}\right] k(t_1) \\ &\quad -\sigma\rho\left[(1 - e^{-\frac{t-t_1}{\tau_1}})(\gamma_1 - \beta_0) - (t - t_1)\beta_d e^{-\frac{t-t_1}{\tau_1}}\right]. \qquad (2.28) \end{aligned}$$

Because $\tau_2 \geq \tau_1 \Rightarrow e^{-\frac{t-t_1}{\tau_2}} - e^{-\frac{t-t_1}{\tau_1}} \geq 0$, the first term in (2.28) is negative. We can define the second term in (2.28) as $\xi(t) = (1 - e^{-\frac{t-t_1}{\tau_1}})(\gamma_1 - \beta_0) - (t - t_1)\beta_d e^{-\frac{t-t_1}{\tau_1}}$.

Note that $\xi(t_1) = 0$ and if $\gamma_1 \geq\ 2(2\beta_0 + \tau_1\beta_d)$ is selected, we have $(\forall t > t_1)$

$$\dot{\xi}(t) = \left(\frac{\gamma_1 - \beta_0}{\tau_1} - \beta_d\right) e^{-\frac{t-t_1}{\tau_1}} + (t-t_1)\frac{\beta_d}{\tau_1}e^{-\frac{t-t_1}{\tau_1}} > (\frac{3\beta_0}{\tau_1} + \beta_d)e^{-\frac{t-t_1}{\tau_1}} > 0,$$

Hence $\xi(t) > 0\ \forall t \in (t_1, t_1 + \triangle_2]$, and we have $\dot{V} < -\sigma\rho(\frac{3\beta_0}{\tau_1} + \beta_d)e^{-\frac{t-t_1}{\tau_1}} < 0$ $\forall t \in (t_1, t_1 + \Delta_1]$. Thus sliding mode exists during the time $t \in (t_1, t_1 + \triangle_2]$. Similarly, for $\sigma(t) < 0$, we can derive the same results.

By repeating the same derivations shown in this part during the interval $t \in [t_r + \sum_{i=1}^{n} \triangle_i, t_r + \sum_{i=1}^{n+1} \triangle_i]$ with $n \geq\ 2$, we can once again derive $\dot{V} < -\sigma\rho(\frac{3\beta_0}{\tau_1} + \beta_d)e^{-\frac{t-t_n}{\tau_1}} < 0$, where $t_n = t_r + \sum_{i=1}^{n} \triangle_i$. This implies that $(\sigma = 0) \cap (\dot{\sigma} = 0)$ $\forall t \in [t_r + \sum_{i=1}^{n} \triangle_i, t_r + \sum_{i=1}^{n+1} \triangle_i]$. By repeating the same derivation infinite times, $\lim_{n\to\infty} \sum_{i=1}^{n} \triangle_i \to \infty$, we can reach the conclusion that the sliding motion is maintained for all $t \in [t_r, \infty)$.

Remark 2.2. *Note that the selection of the controller parameters in Theorem* 2.1 *is based on the worst case, using upper bounds of all the terms on the right hand side of* (2.23)*. In real implementation β_k, as well as the filter gain γ_1, could take lower values.*

When in the sliding mode, it is possible to extract equivalent control signals from the switching control input by means of filtering techniques. This can be seen according to the following analysis. Assume that the control system enters the sliding mode at $t = t_r$ and $u = u_{eq}$. According to (2.5), we can decompose the equivalent control u_{eq} into three continuous components as

$$u_{eq} \ = \ u_{1eq} + u_{2eq} + u_{3eq} = u_c + k(t)u_{seq} + u_v \tag{2.29}$$

which consists of three known factors: $u_c \stackrel{\triangle}{=} u_{1eq}$, k as part of u_{2eq} and $u_v \stackrel{\triangle}{=} u_{3eq}$. The unknown equivalent quantity u_{seq} is a continuous average of the discontinuous

term u_s and reflects the influence from the system disturbance. Comparing (2.4) and (2.29) we can observe

$$k(t)u_{seq} + u_v = -\eta(\mathbf{x}, t). \tag{2.30}$$

If u_v can be made to approximate the system disturbance $\eta(\mathbf{x}, t)$, the switching gain $k(t)$ can be significantly reduced without affecting the existence of the sliding mode. In terms of (2.30), the ultimate objectives of equivalent control are to let $u_v \Rightarrow -\eta$ and $ku_{seq} \Rightarrow 0$. However, there are theoretically infinite number of solutions for (2.30) in which $u_v \neq -\eta$ and $ku_{seq} \neq 0$. In order to drive u_v to approach $-\eta$, it is also necessary to scale down $k(t)$ to zero. The above discussion shows that both low-pass filters, $LPF1$ and $LPF2$, have to work concurrently aiming at acquiring equivalent control and attenuating the switching control gain simultaneously.

Remark 2.3. *Note that (2.10) also gives the constraints on filter parameters – lower bound of γ_1 and the relationship between τ_1 and τ_2. Since there are four design parameters τ_1, γ_1, τ_2 and γ_2, there are degrees of freedom in the selection of the two filter parameters to further influence system performance. A possible and practical way of designing $LPF1$ and $LPF2$ is to incorporate system knowledge in the frequency domain. For instance, from the point of achieving equivalent control in the frequency domain, τ_1 should be made as small as possible so as to increase the bandwidth of $LPF1$ to capture u_{eq} faithfully. τ_2 and γ_2 will affect the attenuating rate of the switching gain $k(t)$ after entering the sliding motion. A smaller τ_2 will render a faster reduction in $k(t)$.*

Remark 2.4. *As a typical kind of nonlinear and discontinuous control strategies, SMC has to be implemented using digital techniques and sampling rate needs to be taken into account. In digital control it is well known, as a rule of thumb, that the Nyquist frequency should be at least 20 times higher than the control system bandwidth. As a consequence, the lower bounds of τ_1 and τ_2 should be $10 \sim 20$ times of the sampling interval. In other words, the control system can only deal*

with nonlinearities, disturbances and tracking tasks within its bandwidth. $LPF1$ *can only learn low frequency components in* u_{eq} *within its bandwidth. Most practical systems do meet this requirement as they can be characterized as low-pass filters themselves. Since most high frequency components in* u_{eq} *are actually dominated by system noise or measurement noise,* $LPF1$ *and* $LPF2$ *of the new SMC scheme are able to work well under such a noisy control environment and improve the control performance.*

2.4 Sliding Motion Recovery Against Disturbance Surging

Any abrupt change in disturbance may violate the sliding mode existence condition because the gain k has been scheduled to a very low level. In such circumstance, the most important thing is to force the system reenter the sliding motion. This can be achieved by letting $LPF2$ respond sufficiently fast to restore the switching gain to the necessary level, and letting $LPF1$ react also sufficiently fast to capture the equivalent control profile immediately after the disturbance surging. In this section we show that the sliding motion can be recovered by the proposed closed-loop filtering mechanism. Before t_1, assume that the system is already in the sliding mode, $|u_v(\mathbf{x},t) + \eta(\mathbf{x},t)| \leq k(t)$. As shown in $Fig.2.2(a)$, at time $t = t_1 > t_r$ there is a large abrupt change in disturbance within the upbound of β_0. If $|u_v(\mathbf{x},t_1^-) + \eta_2(\mathbf{x},t_1^+)| > k(t_1)$, then $|\dot{\sigma}| \neq 0 \Rightarrow |\sigma| > 0$. The system will leave the sliding surface $\sigma = 0$ as shown in $Fig.2.2(b)$. In the following we show that the sliding mode can be recovered in a finite period.

Theorem 2.2. *Assume that at time* $t = t_1 > t_r$*, the system leaves the sliding surface due to a disturbance surging.* $\exists t_2 \in (t_1, t_3]$*,* $t_3 < \infty$*, such that* $\exists t \geq t_2$*,* $\dot{V} \leq -(\gamma_1 - \beta_0)|\sigma\rho|$*, and the sliding motion recovery will be achieved at a finite*

time $t_3 \geq t_2$.

Proof: For simplicity, assume $\rho = (D_{e_n}\sigma)b(\mathbf{x},t) > 0$. Assume $\sigma(t) > 0$ during the disturbance surging. At time $t \in (t_1, t_3]$, $LPF1$ and $LPF2$ can be written as

$$\tau_1 \dot{u}_v + u_v = -\gamma_1 sign(\sigma\rho) = -\gamma_1, \qquad \tau_2 \dot{k}(t) + k(t) = \gamma_2 g(\sigma)$$

$$\begin{aligned} u_v &= e^{-\frac{t-t_1}{\tau_1}} u_v(\mathbf{x},t_1) - \frac{1}{\tau_1}\int_{t_1}^{t} e^{-\frac{t-\tau}{\tau 1}}\gamma_1 d\tau \\ &= e^{-\frac{t-t_1}{\tau_1}}(u_v(\mathbf{x},t_1)+\gamma_1) - \gamma_1 \qquad (2.31) \\ k(t) &= e^{-\frac{t-t_1}{\tau_2}} k(t_1) + \frac{\gamma_2}{\tau_2}\int_{t_1}^{t} g(\sigma) e^{-\frac{t-\tau}{\tau_2}} d\tau, \qquad (2.32) \end{aligned}$$

where $k(t_1) > 0$. Using (2.31) and (2.32), the derivative of the Lyapunov function candidate becomes $(t > t_1)$

$$\begin{aligned} \dot{V} &= \sigma\dot{\sigma} = \sigma\rho(ku_s + u_v + \eta) = \sigma\rho(-k + u_v + \eta) \leq \sigma\rho(-k + u_v + \beta_0) \\ &= \sigma\rho\left[-e^{-\frac{t-t_1}{\tau_2}} k(t_1) - e^{-\frac{t}{\tau_2}}\frac{\gamma_2}{\tau_2}\int_{t_1}^{t} k_g|\sigma|^q e^{\frac{\tau}{\tau_2}} d\tau \right. \\ &\quad \left. + e^{-\frac{t-t_1}{\tau_1}}(u_v(\mathbf{x},t_1)+\gamma_1) - (\gamma_1 - \beta_0)\right]. \end{aligned}$$

Since at $t = t_1$, $u_v(\mathbf{x},t_1)$ is assumed in the $k(t_1)$-neighborhood of $-\eta$, thus $|u_v(\mathbf{x},t_1)| \leq \beta_0 + k(t_1)$. In the sequel

$$\begin{aligned} \dot{V} &\leq \sigma\rho\left[-e^{-\frac{t-t_1}{\tau_2}} k(t_1) - e^{-\frac{t}{\tau_2}}\frac{\gamma_2}{\tau_2}\int_{t_1}^{t} k_g|\sigma|^q e^{\frac{\tau}{\tau_2}} d\tau \right. \\ &\quad \left. + e^{-\frac{t-t_1}{\tau_1}}(\beta_0 + k(t_1) + \gamma_1) - (\gamma_1 - \beta_0)\right] \\ &\leq -\sigma\rho\left[(\gamma_1 - \beta_0) - (\beta_0 + k(t_1) + \gamma_1)e^{-\frac{t-t_1}{\tau_1}}\right]. \qquad (2.33) \end{aligned}$$

Note that V, hence σ, may undergo an increasing period from t_1 to t_2 when t_2 satisfying

$$\begin{aligned} &(\gamma_1 - \beta_0) - (\beta_0 + k(t_1) + \gamma_1)e^{-\frac{t_2-t_1}{\tau_1}} = 0 \\ &\Rightarrow\ t_2 = t_1 + \tau_1 \ln\frac{\beta_0 + k(t_1) + \gamma_1}{\gamma_1 - \beta_0} \end{aligned}$$

which is finite. For any $t > t_2$, the derivative of V is negative,

$$\begin{aligned} \dot{V} &\leq -\sigma\rho\left[(\gamma_1-\beta_0)-(\beta_0+k(t_1)+\gamma_1)e^{-\frac{t-t_2}{\tau_1}}\right]<0 \\ &\Rightarrow \\ \sigma(t)-\sigma(t_2) &\leq -|\rho|_{min}\left[(\gamma_1-\beta_0)(t-t_2)-\tau_1(\beta_0+k(t_1)+\gamma_1)(1-e^{-\frac{t-t_2}{\tau_1}})\right] \\ &\leq -|\rho|_{min}\left[(\gamma_1-\beta_0)(t-t_2)-\tau_1(\beta_0+k(t_1)+\gamma_1)\right]. \end{aligned} \tag{2.34}$$

Thus the maximum recovery time can be calculated according to (2.34) by letting $\sigma(t_3)=0$, which leads to $t_3 \leq\ t_2+\dfrac{\sigma(t_2)+\tau_1(\beta_0+k(t_1)+\gamma_1)}{(\gamma_1-\beta_0)|\rho|_{min}}$. It is immediately obvious that we need only to demonstrate that $|\sigma(t_2)|$ is finite, i.e. no finite escape time phenomenon occurs during the interval $[t_1,\ t_2]$ in which $\dot{V}$ may take positive value. Note that in (2.33), $\forall t \in [t_1,\ t_2]$, the derivative of $\sigma(t)$ satisfies

$$\dot{\sigma}(t) \leq \rho e^{-\frac{t-t_1}{\tau_1}}\left[\beta_0+k(t_1)+\gamma_1\right]. \tag{2.35}$$

Taking the integration on both side of (2.35), noting the fact that $\sigma(t_1)=0$ and $\rho_{max}=(D_{e_n}\sigma)\bar{b}$ is constant, we have

$$\begin{aligned} \int_{t_1}^{t}\dot{\sigma}(\tau)d\tau &\leq \int_{t_1}^{t}\rho e^{-\frac{\tau-t_1}{\tau_1}}\left[\beta_0+k(t_1)+\gamma_1\right]d\tau \\ \Rightarrow \sigma(t)-\sigma(t_1) &= \sigma(t)\leq\ \tau_1\rho_{max}\left[\beta_0+k(t_1)+\gamma_1\right]. \end{aligned} \tag{2.36}$$

Thus at time $t_2 \in (t_1, t_3]$, $t_3<\infty$, $\sigma(t_2)$ is finite.

Similarly, for $\sigma<0$, we can derive the same relationships (2.33) and (2.34), finite $\sigma(t_2)$ and consequently finite t_3, and the sliding motion recovery will be achieved at $t_3 \geq\ t_2$.

Remark 2.5. *The above conclusion shows that the proposed control scheme can be extended practically to disturbances of piecewise continuous nature, provided the discontinuous variations occur less frequently. Frequent occurences of disturbance surging essentially implies a very wide spectrum of frequencies in the disturbance, thereupon a wide spectrum in the equivalent control profile. In such a worst case*

control environment, the most effective way is to retain a high switching gain all the time, as the equivalent control can no longer be extracted by filtering techniques.

2.5 Illustrative Example

Consider a Van der Pol system with an additive disturbance η as shown in Fig.2.3. The dynamics of the system can be written as

$$LC\ddot{v} + L\frac{\partial h(v)}{\partial v}\dot{v} + 2v = u + \eta, \tag{2.37}$$

where $h(v) = -v + \frac{v^3}{3}$. Using the transformation $\frac{dv}{d\tau} = \sqrt{LC}\frac{dv}{dt}$ and $\frac{d^2v}{d\tau^2} = LC\frac{d^2v}{dt^2}$, (2.37) becomes

$$\ddot{v} - \mu(1 - v^2)\dot{v} + 2v = u + \eta, \tag{2.38}$$

where $\mu = \sqrt{\frac{L}{C}}$. In state space, (2.38) can be written as

$$\begin{cases} \dot{x}_1 = x_2 \\ \dot{x}_2 = -2x_1 + \mu(1 - x_1^2)x_2 + u + \eta, \end{cases} \tag{2.39}$$

where $\mu = 3$, $x_1(0) = 1.5$, $x_2(0) = 0$. The disturbance is $\eta = 10sin(5\pi t) + 5sin(2\sqrt{t+1})$. $\beta_0 = 15$ and $\beta_d = 50\pi + 5$. The system (2.39) is to track a model of oscillator - another Van der Pol equation

$$\begin{cases} \dot{x}_{1d}(t) = x_{2d}(t) \\ \dot{x}_{2d}(t) = -x_{1d}(t) + \mu_d(1 - x_{1d}^2)x_{2d}, \end{cases} \tag{2.40}$$

where $\mu_d = 1$, $x_{1d}(0) = 2$, $x_{2d}(0) = 1$. The switching surface is chosen to be $\sigma = e_1 + e_2 = (x_1 - x_{1d}) + (x_2 - \dot{x}_{1d})$.

The control law is

$$\begin{aligned} u_c &= -\left[x_2 - 2x_1 + \mu(1 - x_1^2)x_2 + x_{1d} - x_{2d} - \mu_d(1 - x_{1d}^2)x_{2d}\right] \\ u_s &= -sign(\sigma) \\ u &= u_c + k(t)u_s + u_v, \end{aligned} \tag{2.41}$$

where $u_v(t)$ and $k_s(t) = k(t)$, $\forall t \geq t_r$, are generated by the following filters

$$0.1\dot{u}_v + u_v = \gamma_1 u_s, \qquad 0.1\dot{k} + k = 25\sqrt{|\sigma|},$$

where γ_1 and $k(t_r)$ are selected according to Theorem 2.1. $\beta_k = 20 > \alpha\beta_0$ with $\alpha = 1.32 > 1$ and $t_r = 0.075$. In the simulation, the sampling period is 1 ms (sampling frequency of 1000 Hz).

In the following we mainly compare the new scheme with SMC schemes using a signum function and the SMC scheme with $LPF1$ only. Active SMC schemes, either adaptive type or learning type, are not suitable or not applicable in this particular case because the sole system perturbation $\eta(\mathbf{x}, t)$ is neither parametric nor periodic. The only prior information available in control design is its upper bound. On the other hand, if a problem is specifically catering to adaptive VSC schemes or learning VSC scheme, say either with constant parametric uncertainties or periodic disturbance, we should naturally adopt the most suitable control scheme instead of the proposed one, as the latter may not outperform the most suitable one. In this sense all SMC schemes, passive and active including the proposed one, are complementary to each others, depending on the types of system uncertainties and the availability of system knowledge.

Case 1: Conventional SMC Scheme and SMC Using $LPF1$ Only

The conventional sliding mode control incurs highly switching control signals, as shown in $Fig.2.4$, due to the large gain $k(t)$ used and the discontinuities of control signals crossing the sliding surface.

In (Utkin, 1992), the equivalent control signal is achieved by using a first-order filter $LPF1$ with infinite bandwidth in an open loop fashion. It is said that $LPF1$ output approaches the desired control signal as the time constant of the filter is getting smaller. In $Fig.2.5$, $LPF1$ is put in the closed-loop directly without gain reduction. In $Fig.2.5(a)$, the control profile is highly chattering due to the large

gain k. It is also shown in $Fig.2.5(b)$ that the filtered signal does not match the ideal equivalent control profile.

Case 2: SMC with Closed-Loop Filtering Architecture

Now let us check how does the new SMC work with filtering techniques. $Fig.2.6(a)$ demonstrates the appreciated results: chattering has been reduced to the minimum and the control profile dominated by a 5Hz component is consistent with that of exogenous disturbance. From $Fig.2.6(b)$, we can see that $LPF1$ estimates the disturbance almost perfectly except for the reaching phase. This is possible because the bandwidth of $\eta(\mathbf{x}, t)$ is approximately 5 Hz and that of $LPF1$ is 10 Hz. Consequently $u_v(\mathbf{x}, t)$ is able to compensate the most part of $-\eta(\mathbf{x}, t)$. $Fig.2.7(a)$ further confirms that the produced smooth control waveform is the desired equivalent control which achieves almost perfect tracking. $Fig.2.7(b)$ shows the fast attenuation of the switching gain $k(t)$ using $LPF2$. Due to imperfect factors in the sliding mode, such as limited sampling rate, the switching gain will not completely disappear. However, comparing with the initial value $k(0) = 35$, the effect of gain shaping is immediately obvious. Fig. 2.8 shows the system phase portrait of trajectory tracking under the new control scheme.

Finally let us consider the case with disturbance surging. The disturbance surging happens at time $t_1 = 2.3$ *sec*, where the disturbance changes from $\eta(\mathbf{x}, t_1^-) = 10sin(5\pi t) + 5sin(2\sqrt{t+1})$ to $\eta(\mathbf{x}, t_1^+) = 10sin(5\pi t + 0.5\pi) + 5sin(2\sqrt{t+1} + 0.5\pi)$, as shown in $Fig.2.9$. $Fig.2.10(a)$ shows that the sliding motion can be recovered within about 0.1 *sec*. At the same time, the gain $k(t)$ is automatically scaled up and down by $LPF2$ as shown in $Fig.2.10(b)$.

2.6 Conclusions

In this chapter, two low-pass filters incorporated in the closed loop are adopted into the sliding mode control to acquire equivalent control and shape the switching control gain in the presence of bounded system uncertainties. Based on the new concept of acquiring the equivalent control by gain shaping, the proposed control scheme achieves the following novel properties (1) system disturbances can be compensated quite accurately by the equivalent control approach; (2) the magnitude of the switching gain can be shaped to the very low level while the system retains in the sliding mode; (3) both the time domain and the frequency domain knowledge can be used in the filter design, hence achieving the desired tracking performance; (4) the new control scheme is easy to implement as only two extra simple first-order filters are employed.

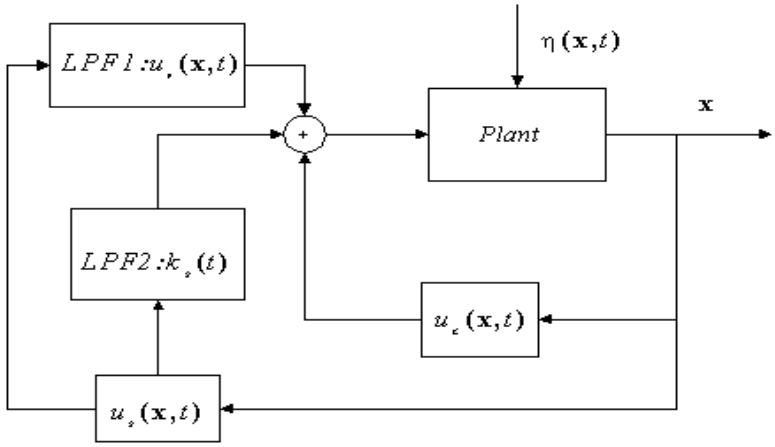

Figure 2.1. The Schematic Diagram of New Sliding Mode Controlled System

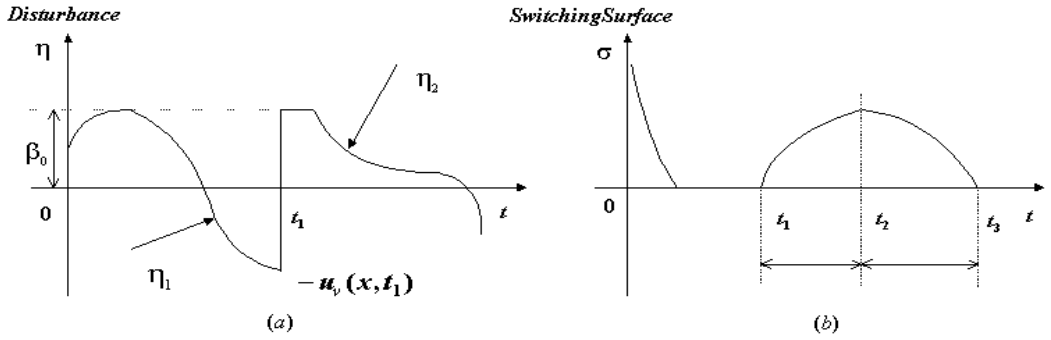

Figure 2.2. The variation of the disturbance and switching surface

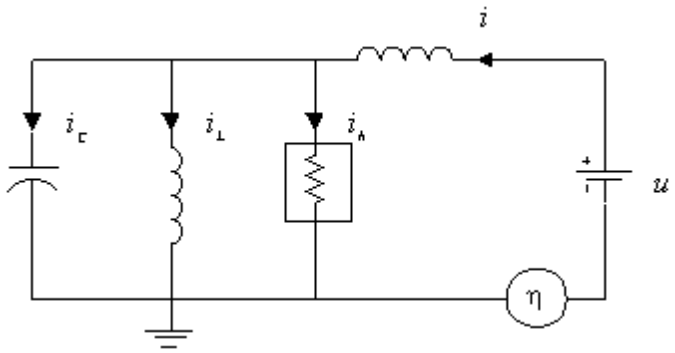

Figure 2.3. The Schematic Diagram of Van der Pol Circuit

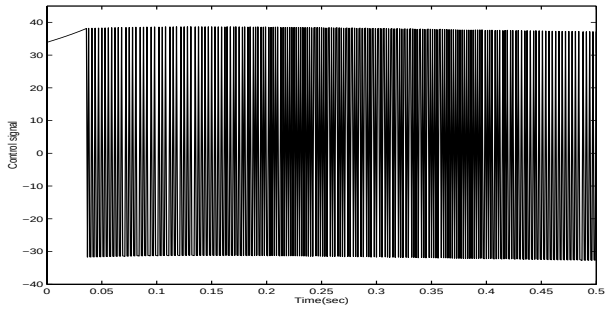

Figure 2.4. Control Signal Profile of the conventional SMC

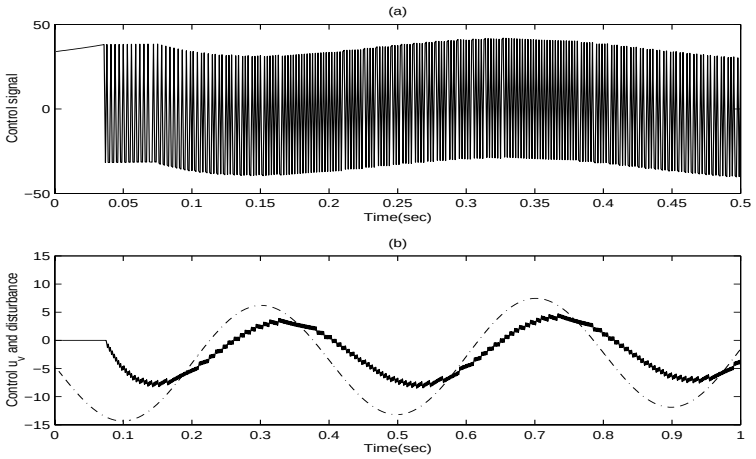

Figure 2.5. Control profiles in closed-loop without tuning the gain: (a) Control signal $u(t)$; (b) Solid line: filtered control term u_v; Dash-dotted line: the system disturbance $-\eta(\mathbf{x}, t)$

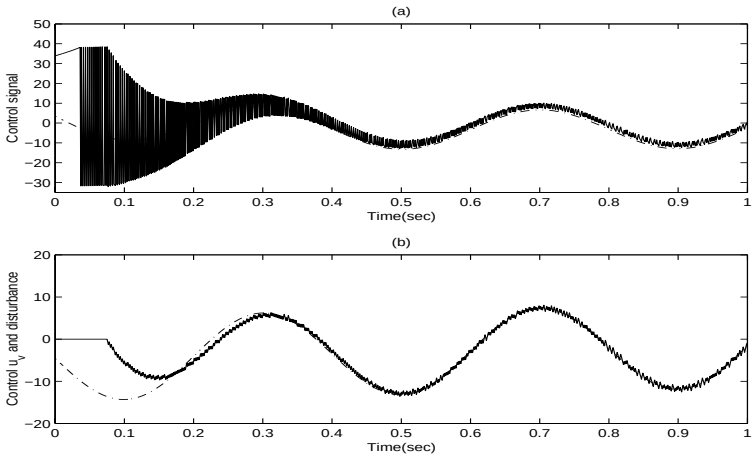

Figure 2.6. (a) Solid line: control profile $u = u_c + ku_s + u_v$; Dash-dotted line - equivalent control u_{eq}); (b) Solid line: filtered control term u_v; Dash-dotted line: disturbance $-\eta(\mathbf{x}, t)$

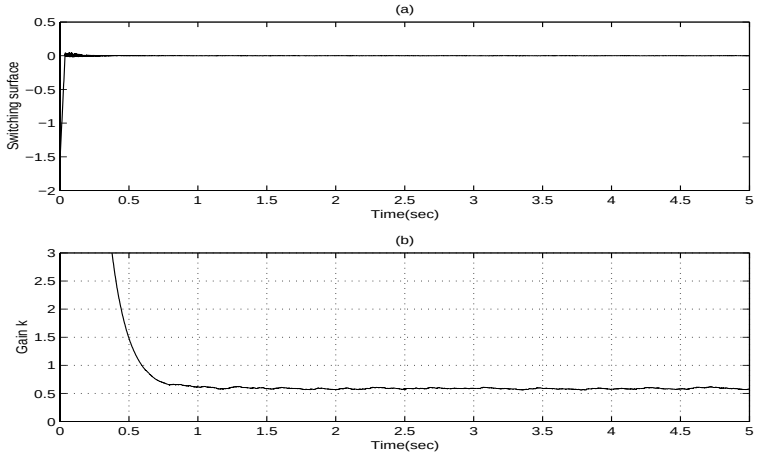

Figure 2.7. (a) Switching surface σ; (b) Gain shaping of switching gain $k(t)$

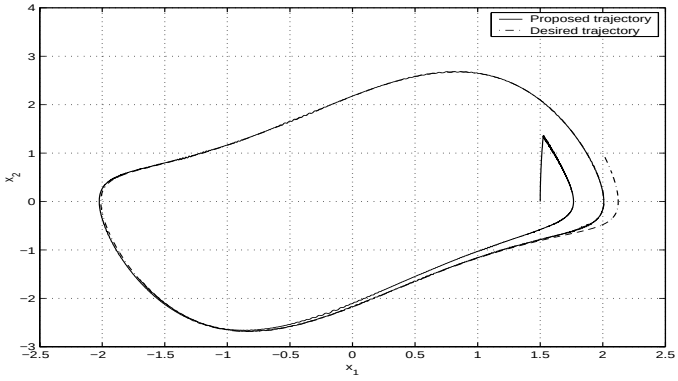

Figure 2.8. The phase portrait of the system

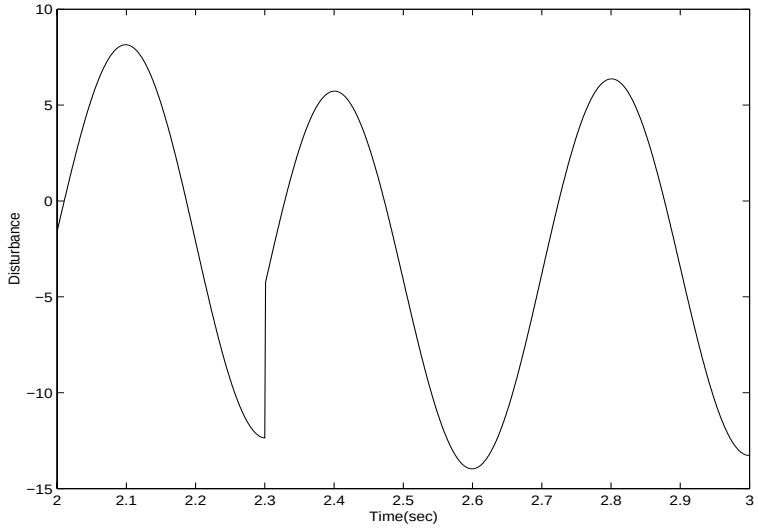

Figure 2.9. Disturbance surging at time $t = 2.3$ *sec*

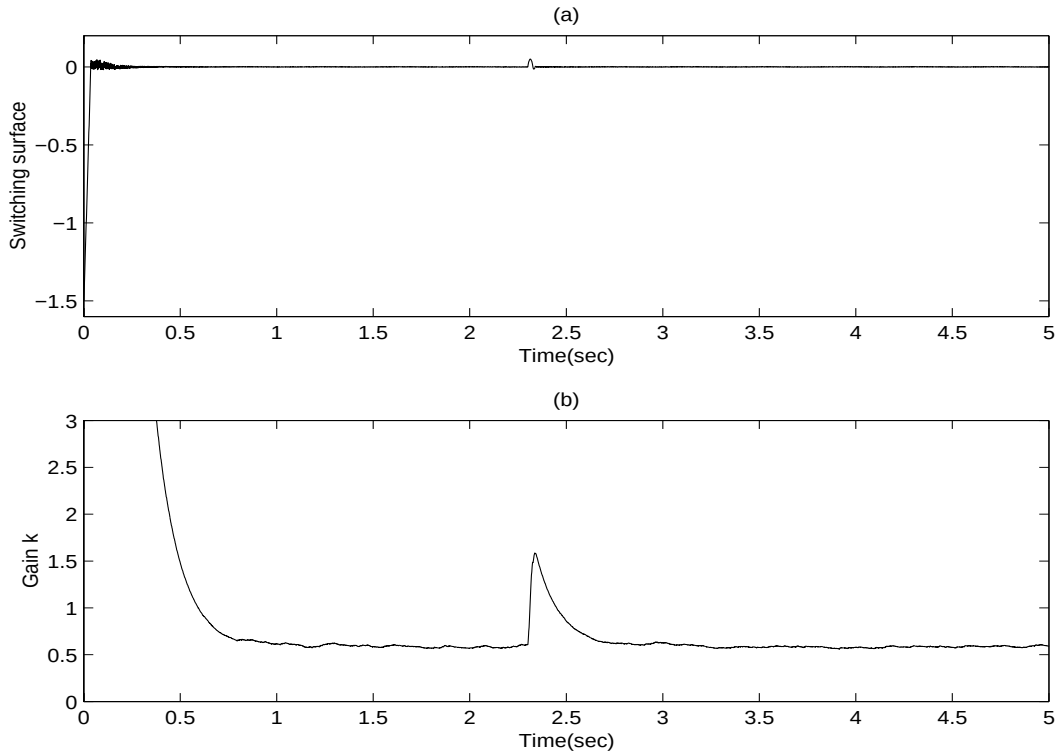

Figure 2.10. Evolution of the switching surface and gain with respect to disturbance surging: (a) Switching surface σ; (b) Gain $k(t)$

Chapter 3

On Nonlinear H^∞ Sliding Mode Control for a Class of Nonlinear Cascaded Systems

3.1 Introduction

Sliding mode control and H^∞ control are well recognized as two major robust control strategies. SMC can handle matched $L_\infty[0,\infty)$ type system disturbance where the upper-bound knowledge is available (Utkin, 1992). On the other hand, nonlinear H^∞ control can deal with $L_2[0,\infty)$ type unmatched disturbance even if the upper-bound knowledge is not available.

In this chapter, sliding mode control is incorporated with nonlinear H^∞ control for a class of cascaded nonlinear systems which consist of a null space dynamics and range space dynamics. A common practice in SMC is to design a switching surface according to the null space dynamics, which must ensure a stable sliding manifold when the system is in the sliding mode (Edwards and Spurgeon, 1998).

For known LTI systems, such design turns to be pole-placement (Zinober, 1994), (Chang and Chen, 2000) or LQR (Young and Ozguner, 1997). For known nonlinear systems, nonlinear optimal design can be applied (Xu and Zhang, 2002). However if there exist uncertaities in the null space nonlinear dynamics, switching surface design becomes extremely difficult. The challenge lies in that we need a systematic design which captures the inherent relationship between the switching surface and the sliding manifold, in the sequel yields a stable sliding manifold. Note that both switching surface and sliding manifold may be highly nonlinear in nature.

Nonlinear H^∞ control offers such a systematic design, which can allow even the presence of unmatched uncertainties of $L_2[0,\infty)$ type, and achieves a desired L_2 gain. The L_2 gain of a nonlinear system has been known to be an useful measure for stabilization and performance, e.g. the finite gain stability and H^∞ disturbance attenuation (Van der Schaft, 1991), (Van der Schaft, 1992). By applying the nonlinear H^∞ control to the null space dynamics, the resulting robust control law defines a suitable switching surface. The L_2 gain property is realized when the sliding mode occurs.

In SMC, designing a suitable reaching control law is as important as designing an appropriate switching surface. Traditionally this control law is to force the system to reach and then stay on the switching surface. Nevertheless, this feature alone is no longer sufficient when the unmatched null space uncertrainties are present. The null space nonlinear dynamics may diverge in a period shorter than the reaching time, if the L_2 gain property does not hold during the reaching phase. Obviously, L_2 gain property should be guaranteed not only for the sliding phase, but also for the reaching phase. This is achieved in the proposed control by again combining SMC and nonlinear H^∞ control.

This chapter is organized as follows. In Section 3.2, the problem is presented. In

Section 3.3, a nonlinear H^∞ switching surface is designed. Section 3.4 proposes a nonlinear H^∞ sliding mode control scheme. Two illustrative examples are given in Section 3.5 to show the effectiveness of the proposed scheme. Section 3.6 draws the conclusions.

3.2 Problem Formulation

Consider the following nonlinear cascaded system

$$\begin{cases} \dot{\mathbf{x}}_1 = \mathbf{f}_1(\mathbf{x}_1, t) + B_1(\mathbf{x}_1, t)\boldsymbol{\varphi}(\mathbf{x}_2) + C_1(\mathbf{x}_1, t)\boldsymbol{\eta}_1 \\ \dot{\mathbf{x}}_2 = \mathbf{f}_2(\mathbf{x}, t) + B_2(\mathbf{x}, t)\left[I + \triangle B_2(\mathbf{x}, t)\right]\left[\mathbf{u} + \boldsymbol{\eta}_2(\mathbf{x}, t)\right] \end{cases} \tag{3.1}$$

where $\mathbf{x} = [\mathbf{x}_1^T,\ \mathbf{x}_2^T]^T$ are physically measurable state vector, $\mathbf{x}_1 \in \mathcal{R}^n$ is the null space dynamics and $\mathbf{x}_2 \in \mathcal{R}^m$ is the range space dynamics, $\mathbf{u} \in \mathcal{R}^m$ denotes the control input, $\boldsymbol{\eta}_1 \in \mathcal{R}^l$ is the external disturbance and $\boldsymbol{\eta}_2 \in \mathcal{R}^m$ is the matched uncertainties. The mappings $\mathbf{f}_1 \in \mathcal{R}^n$, $\boldsymbol{\varphi} \in \mathcal{R}^m$, $\mathbf{f}_2 \in \mathcal{R}^m$, $B_1 \in \mathcal{R}^{n\times m}$, $C_1 \in \mathcal{R}^{n\times l}$ and $B_2 \in \mathcal{R}^{m\times m}$ are known and smooth with respect to $\mathbf{x}$ and continuous with respect to time t. $\triangle B_2 \in \mathcal{R}^{m\times m}$ represent the uncertainties in the control input. $D_{\mathbf{x}_2}\boldsymbol{\varphi} = \dfrac{\partial \boldsymbol{\varphi}}{\partial \mathbf{x}_2} \neq 0$ is bounded in $\mathcal{D} \subset \mathcal{R}^m \cap [0, \infty)$. The relation $m \leq\ n$ holds for the system.

In this chapter, the $\mathbf{x}_1$ subsystem in (3.1) is required to track the desired reference model

$$\dot{\mathbf{x}}_{1d} = \bar{\mathbf{f}}(\mathbf{x}_{1d}, \mathbf{r}(t), t), \tag{3.2}$$

where $\mathbf{r}(t)$ is a smooth reference input. Define $\mathbf{e}_1 = \mathbf{x}_1 - \mathbf{x}_{1d}$. The error dynamics of the $\mathbf{x}_1$ subsystem can be written as

$$\dot{\mathbf{e}}_1 \ = \ \mathbf{f}_1 + B_1\boldsymbol{\varphi} + C_1\boldsymbol{\eta}_1 - \dot{\mathbf{x}}_{1d} = \mathbf{f}_1 + B_1\boldsymbol{\varphi} + C_1\boldsymbol{\eta}_1 - \bar{\mathbf{f}} \tag{3.3}$$

The system (3.1) is assumed to satisfy the following assumptions.

Assumption 3.1. *The control input uncertainty satisfies*

$$\|\triangle B_2\| = \sqrt{\lambda_{max}(\triangle B_2^T \triangle B_2)} \leq \ \varepsilon_{b2}(\mathbf{x}, t),$$

where $0 \leq \ \varepsilon_{b2}(\mathbf{x}, t) < 1$ *is a positive function.*

Assumption 3.2. *The matched uncertainties in* $\mathbf{x}_2$ *subsystem are norm bounded by a known function, i.e.*

$$\|\boldsymbol{\eta}_2\| = \sqrt{\eta_{2,1}^2 + \cdots + \eta_{2,m}^2} \leq \ \phi_2(\mathbf{x}, t),$$

where $\phi_2(\mathbf{x}, t) \geq \ 0$ *is a known positive function.*

Assumption 3.3. *The matrix* $(D_{\mathbf{x}_2}\boldsymbol{\varphi})B_2$ *is of full rank.*

Assumption 3.4. *There exists a function* $\mathbf{g}_1(\cdot)$ *such that the system dynamics* $\dot{\boldsymbol{\xi}} = \mathbf{g}_1(\boldsymbol{\xi}, t)$ *is asymptotically stable. Then we can get the following equation*

$$\mathbf{f}_1(\mathbf{x}_1, t) - \bar{\mathbf{f}}(\mathbf{x}_{1d}, \mathbf{r}(t), t) = \mathbf{g}_1(\mathbf{e}_1, t) + B_1(\mathbf{x}_1, t)\boldsymbol{\zeta}(\mathbf{x}_1, \mathbf{x}_{1d}, \mathbf{r}(t), t),$$

where $\boldsymbol{\zeta}(\cdot)$ *is a smooth function with respect to its arguments.*

According Assumption 3.4 and the error dynamics (3.3), the system (3.1) with the control objective (3.2) can be written as

$$\dot{\mathbf{e}}_1 = \mathbf{g}_1 + B_1(\boldsymbol{\varphi} + \boldsymbol{\zeta}) + C_1\boldsymbol{\eta}_1 \tag{3.4}$$

$$\dot{\mathbf{x}}_2 = \mathbf{f}_2 + B_2(I + \triangle B_2)(\mathbf{u} + \boldsymbol{\eta}_2) \tag{3.5}$$

3.3 Nonlinear H^∞ Sliding Mode Design

The nonlinear H^∞ control aims to obtain a prespecified performance - disturbance attenuation from the external disturbance to the state variable, i.e. the robust L_2 gain ρ_1 from $\boldsymbol{\eta}_1$ to $\mathbf{e}_1$, as defined below

$$\int_0^t \|\mathbf{e}_1\|^2 d\tau \leq \ \beta_1(\mathbf{e}_1(0), 0) + \rho_1^2 \int_0^t \|\boldsymbol{\eta}_1\|^2 d\tau, \qquad \forall \boldsymbol{\eta}_1 \in L_2[0, t), \tag{3.6}$$

where $t \in [0, \infty)$ and $\beta_1(\mathbf{e}_1(0), 0)$ is a positive real valued function depending on the initial conditions.

For $\mathbf{e}_1$ subsystem, $\boldsymbol{\varphi}(\mathbf{x}_2)$ can be regarded as a virtual control input. If $C_1\boldsymbol{\eta}_1$ is absent from the null space dynamics (3.4), the switching surface design can be easily accomplished by choosing $\boldsymbol{\sigma} = \boldsymbol{\varphi}(\mathbf{x}_2) + \boldsymbol{\zeta}$. Once entering the sliding mode, $\boldsymbol{\sigma} = \boldsymbol{\varphi}(\mathbf{x}_2) + \boldsymbol{\zeta} = 0$. Then the error dynamics (3.4) becomes $\dot{\mathbf{e}}_1 = \mathbf{g}_1(\mathbf{e}_1, t)$, that is, the resulting sliding manifold is asymptotically stable and $\mathbf{e} \to 0$ as $t \to \infty$. If $C_1\boldsymbol{\eta}_1$ is present, $\boldsymbol{\sigma} = 0$ renders a sliding manifold

$$\dot{\mathbf{e}}_1 = \mathbf{g}_1 + C_1\boldsymbol{\eta}_1 \tag{3.7}$$

which in the worst case may go divergent due to the strong effect of the disturbance. Since $C_1\boldsymbol{\eta}_1$ could be unmatched, the best we can do is to limit its effect at a prescribed level through the entire reaching and sliding phases. The $L_2[0, \infty)$ nature of $\boldsymbol{\eta}_1$ implies that the effect of disturbance will disappear gradually, therefore the asymptotic convergence of $\mathbf{e}_1$ is still retained.

From L_2 gain property (3.6), we can see that nonlinear H^∞ control is a good candidate to reduce the disturbance effect.

Theorem 3.1. *The L_2 gain (3.6) is achieved for system (3.4) when the following nonlinear H^∞ sliding mode holds*

$$\boldsymbol{\sigma}(\mathbf{x}_1, \mathbf{x}_{1d}, \mathbf{x}_2, t) = \boldsymbol{\sigma}_1(\mathbf{x}_1, \mathbf{x}_{1d}, t) + \boldsymbol{\varphi}(\mathbf{x}_2) = 0, \tag{3.8}$$

$$\boldsymbol{\sigma}_1(\mathbf{x}_1, \mathbf{x}_{1d}, t) = \frac{1}{r_1(\mathbf{x}_1, \mathbf{x}_{1d}, t)} B_1^T (D_{\mathbf{e}_1} V_1)^T + \boldsymbol{\zeta}, \tag{3.9}$$

where $V_1(\mathbf{e}_1, t)$, $\forall \mathbf{e}_1 \in \mathcal{R}^n$ and $t \geq 0$ is a positive definite smooth solution of the following Hamilton-Jacobi inequality

$$\begin{aligned} &D_t V_1 + (D_{\mathbf{e}_1} V_1)\mathbf{g}_1 - (D_{\mathbf{e}_1} V_1)\frac{B_1 B_1^T}{r_1}(D_{\mathbf{e}_1} V_1^T) \\ &+ \frac{1}{4\rho_1^2}(D_{\mathbf{e}_1} V_1) C_1 C_1^T (D_{\mathbf{e}_1} V_1)^T + \mathbf{e}_1^T \mathbf{e}_1 \leq 0, \end{aligned} \tag{3.10}$$

with $r_1(\mathbf{x}_1, \mathbf{x}_{1d}, t) > 0$.

Proof: When in the sliding mode defined in (3.8), we have

$$\boldsymbol{\varphi} = -\frac{1}{r_1} B_1^T (D_{\mathbf{e}_1} V_1)^T - \boldsymbol{\zeta}$$

with V_1 the solution of the Hamilton-Jacobi inequality (3.10). Hence $\boldsymbol{\varphi}$ is a nonlinear H^∞ control law for (3.4) (Shen and Tamura, 1995).

In order to show the L_2 gain property, differentiating the smooth solution $V_1(\mathbf{e}_1, t)$

$$\begin{aligned}
\dot{V}_1 &= D_t V_1 + (D_{\mathbf{e}_1} V_1) \{\mathbf{g}_1 + B_1(\boldsymbol{\varphi} + \boldsymbol{\zeta}) + C_1 \boldsymbol{\eta}_1\} \\
&= D_t V_1 + (D_{\mathbf{e}_1} V_1)\mathbf{g}_1 + (D_{\mathbf{e}_1} V_1) C_1 \boldsymbol{\eta}_1 - (D_{\mathbf{e}_1} V_1) \frac{B_1 B_1^T}{r_1} (D_{\mathbf{e}_1} V_1)^T \\
&= (D_t V_1) + (D_{\mathbf{e}_1} V_1)\mathbf{g}_1 - (D_{\mathbf{e}_1} V_1) \frac{B_1 B_1^T}{r_1} (D_{\mathbf{e}_1} V_1)^T \\
&\quad + \rho_1^2 \boldsymbol{\eta}_1^T \boldsymbol{\eta}_1 + \frac{1}{4\rho_1^2} (D_{\mathbf{e}_1} V_1) C_1 C_1^T (D_{\mathbf{e}_1} V_1)^T - \| \frac{1}{2\rho_1} C_1^T (D_{\mathbf{e}_1} V_1)^T - \rho_1 \boldsymbol{\eta}_1 \|^2 \\
&\leq D_t V_1 + (D_{\mathbf{e}_1} V_1)\mathbf{g}_1 - (D_{\mathbf{e}_1} V_1) \frac{B_1 B_1^T}{r_1} (D_{\mathbf{e}_1} V_1)^T + \rho_1^2 \boldsymbol{\eta}_1^T \boldsymbol{\eta}_1 \\
&\quad + \frac{1}{4\rho_1^2} (D_{\mathbf{e}_1} V_1) C_1 C_1^T (D_{\mathbf{e}_1} V_1)^T. \qquad (3.11)
\end{aligned}$$

If V_1 is the smooth solution of the Hamilton-Jacobi inequality (3.10), then (3.11) becomes

$$\dot{V}_1(\mathbf{e}_1, t) \leq -\mathbf{e}_1^T \mathbf{e}_1 + \rho_1^2 \boldsymbol{\eta}_1^T \boldsymbol{\eta}_1. \qquad (3.12)$$

Integrating both sides of (3.12) from 0 to t yields

$$V_1(\mathbf{e}_1, t) - V_1(\mathbf{e}_1(0), 0) \leq -\int_0^t \|\mathbf{e}_1\|^2 d\tau + \rho_1^2 \int_0^t \|\boldsymbol{\eta}_1\|^2 d\tau. \qquad (3.13)$$

Because $V_1(\mathbf{e}_1, t) \geq 0$, we can achieve the following H^∞ performance from (3.13)

$$\int_0^t \|\mathbf{e}_1\|^2 d\tau \leq \beta_1(\mathbf{e}_1(0), 0) + \rho_1^2 \int_0^t \|\boldsymbol{\eta}_1\|^2 d\tau, \qquad (3.14)$$

where $\beta_1(\mathbf{e}_1(0), 0) = V_1(\mathbf{e}_1(0), 0)$.

3.4 Nonlinear H^∞ Sliding Mode Control Scheme

Traditionally, the SMC in range space is designed in such a way that the reaching condition is guaranteed. This requires a finite reaching time for the states $\mathbf{x}$ to

reach the switching surface $\boldsymbol{\sigma} = \mathbf{0}$, and stay on it afterwards. Often a quadratic function $V_0 = \frac{1}{2}\boldsymbol{\sigma}^T\boldsymbol{\sigma}$ is selected and the reaching control law is such designed that $\dot{V}_0 \leq -\|\boldsymbol{\sigma}\|$, consequently $\boldsymbol{\sigma}$ reaches zero in finite time.

It is worth to note that, in the above SMC design the behavior of the null space dynamics is rather uncertain during the reaching phase. Since $dim(\boldsymbol{\sigma}) = m < dim(\mathbf{x}) = n$, V_0 is not radially unbounded in $\mathbf{x}$, i.e. V_0 is not a Lyapunov function of $\mathbf{x}$. In general $\boldsymbol{\sigma} < \infty$ does not imply the boundedness of the system states $\mathbf{x}$, unless the system enters the designated stable sliding manifold. Will the null space dynamics produce a finite escape time during reaching phase? This will not happen when the null space dynamics is global Lipschitz continuous. A linear null space dynamics is global Lipschitz continuous, thus $\mathbf{x}_1$ would not escape to infinity in any finite time. However, we have to be cautious if there exist non-global Lipschitz continuous (NGLC) components in the null space dynamics. In (Xu and Zhang, 2002), a control Lyapunov function approach is proposed to ensure that the states $\mathbf{x}$ are bounded during the reaching phase. This approach however requires complete knowledge about the null space dynamics. What can we do if there are NGLC type nonlinearities as well as $L_\infty[0, \infty)$ type uncertainties in the null space subsystem?

Obviously, the SMC law has to take both NGLC and uncertain factors into consideration, so as to prevent the finite escape time phenomenon. In this section, we first show that, by incorporating the nonlinear H^∞ control into SMC, the L_2 gain property retains in the reaching phase. Next we prove that the system states are bounded for both reaching and sliding phase. Then we can derive the finite reaching time property for the system to reach the switching surface.

Theorem 3.2. *Consider the nonlinear uncertain system* (3.4) (3.5)*, the system achieves robust L_2 gain ρ_0 ($\rho_0 - \rho_1 > 0$) from $\boldsymbol{\eta}_1$ to $\mathbf{e}_1$ by the following sliding*

mode control law

$$\mathbf{u} = \mathbf{u}_c + \mathbf{u}_s, \tag{3.15}$$

$$\mathbf{u}_c = -\Gamma^{-1}\left[D_t\boldsymbol{\sigma}_1 + (D_{\mathbf{x}_{1d}}\boldsymbol{\sigma}_1)\dot{\mathbf{x}}_{1d} + S(\mathbf{f}_1 + B_1\boldsymbol{\varphi}) + D_{\mathbf{x}_2}\mathbf{f}_2 + \frac{SC_1C_1^TS^T\boldsymbol{\sigma}}{4\rho_m^2}\right], \tag{3.16}$$

$$\mathbf{u}_s = -\left(\frac{\psi}{1-\varepsilon_{b2}}\right)\frac{\Gamma^T\boldsymbol{\sigma}}{\|\Gamma^T\boldsymbol{\sigma}\|}, \tag{3.17}$$

where $S(\mathbf{x}_1, \mathbf{x}_{1d}, t) = D_{\mathbf{x}_1}\boldsymbol{\sigma}_1 \in \mathcal{R}^{m\times n}$, $\Gamma(\mathbf{x}, t) = (D_{\mathbf{x}_2}\boldsymbol{\varphi})B_2 \in \mathcal{R}^{m\times m}$, $\rho_m = \sqrt{\rho_0^2 - \rho_1^2}$, $\psi(\mathbf{x}, \mathbf{x}_{1d}, t) = \varepsilon_{b2}\|\mathbf{u}_c\| + (1+\varepsilon_{b2})\phi_2 + \delta$ *and* $\delta > 0$ *is a positive constant.*

Proof: We first construct a Lyapunov function

$$V(\mathbf{x}, \mathbf{x}_{1d}, t) = V_1(\mathbf{e}_1, t) + V_0(\boldsymbol{\sigma}) = V_1(\mathbf{e}_1, t) + \frac{1}{2}\boldsymbol{\sigma}^T\boldsymbol{\sigma} \geq 0. \tag{3.18}$$

Since $\mathbf{x}_{1d}$ is finite, it is easy to verify that V is radially unbounded in $\mathbf{x}$. Using the switching surface constructed in (3.8), (3.9), and under the control law (3.15)-(3.17), the derivative of V_0 is

$$\begin{aligned}
\dot{V}_0 &= \boldsymbol{\sigma}^T\dot{\boldsymbol{\sigma}} = \boldsymbol{\sigma}^T\left[D_t\boldsymbol{\sigma}_1 + (D_{\mathbf{x}_{1d}}\boldsymbol{\sigma}_1)\dot{\mathbf{x}}_{1d} + (D_{\mathbf{x}_1}\boldsymbol{\sigma}_1)\dot{\mathbf{x}}_1 + (D_{\mathbf{x}_2}\boldsymbol{\varphi})\dot{\mathbf{x}}_2\right] \\
&= \boldsymbol{\sigma}^T\left[D_t\boldsymbol{\sigma}_1 + (D_{\mathbf{x}_{1d}}\boldsymbol{\sigma}_1)\dot{\mathbf{x}}_{1d} + (D_{\mathbf{x}_1}\boldsymbol{\sigma}_1)(\mathbf{f}_1 + B_1\boldsymbol{\varphi})\right] \\
&\quad + \boldsymbol{\sigma}^T(D_{\mathbf{x}_2}\boldsymbol{\varphi})\left[\mathbf{f}_2 + B_2(I + \triangle B_2)(\mathbf{u} + \boldsymbol{\eta}_2)\right] + \boldsymbol{\sigma}^T(D_{\mathbf{x}_1}\boldsymbol{\sigma}_1)C_1\boldsymbol{\eta}_1 \\
&= \boldsymbol{\sigma}^T\left[D_t\boldsymbol{\sigma}_1 + (D_{\mathbf{x}_{1d}}\boldsymbol{\sigma}_1)\dot{\mathbf{x}}_{1d} + S(\mathbf{f}_1 + B_1\boldsymbol{\varphi}) + (D_{\mathbf{x}_2}\boldsymbol{\varphi})\mathbf{f}_2 + \Gamma\mathbf{u}_c\right] + \boldsymbol{\sigma}^TSC_1\boldsymbol{\eta}_1 \\
&\quad + \boldsymbol{\sigma}^T\Gamma\left[\triangle B_2\mathbf{u}_c + (I + \triangle B_2)(\mathbf{u}_s + \boldsymbol{\eta}_2)\right] \\
&= \boldsymbol{\sigma}^T\Gamma\left[\triangle B_2\mathbf{u}_c + (I + \triangle B_2)\boldsymbol{\eta}_2\right] + \boldsymbol{\sigma}^T\Gamma(I + \triangle B_2)\mathbf{u}_s \\
&\quad - \frac{1}{4\rho_m^2}\boldsymbol{\sigma}^TSC_1C_1^TS^T\boldsymbol{\sigma} + \boldsymbol{\sigma}^TSC_1\boldsymbol{\eta}_1 \\
&\leq \|\boldsymbol{\sigma}^T\Gamma\|\left[\varepsilon_{b2}\|\mathbf{u}_c\| + (1+\varepsilon_{b2})\phi_2\right] + \boldsymbol{\sigma}^T\Gamma(I + \triangle B_2)\mathbf{u}_s \\
&\quad - \frac{1}{4\rho_m^2}\boldsymbol{\sigma}^TSC_1C_1^TS^T\boldsymbol{\sigma} + \boldsymbol{\sigma}^TSC_1\boldsymbol{\eta}_1 \qquad (3.19) \\
&\leq -\delta\|\Gamma^T\boldsymbol{\sigma}\| - \frac{1}{4\rho_m^2}\boldsymbol{\sigma}^TSC_1C_1^TS^T\boldsymbol{\sigma} + \boldsymbol{\sigma}^TSC_1\boldsymbol{\eta}_1 \qquad (3.20)
\end{aligned}$$

$$
\begin{aligned}
&= -\delta\|\Gamma^T\boldsymbol{\sigma}\| - \frac{1}{4\rho_m^2}\boldsymbol{\sigma}^T SC_1C_1^T S^T\boldsymbol{\sigma} + \boldsymbol{\sigma}^T SC_1\boldsymbol{\eta}_1 - \rho_m^2\boldsymbol{\eta}_1^T\boldsymbol{\eta}_1 + \rho_m^2\boldsymbol{\eta}_1^T\boldsymbol{\eta}_1 \\
&= -\delta\|\Gamma^T\boldsymbol{\sigma}\| - (\frac{1}{2\rho_m}\boldsymbol{\sigma}^T SC_1 - \rho_m\boldsymbol{\eta}_1^T)(\frac{1}{2\rho_m}S^TC_1^T\boldsymbol{\sigma} - \rho_m\boldsymbol{\eta}_1) + \rho_m^2\boldsymbol{\eta}_1^T\boldsymbol{\eta}_1 \\
&\leq -\delta\|\Gamma^T\boldsymbol{\sigma}\| + \rho_m^2\boldsymbol{\eta}_1^T\boldsymbol{\eta}_1 \qquad (3.21)
\end{aligned}
$$

Using the result (3.12) and (3.21), the derivative of the constructed Lyapunov function V in (3.18) is

$$
\begin{aligned}
\dot{V} &= \dot{V}_1 + \boldsymbol{\sigma}^T\dot{\boldsymbol{\sigma}} \leq -\mathbf{e}_1^T\mathbf{e}_1 + \rho_1^2\boldsymbol{\eta}_1^T\boldsymbol{\eta}_1 - \delta\|\Gamma^T\boldsymbol{\sigma}\| + \rho_m^2\boldsymbol{\eta}_1^T\boldsymbol{\eta}_1 \\
&\leq -\mathbf{e}_1^T\mathbf{e}_1 + \rho_1^2\boldsymbol{\eta}_1^T\boldsymbol{\eta}_1 + (\rho_0^2 - \rho_1^2)\boldsymbol{\eta}_1^T\boldsymbol{\eta}_1 = -\mathbf{e}_1^T\mathbf{e}_1 + \rho_0^2\boldsymbol{\eta}_1^T\boldsymbol{\eta}_1 \qquad (3.22)
\end{aligned}
$$

Integrating both sides of (3.22), we have

$$
\begin{aligned}
-V(\mathbf{x}(0), \mathbf{x}_{1d}(0), 0) &\leq V(\mathbf{x}, \mathbf{x}_{1d}, t) - V(\mathbf{x}(0), \mathbf{x}_{1d}(0), 0) \\
&\leq -\int_0^t \|\mathbf{e}_1\|^2 d\tau + \rho_0^2\int_0^t \|\boldsymbol{\eta}_1\|^2 d\tau, \qquad (3.23) \\
\Rightarrow \int_0^t \|\mathbf{e}_1\|^2 d\tau &\leq \beta(\mathbf{x}(0), \mathbf{x}_{1d}(0), 0) + \rho_0^2\int_0^t \|\boldsymbol{\eta}_1\|^2 d\tau, \qquad (3.24)
\end{aligned}
$$

where $\beta(\mathbf{x}(0), \mathbf{x}_{1d}(0), 0) = V(\mathbf{x}(0), \mathbf{x}_{1d}(0), 0)$. Hence (3.24) holds throughout the entire tracking period, i.e. the H^∞ performance is achieved.

Remark 3.1. *In the nonlinear uncertain system* (3.4)*, if* $\mathbf{g}_1(\mathbf{e}_1, t)$ *can be expressed as* $G_1(\mathbf{e}_1, t)\mathbf{e}_1$*, when* $G_1(\mathbf{e}_1, t)$ *is a matrix-valued smooth function, then the HJB inequality can be simplified into the following differential Riccati inequality*

$$
\frac{1}{2}\dot{P} + \frac{1}{2}(PG_1 + G_1^TP) - P\left[\frac{B_1B_1^T}{r_1} - \frac{1}{4\rho_1^2}C_1C_1^T\right]P + I_{n\times n} \leq 0, \qquad (3.25)
$$

where $P(\mathbf{e}_1, t) \in \mathcal{R}^{n\times n}$ *is a symmetric positive definite smooth matrix. The* $\mathbf{e}_1$ *subsystem warrants a robust* L_2 *gain* ρ_1 *from* $\boldsymbol{\eta}_1$ *to* $\mathbf{e}_1$ *by the nonlinear control law*

$$
\boldsymbol{\varphi} = -\frac{1}{r_1}B_1^TP\mathbf{e}_1 - \boldsymbol{\zeta}, \qquad (3.26)
$$

which also specifies the switching surface as $\boldsymbol{\sigma}_1 = -\boldsymbol{\varphi}$*.*

As the second step, let us prove the boundedness of the system states, which is directly related to the uncertainty $\boldsymbol{\eta}_1$. The following *Corollary* considers two types of $\boldsymbol{\eta}_1$ commonly encountered in control problems.

Corollary 3.1. *With the proposed controller* (3.15) - (3.17)*:*

(*a*) *if* $\boldsymbol{\eta}_1 \in L_2[0,\infty)$*, all the system states are bounded;*

(*b*) *if* $\boldsymbol{\eta}_1 \in L_2[0,\infty) \cap L_\infty[0,\infty)$*,* $\lim_{t\to\infty} \mathbf{e}_1(t) = 0$ *and* $\mathbf{x}_2$ *is bounded.*

Proof: (*a*) If $\boldsymbol{\eta}_1 \in L_2[0,\infty)$, then $\int_0^t \|\boldsymbol{\eta}_1\|^2 d\tau \leq M_d$, where M_d is a finite constant. From (3.23),

$$V(\mathbf{x},\mathbf{x}_{1d},t) - V(\mathbf{x}(0),\mathbf{x}_{1d}(0),0) \leq -\int_0^t \|\mathbf{e}_1\|^2 d\tau + \rho_0^2 \int_0^t \|\boldsymbol{\eta}_1\|^2 d\tau, \quad (3.27)$$

$$\Rightarrow V(\mathbf{x},\mathbf{x}_{1d},t) \leq V(\mathbf{x}(0),\mathbf{x}_{1d}(0),0) + \rho_0^2 M_d. \quad (3.28)$$

Because $V(\mathbf{x},\mathbf{x}_{1d},t)$ is radially unbounded in $\mathbf{x}$, (3.28) means that $\mathbf{x}$ is bounded.

(*b*) If $\boldsymbol{\eta}_1 \in L_2[0,\infty) \cap L_\infty[0,\infty)$, then we have $\int_0^t \|\boldsymbol{\eta}_1\|^2 d\tau \leq M_d$ and $\|\boldsymbol{\eta}_1\| \leq \epsilon_d$, where ϵ_d is a constant. The inequality (3.22) becomes

$$\frac{dV(\mathbf{x},\mathbf{x}_{1d},t)}{dt} \leq -\|\mathbf{e}_1\|^2 + \rho_0^2\epsilon_d^2,$$

which shows that $\|\mathbf{e}_1\| \leq \rho_0\epsilon_d$ is bounded. Thus from the system dynamics (3.4), $\dot{\mathbf{e}}_1$ is bounded and as a result $\mathbf{e}_1$ is uniformly continuous. Note that in (3.24), $\int_0^t \|\mathbf{e}_1\|^2 d\tau$ is bounded because $\boldsymbol{\eta}_1 \in L_2[0,\infty)$. Using *Barbalat's Lemma* (Narendra and Annaswamy, 1989), it is straightforward to reach the conclusion that $\lim_{t\to\infty} \mathbf{e}_1(t) = 0$.

Now we are in a position to derive the finite reaching time property, which is indispensable in any SMC.

Theorem 3.3. *Under the sliding mode control law* (3.15)-(3.17)*, the system* (3.4) *can reach the switching surface* $\boldsymbol{\sigma} = \mathbf{0}$ *in finite time when* $\boldsymbol{\eta}_1 \in L_2[0,\infty)$*.*

Proof: From (3.20), the derivative of V_0 is

$$\begin{aligned} \dot{V}_0 = \boldsymbol{\sigma}^T\dot{\boldsymbol{\sigma}} &\leq -\delta\|\Gamma^T\boldsymbol{\sigma}\| + \boldsymbol{\sigma}^T SC_1\boldsymbol{\eta}_1 - \frac{1}{4\rho_m^2}\boldsymbol{\sigma}^T SC_1C_1^T S^T\boldsymbol{\sigma} \\ &\leq -\delta\|\Gamma^T\boldsymbol{\sigma}\| + \|\boldsymbol{\eta}_1\|\|SC_1\|\|\boldsymbol{\sigma}\| \end{aligned}$$

$$\begin{aligned} &\leq -\delta\underline{\mu}(\Gamma)\|\boldsymbol{\sigma}\| + \bar{\mu}(SC_1)\|\boldsymbol{\eta}_1\|\|\boldsymbol{\sigma}\| \\ \Rightarrow \frac{\boldsymbol{\sigma}^T\dot{\boldsymbol{\sigma}}}{\sqrt{\boldsymbol{\sigma}^T\boldsymbol{\sigma}}} &\leq -\delta\underline{\mu}(\Gamma) + \bar{\mu}(SC_1)\|\boldsymbol{\eta}_1\|, \end{aligned} \tag{3.29}$$

where $\bar{\mu}(A)$ and $\underline{\mu}(A)$ are the maximum and the minimum singular values of a matrix A. Note that $\boldsymbol{\eta}_1 \in L_2[0,\infty) \Rightarrow \int_0^\infty \|\boldsymbol{\eta}_1\|^2 d\tau < \infty$. Therefore $\forall \varepsilon_0 > 0$, $\exists t_0 > 0$, and $t_2 > t_1 > t_0$, such that $\int_{t_1}^{t_2} \|\boldsymbol{\eta}_1\|^2 d\tau < \varepsilon_0$. Using *Hölder inequality* (Lusternik and Sobolev, 1961),

$$\int_{t_1}^{t_2} \|\boldsymbol{\eta}_1\| \cdot 1 d\tau \leq \ (\int_{t_1}^{t_2} \|\boldsymbol{\eta}_1\|^2 d\tau)^{\frac{1}{2}} (\int_{t_1}^{t_2} 1 d\tau)^{\frac{1}{2}} < \sqrt{\varepsilon_0(t_2 - t_1)}. \tag{3.30}$$

From *Assumption* 3.3, Γ is of full rank. From *Corollary* 3.1, $\mathbf{x}$ is bounded. Hence there exist positive constants $\underline{\mu}_c \leq \underline{\mu}(\Gamma)$ and $\bar{\mu}_c \geq \bar{\mu}(SC_1)$. (3.29) becomes

$$\frac{\boldsymbol{\sigma}^T\dot{\boldsymbol{\sigma}}}{\sqrt{\boldsymbol{\sigma}^T\boldsymbol{\sigma}}} \leq -\delta\underline{\mu}_c + \bar{\mu}_c\|\boldsymbol{\eta}_1^T\|. \tag{3.31}$$

By integrating both sides of the inequality (3.31) and using (3.30),

$$\int_{t_1}^{t_2} \frac{\boldsymbol{\sigma}^T\dot{\boldsymbol{\sigma}}}{\sqrt{\boldsymbol{\sigma}^T\boldsymbol{\sigma}}} dt = \int_{t_1}^{t_2} \frac{\dot{V}_0}{\sqrt{2V_0}} dt \leq \ -\int_{t_1}^{t_2} \delta\underline{\mu}_c dt + \int_{t_1}^{t_2} \bar{\mu}_c\|\boldsymbol{\eta}_1\| dt$$

$$\begin{aligned} \sqrt{2V_0}\,|_{V_0(t_1)}^{V_0(t_2)} &= \sqrt{2V_0(t_2)} - \sqrt{2V_0(t_1)} \\ &< -\delta\underline{\mu}_c(t_2 - t_1) + \sqrt{\varepsilon_0}\bar{\mu}_c\sqrt{t_2 - t_1}. \end{aligned} \tag{3.32}$$

In the following part, it is shown that t_2 is finite such that sliding mode can be reached at time $t = t_2 > t_1$ which means that $V_0(t_2) = 0$. Denote $z = \sqrt{t_2 - t_1} > 0$, $q_0 = \delta\underline{\mu}_c > 0$, $q_1 = \sqrt{\varepsilon_0}\bar{\mu}_c > 0$ and $q_2 = \sqrt{2V_0(t_1)} > 0$. Let $V_0(t_2) = 0$, (3.32) can be rewritten as a linear quadratic inequality as

$$q_0 z^2 - q_1 z - q_2 < 0. \tag{3.33}$$

Solving the inequality (3.33), we have

$$0 < z = \sqrt{t_2 - t_1} < \frac{q_1 + \sqrt{q_1^2 + 4q_0q_2}}{2q_0} \quad \Rightarrow t_2 < t_1 + \left(\frac{q_1 + \sqrt{q_1^2 + 4q_0q_2}}{2q_0}\right)^2,$$

which shows that t_2 is finite.

Remark 3.2. *Due to the presence of unmatched disturbance of $L_2[0,\infty)$ type, it is not possible to specify the reaching time t_2.*

The unit vector control law $\mathbf{u}_s$ in (3.17) may incur chattering when the system reaches the sliding mode in finite time. In order to eliminate the chattering phenomenon, $\mathbf{u}_s$ is modified as below

$$\mathbf{u}_s = -\left(\frac{\psi}{1-\varepsilon_{b2}}\right)\frac{\Gamma^T\boldsymbol{\sigma}}{\|\Gamma^T\boldsymbol{\sigma}\|+\epsilon e^{-\nu t}}, \tag{3.34}$$

where ϵ and ν are positive constants. In the following *Corollary*, we show that the L_2 gain property is retained by the smoothing control law (3.34).

Corollary 3.2. *Consider the uncertain nonlinear system* (3.4) (3.5)*, with $\boldsymbol{\eta}_1 \in L_2[0,\infty)$, the controller in* (3.15)*,* (3.16) *and* (3.34) *guarantees that: a finite L_2 gain performance is achieved, all the variables are bounded. Moreover, if $\boldsymbol{\eta}_1 \in L_2[0,\infty)\cap L_\infty[0,\infty)$, the tracking error $\mathbf{e}_1$ converges to zero asymptotically.*

Proof: According to the proof in *Theorem* 3.2, from (3.19), using the smoothing control (3.34), the derivative of V_0 becomes

$$\begin{aligned}
\dot{V}_0 \;\leq\;& (\psi-\delta)\|\boldsymbol{\sigma}^T\Gamma\| - \boldsymbol{\sigma}^T\Gamma(I+\triangle B_2)\left(\frac{\psi}{1-\varepsilon_{b2}}\right)\frac{\Gamma^T\boldsymbol{\sigma}}{\|\Gamma^T\boldsymbol{\sigma}\|+\epsilon e^{-\nu t}} \\
& -\frac{1}{4\rho_m^2}\boldsymbol{\sigma}^T SC_1C_1^TS^T\boldsymbol{\sigma} + \boldsymbol{\sigma}^T SC_1\boldsymbol{\eta}_1 \\
\leq\;& \psi\|\boldsymbol{\sigma}^T\Gamma\| - \frac{\psi\|\Gamma^T\boldsymbol{\sigma}\|^2}{\|\Gamma^T\boldsymbol{\sigma}\|+\epsilon e^{-\nu t}} \\
& -(\frac{\boldsymbol{\sigma}^T SC_1}{2\rho_m} - \rho_m\boldsymbol{\eta}_1^T)(\frac{S^TC_1^T\boldsymbol{\sigma}}{2\rho_m} - \rho_m\boldsymbol{\eta}_1) + \rho_m^2\boldsymbol{\eta}_1^T\boldsymbol{\eta}_1 \\
\leq\;& \frac{\psi\|\Gamma^T\boldsymbol{\sigma}\|\epsilon e^{-\nu t}}{\psi\|\Gamma^T\boldsymbol{\sigma}\|+\epsilon e^{-\nu t}} + \rho_m^2\boldsymbol{\eta}_1^T\boldsymbol{\eta}_1 \leq\; \epsilon e^{-\nu t} + \rho_m^2\boldsymbol{\eta}_1^T\boldsymbol{\eta}_1.
\end{aligned} \tag{3.35}$$

Using (3.12) and (3.35), it is straightforward to get

$$\dot{V} \leq\; -\mathbf{e}_1^T\mathbf{e}_1 + \rho_1^2\boldsymbol{\eta}_1^T\boldsymbol{\eta}_1 + \epsilon e^{-\nu t} + \rho_m^2\boldsymbol{\eta}_1^T\boldsymbol{\eta} = -\mathbf{e}_1^T\mathbf{e}_1 + \rho_0^2\boldsymbol{\eta}_1^T\boldsymbol{\eta}_1 + \epsilon e^{-\nu t}. \tag{3.36}$$

By integrating both sides of (3.36), we have

$$V(\mathbf{x},\mathbf{x}_{1d},t) \;\leq\; V(\mathbf{x}(0),\mathbf{x}_{1d}(0),0) - \int_0^t \|\mathbf{e}_1\|^2 d\tau$$

$$+\rho_0^2 \int_0^t \|\boldsymbol{\eta}_1\|^2 d\tau + \frac{\epsilon}{\nu}(1 - e^{-\nu t}), \tag{3.37}$$

$$\Rightarrow \int_0^t \|\mathbf{e}_1\|^2 d\tau \leq \beta(\mathbf{x}(0), \mathbf{x}_{1d}(0), 0) + \rho_0^2 \int_0^t \|\boldsymbol{\eta}_1\|^2 d\tau + \frac{\epsilon}{\nu}(1 - e^{-\nu t}). \tag{3.38}$$

From the inequality (3.38), a finite L_2 gain performance is achieved. Moreover, as shown in *Corollary* 3.1, the inequality (3.37) implies that all the states of the system are bounded. If $\boldsymbol{\eta}_1 \in L_2[0,\infty) \cap L_\infty[0,\infty)$, we have $\lim_{t\to\infty} \mathbf{e}_1(t) = 0$.

3.5 Illustrative Examples

In this section, we present two examples. In the first example, it is shown that the proposed nonlinear H^∞ sliding mode control can be successfully applied to a nonlinear cascaded system with unmatched uncertainties. In the second example, the proposed method is compared with the suboptimal VSC method. It shows that the existence of NGLC terms in the null space dynamics may lead to divergence during the reaching phase if the control system does not possess the robust L_2 gain property for the entire tracking period.

A. Example 1

Consider a nonlinear uncertain cascaded system

$$\begin{cases} \dot{\mathbf{x}}_1 = \mathbf{f}_1(\mathbf{x}_1, t) + \mathbf{b}_1\varphi(x_2) + C_1(\mathbf{x}_1, t)\boldsymbol{\eta}_1 \\ \dot{x}_2 = f_2(\mathbf{x}, t) + b_2(\mathbf{x}, t)\left[1 + \triangle b_2(\mathbf{x}, t)\right]\left[u + \eta_2(\mathbf{x}, t)\right], \end{cases} \tag{3.39}$$

where

$$\mathbf{f}_1 = G_1 \cdot \mathbf{x}_1 = \begin{bmatrix} 0 & 1 \\ -2 & -4 \end{bmatrix} \begin{bmatrix} x_{11} \\ x_{12} \end{bmatrix}, \mathbf{b}_1 = \begin{bmatrix} 0 \\ 1 \end{bmatrix}, C_1 = \begin{bmatrix} cos(x_{12}) & sin(x_{12}) \\ sin(x_{11}) & cos(x_{11}) \end{bmatrix},$$

$$\boldsymbol{\eta}_1 = \left[e^{-0.1t}, -e^{-0.5t}\right]^T, \ f_2 = x_{11}sin(x_2), \ \triangle b_2 = 0.2cos(x_{12}), \ \eta_2 = sin(\pi t),$$

$$b_2 = 1, \ \varphi(x_2) = x_2, \ x_{11}(0) = x_{12}(0) = 0.5, \ x_2(0) = 0.2, \ \varepsilon_{b,2} = 0.2 \ and \ \phi_2 = 1.$$

The target trajectory is $x_{11d} = 0.2sin(\pi t)$ and $x_{12d} = \dot{x}_{11d} = 0.2\pi cos(\pi t)$. The error dynamics of $\mathbf{x}_1$ subsystem in (3.4) can be expressed as

$$\dot{\mathbf{e}}_1 = G_1\mathbf{e}_1 + \mathbf{b}_1\left[\varphi + \zeta(t)\right] + C_1\boldsymbol{\eta}_1,$$

where $\zeta(t) = -\dot{x}_{12d} - 2x_{11d} - 4x_{12d}$.

Case 1: $\rho_1 = 1.8$

In $\mathbf{x}_1$ subsystem, according to *Remark* 3.1, we first choose $V_1(\mathbf{e}_1, t) = \frac{1}{2}\mathbf{e}_1^T P\mathbf{e}_1$, where P is determined by the differential Riccati inequality (3.25). When $\dot{P} = 0$, $\rho_1 = 1.8$ and $r_1 = 0.1$, from the linear algebraic matrix inequality

$$\frac{1}{2}(PG_1 + G_1^T P) - P\left[\frac{\mathbf{b}_1\mathbf{b}_1^T}{r_1} - \frac{1}{4\rho_1^2}C_1C_1^T\right]P + I_{2\times 2} \leq 0, \tag{3.40}$$

and using the singular value of the matrix C_1, which is 2, we can get a symmetric positive definite smooth matrix $P = \begin{bmatrix} 5.4398 & 0.65719 \\ 0.65719 & 0.262 \end{bmatrix}$. Thus from (3.26), we have $\varphi(\mathbf{x}_1, \mathbf{x}_{1d}, t) = -\frac{1}{r_1}\mathbf{b}_1^T P\mathbf{e}_1 - \zeta(t)$. The switching surface is

$$\sigma = x_2 + \sigma_1 = x_2 - \varphi(\mathbf{x}_1, t) = x_2 + [0\ 10]\,P\mathbf{e}_1 - \zeta(t).$$

From *Theorem* 3.2, choose $\alpha = 1$, $\delta = 0.5$, $\rho_0 = 3.5$, $\rho_m = \sqrt{\rho_0^2 - \rho_1^2} = 3$ and $S = [0\ 10]\,P$, the system possesses the robust L_2 gain ρ_0 from $\boldsymbol{\eta}_1$ to $\mathbf{e}_1$ by the controller $u = u_c + u_s$, where

$$u_c = -\left\{D_t\sigma_1 + [0\ 10]\,P(\mathbf{f}_1 + \mathbf{b}_1 x_2) + f_2 + \frac{1}{4\rho_m^2}SC_1C_1^T S^T\sigma\right\}, \tag{3.41}$$

$$u_s = -\frac{\psi}{0.8}\cdot\frac{\sigma}{|\sigma| + e^{-0.1t}}, \quad \psi = 0.2|u_c| + 1.2. \tag{3.42}$$

Case 2: $\rho_1 = 3$

When $\rho_1 = 3$, according to the design procedure in *Case* 1, $\rho_m = \sqrt{\rho_0^2 - \rho_1^2} = 1.8$ and $P = \begin{bmatrix} 2.7095 & 0.2889 \\ 0.2889 & 0.21183 \end{bmatrix}$. The resulted control law has the same form as in (3.41) and (3.42).

In *Fig.*3.1, it is shown that the tracking error approaches zero asymptotically, i.e., $\lim_{t\to\infty} \mathbf{e}_1(t) = 0$. It is noted that the smaller the value ρ_1 (e.g. $\rho_1 = 1.8$), the better the transient performance in attenuating the effect of external disturbance in $\mathbf{x}_1$ subsystem. *Fig.*3.2 shows the integral of the error signal $\int_0^t \|\mathbf{e}_1\|^2 d\tau$. The desired H^∞ performance (3.6) has been achieved with the prescribed attenuation level ρ_1.

B. Example 2

To make comparisons with the suboptimal VSC method in (Xu and Zhang, 2001), the following cascaded system with matched uncertainties is considered

$$\begin{cases} \dot{\mathbf{x}}_1 = \mathbf{f}_1(\mathbf{x}_1, t) + B_1(\mathbf{x}_1, t)\boldsymbol{\varphi}(\mathbf{x}_2) + C_1(\mathbf{x}_1, t)\boldsymbol{\eta}_1 \\ \dot{\mathbf{x}}_2 = \mathbf{f}_2(\mathbf{x}, t) + B_2(\mathbf{x}, t)\left[I + \triangle B_2(\mathbf{x}, t)\right]\left[\mathbf{u} + \boldsymbol{\eta}_2(\mathbf{x}, t)\right] \end{cases} \tag{3.43}$$

where $\mathbf{f}_1$, $\boldsymbol{\eta}_1$, $\mathbf{x}_1(0)$ and $\varepsilon_{b,2}$ are the same as in example 1, $C_1 = diag(1 + x_{11}^2, 0.5)$, $\boldsymbol{\varphi}(\mathbf{x}_2) = \mathbf{x}_2$, $B_1 = B_2 = I_{2\times 2}$, $\mathbf{f}_2 = [x_{11}sin(x_{21}), x_{12}sin(x_{22})]^T$, $\boldsymbol{\eta}_2 = [sin(\pi t), cos(\pi t)]^T$, $\triangle B_2 = diag\left[0.2cos(x_{12}), 0.2sin(x_{21})\right]$, $\mathbf{x}_2(0) = [0.2, 0.2]^T$ and $\phi_2 = 1.5$.

The designed parameters of the proposed controller are $\rho_1 = 0.3$, $\rho_0 = 3.5$, $r_1 = \frac{4\rho_1^2}{(1+x_{11}^2)^2}$, $P = \begin{bmatrix} p_{11} & p_0 \\ p_0 & p_{22} \end{bmatrix}$, $p_0 = \frac{(-2+\sqrt{4+2\gamma})}{\gamma}$, $\gamma = \frac{(0.75 + 2x_{11}^2 + x_{11}^4)}{(2\rho_1^2)}$, $p_{11} = \gamma p_0 p_{22} + 4p_0 + 2p_{22}$ and $p_{22} = \frac{\left[-4+\sqrt{16+2\gamma(1+p_0)}\right]}{\gamma}$.

In the construction of the suboptimal VSC, the uncertainty $\boldsymbol{\eta}_1$ is not taken into consideration because its upbound is not available. According to (Xu and Zhang, 2001), the switching surface is $\boldsymbol{\sigma} = P_s\mathbf{e}_1 + \mathbf{x}_2 + \boldsymbol{\zeta}$, where $P_s = \begin{bmatrix} 0.774 & 0.098 \\ 0.098 & 0.146 \end{bmatrix}$ with $Q = R = I$ for the optimal control task $\inf_{\boldsymbol{\upsilon}(\cdot)} \int_0^\infty \left[\mathbf{e}_1^T Q \mathbf{e}_1 + \boldsymbol{\upsilon}^T R \boldsymbol{\upsilon}\right] dt$, and $\boldsymbol{\zeta} = [0,\ -\dot{x}_{12d} - 2x_{11d} - 4x_{12d}]^T$.

*Fig.*3.3 shows the tracking error and its integral of the proposed nonlinear H^∞ sliding mode controller. It is straightforward to see that the proposed control

scheme achieves asymptotic convergence. On the contrary, when applying the suboptimal VSC controller (Xu and Zhang, 2001), the system diverges as shown in *Fig*.3.4. This is due to the existence of the NGLC term $1 + x_{11}^2$ in C_1, which results in the finite escape time phenomenon.

3.6 Conclusions

By synthesizing sliding mode control and nonlinear H^∞ techniques, a novel nonlinear H^∞ sliding mode control scheme is developed for tracking control problems. Several fundamental issues of SMC have been explored in this work. First, by means of the nonlinear H^∞ method, a nonlinear switching surface is constructed, which ensures a stable sliding manifold even in the presence of unmatched uncertainties. Second, a new reaching control law in conjunction with a Lyapunov function is proposed to obtain the L_2 gain property for the entire tracking period, guarantee the resulting system behavior in the reaching phase. Third, the nature and effect of $L_2[0, \infty)$ and $L_\infty[0, \infty)$ type system uncertainties have been made clear. In the sequel appropriate control mechanisms can be devised to effectively attenuate or eliminate these influences.

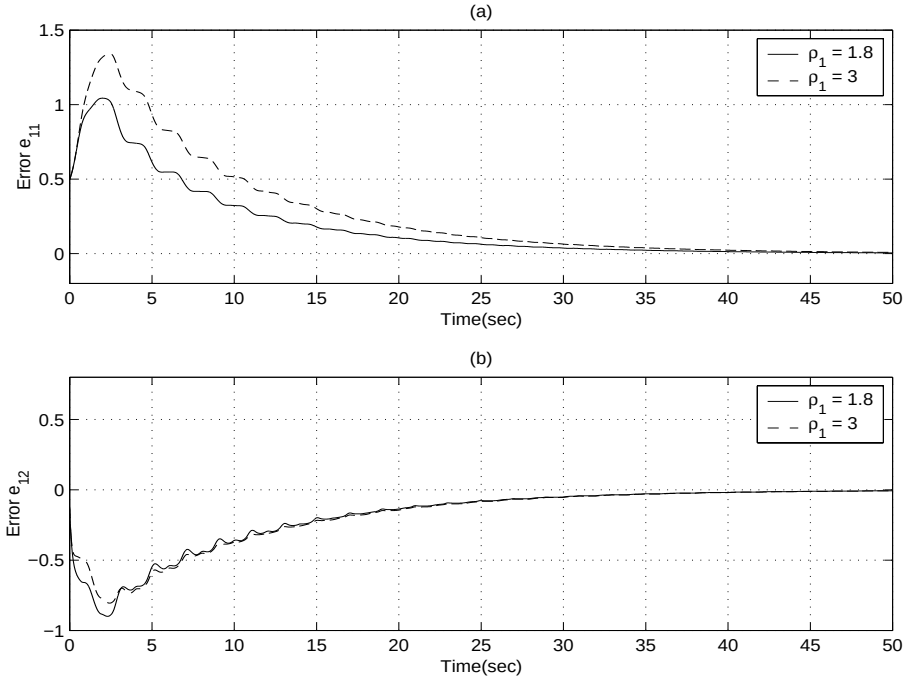

Figure 3.1. The evolution of the tracking error $\mathbf{e}_1$: (a) e_{11}; (b) e_{12} (Solid line - $\rho_1 = 1.8$; Dashed line - $\rho_1 = 3$).

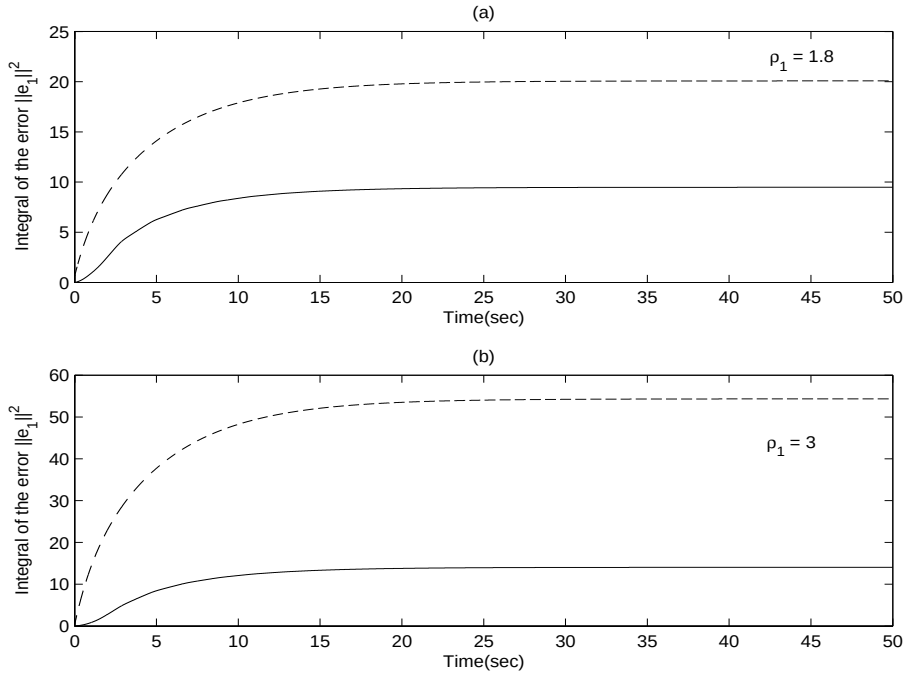

Figure 3.2. (a) Solid line - the integral $\int_0^t \|\mathbf{e}_1\|^2 d\tau$ when $\rho_1 = 1.8$, Dashed line - the term $\beta_1(\mathbf{e}_1(0), 0) + \rho_1^2 \int_0^t \|\boldsymbol{\eta}_1\|^2 d\tau$; (b) Solid line - the integral $\int_0^t \|\mathbf{e}_1\|^2 d\tau$ when $\rho_1 = 3$, Dashed line - the term $\beta_1(\mathbf{e}_1(0), 0) + \rho_1^2 \int_0^t \|\boldsymbol{\eta}_1\|^2 d\tau$.

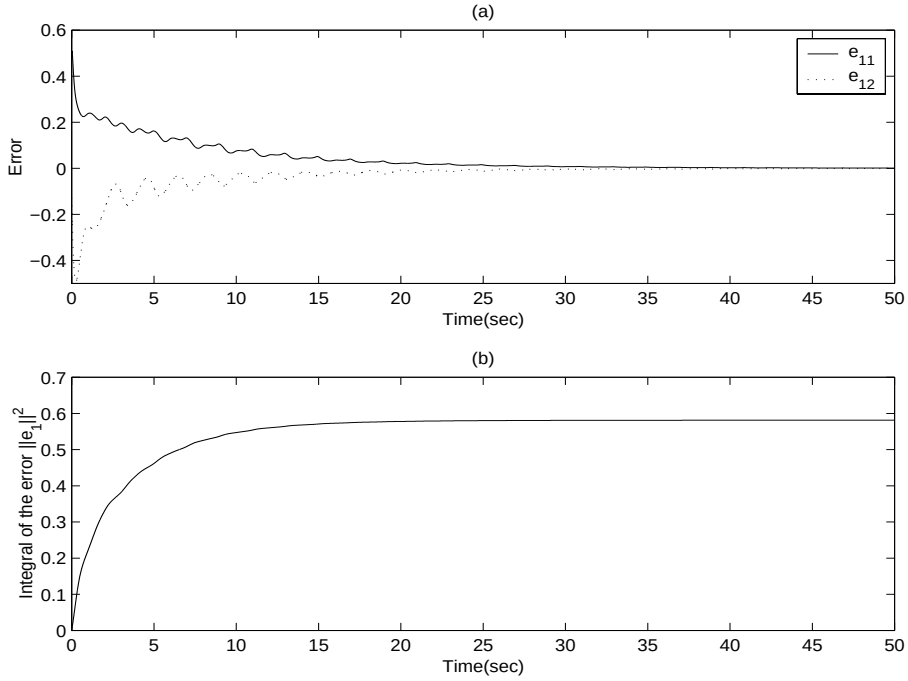

Figure 3.3. (a) The evolution of the tracking error $\mathbf{e}_1$ under the proposed controller; (b) The integral of the tracking error.

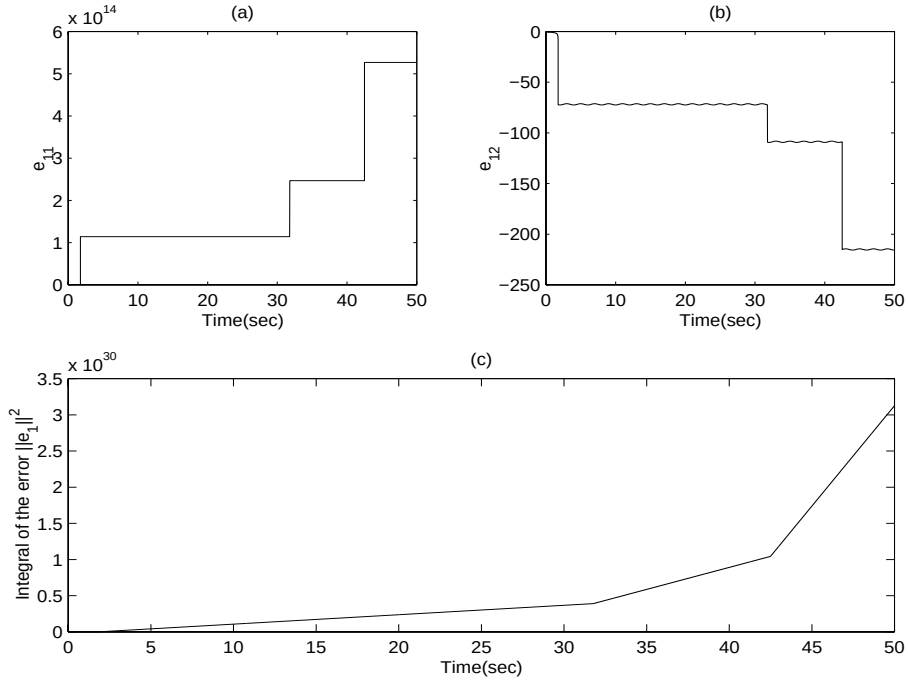

Figure 3.4. The performance under the conventional suboptimal VSC controller: (a) The evolution of the tracking error e_{11}; (b) The evolution of the tracking error e_{12}; (c) The integral $\int_0^t \|\mathbf{e}_1\|^2 d\tau$ of the tracking error $\mathbf{e}_1$.

Chapter 4

Analysis and Design of Integral Sliding Mode Control Based on Lyapunov's Direct Method

4.1 Introduction

The concept of integral sliding mode control (ISMC) has been proposed and defined in (Utkin and Shi, 1996). An integral sliding mode controller is constructed by incorporating an integral term in the switching surface. The main feature of the ISMC is that, when in sliding mode, the sliding manifold spans the entire state space. The main advantage of the ISMC, in the sequel, is the ability to directly design and specify the sliding manifold in the entire state space. This is achieved through the integral term, which provides a direct means for us to shape the sliding manifold based on the knowledge of the system nominal part (Chern *et al.*, 1996), (Wang *et al.*, 1996), (Ackermann and Utkin, 1998). An immediate consequence is that we can easily design a nonlinear ISMC to stabilize the sliding manifold in the

ideal closed-loop.

In this chapter, we concentrate on the ISMC design using Lyapunov's direct method, which offers a systematic way of handling various classes of system nonlinearities and uncertainties. The classical SMC design based on a quadratic form of the switching quantity, on the other hand, is inadequate as it does not span the entire state space in which the property of the sliding manifold is concerned. While a unit vector control is used to ensure the existence of the sliding mode (Edwards and Spurgeon, 1998), a nonlinear feedback based on the system nominal part enters the sliding manifold via the integral switching surface. The resulting sliding manifold, though highly nonlinear, is globally asymptotically stable in the presence of matched system uncertainties.

In this chapter we will in particular discuss the effect of two kinds of unmatched system uncertainties, which can be factorized into the product of a known nonlinear term and an unknown time varying term. When the time varying term is of L_∞, we demonstrate the stability of the sliding manifold, which in turn ensures the boundedness of the system states. When the time varying term is of $L_\infty \cap L_2$, we show the possibility of achieving asymptotic convergence via solving a Hamilton-Jacobien inequality.

The organization of this chapter is as follows. Section 4.2 gives the problem statement and the basic ISMC design. Section 4.3 discusses the disturbance attenuation property for two classes of unmatched uncertainties. Illustrative examples are given in Section 4.4.

4.2 Problem Statement and ISMC Design

A. Problem Statement

Consider the following nonlinear system with both matched and unmatched uncertainties

$$\dot{\mathbf{e}} = \mathbf{f}(\mathbf{e},t) + B(\mathbf{e},t)\left\{[I + \Delta B(\mathbf{e},t)]\,\mathbf{u}(t) + \boldsymbol{\eta}_m(\mathbf{e},t)\right\} + \boldsymbol{\eta}_u(\mathbf{e},t), \quad (4.1)$$

where $\mathbf{e} \in \mathcal{R}^n$ is a vector of physically measurable system representative variables e.g. the tracking errors, $\mathbf{u} \in \mathcal{R}^m$ is a vector of control inputs. $\mathbf{f} \in \mathcal{R}^n$ and $B \in \mathcal{R}^{n\times m}$ are known nonlinear vector-valued and matrix-valued functions. $\boldsymbol{\eta}_m \in \mathcal{R}^m$ and $\Delta B \in \mathcal{R}^{m\times m}$ represent the matched uncertainties, and $\boldsymbol{\eta}_u \in \mathcal{R}^n$ the unmatched uncertainties. All functions are continuous with respect to the arguments.

Assumption 4.1. *ΔB, $\boldsymbol{\eta}_m$ and $\boldsymbol{\eta}_u$ are bounded in Euclidean norm by known nonlinear functions as,*

$$\forall(\mathbf{e},t) \in \mathcal{R}^n \times \mathcal{R}^+, \quad \|\Delta B\| \le \beta_b(\mathbf{e},t) < 1, \quad \|\boldsymbol{\eta}_m\| \le \beta_m(\mathbf{e},t), \quad \|\boldsymbol{\eta}_u\| \le \beta_u(\mathbf{e},t).$$

Assumption 4.2. *The system nominal part of (4.1),*

$$\dot{\mathbf{e}}(t) = \mathbf{f}(\mathbf{e},t) + B(\mathbf{e},t)\mathbf{u}(t),$$

is globally asymptotically stabilizable via a nonlinear control $\mathbf{u} = \boldsymbol{\kappa}(\mathbf{e},t)$.

Remark 4.1. *In whatever control problems including SMC, the necessity for such a stabilizing control $\boldsymbol{\kappa}(\mathbf{e},t)$ is obvious.*

It is well known that Lyapunov's direct method provides a systematic way of handling various types of system nonlinearities and uncertainties (Qu, 1998). Thus we obtain the following property, which can be derived from Assumption 2 according to the converse theorems.

There is a nonempty set of *Lyapunov* Functions, $\mathcal{V}$, such that, for any choice of $\mathcal{C}^1$ function $V(\mathbf{e},t) \in \mathcal{V} : \mathcal{R}^n \times \mathcal{R}^+ \to \mathcal{R}^+$,

$$\begin{aligned} \gamma_1(\|\mathbf{e}\|) \le V(\mathbf{e},t) &\le \gamma_2(\|\mathbf{e}\|), \\ D_tV + (D_{\mathbf{e}}V)\left[\mathbf{f}(\mathbf{e},t) + B(\mathbf{e},t)\boldsymbol{\kappa}(\mathbf{e},t)\right] &\le -\gamma_3(\|\mathbf{e}\|) - \gamma_4(\mathbf{e},t), \end{aligned} \quad (4.2)$$

where $\gamma_1, \gamma_2 : \mathcal{R}^+ \to \mathcal{R}^+$ are class $\mathcal{K}_\infty$ functions, $\gamma_3 : \mathcal{R}^+ \to \mathcal{R}^+$ is a class $\mathcal{K}$ function and γ_4 is a nonnegative function.

In the literature of SMC (Yu and Man, 1998) (Chien and Fu, 1999) (Young and Ozguner, 1999), a typical *linear* sliding surface is $\boldsymbol{\sigma} = H\mathbf{e}(t)$, with $H \in \mathcal{R}^{m\times n}$ a constant matrix and $HB(\mathbf{e}, t)$ uniformly invertible. Using a quadratic function of the switching quantity $\boldsymbol{\sigma}$, for instance $V_0 = \frac{1}{2}\boldsymbol{\sigma}^T\boldsymbol{\sigma}$, we can easily derive a switching control law such that $\dot{V}_0 < -\alpha\|\boldsymbol{\sigma}\|$ where $\alpha > 0$, and $\boldsymbol{\sigma} = 0$ can be reached in finite time. However, $\boldsymbol{\sigma} = 0$ does not warrant a stable $\mathbf{e}$, unless the resulting sliding manifold is stable. Using the equivalent control technique we can derive the sliding manifold, in this case, is

$$\dot{\mathbf{e}} = [I - B(HB)^{-1}H](\mathbf{f} + \boldsymbol{\eta}_u). \tag{4.3}$$

Even without considering $\boldsymbol{\eta}_u$, it would be a very hard problem to justify the stability property of the sliding manifold (4.3), due to the highly nonlinear factors in B, $(HB)^{-1}$ and $\mathbf{f}$. It is an even harder problem in designing H so as to stabilize the nonlinear dynamics (4.3). Often the nonlinear sliding manifold is not stabilizable by a constant matrix H. Since the ultimate objective is to stabilize $\mathbf{e}$ in the entire state space, ISMC provides a means for us to directly design the sliding manifold.

B. Integral Sliding Mode Control Design

A *nonlinear* integral-type switching surface is constructed as follows

$$\boldsymbol{\sigma}(\mathbf{e}, t) = H\mathbf{e}(t) - H\mathbf{e}(0) - \int_0^t H\left[\mathbf{f}(\mathbf{e}, \tau) + B(\mathbf{e}, \tau)\boldsymbol{\kappa}(\mathbf{e}, \tau)\right] d\tau. \tag{4.4}$$

A unit vector SMC law is designed as

$$\begin{aligned} \mathbf{u}(t) &= \boldsymbol{\kappa}(\mathbf{e}, t) + \mathbf{u}_s \\ \mathbf{u}_s &= \begin{cases} -\beta(\mathbf{e}, t)\frac{(HB)^T\boldsymbol{\sigma}}{\|(HB)^T\boldsymbol{\sigma}\|}, & \boldsymbol{\sigma} \neq \mathbf{0}, \\ \mathbf{0}, & \boldsymbol{\sigma} = \mathbf{0}, \end{cases} \end{aligned} \tag{4.5}$$

where

$$\beta(\mathbf{e},t) \geq \frac{1}{1-\beta_b(\mathbf{e},t)}\left\{\beta_b(\mathbf{e},t)\|\boldsymbol{\kappa}(\mathbf{e},t)\| + \beta_m(\mathbf{e},t) + \|(HB)^{-1}H\|\beta_u(\mathbf{e},t) + \alpha\right\},$$

and α is a positive constant.

Let us first show the attractiveness of the switching surface $\boldsymbol{\sigma} = \mathbf{0}$ under the SMC law (4.5). Differentiating $\boldsymbol{\sigma}$ in (4.4) yields

$$\begin{aligned}\dot{\boldsymbol{\sigma}} &= H\dot{\mathbf{e}} - H\mathbf{f} - HB\boldsymbol{\kappa} \\ &= H[\mathbf{f} + B(I+\Delta B)(\boldsymbol{\kappa}+\mathbf{u}_s) + B\boldsymbol{\eta}_m + \boldsymbol{\eta}_u] - H\mathbf{f} - HB\boldsymbol{\kappa} \\ &= HB(I+\Delta B)\mathbf{u}_s + HB\Delta B\boldsymbol{\kappa} + HB\boldsymbol{\eta}_m + H\boldsymbol{\eta}_u. \end{aligned} \tag{4.6}$$

Now choose the quadratic function $V_0 = \frac{1}{2}\boldsymbol{\sigma}^T\boldsymbol{\sigma}$. Under the SMC law (4.5), Assumption 4.1 and expression (4.6), when $\boldsymbol{\sigma} \neq 0$, the derivative of V_0 is

$$\begin{aligned}\dot{V}_0 &= \boldsymbol{\sigma}^T\dot{\boldsymbol{\sigma}} = \boldsymbol{\sigma}^T HB\left[(I+\Delta B)\mathbf{u}_s + \Delta B\boldsymbol{\kappa} + \boldsymbol{\eta}_m + (HB)^{-1}H\boldsymbol{\eta}_u\right] \\ &= \boldsymbol{\sigma}^T HB\left[-\beta\frac{(HB)^T\boldsymbol{\sigma}}{\|(HB)^T\boldsymbol{\sigma}\|} - \Delta B\beta\frac{(HB)^T\boldsymbol{\sigma}}{\|(HB)^T\boldsymbol{\sigma}\|} + \Delta B\boldsymbol{\kappa} + \boldsymbol{\eta}_m + (HB)^{-1}H\boldsymbol{\eta}_u\right] \\ &\leq -\left[(1-\beta_b)\beta - \beta_b\|\boldsymbol{\kappa}\| - \beta_m - \|(HB)^{-1}H\|\beta_u\right]\|(HB)^T\boldsymbol{\sigma}\| \\ &\leq -\alpha\|(HB)^T\boldsymbol{\sigma}\|. \end{aligned}$$

This shows that the system will reach the switching surface in finite time and remain on it. On the other hand, from (4.4) we can see the zero initial value $\boldsymbol{\sigma}(t) = \mathbf{0}$ at $t = 0$. Therefore the sliding mode exists $\forall t \geq 0$.

Next we derive the sliding manifold. When the system is in the sliding mode, $\mathbf{u} = \mathbf{u}_{eq}$ and the equivalent control input $\mathbf{u}_{eq}$ can be obtained from $\dot{\boldsymbol{\sigma}} = 0$. Substituting $\mathbf{u}_{eq}$ into (4.1), the sliding manifold is

$$\dot{\mathbf{e}}(t) = \mathbf{f}(\mathbf{e},t) + B(\mathbf{e},t)\boldsymbol{\kappa}(\mathbf{e},t) + \left\{I - B(\mathbf{e},t)[HB(\mathbf{e},t)]^{-1}H\right\}\boldsymbol{\eta}_u(\mathbf{e},t). \tag{4.7}$$

Comparing the integral sliding manifold (4.7) with the conventional one (4.3), we can clearly see the similarities and difference. Both are able to reject the matched

uncertainty $\boldsymbol{\eta}_m$ perfectly, and both are perturbed by the unmatched uncertainty $\boldsymbol{\eta}_u$ through $I - B(HB)^{-1}H$. The major difference is, the ISMC generates a stabilizing control component $\mathbf{f} + B\boldsymbol{\kappa}$, which can be designed based on the system nominal part and the Lyapunov's direct method. Moreover, H can be selected separately to minimize the nonlinear term $I - B(HB)^{-1}H$, thereafter minimize the effect from $\boldsymbol{\eta}_u$. On the contrary, in (4.3) we can only rely on H to suppress the unmatched uncertainty, the effect is rather limited. The selection or design of H is in general a difficult task even for linear systems.

From Assumption 2 or the property (4.2), we can discuss the tracking performance in terms of the sliding manifold (4.7). If $\boldsymbol{\eta}_u(\mathbf{e}, t)$ is a lumped uncertainty with the bounding function $\beta_u(\mathbf{e}, t)$ as the only *a priori* knowledge, we can only draw boundedness conclusions about the tracking error $\mathbf{e}$, as shown below. Note that

$$\begin{aligned} \dot{V}(\mathbf{e}, t) &= D_t V + (D_{\mathbf{e}} V)(\mathbf{f} + B\boldsymbol{\kappa}) + (D_{\mathbf{e}} V)[I - B(HB)^{-1}H]\boldsymbol{\eta}_u \\ &\leq -\gamma_3(\|\mathbf{e}\|) - \gamma_4(\mathbf{e}, t) + \beta_a(\mathbf{e}, t), \end{aligned} \tag{4.8}$$

where $\beta_a = \|D_{\mathbf{e}} V[I - B(HB)^{-1}H]\|\beta_u$. From (4.8), the boundedness of the closed loop system is determined by the nature and size of the unmatched uncertainties, equivalently, the function $\beta_a(\mathbf{e}, t)$. The closed-loop dynamics in the sliding manifold (4.7) is:

(a) globally asymptotically stable if

$$\beta_a(\mathbf{e}, t) < \gamma_3(\|\mathbf{e}\|) + \gamma_4(\mathbf{e}, t),\ \forall (\mathbf{e}, t) \in (\mathcal{R}^n \times \mathcal{R}^+) \cap (\mathbf{e} \neq \mathbf{0});$$

(b) globally uniformly ultimately bounded if

$$\lim_{r \to \infty} \sup_{\|\mathbf{e}\| \geq r} \sup_{t \geq t_0} \left[\gamma_3(\|\mathbf{e}\|) + \gamma_4(\mathbf{e}, t)\right] / \beta_a(\mathbf{e}, t) > 1\ ;$$

(c) locally uniformly ultimately bounded if

$$\gamma_3(\|\mathbf{e}\|) + \gamma_4(\mathbf{e}, t) > \beta_a(\mathbf{e}, t),\ \forall (\mathbf{e}, t) \in (\mathcal{R}^n \times \mathcal{R}^+) \cap (\eta_1 < \|\mathbf{e}\| < \eta_2)$$

where $\gamma_1(\eta_2) > \gamma_2(\eta_1)$ to ensure $V(\eta_1) < V(\eta_2)$ so as to be consistent with $\dot{V}(\mathbf{e}, t) < 0,\ \forall(\mathbf{e}, t) \in (\mathcal{R}^n \times \mathcal{R}^+) \cap (\eta_1 < \|\mathbf{e}\| < \eta_2)$.

Remark 4.2. *If $\boldsymbol{\eta}_u = 0$, the sliding manifold (4.7) becomes $\dot{\mathbf{e}} = \mathbf{f} + B\boldsymbol{\kappa}$, which is asymptotically stable. However, when under the linear sliding surface $\boldsymbol{\sigma} = H\mathbf{e}$, the sliding manifold is $\dot{\mathbf{e}} = [I - B(HB)^{-1}H]\,\mathbf{f}$, which can hardly be designed to ensure an asymptotically stable sliding manifold.*

Remark 4.3. *In addition, the system nominal part $\dot{\mathbf{e}} = \mathbf{f} + B\boldsymbol{\kappa}$ can also be designed to meet various control specifications, such as pole-placement or LQR for linear cases, and nonlinear/inverse optimality for nonlinear cases, etc.*

4.3 On Unmatched Disturbance Attenuation

From the result of (4.8), we can observe one problem in the integral SMC design, that the known function $D_{\mathbf{e}}V[I - B(HB)^{-1}H]$ has been treated as a gain of the unmatched perturbation. This may give rise to a new problem, that the class $\mathcal{K}$ function γ_3 may not be able to suppress β_a due to the term $D_{\mathbf{e}}V[I - B(HB)^{-1}H]$. For instance, if a quadratic Lyapunov function $V(\mathbf{e})$ is selected, which is very common in nonlinear control system design, then $\|D_{\mathbf{e}}V\|$ is a class $\mathcal{K}_\infty$ function instead of a class $\mathcal{K}$ function. On the other hand, the system knowledge regarding $D_{\mathbf{e}}V[I - B(HB)^{-1}H]$ is not fully taken into consideration in the above control design.

In the literature of H^2/H^∞, in particular the nonlinear H^∞ control, attention has been paid to the more detailed classification of the system uncertainties, whether matched or unmatched. With the availability of more knowledge on the system uncetrainties, more appropriate controllers can be designed to achieve better control performance. Analogously, here we will specify the types of unmatched uncertain-

ties and look for more appropriate integral SMC. Assume that the unmatched uncertainties $\boldsymbol{\eta}_u$ can be separated into two terms, $\boldsymbol{\eta}_u = E(\mathbf{e})\mathbf{w}(t)$, where $E(\cdot) \in \mathcal{R}^{n\times l}$ is a known matrix valued function of the states, and $\mathbf{w}(\cdot) \in \mathcal{R}^l$ is either $L_\infty[0,\infty)$ or $L_2[0,\infty) \cap L_\infty[0,\infty)$ with known bounds.

In such circumstance, the sliding manifold (4.7) can be written as

$$\dot{\mathbf{e}}(t) = \mathbf{f}(\mathbf{e},t) + B(\mathbf{e},t)\boldsymbol{\kappa}(\mathbf{e},t) + N(\mathbf{e},t)\mathbf{w}(t) \tag{4.9}$$

where $N(\mathbf{e},t) = [I - B(HB)^{-1}H]E$. Now we are able to give a concrete design of the nominal control law $\boldsymbol{\kappa}$, which incorporates all the available system knowledge.

Theorem 4.1. *Choose a class $\mathcal{K}$ function γ_3, and let*

$$\gamma_4(\mathbf{e},t) = \frac{1}{4\rho^2}(D_{\mathbf{e}}V)NN^T(D_{\mathbf{e}}V)^T,$$

where ρ is a constant. For the sliding manifold (4.9), the nominal control $\boldsymbol{\kappa}$ is designed as a nonlinear feedback law

$$\boldsymbol{\kappa} = -\frac{1}{r}B^T(D_{\mathbf{e}}V)^T, \qquad r(\mathbf{e},t) > 0. \tag{4.10}$$

Here $r(\mathbf{e},t)$ and ρ are chosen to satisfy the following Hamilton-Jacobien inequality

$$D_tV + (D_{\mathbf{e}}V)\mathbf{f} - (D_{\mathbf{e}}V)\frac{BB^T}{r}(D_{\mathbf{e}}V)^T + \gamma_3(\|\mathbf{e}\|) + \gamma_4(\mathbf{e},t) \leq\ 0. \tag{4.11}$$

Under the control (4.10), we have the following properties.

(1) $\forall \mathbf{w} \in L_\infty[0,\infty)$, *the sliding manifold* (4.9) *is uniformly bounded;*

(2) $\forall \mathbf{w} \in L_2[0,\infty) \cap L_\infty[0,\infty)$, *the sliding manifold* (4.9) *is asymptotically stable, i.e.* $\lim_{t\to\infty} \mathbf{e}(t) = 0$.

Proof: Under the feedback controller (4.10), we have

$$\begin{aligned}
\dot{V}(\mathbf{e},t) &= D_tV + (D_{\mathbf{e}}V)(\mathbf{f} + B\boldsymbol{\kappa}) + (D_{\mathbf{e}}V)N\mathbf{w} \\
&= D_tV + (D_{\mathbf{e}}V)\mathbf{f} - (D_{\mathbf{e}}V)\frac{BB^T}{r}(D_{\mathbf{e}}V)^T + (D_{\mathbf{e}}V)N\mathbf{w}
\end{aligned}$$

$$\begin{aligned} &\leq -\gamma_3(\|\mathbf{e}\|) - \gamma_4(\mathbf{e},t) + (D_{\mathbf{e}}V)N\mathbf{w} \\ &= -\gamma_3(\|\mathbf{e}\|) - \frac{1}{4\rho^2}(D_{\mathbf{e}}V)NN^T(D_{\mathbf{e}}V)^T + (D_{\mathbf{e}}V)N\mathbf{w} \\ &= -\gamma_3(\|\mathbf{e}\|) + \rho^2\mathbf{w}^T\mathbf{w} - \|\frac{1}{2\rho}N^T(D_{\mathbf{e}}V)^T - \rho\mathbf{w}\|^2 \\ &\leq -\gamma_3(\|\mathbf{e}\|) + \rho^2\mathbf{w}^T\mathbf{w}. \end{aligned} \tag{4.12}$$

Comparing with (4.8), it can be seen that the system perturbation is reduced to a state independent term $\rho^2\mathbf{w}^T\mathbf{w}$. When $\mathbf{w} \in L_\infty[0,\infty)$, there exists a constant $\beta_c > 0$ such that $\rho^2\mathbf{w}^T\mathbf{w} \leq \beta_c$. Hence $\gamma_3(\|\mathbf{e}\|)$ can be chosen with a positive constant ε to satisfy $\gamma_3(\varepsilon) > \beta_c$. This implies, with simply a class $\mathcal{K}$ function γ_3, we can achieve the uniform bound $\|\mathbf{e}\| \leq \varepsilon = \gamma_3^{-1}(\beta_c)$.

When $\mathbf{w}\in L_2[0,\infty) \cap L_\infty[0,\infty)$, integrating from 0 to t the inequality (4.12) which is

$$\dot{V}(\mathbf{e},t) \leq -\gamma_3(\|\mathbf{e}\|) + \rho^2\mathbf{w}^T\mathbf{w},$$

yields

$$V(\mathbf{e},t) - V(\mathbf{e}(0),0) \leq -\int_0^t \gamma_3(\|\mathbf{e}\|)d\tau + \rho^2\int_0^t \|\mathbf{w}\|^2 d\tau. \tag{4.13}$$

Because $V(\mathbf{e},t) \geq 0$, from (4.13) we can derive

$$\int_0^t \gamma_3(\|\mathbf{e}\|)d\tau \leq V(\mathbf{e}(0),0) + \rho^2\int_0^t \|\mathbf{w}\|^2 d\tau < \infty. \tag{4.14}$$

From the boundedness of $\mathbf{e}$ and $\boldsymbol{\kappa}$, $\dot{\mathbf{e}}$ is bounded. As a result $\gamma_3(\|\mathbf{e}\|)$ is uniformly continuous. According to *Barbalat's Lemma* (Narendra and Annaswamy, 1989), we can conclude that

$$\lim_{t\to\infty} \gamma_3(\|\mathbf{e}(t)\|) = 0 \Rightarrow \lim_{t\to\infty} \mathbf{e}(t) = 0.$$

Remark 4.4. *Generally speaking, it may not be so straightforward to solve the Hamilton-Jacobien inequality (4.11) for arbitrary nonlinear systems. If* $\mathbf{f}(\mathbf{e},t)$ *can be expressed to be* $F(\mathbf{e},t)\mathbf{e}$*, where* F *is continuous with respect to the arguments,*

then we can choose a quadratic $\gamma_3(\|\mathbf{e}\|) = \mathbf{e}^T\mathbf{e}$. *As a consequence, the Hamilton-Jacobien inequality (4.11) renders to a differential Riccati inequality*

$$\frac{1}{2}\dot{P} + \frac{1}{2}(PF + F^TP) - P\left[\frac{BB^T}{r} - \frac{1}{4\rho^2}NN^T\right]P + I_{n\times n} \leq 0, \tag{4.15}$$

with $P(\mathbf{e}, t) \in \mathcal{R}^{n\times n}$ *a symmetric positive definite smooth matrix.*

4.4 Illustrative Examples

Consider the system (4.1) with the following parameters

$$\mathbf{f} = F\mathbf{e} = \begin{bmatrix} 0 & 1 \\ -2 & -4 \end{bmatrix}\mathbf{e}, \qquad \mathbf{b} = \begin{bmatrix} 0 \\ 1 \end{bmatrix}, \qquad E = \begin{bmatrix} cos(e_2) & sin(e_2) \\ sin(e_1) & cos(e_1) \end{bmatrix},$$

$\Delta b = 0.2cos(e_2)$, $e_1(0) = e_2(0) = 0.5$, and $\eta_m = sin(\pi t)$. The known bounds are $\beta_b = 0.2$, $\beta_m = 1$ and $\beta_u = \sqrt{2}\,\|E(\mathbf{e})\|$. The switching surface is chosen according to (4.4), where $H = [1, 2]$. A saturation function with boundary layer 0.02 is used to smooth the switching control part. The sampling interval in the simulation is $T_s = 1ms$.

According to *Remark* 4.4, we choose $V(\mathbf{e}, t) = \frac{1}{2}\mathbf{e}^TP\mathbf{e}$, where P is determined by the differential Riccati inequality (4.15). Since F is a constant matrix, we can choose a constant matrix P. Choose $\gamma_3 = \mathbf{e}^T\mathbf{e}$, $\rho = 1.2$ and $r = 0.1$. In order to solve the linear algebraic matrix inequality

$$\frac{1}{2}(PF + F^TP) - P\left[\frac{\mathbf{b}\mathbf{b}^T}{r} - \frac{1}{4\rho^2}NN^T\right]P + I_{2\times 2} \leq 0,$$

we use the singular value of the matrix N, which is 1. A solution is

$$P = \begin{bmatrix} 8.9774 & 1.1376 \\ 1.1376 & 0.32734 \end{bmatrix}.$$

Next from (4.10), we have $\kappa(\mathbf{e}, t) = -\frac{1}{r}\mathbf{b}^TP\mathbf{e}$.

Case 1. Unmatched uncertainty $\mathbf{w} \in L_\infty[0,\infty)$

The unmatched uncertainty is $\mathbf{w} = [0.05sin(0.5t),\ 0.05cos(0.5t)]^T$. $Fig.4.1$ shows (solid line) that the error states e_1 and e_2 of the system are bounded but cannot be eliminated, due to the existence of the unmatched L_∞ type uncertainty. On the other hand, ISMC achieves asymptotic convergence when $\mathbf{w} = 0$, that is, ISMC rejects the matched uncertainty η_m perfectly. As shown in $Fig.4.2$, the proposed scheme is compared with the conventional scheme with linear sliding surface (H is same and $\kappa = -(H\mathbf{b})^{-1}H\mathbf{f}$). Note that in this example, the resulting sliding manifold can also be stabilizable by a linear sliding surface, since the term $\mathbf{f}$ is a linear function of the states. However, the tracking performance is not as good as the proposed scheme because of larger error bound and slower convergence rate.

Case 2. Unmatched uncertainty $\mathbf{w} \in L_2[0,\infty) \cap L_\infty[0,\infty)$

The unmatched uncertainty is $\mathbf{w} = [e^{-0.1t}, -e^{-0.5t}]^T \in L_2[0,\infty)$. As shown in $Fig.4.3$, the tracking error $\mathbf{e}$ of the system approaches zero asymptotically. As shown in $Fig.4.4$, the proposed scheme isalso compared with the conventional scheme with linear sliding surface. Note that the tracking performance is not as good as the proposed scheme because of also compared with the conventional scheme with linear sliding surface. Note that the tracking performance is also not as good as the proposed scheme.

4.5 Conclusions

In this chapter, the feature of integral SMC was first highlighted and compared with conventional SMC. The ISMC leads to a sliding manifold that spans the whole state space. Using Lyapunov's direct method, it is easy to design a nonlinear nominal control law to stabilizing the sliding manifold. In particularly with L_∞ or $L_2 \cap L_\infty$

type unmatched uncertainties, the ISMC achieves either uniform boundedness or asymptotic stability. Illustrative examples have demonstrated the effectiveness of the ISMC.

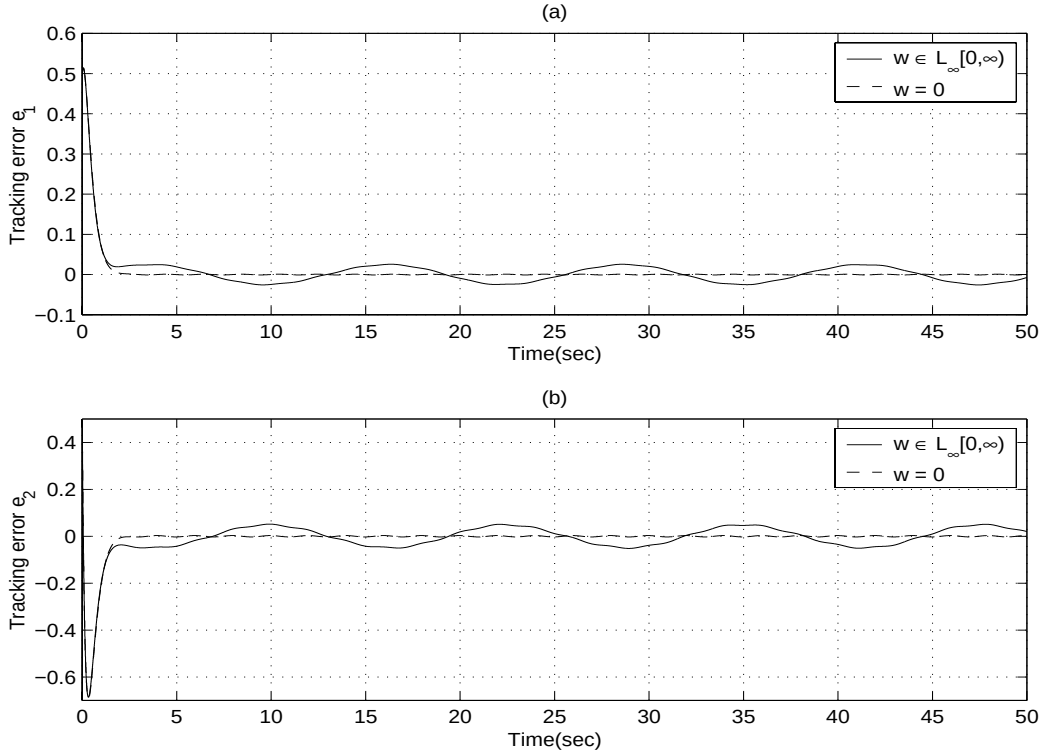

Figure 4.1. The evolution of tracking error: (a) Evolution of e_1; (b) Evolution of e_2.

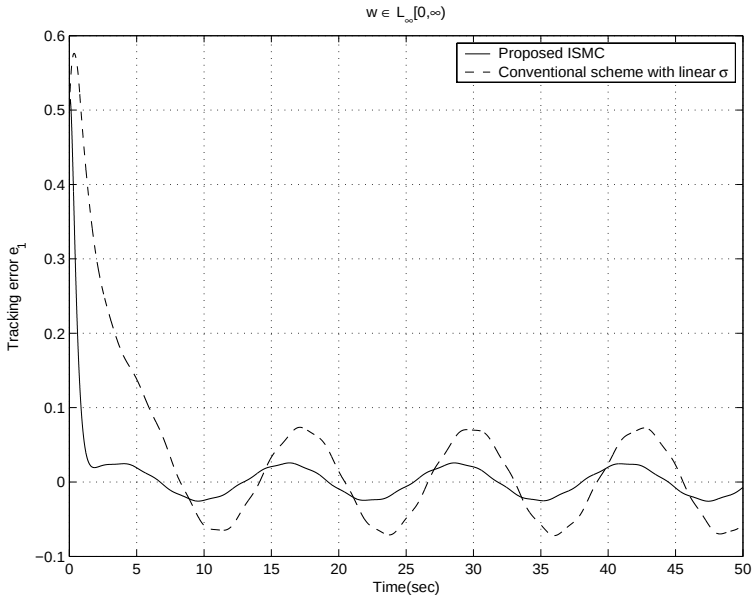

Figure 4.2. The comparisons of the tracking error e_1 when $w \in L_\infty[0, \infty)$.

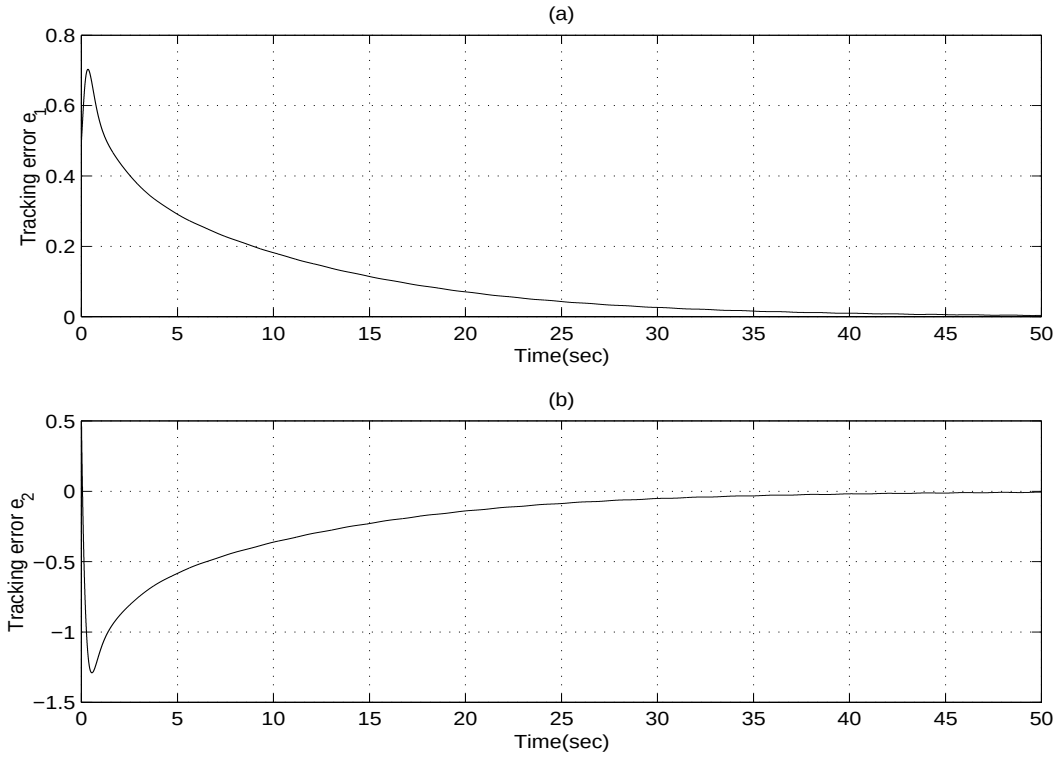

Figure 4.3. The evolution of the tracking error: (a) Evolution of e_1; (b) Evolution of e_2.

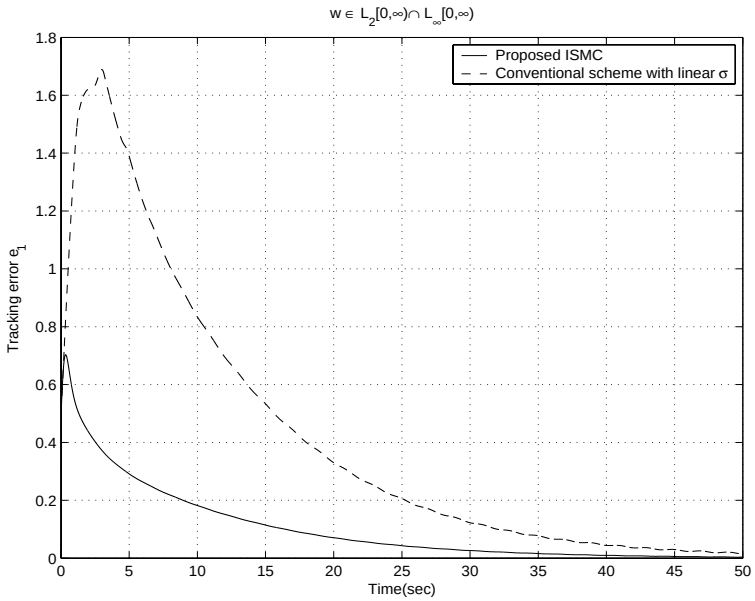

Figure 4.4. The comparisons of the tracking error e_1 when $w \in L_2[0,\infty) \cap L_\infty[0,\infty)$.

Chapter 5

Adaptive Variable Structure Control Design Without a Priori Knowledge of Control Directions

5.1 Introduction

Most of the existing VSC schemes are proposed to deal with the control task when the control directions are known *a priori*. In this chapter, we will show the possibility of performing tracking control without prior knowledge of control directions, which is a challenging problem in general for any control methods. Up to now, there are mainly two approaches to address this problem. One approach is to incorporate the technique of Nussbaum-type gains into the control design. The first result was proposed by Nussbaum (Nussbaum, 1983), and later extended to adaptive control systems (Ryan, 1991), (Ye and Jiang, 1998). Note that those adaptive control schemes were developed to deal with parametric uncertainties. Another approach is to directly estimate unknown parameters involved in the control di-

rections (Mudgett and Morse, 1985) (Brogliato and Lozano, 1992), (Brogliato and Lozano, 1994), (Kaloust and Qu, 1995). In this chapter, the first approach is integrated with the typical variable structure control (VSC). By incorporating a Nussbaum-type function, the new adaptive VSC law can ensure the convergence of the tracking error in the existence of non-parametric uncertainties.

The chapter is organized as follows. In Section 5.2, the problem formulation is presented. In Section 5.3, the new adaptive variable structure control scheme design and the convergence property are given. In Section 5.4, a numerical example is presented which demonstrates the effectiveness of the proposed scheme. Finally, Section 5.5 gives the conclusions. For simplicity, we focus on SISO nonlinear uncertain systems in this chapter.

5.2 Problem Formulation

Consider the following uncertain nonlinear system

$$\dot{x} = \eta(x,t) + bu(x,t), \tag{5.1}$$

where $x \in \mathcal{R}$ is a physically measurable state, $b \neq 0$ is an unknown constant parameter and $u \in \mathcal{R}$ is the control input. η is a lumped disturbance. The sign of b, which determines the control direction, is assumed to be unknown.

The system is required to track the trajectory $x_d \in \mathcal{C}^1[0,\infty)$. The switching surface is selected as $\sigma = x_d - x$.

Assumption 5.1. *$\eta(x,t)$ is norm bounded by a known non-negative bounding function, i.e., $|\eta(x,t)| \leq \beta_\eta(x,t)$. $\forall x$ in any closed set, $\exists \beta$, $\beta_\eta(x,t) < \beta$, where β is a finite constant.*

When the parameter b is known, this tracking problem can be solved simply by the

classical variable structure control. When b is unknown, we need to look for a new adaptive VSC approach. In this chapter, the following Nussbaum-type function will be used in the controller design.

Definition 5.1. *(Nussbaum, 1983) $v(\star)$ is an even smooth Nassbaum-type function, if the function has the following properties*

$$\begin{aligned} \limsup_{s\to\infty} \frac{1}{s}\int^{s} v(k)dk &= \infty, \\ \liminf_{s\to\infty} \frac{1}{s}\int^{s} v(k)dk &= -\infty. \end{aligned}$$

An example of such a continuous function is $v(k) = k^2 cos(k)$. Regarding the Nussbaum-type function, the following property holds (Ye and Jiang, 1998).

Property 5.1. *Let $V(\star)$ and $k(\star)$ be smooth functions defined on $[0, T)$ with $V(t) \geq 0$, $\forall t \in [0, T)$, $v(\star)$ be an even smooth Nassbaum-type function, and b a nonzero constant. If the following inequality holds*

$$V(t) \leq \int_0^{k(t)} [bv(\omega) + 1]\, d\omega + c, \qquad \forall t \in [0, T),$$

where c is an arbitrary constant, then $V(t)$, $k(t)$ and $\int_0^{k(t)} [bv(\omega) + 1]\, d\omega$ must be bounded on $[0, T)$.

5.3 Adaptive Variable Structure Controller Design

The adaptive variable structure controller is designed as

$$u(x,t) = v(k(t))z(x,t) \tag{5.2}$$

$$\dot{k}(t) = -z(x,t)\sigma$$

$$z(x,t) = -\sigma - \dot{x}_d - (\beta_\eta + \varepsilon)sign(\sigma), \tag{5.3}$$

where $v(\star)$ is an even smooth Nussbaum-type function and ε is a positive constant.

Theorem 5.1. *For system* (5.1) *under the adaptive variable structure controller* (5.2) *and* (5.3), $\sigma \to 0$ *as* $t \to \infty$.

Proof: Selecting a Lyapunov function candidate $V = \frac{1}{2}\sigma^2$. Under the control law (5.2), the time derivative of V is

$$\begin{aligned}
\dot{V} &= \sigma\dot{\sigma} = \sigma\dot{e} = \sigma(\dot{x}_d - \eta - bu) \\
&= \sigma\left[\dot{x}_d - \eta - bv(k)z\right] = \sigma\left[\dot{x}_d - \eta - bv(k)z - z + z\right] \\
&= \sigma\dot{x}_d + \left[bv(k)+1\right]\dot{k} + \sigma\left[-\sigma - \dot{x}_d - (\beta_\eta + \varepsilon)sign(\sigma)\right] - \sigma\eta \\
&\leq -\sigma^2 + \left[bv(k)+1\right]\dot{k} - \sigma\beta_\eta sign(\sigma) + \beta_\eta|\sigma| \\
&= -\sigma^2 + \left[bv(k)+1\right]\dot{k}. \qquad (5.4)
\end{aligned}$$

Integrating both sides of the inequality (5.4) from 0 to t, we have

$$\begin{aligned}
V(t) &\leq V(0) - \int_0^t \sigma^2 d\tau + \int_0^t \left[bv(k)+1\right]\dot{k}d\tau \qquad (5.5) \\
&\leq V(0) + \int_0^t \left[bv(k)+1\right]\dot{k}d\tau \\
&= V(0) + \int_0^{k(t)} \left[bv(\omega)+1\right]d\omega. \qquad (5.6)
\end{aligned}$$

Hence, according to *Property*, $V(t)$, $k(t)$ and $\int_0^{k(t)} \left[bv(\omega)+1\right]d\omega$ are bounded , i.e., $\exists\beta_V < \infty$, $\beta_k < \infty$, $\beta_i < \infty$, such that

$$V(t) \leq \beta_V, \qquad k(t) \leq \beta_k, \qquad \int_0^{k(t)} \left[bv(\omega)+1\right]d\omega \leq \beta_i.$$

Note that $\sigma = 2\sqrt{V(t)} \leq 2\sqrt{\beta_V}$ implies $\sigma \in L_\infty$, in the sequel $x \in L_\infty$ and $\beta_\eta \in L_\infty$.

From (5.5), we have

$$\int_0^t \sigma^2 d\tau \leq V(0) + \int_0^{k(t)} \left[bv(\omega)+1\right]d\omega = V(0) + \beta_i, \qquad (5.7)$$

where $V(0) = \frac{1}{2}\sigma(0)^2$ is a finite positive constant. Hence, σ is square integrable which means $\sigma \in L_2$.

Furthermore, in the controller (5.2), the smooth function $v(k)$ is bounded because $k(t)$ is bounded. In (5.3), $z(\star)\in L_\infty$ because $\sigma \in L_\infty$. Thus $u(\star) \in L_\infty$ which means that $\dot{\sigma} = \dot{x}_d - \eta - bu$ is bounded. According to Barbalat's lemma (Narendra and Annaswamy, 1989), $\sigma \in L_\infty \cap L_2$ and the boundedness of $\dot{\sigma}$ warrants $\lim_{t\to\infty} \sigma = 0$.

Remark 5.1. *The above result can be easily extended to higher order systems*

$$\begin{cases} \dot{x}_i(t) = x_{i+1}(t), & i = 1, 2, \cdots, n-1, \\ \dot{x}_n(t) = \eta(\mathbf{x}, t) + bu(\mathbf{x}, t), \end{cases}$$

where $\mathbf{x} = [x_1, x_2, \cdots, x_n]^T$. *Denote* $\mathbf{x}_d = [x_{1d}, x_{2d}, \cdots, x_{nd}]^T$ *the target trajectory, and* $e_1 = x_1 - x_{1d}$, $e_i = \dot{e}_{i-1}$, $i = 2, 3, \cdots, n$ *the tracking errors. Choose the switching surface*

$$\sigma = \sigma(e_1, e_2, \cdots, e_n), \quad \frac{\partial \sigma}{\partial e_n} \neq 0. \tag{5.8}$$

Then the adaptive variable structure control law can be designed analogous to (5.2) *and* (5.3)*, as below, which achieves the asymptotic tracking convergence*

$$\begin{aligned} u(x,t) &= v(k(t))z(x,t) \\ \dot{k}(t) &= -\alpha z(x,t)\sigma \\ z(x,t) &= -\sigma - g(\mathbf{x},t) - \dot{x}_{nd} - (\beta_\eta + \varepsilon) sign(\alpha\sigma), \end{aligned}$$

where $g = \left(\frac{\partial \sigma}{\partial e_n}\right)^{-1} \sum_{i=1}^{n-1} \frac{\partial \sigma}{\partial e_n} e_{i+1}$ *and* $\alpha = \frac{\partial \sigma}{\partial e_n}$.

5.4 Illustrative Example

Consider the uncertain nonlinear system (5.1) with $x(0) = 0.5$, $b = 1$ and $\eta(x,t) = 2x^2 sin(\pi t)$. The control direction, the sign of b, is assumed unknown. The known bound of η is $\beta_\eta = 2x^2$. The system is required to track the target trajectory $x_d(t) = 0.2 + 0.2 sin^2(\pi t)$. The switching surface is chosen to be $\sigma = x_d - x$.

The simulation is carried out by applying the proposed adaptive variable structure control law (5.2) and (5.3) with $\varepsilon = 0.5$. Note that any small value of $\varepsilon > 0$ can be selected and hence a little influence on the system performance. It is clearly shown in $Fig.5.1$ that $\sigma = 0$ is achieved. The boundedness of the adapting parameter $k(t)$ is shown in $Fig.5.2$.

5.5 Conclusions

In order to deal with the tracking problem without any prior knowledge with regards to the control directions, a Nussbaum function is incorporated into the adaptive variable structure controller. Based on Lyapunov's direct method, the system with zero tracking error is ensured under the proposed control scheme. The effectiveness of the adaptive VSC design is demonstrated through a numerical example.

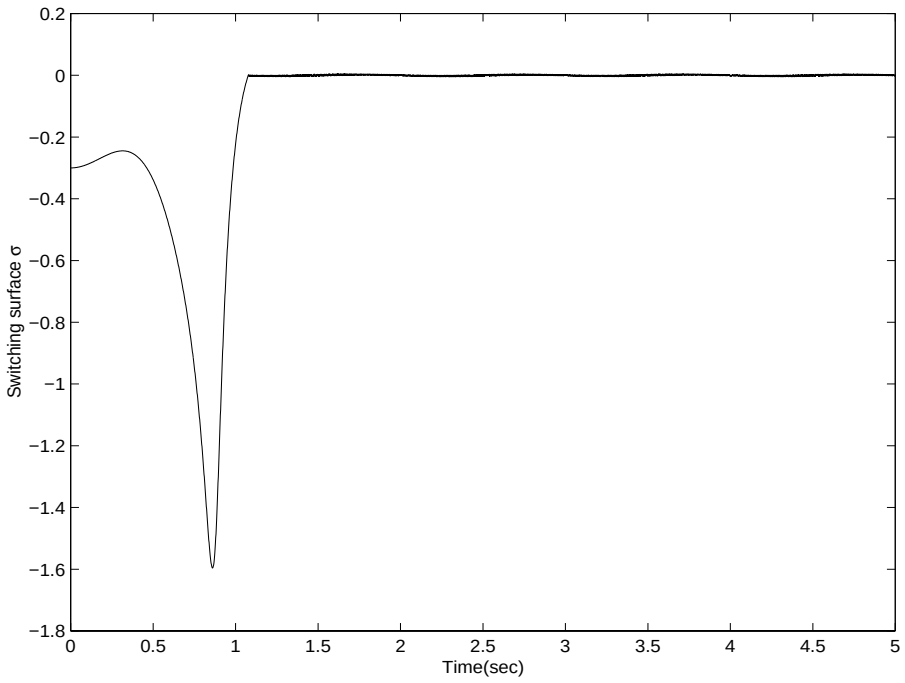

Figure 5.1. The evolution of the switching surface $\sigma(x, t)$.

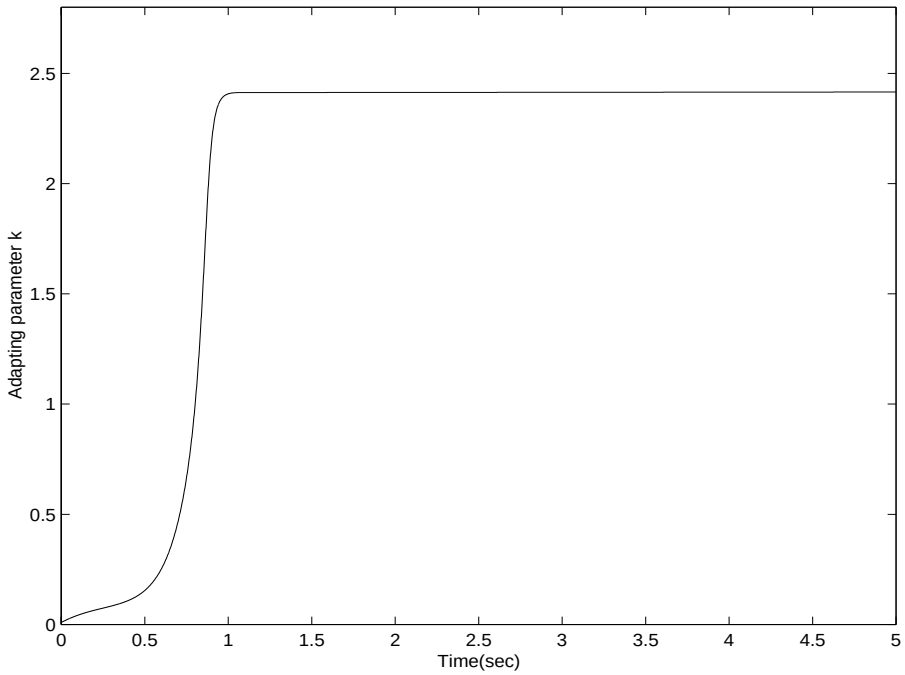

Figure 5.2. The evolution of the adapting parameter $k(t)$.

Chapter 6

A New Fractional Interpolation Based Smoothing Scheme for Variable Structure Control

6.1 Introduction

The ideal sliding mode in VSC requires infinite switching frequency which is not achievable in practice due to the limited sampling rate in digital implementation. On the other hand, a typical switching mechanism in VSC tries to realize an infinitely high gain crossing the switching surface to suppress any norm-bounded non-vanishing uncertainties. As a consequence, a finite switching frequency associated with extremely high control gain will cause undesirable chattering which may excite unmodeled high frequency system dynamics and is harmful to actuation mechanism.

In practice, most control tasks are considered as being accomplished as long as the tracking error eventually enters a pre-specified tracking precision bound which is

non-infinitesimal. This fact implies that the control system needs only a finite instead of an infinite gain nearby the equilibrium. Based on this, various smoothing schemes have been proposed. In (Slotine, 1984) and (Xu *et al.*, 1989), a saturation function with boundary layer is introduced to replace the signum function. It uses a proportional gain inside the precision bound, and a saturated control gain elsewhere. Another well known smoothing scheme has been proposed and explored by (Burton and Zinober, 1986) and (Zinober, 1994), in which a fractional interpolation with state dependent offset is introduced to replace the signum function. Comparing the two schemes, the former is not as smooth as the latter, but ensures the global convergence to the precision bound. The main problem with the fractional interpolation scheme is the lack of quantified design to guarantee the tracking accuracy.

In this chapter, a new fractional interpolation is developed, which retains the advantages of the above two smoothing schemes: its equivalent gain is as smooth as the fractional interpolation, and as adequate and moderate as the saturation function. Moreover, the new scheme enjoys one more feature: the equivalent gain nearby the vicinity of the equilibrium can be further adjusted to vary from the saturation type to the signum type.

The chapter is organized as follows. Section 6.2 gives the problem formulation and the review of the two existing smoothing schemes. In Section 6.3, the properties of the new fractional interpolation scheme are analyzed. Section 6.4 compares the new scheme with the two existing smoothing schemes through an example and shows the advantages of the proposed scheme. Finally Section 6.5 draws the conclusions.

6.2 Problem Statement

6.2.1 System Description

It is well known in VSC that chattering is likely to occur when a high gain is required to suppress norm-bounded uncertainties. The underlying part of the problem is then on the introduction of an appropriate smoothing function to lower the gain around the equilibrium, hence eliminate chattering and achieve specified tracking accuracy. To focus on this, we consider the following system as the simplest but the typical circumstance

$$\begin{cases} \dot{x}_i(t) = x_{i+1}(t), \quad i = 1, 2, \cdots, n-1 \\ \dot{x}_n(t) = u(\mathbf{x}, t) + \eta(\mathbf{x}, t) \end{cases} \tag{6.1}$$

where $t \in \mathcal{R}^+$; $\mathbf{x} = [x_1, x_2, \cdots, x_n]^T$ is the physically measurable state; $u(\mathbf{x}, t)$ is the system control input; and $\eta(\mathbf{x}, t)$ is a norm-bounded uncertainty satisfying the following assumption.

Assumption 6.1. *$|\eta(\mathbf{x}, t)| < \beta(\mathbf{x}, t)$, where $\beta(\mathbf{x}, t)$ is a known positive function.*

The switching surface is chosen as $\sigma = e_n + \sum_{i=1}^{n-1} c_i e_i$, where c_i, $i = 1, 2, \cdots, n-1$, are chosen such that $\lambda^{n-1} + c_{n-1}\lambda^{n-2} + \cdots + c_2\lambda + c_1$ is a Hurwitz polynomial.

6.2.2 Control Task

The original control objective is to track the desired trajectory $\mathbf{x}_d$ described by

$$\begin{cases} \dot{x}_{id} = x_{(i+1)d}, \quad i = 1, 2, \cdots, n-1 \\ \dot{x}_{nd} = \psi(\mathbf{x}_d(t), r(t), t) \end{cases}$$

where $\mathbf{x}_d = [x_{1d}, x_{2d}, \cdots, x_{nd}]^T$; $\psi \in C^1[0, \infty)$ with respect to all arguments and $r(t)$ is a reference input. The tracking errors are defined as $e_1 = x_1 - x_{1d}$, $e_i = \dot{e}_{i-1}$, $i = 2, 3, \cdots, n$.

A typical VSC law is

$$\begin{aligned} u &= u_c + u_s, \\ u_c &= \dot{x}_{nd} - \sum_{i=1}^{n-1} c_i e_{i+1}, \qquad u_s = -k\ sign(\sigma), \end{aligned} \tag{6.2}$$

where u_c denotes the feed-forward compensation term generated by $\dot{\sigma} = 0$ in the absence of uncertainties and u_s is the switching control used to suppress the norm-bounded system uncertainty. $k = \beta + \varepsilon$ and ε is a positive constant to ensure finite reaching time.

In practice perfect tracking can hardly be achieved. It is common to introduce a tracking precision bound $\alpha > 0$ and the corresponding control objective is $|\sigma(t)| \leq \alpha,\ \forall t > t_r$, where $t_r > 0$ is a finite reaching time.

6.2.3 Existing Smoothing Schemes

In (*Zinober*, 1994), it was proposed that the signum function $sign(\sigma)$ be replaced by the following fractional interpolation

$$\frac{\sigma}{|\sigma| + \delta}, \tag{6.3}$$

where δ is a positive constant. It provides very smooth control action. Rewrite the switching control

$$u_s = -k\frac{\sigma}{|\sigma| + \delta} = -k_1\ sign(\sigma). \tag{6.4}$$

The equivalent switching control gain k_1 can be calculated as

$$\begin{aligned} k_1 &= k\ f(\sigma, \delta), \\ f(\sigma, \delta) &= \frac{|\sigma|}{|\sigma| + \delta}. \end{aligned} \tag{6.5}$$

The main drawback of (6.4) is that the tracking precision bound α cannot be determined and ensured by the selection of δ. Since $f(\sigma, \delta) < 1\ \forall\delta$, the equivalent

switching gain k_1 will be lower than the necessary level k and may cause large tracking error.

Another well adopted smoothing scheme is to replace the signum function with a saturation function

$$u_s = -k\ sat(\sigma, \alpha) \quad = \quad \begin{cases} -k\ sign(\sigma) & |\sigma| \geq\ \alpha \\ -k\ \frac{\sigma}{\alpha} & |\sigma| < \alpha \end{cases} \tag{6.6}$$

The equivalent switching gain is

$$\begin{aligned} u_s &= -k_2\ sign(\sigma), \\ k_2 &= \begin{cases} -k & |\sigma| \geq\ \alpha \\ -k\ \frac{|\sigma|}{\alpha} & |\sigma| < \alpha. \end{cases} \end{aligned}$$

Note that the equivalent switching gain outside the bound α is at the necessary level k, hence the tracking precision is guaranteed. This is the main reason why (6.6) is so popular. However it is less smooth compared with (6.4), as the saturation function is only piecewise smooth. Moreover, once α is fixed, inside the precision bound it is in fact a fixed proportional control with the gain k/α which cannot be further adjusted. It is worth mentioning that saturation based smoothing with varying boundary layer (Slotine, 1984) and (Xu *et al.*, 1989) can improve the smoothness property. Nevertheless it is complicated due to the dynamic compensation nature, and the varying boundary layer sacrifices the tracking accuracy.

The new smoothing scheme to be detailed in the next section is able to overcome all above shortcomings.

6.3 New Fractional Interpolation Scheme

6.3.1 New Switching Control Law

The switching control with new fractional interpolation is

$$u_s = -k \frac{(|\sigma| + \delta_1)\sigma}{(|\sigma| + \delta)^2} = -k_3 \, sign(\sigma) \tag{6.7}$$

where the equivalent switching gain is

$$\begin{aligned} k_3 &= k \; g(\sigma, \delta, \delta_1), \\ g(\sigma, \delta, \delta_1) &= \frac{(|\sigma| + \delta_1)|\sigma|}{(|\sigma| + \delta)^2}, \end{aligned} \tag{6.8}$$

where δ and δ_1 are two design parameters. Comparing with (6.5), we can see that the only difference is the replacement of the smoothing function $f(\sigma, \delta)$ by a new smoothing function $g(\sigma, \delta, \delta_1)$.

6.3.2 Property Analysis

In order to acquire all advantages of the two existing smoothing schemes, the following three properties are required.

$P1^\circ$. The equivalent control gain $k_3 \geq k$ when $|\sigma| \geq \alpha$.

That is, the equivalent gain must be adequate outside the precision bound.

$P2^\circ$. The switching control is smooth in the large.

That is, the partial derivative $D_\sigma u_s$ is continuous $\forall \sigma$.

It should be noted that the first two properties can be easily achieved by a simple linear control law, for instance a proportional control $u_s = \frac{k}{\alpha}\sigma$. It is equally important to limit the control action outside the precision bound as the saturation scheme does. This is described by the third property.

$P3^\circ$. The equivalent switching control gain $k_3 \Rightarrow k$ as $|\sigma| \Rightarrow \infty$.

The main result of this work is summarized in the following proposition.

Proposition 6.1. *The proposed control law (6.7) with*

$$\delta_1 = 2\delta + \frac{\delta^2}{\alpha} \tag{6.9}$$

ensures all the three properties.

Proof: $P1^\circ$: When $|\sigma| = \alpha$,

$$k_3 = k\ g(\alpha, \delta, \delta_1) = \frac{k(\alpha + 2\delta + \frac{\delta^2}{\alpha})\alpha}{(\alpha + \delta)^2} = k.$$

When $|\sigma| > \alpha$,

$$k_3 = \frac{k(|\sigma| + 2\delta + \frac{\delta^2}{\alpha})|\sigma|}{(|\sigma| + \delta)^2} = k\left[1 + \frac{\delta^2(|\sigma| - \alpha)}{\alpha(|\sigma| + \delta)^2}\right] > k.$$

The control gain is adequate outside the precision bound.

$P2^\circ$: From (6.7) it is straightforward to see that u_s is smooth at the point $\sigma \neq 0$. Thus we need only to show this property at $\sigma = 0$. First we can derive

$$\lim_{\sigma \to 0^+} u_s = \lim_{\sigma \to 0^+} -\frac{k(|\sigma| + \delta_1)\sigma}{(|\sigma| + \delta)^2} = \lim_{\sigma \to 0^-} u_s = \lim_{\sigma \to 0^-} -\frac{k(|\sigma| + \delta_1)\sigma}{(|\sigma| + \delta)^2} = 0.$$

For $\sigma < 0$, we have

$$u_s = -\frac{k(-\sigma + \delta_1)\sigma}{(-\sigma + \delta)^2} = \frac{k(\sigma - \delta_1)\sigma}{(\sigma - \delta)^2}, \quad \Rightarrow D_\sigma u_s = \frac{k(\sigma\delta_1 - 2\delta\sigma + \delta\delta_1)}{(\sigma - \delta)^3}. \tag{6.10}$$

Thus

$$\lim_{\sigma \to 0^-} D_\sigma u_s = \lim_{\sigma \to 0^-} \frac{k(\sigma\delta_1 - 2\delta\sigma + \delta\delta_1)}{(\sigma - \delta)^3} = -\frac{k\delta_1}{\delta^2}. \tag{6.11}$$

Similarly, we can derive for $\sigma > 0$,

$$u_s = -\frac{k(\sigma + \delta_1)\sigma}{(\sigma + \delta)^2}, \qquad \Rightarrow D_\sigma u_s = -\frac{k(-\sigma\delta_1 + 2\delta\sigma + \delta\delta_1)}{(\sigma + \delta)^3},$$

and

$$\lim_{\sigma\to 0^+} D_\sigma u_s = \lim_{\sigma\to 0^+} -\frac{k(-\sigma\delta_1 + 2\delta\sigma + \delta\delta_1)}{(\sigma+\delta)^3} = -\frac{k\delta_1}{\delta^2}. \tag{6.12}$$

At the point $\sigma = 0$,

$$D_\sigma u_s = \lim_{\triangle\sigma\to 0} \frac{u_s(\triangle\sigma) - u_s(0)}{\triangle\sigma} = -\frac{k(|\triangle\sigma| + \delta_1)\triangle\sigma}{(|\triangle\sigma| + \delta)^2 \triangle\sigma} = -\frac{k\delta_1}{\delta^2}. \tag{6.13}$$

The results of (6.11), (6.12) and (6.13) show that $D_\sigma u_s$ is continuous at the point $\sigma = 0$.

P3°: When $|\sigma| \to \infty$, using (6.8),

$$\lim_{|\sigma|\to\infty} g(\sigma, \delta, \delta_1) = 1 \Rightarrow \lim_{|\sigma|\to\infty} k_3 = k.$$

That is, the control action will be kept at the necessary level when the system state is far away from the switching surface $\sigma = 0$.

Remark 6.1. *Since the equivalent switching control gain is very low near the equilibrium, the chattering can be significantly reduced or even eliminated.*

6.3.3 Selection of Parameter δ

Note that the three properties of the new smoothing scheme are derived without any specification on the parameter δ, which is an extra degree of freedom in controller design. To facilitate the controller design, it is useful to investigate the relationship between the function $g(\sigma, \delta, \delta_1)$ and δ. The partial derivative of the function g with respect to δ is

$$D_\delta g = \frac{2|\sigma|\delta(|\sigma| - \alpha)}{(|\sigma| + \delta)^3\alpha}.$$

Therefore with increasing δ, the equivalent switching gain will increase outside the precision bound and decrease inside the precision bound. It can also be seen from (6.7) that u_s becomes the typical switching controller $k\ sign(\sigma)$ as $\delta \to 0$.

$Fig.6.1(a)$ compares two fractional interpolation schemes with $\alpha = \delta = 0.1$. $Fig.6.1(b)$ compares the new interpolation scheme with saturation scheme with $\alpha = 0.1$, $\delta = 0.5$ and $\delta = 0.01$ respectively. From $Fig.6.1(a)$, the new smoothing scheme does possess the highly preferred three properties, whereas the conventional one does not. From $Fig.6.1(b)$, the proposed smoothing scheme has a smoother shape and an adjustable gain within the precision bound in comparison with the saturation scheme.

6.4 Illustrative Example

Consider the following system

$$\begin{cases} \dot{x}_1(t) = x_2(t) \\ \dot{x}_2(t) = u(\mathbf{x}, t) + \eta(\mathbf{x}, t) \end{cases}$$

where the initial states are $x_1(0) = 1.5$, $x_2(0) = 0$ and d is a disturbance with a known upper bound $\beta = 10$. The reference signals are $x_{1d} = 1 - sin(t)$ and $x_{2d} = \dot{x}_{1d} = -cos(t)$. The switching surface is chosen to be $\sigma = e_2 + 5e_1$ where $e_1 = x_1 - x_{1d}$, $e_2 = x_2 - x_{2d}$. From equation (6.2), the controller consists of $u_c = \dot{x}_{2d} - 5e_2 = sin(t) - 5e_2$, and $u_s = -k\ sat(\sigma, \alpha)$ in the saturation scheme, $u_s = -k\ f(\sigma, \delta) sign(\sigma)$ in the conventional interpolation scheme and $u_s = -k\ g(\sigma, \delta, \delta_1) sign(\sigma)$ in the proposed scheme. $k = \beta + \varepsilon = 10 + 0.1 = 10.1$ and the selections of δ and α will be presented in the following case studies. The sampling interval is $T_s = 0.02$ sec.

Case 1: Comparison with the conventional fractional interpolation scheme

The disturbance is selected to be $\eta = 10$. Choose $\delta = 0.2$, $\alpha = 0.1$ and δ_1 according to (6.9). As shown in $Fig.6.2$, the error bound is very large. By choosing a

Lyapunov function $V = \frac{1}{2}\sigma^2$, it is easy to estimate the error bound.

$$\begin{aligned} \dot{V} &= \sigma(u + \eta - \dot{x}_{2d} + 5e_2) = \sigma(-kf + \eta) \leq \frac{|\sigma|(-\varepsilon|\sigma| + \beta\delta)}{|\sigma| + \delta} \\ \Rightarrow |\sigma| &= \frac{\beta\delta}{\varepsilon} = 10 \times 0.2/0.1 = 20. \end{aligned}$$

This is due to the inadequate control gain which is further provoked by the fact that η is almost the same size as the switching gain k. Shown in $Fig.6.3$, by using the proposed control scheme, the system enters the desired precision bound $\alpha = 0.1$.

Case 2: Comparison with the saturation scheme

In this case, the disturbance is $\eta(\mathbf{x}, t) = 5sin(10t) + 5cos(x_2)$ with a known upper bound $\beta = 10$. The comparison results using the proposed and the saturation schemes are shown as in $Fig.6.4$, $Fig.6.5$ and $Fig.6.6$ respectively. When the given precision bound is large ($\alpha = 0.5$), it is possible to increase the equivalent switching gain within the bound as long as it does not incur chattering. This can be easily achieved by reducing the value of δ. By choosing $\delta = 0.25$, the tracking error of the proposed scheme is about 50% of the saturation one, whereas the control files are equally smooth ($Fig.6.4$).

When a tougher tracking precision bound $\alpha = 0.1$ is given, the gain of the saturation scheme is inevitably increased and may lead to chattering (see $Fig.6.5$). By contrast, the proposed scheme retains a smooth control profile. In other words, the new fractional interpolation is smoother than the saturation function.

6.5 Conclusions

In this chapter, a new fractional interpolation based smoothing scheme is proposed for variable structure control. The new properties of the proposed scheme has been analyzed and well presented in the chapter. Compared with the conventional

fractional interpolation scheme, the proposed scheme is able to force the system enter the specified precision bound, meanwhile retains one extra degree of freedom in the controller design. Compared with saturation based smoothing scheme, the proposed scheme also shows superior performance owing to its smoothness and adjustable control gain. Finally, simulation results are given to show the effectiveness of the proposed control scheme.

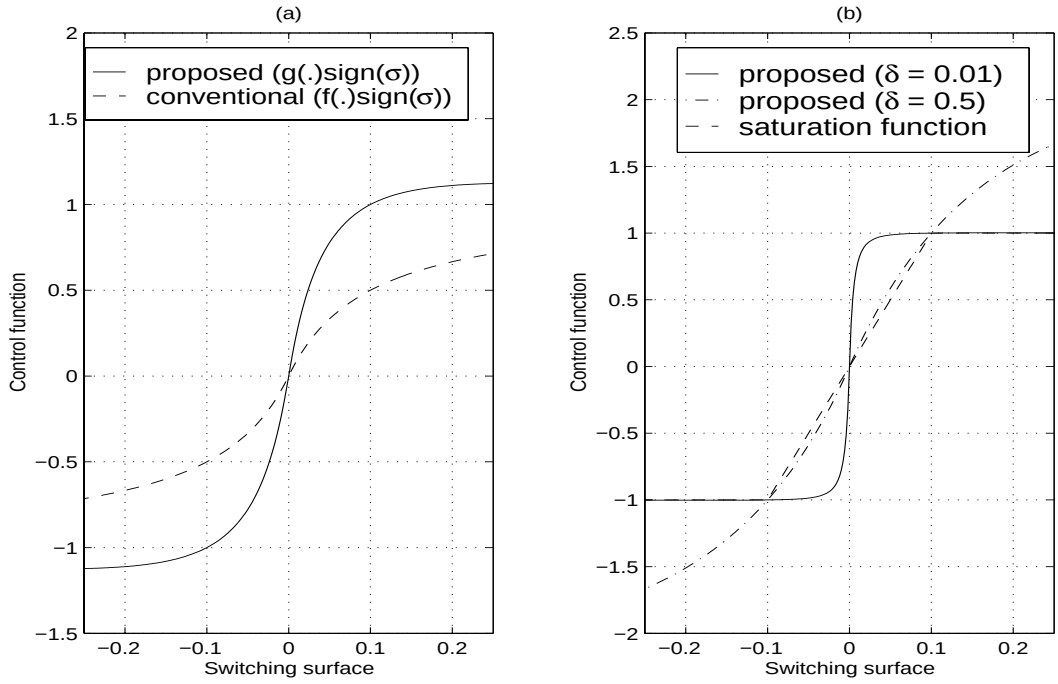

Figure 6.1. (a) The comparison of two fractional interpolation schemes; (b) The comparison of new fractional interpolation and saturation schemes.

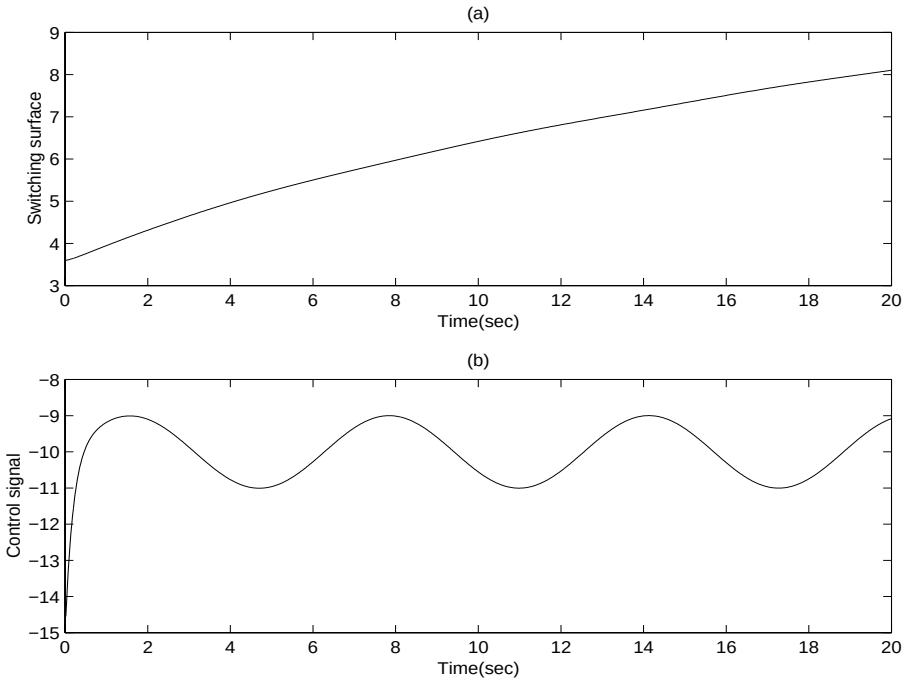

Figure 6.2. The control performance with conventional interpolation scheme: (a) Switching surface; (b) Control signal.

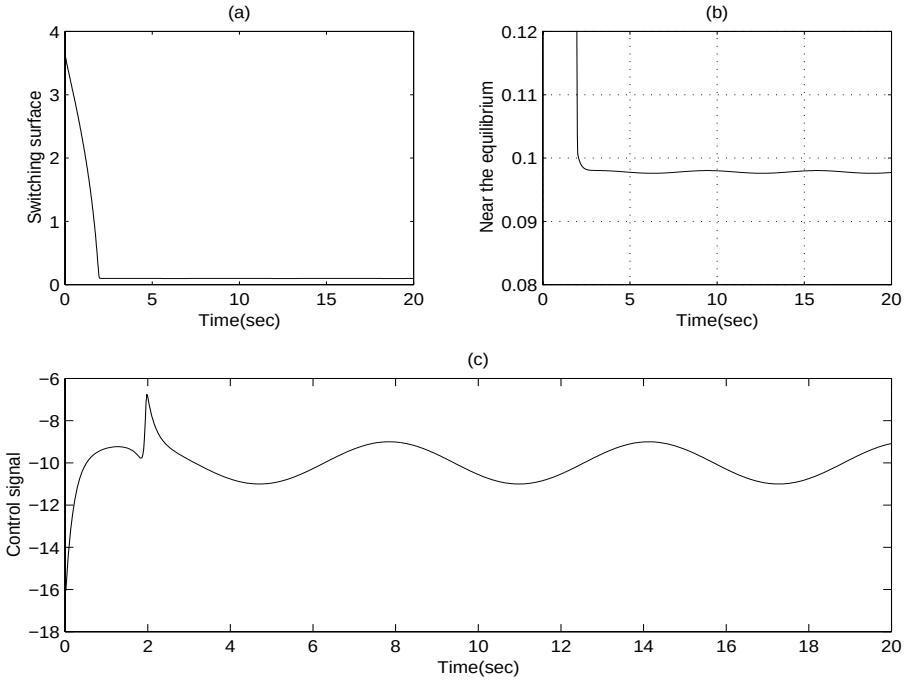

Figure 6.3. The control performance of the proposed control scheme: (a) Switching surface; (b) Switching surface near the equilibrium; (c) Control signal.

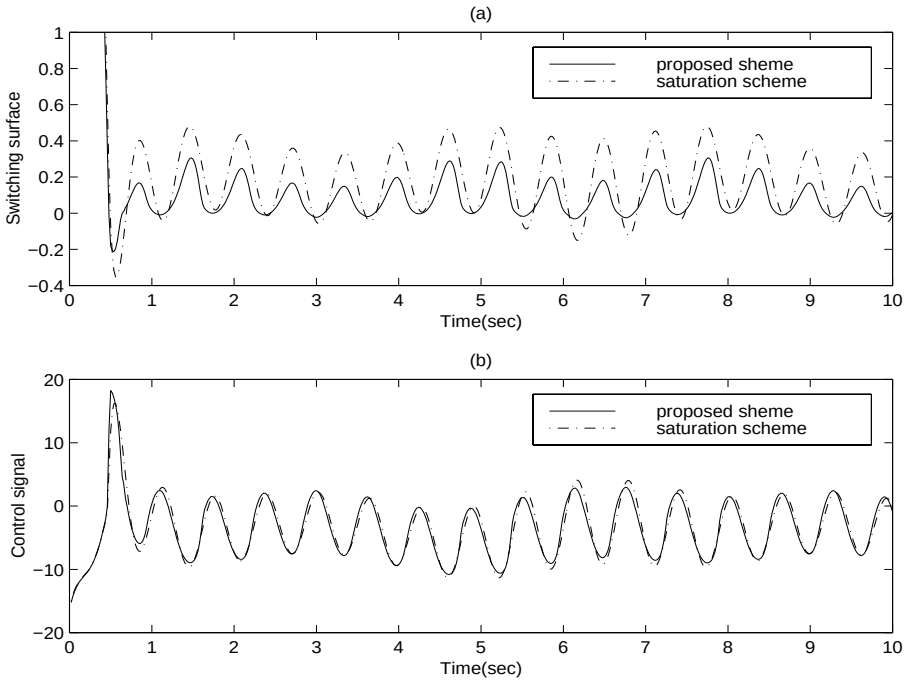

Figure 6.4. Performance of the proposed smoothing scheme ($\delta = 0.25$, $\alpha = 0.5$): (a) Switching surface; (b) Control signal.

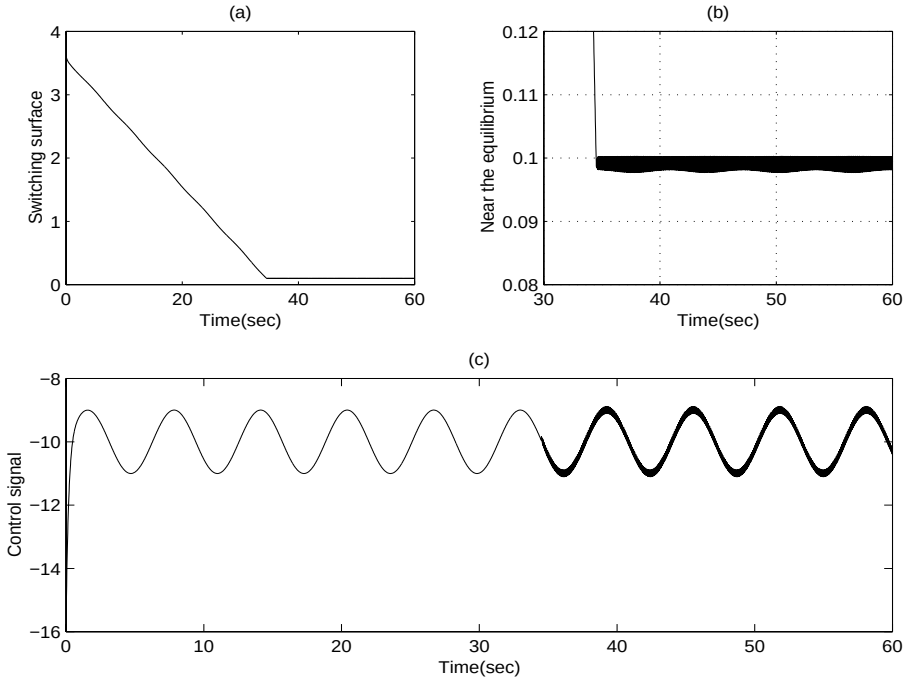

Figure 6.5. Performance of the saturation scheme ($\alpha = 0.1$): (a) Switching surface; (b) Switching surface near the equilibrium; (c) Control signal.

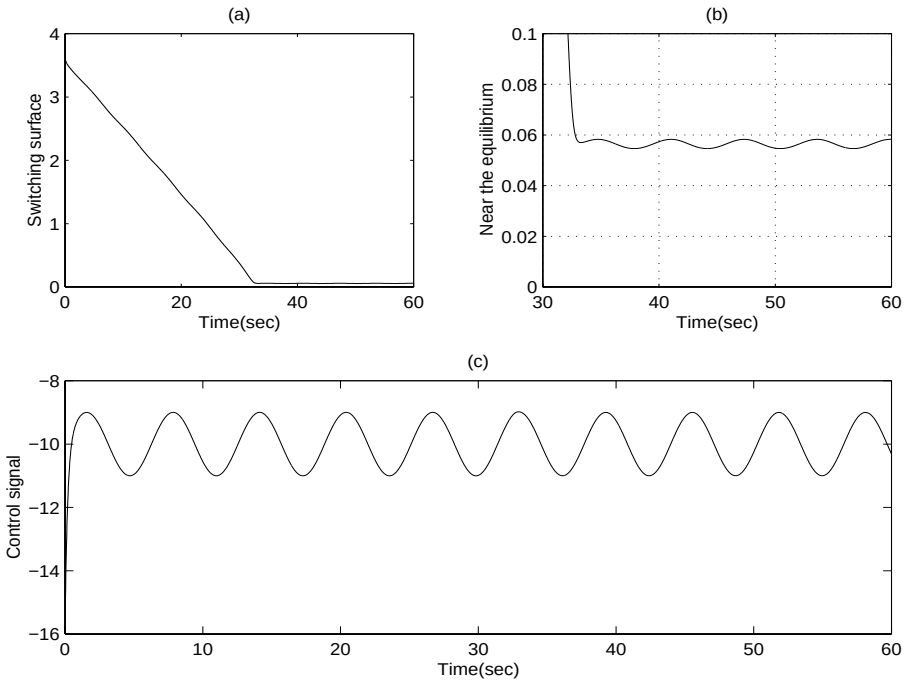

Figure 6.6. Performance of the proposed control scheme ($\delta = 0.01$, $\alpha = 0.1$): (a) Switching surface; (b) Switching surface near the equilibrium; (c) Control signal.

Chapter 7

Gain Shaped Sliding Mode Control of Multi-link Robotic Manipulators

7.1 Introduction

Nowadays, robotic manipulators are widely used in different industries and highly motivated industrial automation. Among numerous control approaches developed for robotic manipulators hitherto, there are four typical approaches of particular interests: 1) sliding mode control approach;2) adaptive control approach; 3) adaptive robust control approach; 4) learning control approach. Each approach has its attractive features and limitations. SMC, as one of the most robust control approaches, makes the robotic control system insensitive to parametric uncertainties and norm-bounded disturbances. On the other hand, as aforementioned, the control performance is limited either due to its high gain chattering nature or due to the introduction of smoothing technique approach as the trade-off. The main

disadvantage of the adaptive controller for robotic manipulators is the lack of robustness to norm-bounded disturbances. The adaptive robust control approach, Although it enhances the robustness to certain extent, is not able to generate the desired equivalent control signal. Consequently, it is still feedback dominant. The learning control approach for robotic manipulators is confined to periodic control circumstances.

In (Utkin, 1977), it has been shown that equivalent control can be obtained using a first-order filter provided that system is in sliding mode and the filter has infinite bandwidth. Note that the second condition is needed only when equivalent control signals possess infinite bandwidth. However, in most practical circumstances, it is not necessary to consider such extreme cases as requiring infinite bandwidth. Most control tasks and control processes or actuators are predominated by frequency band much lower than Nyquist frequency. From sampling theorem, it is also well known that none of control strategies can work near Nyquist frequency. The sliding mode control, as one of the typical nonlinear control strategies implemented using digital techniques, cannot be exempted from this general rule. As a consequence, for most practical control problems, it is sufficient to consider a finite band of frequency components in equivalent control.

In this chapter, from the viewpoint of gain scaling and equivalent control theory, a gain shaped SMC scheme using signal processing techniques is proposed for robotic manipulators to perform tracking control tasks (Xu *et al.*, 2000*d*), (Xu *et al.*, 2000*e*). Based upon the reasonable assumption that the actual frequency band in equivalent control is far lower than the sampling frequency, a class of low-pass filters (LPF1) is employed to acquire equivalent control signals from the switching control signals by the "averaging" operation. Nevertheless, LPF1 alone cannot fully extract the equivalent control signals if its output is to be put into the process as the feedforward compensation because the existence of the switching control part

with high switching gain will interfere with the low-pass filter. Moreover, adding the feedforward compensation does not immediately warrant an auto-shaping of the switching control. Hence the chattering phenomenon incurred by high gain still remains. To facilitate the acquisition of the equivalent control and reduce the switching gain, a second class of low-pass filters (LPF2) is incorporated to shape the switching gain directly.

It is worthwhile to point out that the variable structure control system exhibits distinct behavior in reaching and sliding phases. Therefore it is possible and necessary to design different control schemes better catering to the two phases respectively. During reaching phase, it is mandatory to use high gain so as to ensure the global attractiveness of the switching surface. While in sliding mode, however, it is possible to extract the equivalent control signals from the switching control inputs by means of filtering techniques, and scale down switching control gains accordingly. In this chapter we present two sufficient conditions in the construction of low-pass filters LPF1 and LPF2, under which the sliding motion is guaranteed when LPF1 and LPF2 work concurrently. We further discuss the use of extra degrees of freedom in the design of filter parameters, which allows the incorporation of frequency domain system knowledge and improves control performance.

In this chapter we further show another important property of the gain shaped SMC: the control system is able to reenter the sliding motion in finite time once the system is knocked away from the sliding surface due to any unexpected disturbance surge. The control gain originally being shaped low by LPF2 will automatically scale up so as to recover the sliding motion.

The proposed gain shaped SMC of multi-link robotic manipulators is not simply an extention of the SMC scheme with closed-loop filtering architecture as in Chapter 2. There are numerous differences between these two works. In Chapter 2, a single-

input and single-output can only be developed, however, it is a multi-input multi-output case in the gain shaped SMC of multi-link robotic manipulators. Hence two classes of low pass filters are applied. Furthermore, combined with the using of a set of saturating bounds on the torque control input, the passivity property of the robotic manipulators holds for the torque and the velocity is used to ensure the convergence in case of uncertainty surging.

The chapter is organized as follows. In Section 7.2, the robotic dynamics, the concept of equivalent control and the gain shaped SMC are presented. In Section 7.3, the convergence properties in reaching phase and sliding mode respectively are analyzed and sufficient convergence conditions are given. Section 7.4 addresses the disturbance surging problem and shows the desired finite time recovery property of the sliding mode associated with the gain shaped SMC. In Section 7.5, an illustrative example of a two-link robotic manipulator is presented which demonstrates the effectiveness of the proposed scheme. Finally, Section 7.6 gives the conclusions.

7.2 Gain Shaped SMC of Multi-link Robotic Manipulators

A. Problem Formulation

The dynamic equation of the n degree-of-freedom robot manipulator is

$$M(\mathbf{q})\ddot{\mathbf{q}} + C(\mathbf{q}, \dot{\mathbf{q}})\dot{\mathbf{q}} + \mathbf{g}(\mathbf{q}) = E(\mathbf{q}, \dot{\mathbf{q}}, \ddot{\mathbf{q}})\mathbf{r} = \boldsymbol{\psi}(\mathbf{u}). \tag{7.1}$$

where $M(\mathbf{q})$ is an $n \times n$ inertia matrix which is symmetric positive definite, $C(\mathbf{q}, \dot{\mathbf{q}})\dot{\mathbf{q}}$ is an n-vector of Centripetal and Coriolis torques with $C(\mathbf{q}, \dot{\mathbf{q}})$ being an $n \times n$ matrix, and $\mathbf{g}(\mathbf{q})$ is an n-vector of gravitational torques, $\mathbf{q}$ is an n-vector of joint angular positions, $\dot{\mathbf{q}}$ is an n-vector of joint velocities, $\mathbf{u}$ is an n-vector input torque.

$\mathbf{r}$ is a constant p-dimensional vector of inertia parameters and E is an $n \times p$ matrix of known functions of the generalized coordinates and their higher derivatives. $\boldsymbol{\psi}(\mathbf{u}) = [\psi_1(u_1), \psi_2(u_2), \cdots, \psi_n(u_n)]^T$, where

$$\psi_i(u_i) = \begin{cases} u_i^* sign(u_i) & |u_i| \geq u_i^* \\ u_i & |u_i| < u_i^* \end{cases}$$

is a set of saturating bounds. Most real robotic systems have limited actuation output so that u_i^* can be determined according to the hardware limitations. Otherwise a sufficiently large u_i^* can be set, in which the given tracking task is realizable.

Definition 7.1. *Define* $[\star]_{ij}$ *the* i*th row and* j*th column entry in a matrix* $[\star]$ *and* $[\star]_i$ *the* i*th component in a column vector* $[\star]$*, the relation that two* $n \times n$ *diagonal matrices* A *and* B *satisfy* $[A]_{ii} \leq [B]_{ii}$*,* $i = 1, 2, \cdots, n$*, is defined as* $A \leq B$ *and the relation that two* $n \times 1$ *vectors* $\mathbf{x}$ *and* $\mathbf{y}$ *satisfy* $[\mathbf{x}]_i \leq [\mathbf{y}]_i$*,* $i = 1, 2, \cdots, n$*, is defined as* $\mathbf{x} \leq \mathbf{y}$*.*

Definition 7.2. *Define*

$$|W| = \begin{bmatrix} |w_{11}| & \cdots & |w_{1n}| \\ \vdots & \ddots & \vdots \\ |w_{n1}| & \cdots & |w_{nn}| \end{bmatrix}, \qquad |\mathbf{x}| = [|x_1|, \cdots, |x_n|]^T,$$

where W *is an* $n \times n$ *matrix,* $\mathbf{x}$ *is an* $n \times 1$ *vector and* $|\star|$ *denotes the absolute value.*

Assumption 7.1. *The parameter vector* $\mathbf{r}$ *is uncertain but the modeling error is bounded*

$$|\tilde{\mathbf{r}}| = |\mathbf{r} - \mathbf{r}_0| \leq \bar{\mathbf{r}} \tag{7.2}$$

where $\mathbf{r}_0 \in \mathcal{R}^p$ *is the known nominal part of the parameter vector.*

The system is required to track the desired trajectory $\mathbf{q}_d \in \mathcal{R}^n$. Define the tracking error as $\mathbf{e} = \mathbf{q} - \mathbf{q}_d$. The switching surface here is chosen as

$$\sigma_i = \dot{q}_i - \dot{q}_{di} + \lambda_i(q_i - q_{di}) = \dot{e}_i + \lambda_i e_i. \tag{7.3}$$

where λ_i is the coefficient of a Hurwitz polynomial, $e_i = q_i - q_{di}$ is the tracking error of the ith state. Define $\dot{q}_{ri} = \dot{q}_{di} - \lambda_i e_i$, then (7.3) becomes $\sigma_i = \dot{q}_i - \dot{q}_{ri}$. The switching surface can be simply expressed as $\boldsymbol{\sigma} = \dot{\mathbf{q}} - \dot{\mathbf{q}}_r$ where $\mathbf{q} = [q_1, \cdots, q_n]^T$, $\mathbf{q}_r = [q_{r1}, \cdots, q_{rn}]^T$ and $\Lambda = diag(\lambda_1, \cdots, \lambda_n)$.

B. Concept of Equivalent Control

If system is in sliding mode, then $\boldsymbol{\sigma} = \mathbf{0}$ and the dynamics $\dot{\boldsymbol{\sigma}} = \mathbf{0}$ are satisfied at the same time. By solving the equation $\boldsymbol{\sigma} = \mathbf{0}$ and $\dot{\boldsymbol{\sigma}} = \mathbf{0}$ for the control input, we obtain the equivalent control, $\mathbf{u}_{eq}$, which can be interpreted as the continuous control law that would maintain $\dot{\boldsymbol{\sigma}} = \mathbf{0}$. According to (7.3)

$$\boldsymbol{\sigma} = \mathbf{0} \qquad \Rightarrow \dot{\mathbf{q}} = \dot{\mathbf{q}}_\mathbf{r}, \qquad \dot{\boldsymbol{\sigma}} = \mathbf{0} \qquad \Rightarrow \ddot{\mathbf{q}} = \ddot{\mathbf{q}}_\mathbf{r}. \tag{7.4}$$

The equivalent control can be written as

$$\mathbf{u}_{eq} = M(\mathbf{q})\ddot{\mathbf{q}}_r + C(\mathbf{q}, \dot{\mathbf{q}})\dot{\mathbf{q}}_r + \mathbf{g}(\mathbf{q}) = \mathbf{u}_c - \left[\tilde{M}(\mathbf{q})\ddot{\mathbf{q}}_r + \tilde{C}(\mathbf{q}, \dot{\mathbf{q}})\dot{\mathbf{q}}_r + \tilde{\mathbf{g}}(\mathbf{q})\right] \tag{7.5}$$

where $\tilde{M} = \hat{M} - M$, $\tilde{C} = \hat{C} - C$, $\tilde{\mathbf{g}} = \hat{\mathbf{g}} - \mathbf{g}$ and $\mathbf{u}_c$ denotes the feedforward compensation term generated by $\dot{\boldsymbol{\sigma}} = \mathbf{0}$ in the absence of uncertainties (i.e. $\mathbf{r} = \mathbf{r}_0$)

$$\mathbf{u}_c = \hat{M}(\mathbf{q})\ddot{\mathbf{q}}_r + \hat{C}(\mathbf{q}, \dot{\mathbf{q}})\dot{\mathbf{q}}_r + \hat{\mathbf{g}}(\mathbf{q}) = E(\mathbf{q}, \dot{\mathbf{q}}_r, \ddot{\mathbf{q}}_r)\mathbf{r}_0. \tag{7.6}$$

C. Gain Shaped SMC

The gain shaped SMC is constructed as below

$$\mathbf{u} = \mathbf{u}_c + K\mathbf{u}_s + \mathbf{u}_v, \tag{7.7}$$

where $\mathbf{u}_s = [u_{s1}, u_{s2}, \cdots, u_{sn}]^T$ is an n-vector switching quantity with

$$u_{si} \;\; = \;\; -sign(\sigma_i), \qquad i = 1, 2, \cdots, n, \tag{7.8}$$

$K(t) = diag(k_1(t), \cdots, k_n(t))$ is a diagonal gain matrix.

The continuous term $\mathbf{u}_v$ is generated by a class of first-order filters (denoted as LPF1)

$$T_1\dot{\mathbf{u}}_v + \mathbf{u}_v = \Gamma_1\mathbf{u}_s.$$

and is added to the control input once all system states enter the sliding mode at $t = t_r$ with zero initial condition $\mathbf{u}_v(t_r) = \mathbf{0}$ and $\mathbf{u}_v = [u_{v1}, u_{v2}, \cdots, u_{vn}]^T$. Parametric matrices $T_1 = diag(\tau_{11}, \tau_{12}, \cdots, \tau_{1n})$, $\Gamma_1 = diag(\gamma_{11}, \gamma_{12}, \cdots, \gamma_{1n})$ are positive definite and diagonal entries of Γ_1 are functions of $\mathbf{q}$, $\dot{\mathbf{q}}$, $\mathbf{q}_d$, $\dot{\mathbf{q}}_d$, $\ddot{\mathbf{q}}_d$, $\mathbf{q}_d^{(3)}$.

The component k_i of the gain matrix K is chosen as bellows

$$\begin{cases} k_i(t) \geq \left|\left[\tilde{M}(\mathbf{q})\ddot{\mathbf{q}}_r + \tilde{C}(\mathbf{q},\dot{\mathbf{q}})\dot{\mathbf{q}}_r + \tilde{\mathbf{g}}(\mathbf{q})\right]_i\right| + \varepsilon_i & \forall t \in [0, t_r] \\ k_i(t) = k_{il}(t) & \forall t \in (t_r, \infty) \end{cases} \tag{7.9}$$

where the constant ε_i are strictly positive and the diagonal elements of the matrix H=$diag(\varepsilon_1, \cdots, \varepsilon_n)$, t_r is the reaching time. $K(t) = K_l(t)$, $\forall t \in (t_r, \infty)$, are generated by another class of first-order filters (denoted as LPF2)

$$T_2\dot{K}_l + K_l = \Gamma_2 F(\boldsymbol{\sigma}), \tag{7.10}$$

$$F(\boldsymbol{\sigma}) = K_g|S|, \tag{7.11}$$

where the initial condition $K_l(t_r)$ is chosen to satisfy the 1st condition in equation (7.9); $|S| = diag(|\sigma_1|, \cdots, |\sigma_n|)$; $F(\boldsymbol{\sigma}) = diag(f_1(\sigma_1), f_2(\sigma_2), \cdots, f_n(\sigma_n))$ whose diagonal entry $f_i(\sigma_i)$ is a continuous even function of the switching surface σ_i, $f_i(\sigma_i) = 0$ only when $\sigma_i = 0$; $T_2 = diag(\tau_{21}, \tau_{22}, \cdots, \tau_{2n})$, $\Gamma_2 = diag(\gamma_{21}, \gamma_{22}, \cdots, \gamma_{2n})$, $K_g = diag(k_{g1}, k_{g2}, \cdots, k_{gn})$ whose diagonal entries are all positive constant parameters.

The schematic diagram of the proposed gain shaped control system is shown in *Fig.*7.1.

Remark 7.1. *Without using* $\mathbf{u}_v$*, and choosing*

$$k_i(t) \geq \left|\left[\tilde{M}(\mathbf{q})\ddot{\mathbf{q}}_r + \tilde{C}(\mathbf{q},\dot{\mathbf{q}})\dot{\mathbf{q}}_r + \tilde{\mathbf{g}}(\mathbf{q})\right]_i\right| + \varepsilon_i, \quad i = 1, 2, \cdots, n,$$

the reaching condition of the sliding mode is guaranteed by the switching control $K\mathbf{u}_s$. *In most SMC, after entering sliding mode,* $K\mathbf{u}_s$ *is kept invariant and chattering is incurred inevitably. The purpose of introducing LPF1 and LPF2 is to extract equivalent control and hence scale down the switching gain* $K(t)$.

7.3 Convergence Analysis

Since the variable structure control system exhibits distinct behavior in reaching and sliding phases, it is better to design different control schemes according to the two phases respectively. During reaching phase, it is mandatory to use high gain so as to ensure the global attractiveness of the switching surface. While in the sliding mode, however, it is possible to extract equivalent control signals from the switching control input by means of filtering techniques. Here we decompose the equivalent control $\mathbf{u}_{eq}$ into three components as

$$\mathbf{u}_{eq} = \mathbf{u}_{1eq} + \mathbf{u}_{2eq} + \mathbf{u}_{3eq} = \mathbf{u}_c + K(t)\mathbf{u}_{seq} + \mathbf{u}_v, \tag{7.12}$$

which consists of three known factors $\mathbf{u}_c \triangleq \mathbf{u}_{1eq}$, $K(t)$ as part of $\mathbf{u}_{2eq}$ and $\mathbf{u}_v \triangleq \mathbf{u}_{3eq}$. The unknown equivalent quantity $\mathbf{u}_{seq}$, which is a continuous average of the discontinuous term $\mathbf{u}_s$, reflects the influence of the system uncertainties or disturbances.

Comparing (7.5) and (7.12) we have

$$K(t)\mathbf{u}_{seq} + \mathbf{u}_v = -\left[\tilde{M}(\mathbf{q})\ddot{\mathbf{q}}_r + \tilde{C}(\mathbf{q},\dot{\mathbf{q}})\dot{\mathbf{q}}_r + \tilde{\mathbf{g}}(\mathbf{q})\right] \tag{7.13}$$

where $K(t) = K_l(t)$, $\forall t \geq t_r$. When the system is in the sliding mode, (7.4) is satisfied. Thus we can formulate the system uncertainties as

$$\begin{aligned}
\boldsymbol{\eta}(\mathbf{q},\dot{\mathbf{q}},\mathbf{q}_d,\dot{\mathbf{q}}_d,\ddot{\mathbf{q}}_d) &\triangleq \tilde{M}(\mathbf{q})\ddot{\mathbf{q}}_r + \tilde{C}(\mathbf{q},\dot{\mathbf{q}})\dot{\mathbf{q}}_r + \tilde{\mathbf{g}}(\mathbf{q}) = E(\mathbf{q},\dot{\mathbf{q}},\mathbf{q}_d,\dot{\mathbf{q}}_d,\ddot{\mathbf{q}}_d)\tilde{\mathbf{r}} \\
\dot{\boldsymbol{\eta}}(\mathbf{q},\dot{\mathbf{q}},\mathbf{q}_d,\dot{\mathbf{q}}_d,\ddot{\mathbf{q}}_d) &\triangleq \dot{\tilde{M}}(\mathbf{q})\ddot{\mathbf{q}}_r + \tilde{M}(\mathbf{q})\mathbf{q}_r^{(3)} + \dot{\tilde{C}}(\mathbf{q},\dot{\mathbf{q}})\dot{\mathbf{q}}_r + \tilde{C}(\mathbf{q},\dot{\mathbf{q}})\ddot{\mathbf{q}}_r + \dot{\tilde{\mathbf{g}}}(\mathbf{q}) \\
&= E_d(\mathbf{q},\dot{\mathbf{q}},\mathbf{q}_d,\dot{\mathbf{q}}_d,\ddot{\mathbf{q}}_d,\mathbf{q}_d^{(3)})\tilde{\mathbf{r}}
\end{aligned}$$

where E and E_d are $n \times p$ matrices, E_d is the derivative of E, $\tilde{\mathbf{r}} \in \mathcal{R}^p$ is the uncertain parameter vector which satisfies Assumption 7.1.

The relation (7.13) can be rewritten as

$$K(t)\mathbf{u}_{seq} + \mathbf{u}_v = -\boldsymbol{\eta}(\mathbf{q}, \dot{\mathbf{q}}, \mathbf{q}_d, \dot{\mathbf{q}}_d, \ddot{\mathbf{q}}_d) = -E(\mathbf{q}, \dot{\mathbf{q}}, \mathbf{q}_d, \dot{\mathbf{q}}_d, \ddot{\mathbf{q}}_d)\tilde{\mathbf{r}}. \tag{7.14}$$

If $\mathbf{u}_v$ can be made to approximate the system uncertainties $-\boldsymbol{\eta}$, the switching gain K can be significantly reduced without affecting the existence of the sliding mode. In terms of (7.13) the ultimate objectives of equivalent control are to achieve $\mathbf{u}_v = -\boldsymbol{\eta}$ and $K\mathbf{u}_{seq} = 0$. However, there are also theoretically infinite number of solutions for (7.13) in which $\mathbf{u}_v \neq -\boldsymbol{\eta}$ and thereafter $K\mathbf{u}_{seq} \neq 0$. In order to drive $\mathbf{u}_v$ to approach $-\boldsymbol{\eta}$, it is also necessary to scale down K to zero. The above discussion shows that both low-pass filters, LPF1 and LPF2, have to work concurrently aiming at acquiring equivalent control and nullifying the switching control gain simultaneously.

A positive Lyapunov function is chosen as

$$V(t) \;=\; \frac{1}{2}\boldsymbol{\sigma}^T M \boldsymbol{\sigma} > 0. \tag{7.15}$$

Note that the matrix $\dot{M} - 2C$ is a skew-symmetric matrix. Thus the derivative of V becomes

$$\dot{V}(t) = \boldsymbol{\sigma}^T M \dot{\boldsymbol{\sigma}} + \frac{1}{2}\boldsymbol{\sigma}^T \dot{M} \boldsymbol{\sigma} = \boldsymbol{\sigma}^T (M\ddot{\mathbf{q}} - M\ddot{\mathbf{q}}_r) + \boldsymbol{\sigma}^T C \boldsymbol{\sigma}$$

and substituting $M\ddot{\mathbf{q}}$ from the system dynamics,

$$\begin{aligned} M\ddot{\mathbf{q}} &= \mathbf{u} - C\dot{\mathbf{q}} - \mathbf{g} = \mathbf{u} - C(\boldsymbol{\sigma} + \dot{\mathbf{q}}_r) - \mathbf{g} \\ \Rightarrow \dot{V}(t) &= \boldsymbol{\sigma}^T (\mathbf{u} - M\ddot{\mathbf{q}}_r - C\dot{\mathbf{q}}_r - \mathbf{g}). \end{aligned} \tag{7.16}$$

In the rest of this section we will derive the sufficient conditions of maintaining the sliding mode when using the gain shaped SMC, which are summarized in following

two theorems. The convergence property of the control scheme (7.7) is guaranteed for both reaching phase and sliding phase respectively as shown below.

A. Convergence Analysis in the Reaching Phase

In the reaching phase ($t \in [0, t_r]$), $K(t)$ satisfies equation (7.9) and $\mathbf{u} = \mathbf{u}_c + K(t)\mathbf{u}_s$, the derivative of V satisfies $\dot{V}(t) \leq -\sum_{i=1}^{n} \varepsilon_i |\sigma_i|$. Thus the system is convergent during the reaching phase and the surface $\boldsymbol{\sigma} = \mathbf{0}$ is reached in finite time (Slotine and Li, 1991). The upper bound of the reaching time can be calculated as bellows. Consider the Lyapunov function given in (7.15)

$$V(t) = \frac{1}{2}\boldsymbol{\sigma}^T M \boldsymbol{\sigma} \leq \frac{1}{2}\lambda_{max}\boldsymbol{\sigma}^T\boldsymbol{\sigma} \qquad \Rightarrow \boldsymbol{\sigma}^T\boldsymbol{\sigma} \geq \sqrt{\frac{2V(t)}{\lambda_{max}}}, \tag{7.17}$$

where λ_{max} is maximum eigenvalue of the inertia matrix $M(\mathbf{q})$. Note that $V(t_r) = 0$ at the time system entering the sliding motion and $V(0) \leq \frac{1}{2}\lambda_{max}\boldsymbol{\sigma}(0)^T\boldsymbol{\sigma}(0)$. The derivative of V satisfies

$$\dot{V} \leq -\sum_{i=1}^{n} \varepsilon_i |\sigma_i| \leq -\varepsilon_{min} \sum_{i=1}^{n} |\sigma_i| \leq -\varepsilon_{min}\sqrt{\boldsymbol{\sigma}^T\boldsymbol{\sigma}} \leq -\varepsilon_{min}\sqrt{\frac{2V}{\lambda_{max}}}. \tag{7.18}$$

By integrating equation (7.18)

$$\int_0^{t_r} \frac{\dot{V}}{\sqrt{V}} dt \leq -\int_0^{t_r} \varepsilon_{min}\sqrt{\frac{2}{\lambda_{max}}} dt, \quad \Rightarrow 2\sqrt{V} \,|_{V(0)}^{V(t_r)} \leq -(\varepsilon_{min}\sqrt{\frac{2}{\lambda_{max}}})t_r$$

$$\begin{aligned} -2\sqrt{V(0)} &\leq -(\varepsilon_{min}\sqrt{\frac{2}{\lambda_{max}}})t_r \\ \Rightarrow t_r &\leq \frac{2\sqrt{V(0)}\sqrt{\frac{\lambda_{max}}{2}}}{\varepsilon_{min}} \leq \frac{\lambda_{max}}{\varepsilon_{min}}\sqrt{\boldsymbol{\sigma}(0)^T\boldsymbol{\sigma}(0)}. \end{aligned} \tag{7.19}$$

Note that (7.19) is a conservative estimate, in practical, the real reaching time could be far less than the value derived in (7.19).

B. Convergence Analysis in the Sliding Phase

Theorem 7.1. *Assume that the control system is in the sliding mode at $t = t_r$, if the condition $|\mathbf{u}_{seq}(t)| < \boldsymbol{\theta}$, $\forall t > t_r$ holds, where $\boldsymbol{\theta} = [1, 1, \cdots, 1]^T$ is an n-vector, then the sliding mode retains $\forall t > t_r$.*

Proof: Using equations (7.6), (7.7) and (7.13), the derivative of V becomes

$$\begin{aligned}\dot{V}(t) &= \boldsymbol{\sigma}^T(\mathbf{u} - M\ddot{\mathbf{q}}_r - C\dot{\mathbf{q}}_r - \mathbf{g}) = \boldsymbol{\sigma}^T\left[\mathbf{u}_c + K(t)\mathbf{u}_s + \mathbf{u}_v - M\ddot{\mathbf{q}}_r - C\dot{\mathbf{q}}_r - \mathbf{g}\right] \\ &= \boldsymbol{\sigma}^T\left[K(t)\mathbf{u}_s + \mathbf{u}_v + (\tilde{M}\ddot{\mathbf{q}}_r + \tilde{C}\dot{\mathbf{q}}_r + \tilde{\mathbf{g}})\right] \\ &= \boldsymbol{\sigma}^T\left[K(t)\mathbf{u}_s - K(t)\mathbf{u}_{seq}\right] \leq -\sum_{i=1}^{n} k_i(t)\left[1 - |u_{seqi}(t)|\right]|\sigma_i|.\end{aligned}$$

In the case that $k_i(t) \neq 0$ and $|u_{seqi}(t)| < 1$, $i = 1, 2, \cdots, n$, then $\dot{V} < 0$ and σ_i will converge to zero. In case $k_i(t) = k_{li}(t) = 0$, $i = 1, 2, \cdots, n$, from relation (7.10) we can see that $\sigma_i = 0$ and system is already in sliding mode.

Theorem 7.2. *If the parametric matrices of the filters T_1, Γ_1, T_2 are chosen to satisfy the following conditions*

$$\begin{cases} T_2 \geq T_1 \\ \Gamma_1\boldsymbol{\theta} \geq \alpha|E|\bar{\mathbf{r}} + T_1|E_d|\bar{\mathbf{r}} + \boldsymbol{\rho} \end{cases} \tag{7.20}$$

then $|\mathbf{u}_{seq}(t)| < \boldsymbol{\theta}$, $\forall t > t_r$, where $\alpha > 1$ is a constant, $\boldsymbol{\theta} = [1, 1, \cdots, 1]^T$ is an n-vector with each element equal one and $\boldsymbol{\rho} = [\rho_1, \cdots, \rho_n]^T$, $\rho_i > 0$, $i = 1, \cdots, n$, is a constant.

Proof: When the system is in the sliding mode, the following equation holds

$$T_1\dot{\mathbf{u}}_v + \mathbf{u}_v = \Gamma_1\mathbf{u}_{seq}. \tag{7.21}$$

In order to explore the dynamic relationship among $\mathbf{u}_{seq}$, $\mathbf{d}$ and $\mathbf{u}_v$ specified by equation (7.14), taking the derivative of equation (7.14) yields

$$\dot{K}(t)\mathbf{u}_{seq} + K(t)\dot{\mathbf{u}}_{seq} + \dot{\mathbf{u}}_v = -\dot{\boldsymbol{\eta}} = -E_d(\mathbf{q}, \dot{\mathbf{q}}, \mathbf{q}_d, \dot{\mathbf{q}}_d, \ddot{\mathbf{q}}_d, \mathbf{q}_d^{(3)})\tilde{\mathbf{r}}. \tag{7.22}$$

Substituting (7.10), (7.14) and (7.21) into (7.22) leads to

$$\begin{aligned}K(t)\dot{\mathbf{u}}_{seq} + \left[T_2^{-1}\Gamma_2 F(\boldsymbol{\sigma}) + T_1^{-1}\Gamma_1 + T_1^{-1}K(t) - T_2^{-1}K(t)\right]\mathbf{u}_{seq} \\ = -(T_1^{-1}\boldsymbol{\eta} + \dot{\boldsymbol{\eta}}) = -(T_1^{-1}E\tilde{\mathbf{r}} + E_d\tilde{\mathbf{r}}).\end{aligned} \tag{7.23}$$

Define $N(t) = T_2^{-1}\Gamma_2 F(\boldsymbol{\sigma}) + T_1^{-1}\Gamma_1 + T_1^{-1}K(t) - T_2^{-1}K(t)$. Since matrices $K(t)$, T_1, T_2, Γ_1, Γ_2 and function $F(\boldsymbol{\sigma})$ are positive definite, if we choose $T_2 \geq T_1$, i.e. the first condition of (7.20), then

$$\begin{aligned} N(t) &= T_2^{-1}\Gamma_2 F(\boldsymbol{\sigma}) + T_1^{-1}\Gamma_1 + T_1^{-1}K(t) - T_2^{-1}K(t) \\ &\geq N_{min} \triangleq T_1^{-1}\Gamma_1 > \mathbf{0}. \end{aligned} \tag{7.24}$$

Now rewrite (7.23) as

$$\begin{aligned} K(t)\dot{\mathbf{u}}_{seq} + N(t)\mathbf{u}_{seq} &= -(T_1^{-1}E\tilde{\mathbf{r}} + E_d\tilde{\mathbf{r}}) \\ \dot{\mathbf{u}}_{seq} &= -K(t)^{-1}N(t)\mathbf{u}_{seq} - K(t)^{-1}(T_1^{-1}E\tilde{\mathbf{r}} + E_d\tilde{\mathbf{r}}). \end{aligned} \tag{7.25}$$

Since $\mathbf{u}_v(t_r) = \mathbf{0}$, according to (7.9) and (7.14), the absolute value of $\mathbf{u}_{seq}$ at $t = t_r$ is

$$\begin{aligned} |\mathbf{u}_{seq}(t_r)| &= \left|-K(t_r)^{-1}\left[E(\mathbf{q},\dot{\mathbf{q}},\mathbf{q}_d,\dot{\mathbf{q}}_d,\ddot{\mathbf{q}}_d)\tilde{\mathbf{r}} + \mathbf{u}_v(t_r)\right]\right| \\ &= \left|K(t_r)^{-1}E(\mathbf{q},\dot{\mathbf{q}},\mathbf{q}_d,\dot{\mathbf{q}}_d,\ddot{\mathbf{q}}_d)\tilde{\mathbf{r}}\right| \\ &\leq \left[\frac{\left|\left[\tilde{M}\ddot{\mathbf{q}}_r + \tilde{C}\dot{\mathbf{q}}_r + \tilde{\mathbf{g}}\right]_1\right|}{\left|\left[\tilde{M}\ddot{\mathbf{q}}_r + \tilde{C}\dot{\mathbf{q}}_r + \tilde{\mathbf{g}}\right]_1\right| + \varepsilon_1}, \cdots, \frac{\left|\left[\tilde{M}\ddot{\mathbf{q}}_r + \tilde{C}\dot{\mathbf{q}}_r + \tilde{\mathbf{g}}\right]_n\right|}{\left|\left[\tilde{M}\ddot{\mathbf{q}}_r + \tilde{C}\dot{\mathbf{q}}_r + \tilde{\mathbf{g}}\right]_n\right| + \varepsilon_n}\right]^T \\ &< \boldsymbol{\theta}. \end{aligned} \tag{7.26}$$

The solution of (7.25) at time $t \geq t_r$ is as the following,

$$\begin{aligned} \mathbf{u}_{seq}(t) &= e^{-\int_{t_r}^{t} K(\tau)^{-1}N(\tau)d\tau}\mathbf{u}_{seq}(t_r) \\ &\quad + \int_{t_r}^{t} e^{-\int_{\tau}^{t} K(s)^{-1}N(s)ds}K(\tau)^{-1}\left[-(T_1^{-1}E\tilde{\mathbf{r}} + E_d\tilde{\mathbf{r}})\right]d\tau. \end{aligned}$$

Using inequality (7.24) we obtain the upper bound of $|\mathbf{u}_{seq}(t)|$

$$\begin{aligned} |\mathbf{u}_{seq}(t)| &\leq e^{-\int_{t_r}^{t} K(\tau)^{-1}N_{min}d\tau}\,|\mathbf{u}_{seq}(t_r)| \\ &\quad + \int_{t_r}^{t} e^{-\int_{\tau}^{t} K(s)^{-1}N_{min}ds}K(\tau)^{-1}\left|T_1^{-1}E\tilde{\mathbf{r}} + E_d\tilde{\mathbf{r}}\right|d\tau \\ &\leq e^{-\int_{t_r}^{t} K(\tau)^{-1}N_{min}d\tau}|\mathbf{u}_{seq}(t_r)| \end{aligned}$$

$$
\begin{aligned}
&+\int_{t_r}^{t} e^{-\int_{\tau}^{t} K(s)^{-1}N_{min}ds}\left[K(\tau)^{-1}N_{min}\right]N_{min}^{-1}\left|T_1^{-1}E\tilde{\mathbf{r}}+E_d\tilde{\mathbf{r}}\right|d\tau\\
\leq\ & e^{-\int_{t_r}^{t} K(\tau)^{-1}N_{min}d\tau}|\mathbf{u}_{seq}(t_r)|\\
&+\int_{t_r}^{t} e^{-\int_{\tau}^{t} K(s)^{-1}N_{min}ds}\left[K(\tau)^{-1}N_{min}\right]N_{min}^{-1}(T_1^{-1}|E|\bar{\mathbf{r}}+|E_d|\bar{\mathbf{r}})d\tau\\
=\ & e^{-\int_{t_r}^{t} K(\tau)^{-1}N_{min}d\tau}|\mathbf{u}_{seq}(t_r)|\\
&+\int_{t_r}^{t} e^{-\int_{\tau}^{t} K(s)^{-1}N_{min}ds}\left[K(\tau)^{-1}N_{min}\right]\Gamma_1^{-1}(|E|\bar{\mathbf{r}}+T_1|E_d|\bar{\mathbf{r}})d\tau. \qquad (7.27)
\end{aligned}
$$

If we choose $\Gamma_1\boldsymbol{\theta} \geq \alpha|E|\bar{\mathbf{r}}+T_1|E_d|\bar{\mathbf{r}}+\boldsymbol{\rho} > |E|\bar{\mathbf{r}}+T_1|E_d|\bar{\mathbf{r}}$, namely the second condition of (7.20), then $\Gamma_1^{-1}(|E|\bar{\mathbf{r}}+T_1|E_d|\bar{\mathbf{r}}) < \boldsymbol{\theta}$. Thus (7.27) becomes

$$
\begin{aligned}
|\mathbf{u}_{seq}(t)| \ <\ & e^{-\int_{t_r}^{t} K(\tau)^{-1}N_{min}d\tau}|\mathbf{u}_{seq}(t_r)|\\
&+\int_{t_r}^{t} e^{-\int_{\tau}^{t} K(s)^{-1}N_{min}ds}\left[K(\tau)^{-1}N_{min}\right]d\tau\boldsymbol{\theta}. \qquad (7.28)
\end{aligned}
$$

Define $\boldsymbol{\phi}(\tau) = N_{min}^{-1}K(\tau)$, a diagonal matrix whose diagonal elements $\phi_i(\tau)$, $i = 1, 2, \cdots, n$, are all continuous and positive functions over the interval $[t_r, t]$. Consider $\Phi(t)-\Phi(t_r) = \int_{t_r}^{t}\boldsymbol{\phi}(s)^{-1}ds$, then $\dot{\Phi}(t) = \boldsymbol{\phi}(t)^{-1}$ and $\int_{t_r}^{t}\boldsymbol{\phi}(\tau)^{-1}d\tau = \Phi(t)-\Phi(t_r)$. In the sequel

$$
\begin{aligned}
\int_{t_r}^{t} e^{-\int_{\tau}^{t}\boldsymbol{\phi}(s)^{-1}ds}\boldsymbol{\phi}(\tau)^{-1}d\tau \ &= \ \int_{t_r}^{t} e^{\Phi(\tau)-\Phi(t)}\boldsymbol{\phi}(\tau)^{-1}d\tau = e^{-\Phi(t)}\int_{t_r}^{t} e^{\Phi(\tau)}\boldsymbol{\phi}(\tau)^{-1}d\tau\\
&= \ e^{-\Phi(t)}\int_{t_r}^{t} e^{\Phi(\tau)}d\Phi(\tau) = e^{-\Phi(t)}e^{\Phi(\tau)}\ |_{t_r}^{t}\\
&= \ I - e^{[\Phi(t_r)-\Phi(t)]} = I - e^{-\int_{t_r}^{t}\boldsymbol{\phi}(\tau)^{-1}d\tau}. \qquad (7.29)
\end{aligned}
$$

Using (7.26) and (7.29), then (7.28) becomes

$$
\begin{aligned}
|\mathbf{u}_{seq}(t)| \ <\ & e^{-\int_{t_r}^{t}\boldsymbol{\phi}(\tau)^{-1}d\tau}|\mathbf{u}_{seq}(t_r)| + \int_{t_r}^{t} e^{-\int_{\tau}^{t}\boldsymbol{\phi}(s)^{-1}ds}\boldsymbol{\phi}(\tau)^{-1}d\tau\boldsymbol{\theta}\\
<\ & e^{-\int_{t_r}^{t}\boldsymbol{\phi}(\tau)^{-1}d\tau}|\mathbf{u}_{seq}(t_r)| + (I - e^{-\int_{t_r}^{t}\boldsymbol{\phi}(\tau)^{-1}d\tau})\boldsymbol{\theta}\\
=\ & e^{-\int_{t_r}^{t} K(\tau)^{-1}N_{min}d\tau}|\mathbf{u}_{seq}(t_r)| + (I - e^{-\int_{t_r}^{t} K(\tau)^{-1}N_{min}d\tau})\boldsymbol{\theta}\\
<\ & e^{-\int_{t_r}^{t} K(\tau)^{-1}N_{min}d\tau}\boldsymbol{\theta} + (I - e^{-\int_{t_r}^{t} K(\tau)^{-1}N_{min}d\tau})\boldsymbol{\theta} = \boldsymbol{\theta}.
\end{aligned}
$$

Remark 7.2. *Note that (7.20) only shows the lower bound of Γ_1 and the relationship between T_1 and T_2. Therefore there are degrees of freedom in the selection*

of the two classes of filters' parameters T_1, Γ_1, T_2 and Γ_2 to further improve the system performance. A possible and practical way of designing LPF1 and LPF2 is to incorporate the system knowledge in frequency domain. For instance, from the point of achieving equivalent control in frequency domain, T_1 should be made as small as possible so as to increase the bandwidth of LPF1 to capture $\mathbf{u}_{eq}$ faithfully. T_2 and Γ_2 will affect the attenuating rate of the switching gain $K(t)$ after entering the sliding motion. A smaller T_2 will render a faster reduction in $K(t)$. Let us further consider extreme cases where an abrupt change in system occurs and violates the sliding mode condition. In such circumstance, the most important thing is to restore the switching gain to the necessary level, thereafter force the system reenter the sliding motion. It is immediately obvious that a small T_2, a large Γ_2 and a fast increasing function $F(\cdot)$ with respect to $\boldsymbol{\sigma}$ will facilitate the switching gain recovery.

Remark 7.3. *As a typical kind of nonlinear and discontinuous control strategies, SMC has to be implemented using digital techniques and sampling rate needs to be taken into account. In digital control it is well known, as a rule of thumb, that the Nyquist frequency should be at least 20 times higher than the control system bandwidth. As a consequence, the lower bounds of T_1 and T_2 should be $10 \sim 20$ times of the sampling interval. In other words, the control system can only deal with nonlinearities, uncertainties and tracking tasks within its bandwidth. LPF1 can only learn low frequency components in $\mathbf{u}_{eq}$ within its bandwidth. Most practical systems do meet this requirement as they can be characterized as low-pass filters themselves. Since most high frequency components in $\mathbf{u}_{eq}$ are actually dominated by system noise or measurement noise, characterized by low-pass filters LPF1 and LPF2, the gain shaped SMC are able to work well under such a noisy control environment.*

7.4 Sliding Motion Recovery Analysis in Case of Disturbance Surging

In this section, let us consider the disturbance surging problem, namely, there is an abrupt change in parametric uncertainty or disturbance which violates the sliding mode existence condition. This situation may occur because the gain K may have been shaped to a very low level while in the sliding mode. In such circumstance, the most important thing is to force the system reenter the sliding motion by restoring the switching gain to the necessary level. Assume that the system is already in the sliding mode up to t_1, $|\mathbf{u}_v(t_1)| = |\boldsymbol{\eta}_2(\mathbf{q}, \dot{\mathbf{q}}, \mathbf{q}_d, \dot{\mathbf{q}}_d, \ddot{\mathbf{q}}_d)| = E(\mathbf{q}, \dot{\mathbf{q}}, \mathbf{q}_d, \dot{\mathbf{q}}_d, \ddot{\mathbf{q}}_d)\tilde{\mathbf{r}}_2$ and $K(t_1) = 0$. As shown in $Fig.7.2(a)$, at time $t = t_1$ a parametric disturbance occurs abruptly within the parameter upbound of $\bar{\mathbf{r}}$. If $\mathbf{u}_v(t_1^-) \neq -\left[\boldsymbol{\eta}_2(\mathbf{q}, \dot{\mathbf{q}}, \mathbf{q}_d, \dot{\mathbf{q}}_d, \ddot{\mathbf{q}}_d)|_{t=t_1^+}\right]$, then $|\dot{\boldsymbol{\sigma}}| \neq \mathbf{0} \Rightarrow |\boldsymbol{\sigma}| > \mathbf{0}$. The system will leave the sliding surface $\boldsymbol{\sigma} = \mathbf{0}$ as shown in $Fig.7.2(b)$. In the following we show that the sliding motion can be recovered in a finite period by the proposed gain shaping mechanism when there is an abrupt change in parametric uncertainty.

Theorem 7.3. *Assume that at time $t = t_1$, the system leaves the sliding surface due to a parametric uncertainty surging. $\exists t_2 \in (t_1, t_3]$, $t_3 < \infty$, such that $\forall t \geq t_2$, $\dot{V} \leq -|\boldsymbol{\sigma}|^T \boldsymbol{\rho}$, and the sliding motion recovery will be achieved at a finite time $t_3 \geq t_2$.*

Proof: At time $t \in (t_1, t_3]$, LPF1 and LPF2 ($K_l(t) = K(t)$) can be written as

$$
\begin{aligned}
T_1\dot{\mathbf{u}}_v + \mathbf{u}_v &= -\Gamma_1 sign(\boldsymbol{\sigma}), \qquad T_2\dot{K} + K = \Gamma_2 F(\boldsymbol{\sigma}) \\
\mathbf{u}_v(t) &= e^{-T_1^{-1}(t-t_1)}\mathbf{u}_v(t_1) + \int_{t_1}^{t} e^{-T_1^{-1}(t-\tau)}(-T_1^{-1}\Gamma_1 sign(\boldsymbol{\sigma}))d\tau \quad (7.30) \\
K(t) &= e^{-T_2^{-1}(t-t_1)}K(t_1) + \int_{t_1}^{t} e^{-T_2^{-1}(t-\tau)}T_2^{-1}\Gamma_2 F(\boldsymbol{\sigma})d\tau \\
&= \int_{t_1}^{t} e^{-T_2^{-1}(t-\tau)}T_2^{-1}\Gamma_2 K_g|S|d\tau, \quad (7.31)
\end{aligned}
$$

where $K(t_1) = \mathbf{0}$. Using (7.2), (7.20), (7.30) and (7.31), the derivative of the Lyapunov function becomes ($t > t_1$)

$$\begin{aligned}
\dot{V} &= \boldsymbol{\sigma}^T M\dot{\boldsymbol{\sigma}} + \frac{1}{2}\boldsymbol{\sigma}^T\dot{M}\boldsymbol{\sigma} = \boldsymbol{\sigma}^T M\dot{\boldsymbol{\sigma}} + \boldsymbol{\sigma}^T C\boldsymbol{\sigma} = \boldsymbol{\sigma}^T(M\ddot{\mathbf{q}} - M\ddot{\mathbf{q}}_r) + \boldsymbol{\sigma}^T C\boldsymbol{\sigma} \\
&= \boldsymbol{\sigma}^T(\mathbf{u} - M\ddot{\mathbf{q}}_r - C\dot{\mathbf{q}}_r - \mathbf{g}) = \boldsymbol{\sigma}^T(\mathbf{u}_c + K\mathbf{u}_s + \mathbf{u}_v - M\ddot{\mathbf{q}}_r - C\dot{\mathbf{q}}_r - \mathbf{g}) \\
&= \boldsymbol{\sigma}^T(K\mathbf{u}_s + \mathbf{u}_v + E\tilde{\mathbf{r}}_2) = \boldsymbol{\sigma}^T(-Ksign(\boldsymbol{\sigma}) + \mathbf{u}_v + E\tilde{\mathbf{r}}_2) \\
&= -|\boldsymbol{\sigma}|^T \int_{t_1}^{t} e^{-T_2^{-1}(t-\tau)} T_2^{-1}\Gamma_2 K_g |S| d\tau\boldsymbol{\theta} + \boldsymbol{\sigma}^T e^{-T_1^{-1}(t-t_1)}\mathbf{u}_v(t_1) \\
&\quad + \boldsymbol{\sigma}^T \int_{t_1}^{t} e^{-T_1^{-1}(t-\tau)}(-T_1^{-1}\Gamma_1 sign(\boldsymbol{\sigma}))d\tau + \boldsymbol{\sigma}^T E\tilde{\mathbf{r}}_2 \\
&\leq -|\boldsymbol{\sigma}|^T \int_{t_1}^{t} e^{-T_2^{-1}(t-\tau)} T_2^{-1}\Gamma_2 K_g |S| d\tau\boldsymbol{\theta} - |\boldsymbol{\sigma}|^T \int_{t_1}^{t} e^{-T_1^{-1}(t-\tau)}(T_1^{-1}\Gamma_1\boldsymbol{\theta})d\tau \\
&\quad + |\boldsymbol{\sigma}|^T e^{-T_1^{-1}(t-t_1)}|\mathbf{u}_v(t_1)| + |\boldsymbol{\sigma}|^T |E|\bar{\mathbf{r}} \\
&= -|\boldsymbol{\sigma}|^T \left[\int_{t_1}^{t} e^{-T_2^{-1}(t-\tau)} T_2^{-1}\Gamma_2 K_g |S| d\tau\boldsymbol{\theta} - e^{-T_1^{-1}(t-t_1)}|\mathbf{u}_v(t_1)|\right] \\
&\quad -|\boldsymbol{\sigma}|^T \left[(I - e^{-T_1^{-1}(t-t_1)})\Gamma_1\boldsymbol{\theta} - |E|\bar{\mathbf{r}})\right] \\
&\leq -|\boldsymbol{\sigma}|^T \left[\int_{t_1}^{t} e^{-T_2^{-1}(t-\tau)} T_2^{-1}\Gamma_2 K_g |S| d\tau\boldsymbol{\theta} - e^{-T_1^{-1}(t-t_1)}|\mathbf{u}_v(t_1)|\right] \\
&\quad -|\boldsymbol{\sigma}|^T \left[(I - e^{-T_1^{-1}(t-t_1)})(\alpha|E|\bar{\mathbf{r}} + \boldsymbol{\rho}) - |E|\bar{\mathbf{r}})\right] \\
&= -|\boldsymbol{\sigma}|^T (I - e^{-T_1^{-1}(t-t_1)})\boldsymbol{\rho} \\
&\quad -|\boldsymbol{\sigma}|^T \left[\int_{t_1}^{t} e^{-T_2^{-1}(t-\tau)} T_2^{-1}\Gamma_2 K_g |S| d\tau\boldsymbol{\theta} - e^{-T_1^{-1}(t-t_1)}|\mathbf{u}_v(t_1)|\right] \\
&\quad -|\boldsymbol{\sigma}|^T \left[(\alpha I - I - \alpha e^{-T_1^{-1}(t-t_1)})|E|\bar{\mathbf{r}}\right]. \qquad (7.32)
\end{aligned}$$

Note that the passivity property of the robotic manipulators holds for the torque $\mathbf{u}$ and velocity $\dot{\mathbf{q}}$. In the worst case we will still have finite energy injection over a finite period by the saturated actuation $\mathbf{u}^*$. Thus $\dot{\mathbf{q}}$ is finite for any finite period, in the sequel $\mathbf{q}$, $\ddot{\mathbf{q}}$ and $\boldsymbol{\sigma}(t)$ are all finite for any finite $t \in [t_1, \infty)$. According to the last line of (7.32), $e^{-T_1^{-1}(t-t_1)}$ is monotonously decaying, thus $\exists t_\sigma > t_1$ and $\exists t_\gamma > t_1$ such that

$$\int_{t_1}^{t_\sigma} e^{-T_2^{-1}(t_\sigma-\tau)} T_2^{-1}\Gamma_2 K_g |S| d\tau\boldsymbol{\theta} - e^{-T_1^{-1}(t_\sigma-t_1)}|\mathbf{u}_v(t_1)| \geq \mathbf{0},$$

and

$$\alpha I - I - \alpha e^{-T_1^{-1}(t_\gamma - t_1)} \geq \mathbf{0}$$

Therefore $\exists t_2 = max\{t_\sigma, t_\gamma\} < \infty$, such that $\forall t > t_2$ (7.32) becomes

$$\dot{V} \leq -|\boldsymbol{\sigma}|^T (I - e^{-T_1^{-1}(t_2 - t_1)})\boldsymbol{\rho}. \tag{7.33}$$

Finally, the recovery time will be

$$t_3 \leq t_2 + \frac{\lambda_{max}}{\left[(I - e^{-T_1^{-1}(t_2 - t_1)})\boldsymbol{\rho}\right]_{min}} \sqrt{\boldsymbol{\sigma}(t_2)^T \boldsymbol{\sigma}(t_2)}.$$

7.5 Illustrative Example

Consider a planar, two-link, articulated robotic manipulator in the vertical plane whose dynamics can be written as

$$\begin{bmatrix} h_{11} & h_{12} \\ h_{21} & h_{22} \end{bmatrix} \begin{bmatrix} \ddot{q}_1 \\ \ddot{q}_2 \end{bmatrix} + \begin{bmatrix} -h\dot{q}_2 & -h(\dot{q}_1 + \dot{q}_2) \\ -h\dot{q}_1 & 0 \end{bmatrix} \begin{bmatrix} \dot{q}_1 \\ \dot{q}_2 \end{bmatrix} + \begin{bmatrix} g_1 \\ g_2 \end{bmatrix} = \begin{bmatrix} u_1 \\ u_2 \end{bmatrix}.$$

with $\mathbf{q} = [q_1, q_2]^T$ being the two joint angular displacements, $\mathbf{u} = [u_1, u_2]^T$ being the joint inputs, and

$$\begin{aligned}
h_{11} &= I_1 + m_1 l_{c1}^2 + I_2 + m_2 l_{c2}^2 + m_2 l_1^2 + 2m_2 l_1 l_{c2} cos(q_2) \stackrel{\triangle}{=} c_1 + c_2 cos(q_2) \\
h_{12} &= h_{21} = I_2 + m_2 l_{c2}^2 + m_2 l_1 l_{c2} cos(q_2) \stackrel{\triangle}{=} c_3 + c_4 cos(q_2) \\
h_{22} &= I_2 + m_2 l_{c2}^2 \stackrel{\triangle}{=} c_3 \\
h &= m_2 l_1 l_{c2} sin(q_2) \stackrel{\triangle}{=} c_4 sin(q_2) \\
g_1 &= m_1 l_{c1} g cos(q_1) + m_2 g \left[l_{c2} cos(q_1 + q_2) + l_1 cos(q_1) \right] \\
&\stackrel{\triangle}{=} c_5 cos(q_1) + c_6 cos(q_1 + q_2) \\
g_2 &= m_2 l_{c2} g cos(q_1 + q_2) \stackrel{\triangle}{=} c_6 cos(q_1 + q_2).
\end{aligned}$$

In the model, the second terms represent all Centripetal, Coriolis and gravity terms. The pairs $\{m_1, m_2\}$, $\{I_1, I_2\}$, $\{l_1, l_2\}$, $\{l_{c1}, l_{c2}\}$ are the masses, moments of inertia,

lengths, center of gravity coordinates of the two robotic arms respectively. The coefficients $\{c_1, \cdots, c_6\}$ are appropriate unknown constants. For simplicity, the unknown payload is also included in m_2. In the simulation, the following values are assigned to the parameters: $m_1 = 4kg$, $m_2 = 3kg$, $l_1 = 0.5m$, $l_2 = 0.5m$, $l_{c1} = 0.3m$, $l_{c2} = 0.25m$, $I_1 = 0.4kg \cdot m^2$, $I_2 = 0.25kg \cdot m^2$, $g = 9.8N/kg$. In the controller design we assume a maximum uncertainties of 50% on the mass properties of the 2nd robot link of the system. The robot initially resets at $q_1(0) = 30°$; $q_2(0) = 120°$, is commanded a desired trajectory $q_{1d}(t) = 30° \left[1 - cos(2\pi t)\right]$ and $q_{2d}(t) = 45° \left[1 - cos(2\pi t)\right]$. The sampling interval is $T_s = 1msec$.

Case 1: Conventional SMC.

In order to compare the proposed scheme with the conventional SMC method, a basic sliding mode controller is designed for the two-link robotic manipulator

$$\begin{aligned} \mathbf{u} &= \hat{M}\ddot{\mathbf{q}}_r + \hat{C}\dot{\mathbf{q}}_r + \hat{\mathbf{g}} + \mathbf{u}_{sign} \\ \mathbf{u}_{sign} &= -Ksign(\boldsymbol{\sigma}) = [k_1 sign(-\sigma_1), k_2 sign(-\sigma_2)]^T. \end{aligned} \tag{7.34}$$

The switching surface is

$$\boldsymbol{\sigma} = \dot{\tilde{\mathbf{q}}} + \Lambda\tilde{\mathbf{q}} = \dot{\mathbf{q}} - \dot{\mathbf{q}}_r$$

where $\dot{\mathbf{q}}_r = \dot{\mathbf{q}}_d - \Lambda\tilde{\mathbf{q}}$ and $\Lambda = 5I$. The control gain is chosen as

$$k_i(t) = \left| \left[\tilde{M}(\mathbf{q})\ddot{\mathbf{q}}_r + \tilde{C}(\mathbf{q}, \dot{\mathbf{q}})\dot{\mathbf{q}}_r + \tilde{\mathbf{g}} \right]_i \right| + \varepsilon_i, \qquad i = 1, 2, \tag{7.35}$$

where $\varepsilon_1 = \varepsilon_2 = 1$, $\tilde{M} = \hat{M} - M$, $\tilde{C} = \hat{C} - C$, $\tilde{\mathbf{g}} = \hat{\mathbf{g}} - \mathbf{g}$. The corresponding position errors and control torques are plotted in $Fig.7.3$ and $Fig.7.4$. From figures we find that the chattering phenomenon appears. This is due to the large switching gain K used and the discontinuities of control signals crossing the sliding surfaces.

Case 2: SMC with passive smoothing scheme.

To alleviate the high-frequency phenomenon of control torque, the smoothing method using saturation function, as one of the most widely used passive SMC

methods, is implemented by replacing the signum function $\mathbf{u}_{sign}$ in control (7.34) with the following saturation function

$$\mathbf{u}_{sat} = [k_1 sat(\sigma_1/\varphi_1), k_2 sat(\sigma_2/\varphi_2)]^T, \tag{7.36}$$

where φ_1 and φ_2 are the boundary layers. The tracking accuracy and the smoothness of control signal are compared in $Fig.7.5$ and $Fig.7.6$ where $\varphi_1 = \varphi_2 = 0.5$ and $\varphi_1 = \varphi_2 = 0.05$ respectively. The thinner the boundary layer, the better the tracking accuracy; the wider the boundary layer, the smoother the control signal. This is a reasonable compromise which makes balance between torque smoothness and tracking accuracy. Note that, within the boundary layer, the system is under proportional control and sliding mode is not guaranteed.

Case 3: The proposed gain shaped SMC with filtering.

In the new gain shaped SMC scheme (7.7), we adopt the filtering techniques to generate the smooth and continuous control signal by automatically reducing the switching gain without destroying the existence condition of the sliding motion and in the sequel achieve better performance. The parameters chosen for the two classes of low-pass filters are: (1) $T_1 = T_2 = diag(0.1, 0.1)$ which is larger than the lower bounds discussed in 7.3; (2) $\Gamma_2 = diag(1, 1)$; (3) $F(\boldsymbol{\sigma}) = diag(|\sigma_1|, |\sigma_2|)$, where $K_g = I_2$; (4) $\Gamma_1[1, 1]^T = \alpha|E|\bar{\mathbf{r}} + T_1|E_d|\bar{\mathbf{r}} + \boldsymbol{\rho}$, where $\alpha = 1.1$ and $\boldsymbol{\rho} = [1, 1]^T$.

From $Fig.7.7$ (a) and (b), the desired control signal is apparently smoother than that of the conventional SMC scheme and smoother than SMC with boundary layer $\varphi_1 = \varphi_2 = 0.05$. The chattering of control torque u_2 observed in $Fig.7.7$ (b) is caused by the fact that σ_2 reaches the sliding surface ahead of σ_1. Therefore, the control system is a conventional SMC until the first time it reaches the switching surface $\sigma_1 = 0$, where $t_r = 0.475$ *sec.* From $Fig.7.7$ (c) and (d), note that the bandwidth of filtered control profiles which are the estimation of the uncertainties is dominated by $1Hz$ and is much lower than the cut-off frequency $\omega_{1c} = \omega_{2c} = 10Hz$

of LPF1. $Fig.7.8$ shows the fast attenuation of the switching gain $K(t)$ using LPF2. Due to imperfect factors in sliding mode such as limited sampling rate, the switching gain will not disappear completely. However, comparing with the initial value $K_l(t_r) = [27.8, 25.9]^T$, the effect of gain shaping is immediately obvious.

$Fig.7.7$ also demonstrates the appreciated results: chattering has been reduced substantially after a short transient period, the control profiles are much smoother than those of conventional SMC and SMC with boundary layer $\varphi_1 = \varphi_2 = 0.05$. $Fig.7.9$ further confirms the tracking accuracy under the proposed scheme. It shows that the tracking error in $Fig.7.9$ (b) is about one tenth of that of conventional SMC and SMC with saturation function. Moreover, the sliding motion is guaranteed even when $K(t)$ is shaped near to zero, which implies that the equivalent control is realized.

$Fig.7.10(a)(b)$ shows that the sliding motion can be recovered about 0.5 *sec* after the parametric uncertainty surge at time $t = 2.5$ *sec*. In this case, the parametric uncertainty is varied from 40% to 25% of the nominal mass properties of the robotics. At the same time, the gain K is automatically scaled up and down by LPF2 as shown in $Fig.7.10(c)(d)$.

7.6 Conclusions

In this chapter, in the controller design of robotic manipulators, filtering techniques are incorporated into sliding mode control to shape the switching control gain and to acquire equivalent control in the presence of bounded system uncertainties. The proposed control scheme for robotic manipulators possesses the following novel properties: system uncertainties can be mostly estimated and compensated; the magnitude of the switching control gain can be shaped to the minimum level while

retaining the system in the sliding mode; both time domain and frequency domain knowledge can be used in the filter design; only two classes of first-order filters are employed and thus the controller is easily implemented. It is also worthwhile to point out that in this new SMC scheme control inputs are shaped directly by filtering and gain shaping, which is analogous to many other advanced control approaches such as H_∞. From this point of view, the proposed approach provides one more degree of freedom in SMC construction in addition to the well established switching surfaces design.

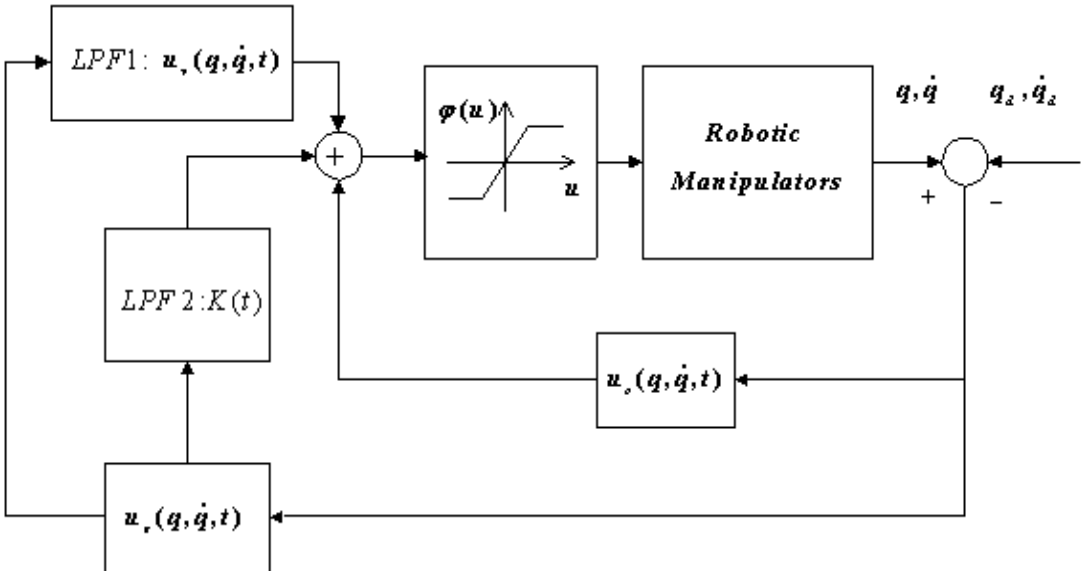

Figure 7.1. The schematic diagram of gain shaped SMC

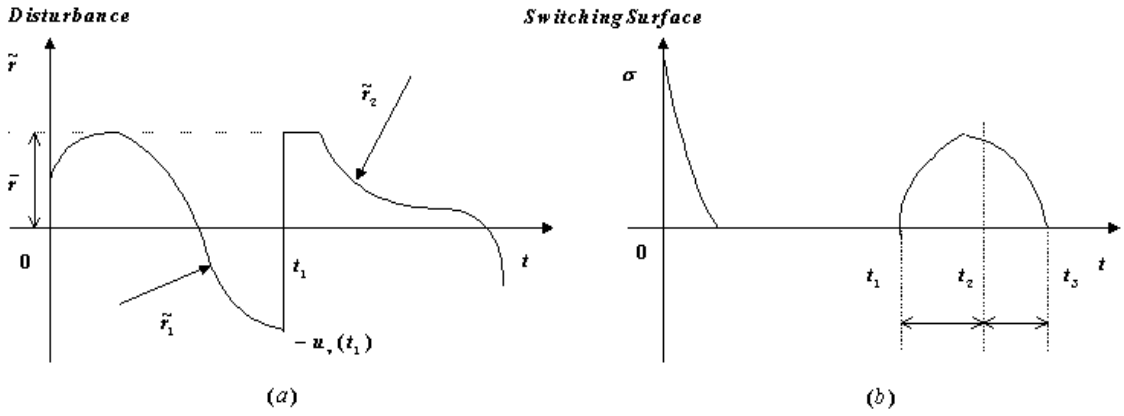

Figure 7.2. The variation of the disturbance and switching surface

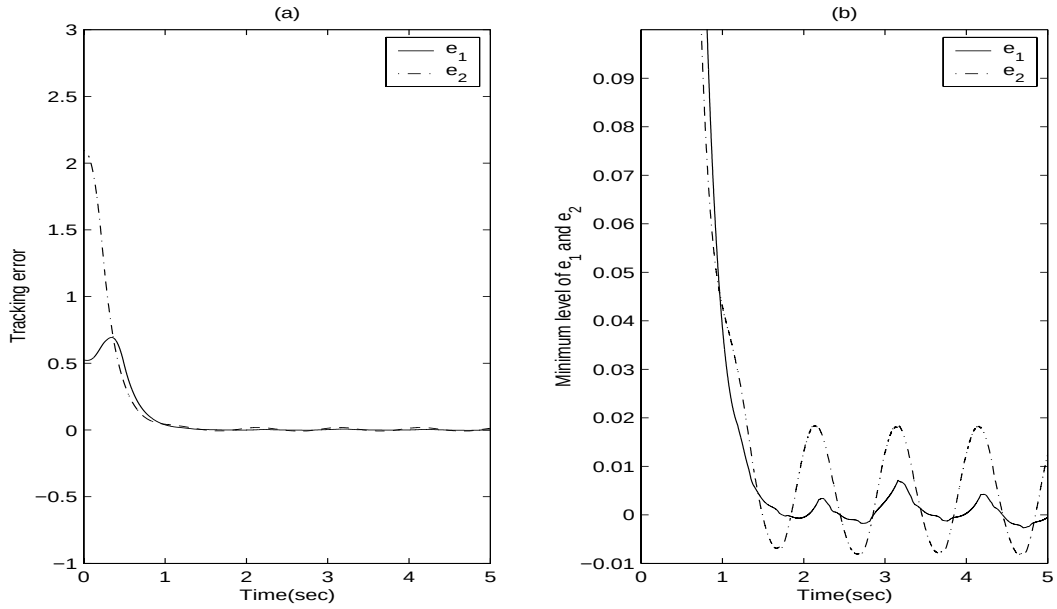

Figure 7.3. Tracking error profiles of the conventional SMC: (a) Global view; (b) Zoomed view.

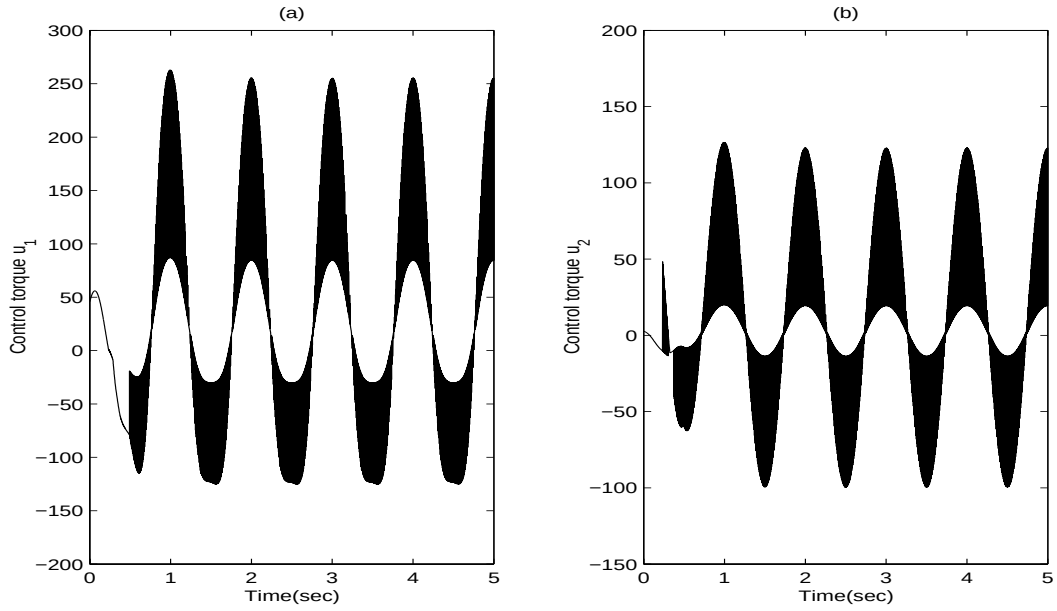

Figure 7.4. Control signal profiles of the conventional SMC: (a) Torque u_1; (b) Torque u_2.

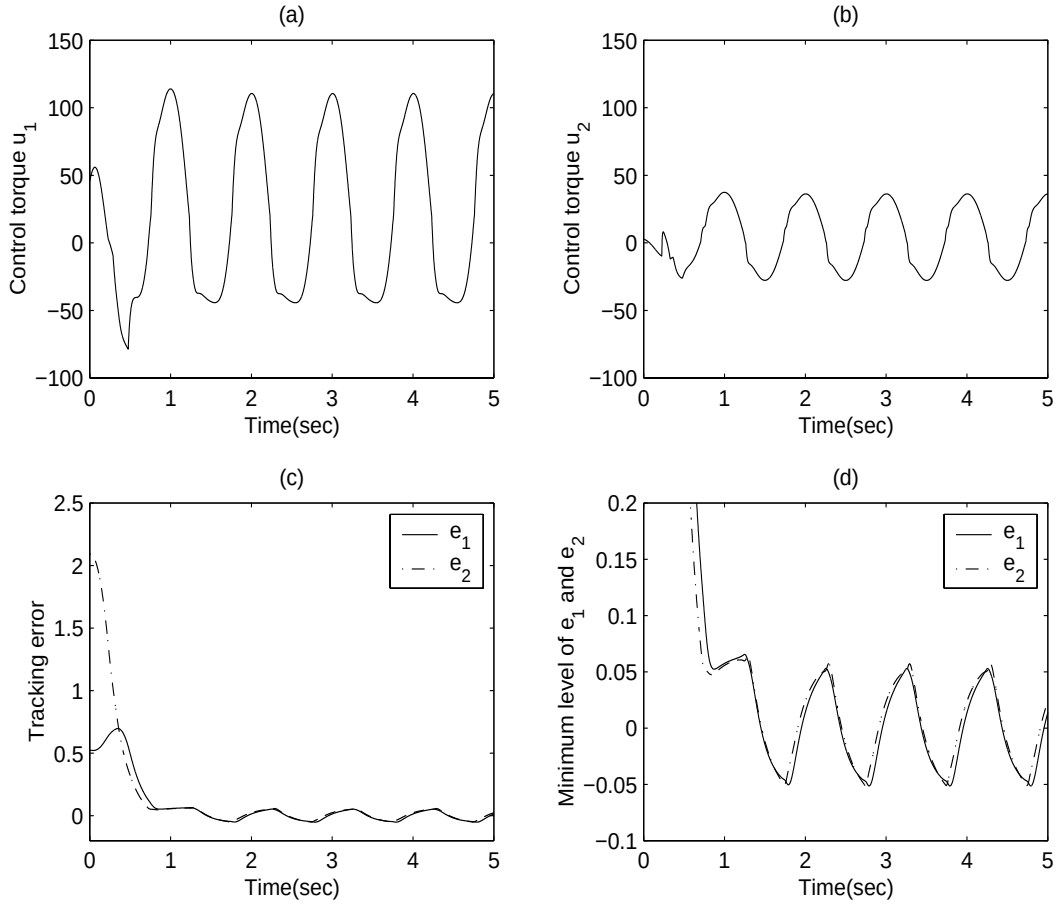

Figure 7.5. Control signal and tracking error profiles of the SMC with saturation function $\varphi_1 = \varphi_2 = 0.5$: (a) Torque u_1; (b) Torque u_2; (c) Tracking errors e_1 and e_2; (d) Zoomed e_1 and e_2 near the equilibrium.

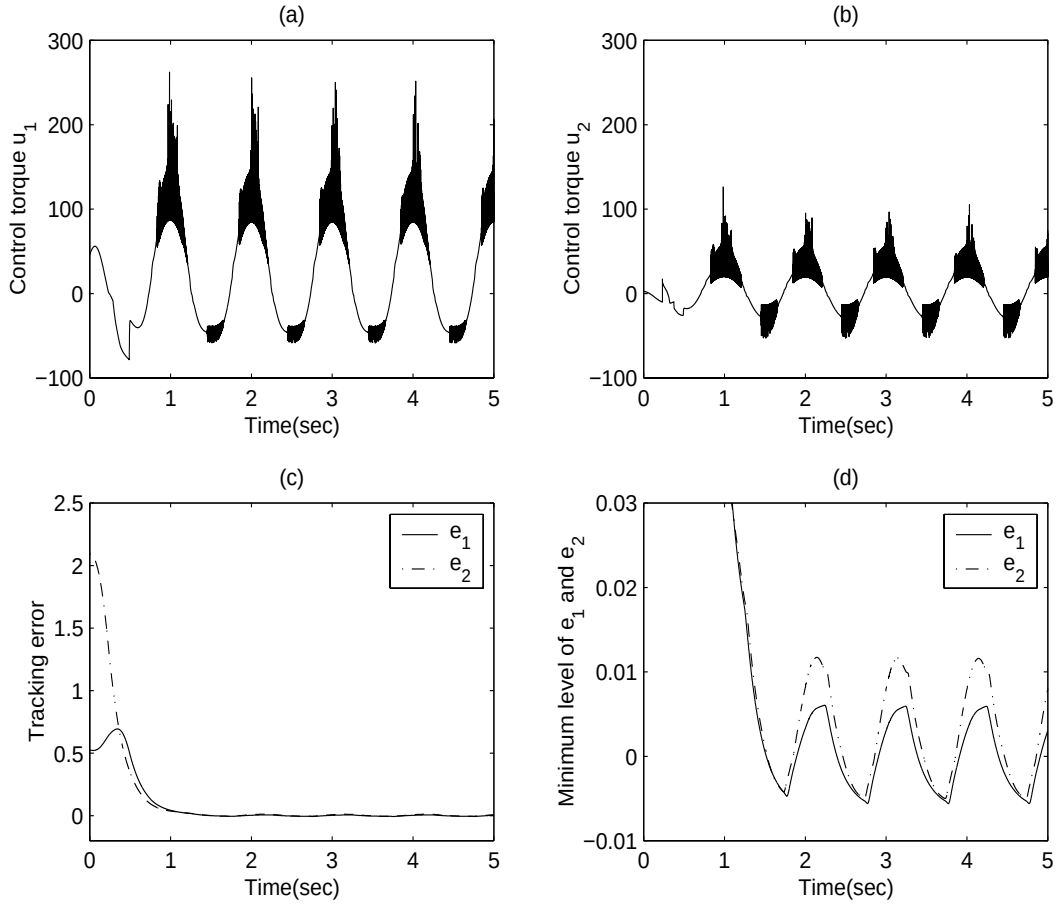

Figure 7.6. Control signal and tracking error profiles of the SMC with saturation function $\varphi_1 = \varphi_2 = 0.05$: (a) Torque u_1; (b) Torque u_2; (c) Tracking errors e_1 and e_2; (d) Zoomed e_1 and e_2 near the equilibrium.

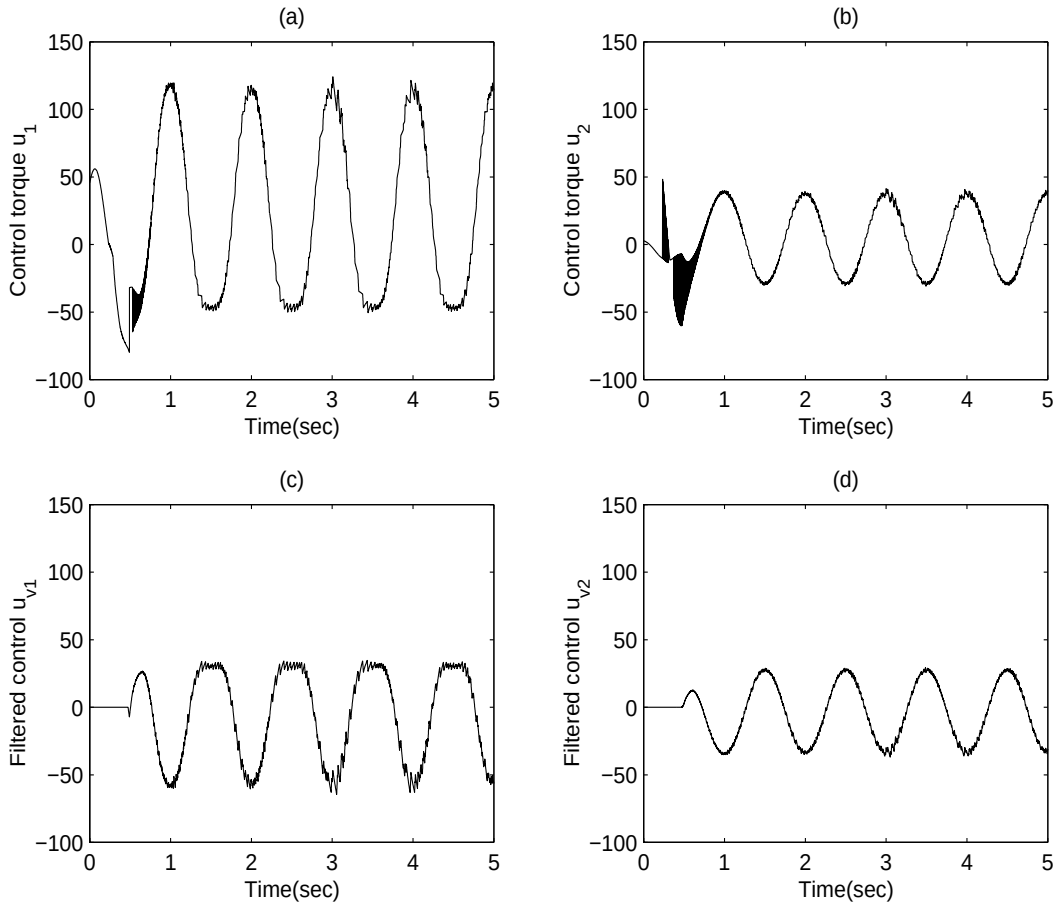

Figure 7.7. Control signal profiles $\mathbf{u}$ and filtered control profiles $\mathbf{u}_v$: (a) Torque u_1; (b) Torque u_2; (c) Filtered control u_{v1}; (d) Filtered control u_{v2}.

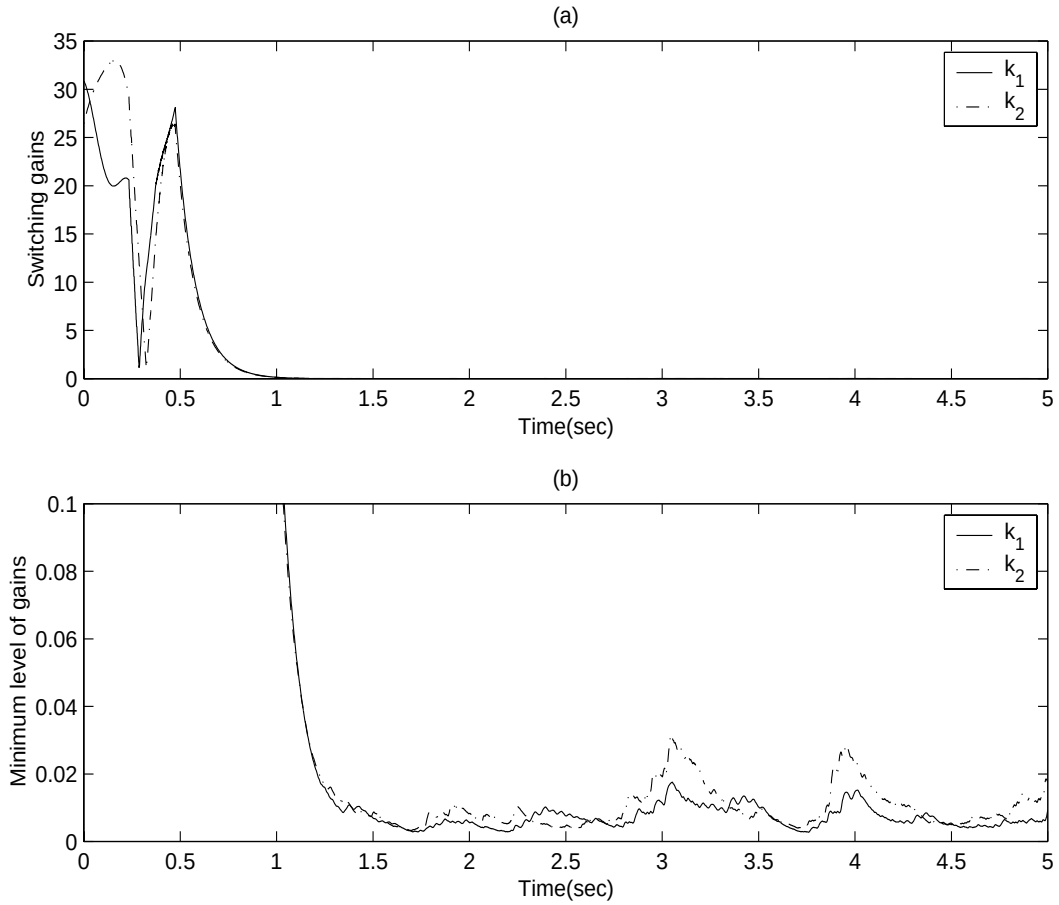

Figure 7.8. (a) Shaped switching gains ; (b) Zoomed gain profiles near the equilibrium.

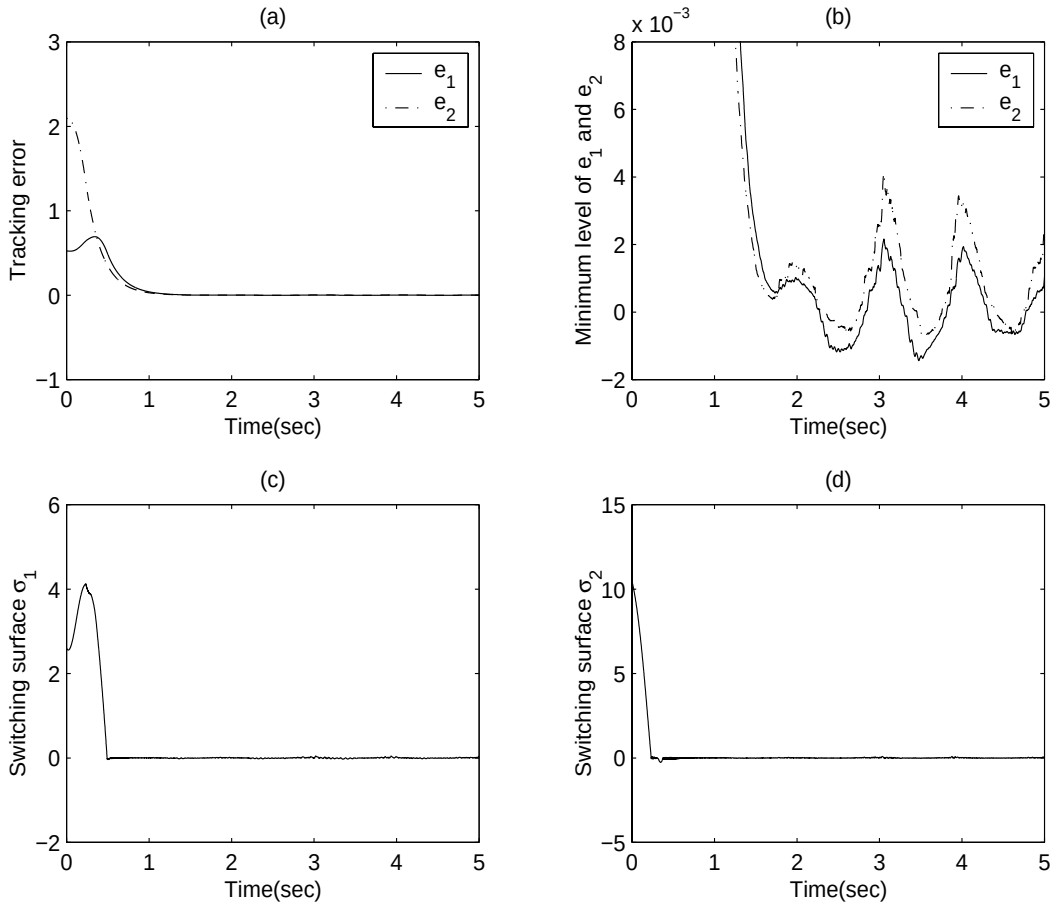

Figure 7.9. (a) Tracking errors e_1 and e_2; (b) Zoomed e_1 and e_2 near the equilibrium; (c) Switching surface σ_1; (d) Switching surface σ_2.

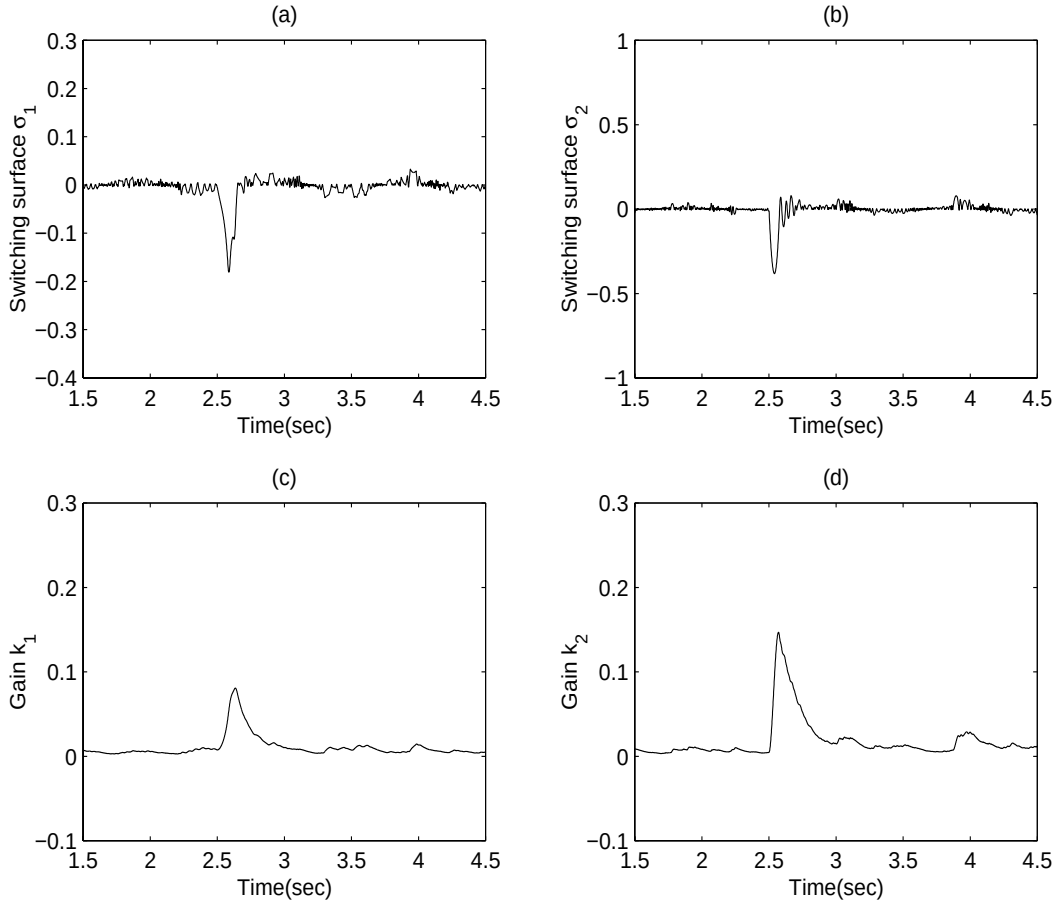

Figure 7.10. The evolution of switching surfaces and gains with respect to disturbance surging: (a) Switching surface σ_1; (b) Switching surface σ_2; (c) Gain $k_1(t)$; (d) Gain $k_2(t)$.

Chapter 8

A Modular Control Scheme for PMSM Speed Control with Pulsating Torque Minimization

8.1 Introduction

The concept of system modularization has been broadly applied to hardware construction of engineering systems ranging from personal computers to aeroplanes. It greatly facilitates design, development, diagnosis, maintenence and upgrading of a particular module according to the relatively independent functionality. In this work, we apply the same concept to a Permanent Magnet Synchronous Motor (PMSM) speed control system which is the integration of a number of control algorithms and supporting hardware components. Based on individual functionality, the existing PMSM control system can be divided into three independent modules: PI speed control module, reference current generating module, and PI current control module. The task of the PI speed control module is to eliminate offset between

the desired and actual motor speed by generating an appropriate reference torque. Since a PI controller only offers finite gain for time varying signals, this module is more suitable for constant speed control tasks. Similarly, the PI current control module is able to perfectly follow a constant reference current. However, PI current control module has much higher feedback gain and thus a higher bandwidth in the inner current loop. This is because the PMSM electrical time constant is much smaller than the mechanical time constant. Consequently, the PI current control module can also accurately track a time varying reference up to a certain bandwidth. In most practical PMSM control, the reference current generating module is simply the inverse of torque coefficient to convert reference torque into reference current assuming that flux due to permanent magnet is a constant.

PMSM control with above three modules has been widely and successfully applied to servo speed control tasks, in which the sole objective is to track a constant reference speed. By virtue of internal model principle, PI speed control module should be adequate to track a given set point and eliminate steady state off-set. However, the existence of parasitic torque pulsation limits the application of PMSM as high performance servo.

The torque pulsation in PMSM is generated due to a number of factors, including the distortion of the stator flux linkage distribution, variable magnetic reluctance at the stator slots, and secondary phenomena such as current measurement off-set as well as scaling errors (Jahns and Soong, 1996). The resulting torque ripples and consequently speed oscillations deteriorate the performance of the drive in high-performance servo applications. Since the pulsating torque consists mainly of 1st, 2nd, 6th and 12th harmonics, it can be regarded as a periodic disturbance with known period. It will be shown in this article that those harmonics enter the process in both additive and multiplicative ways. This make it difficult for a simple PI control module to reject those uncertainties. An effective approach

catering to this problem is iterative learning control (ILC) (Moore and Xu, 2000). An ILC module is inserted in between two PI control modules to replace the conventional reference current generating module. The main role of the ILC module is to supply an internal model which can compensate any periodic components in the torque. In the ILC module, the tracking error between the desired and the actual oscillatory torque is stored over one entire cycle in dynamic memory, and then used to generate the reference q-axis current for the next cycle. Thus the iteratively generated reference current takes all the periodic factors into account. Since the motor torque is directly proportional to the q-axis current, in the ILC module the P-type ILC method is applied, which incorporates both the previous cycle error information and current cycle error feedback (Sahoo *et al.*, 1999), (Lam *et al.*, 1999). By virtue of incorporating internal model, ILC module achieves the desirable feedforward compensation for all torque harmonics with unknown magnitudes, hence can outperform pure error feedback based control approaches. On the other hand, by incorporating feedback, ILC module is also robust in comparison with feedforward control approaches (Hung and Ding, 1993) (Marchand and Razek, 1993) (Hanselman, 1994).

Note that the replacement of conventional reference current generating module by the ILC module minimizes the reconfiguration of the control system, as two existing PI control modules retain and work with the new ILC module. Advanced control methods such as adaptive control, robust control or the integrated ones, were also proposed to improve the control accuracy (Dawson *et al.*, 1994) (Chung *et al.*, 1998) (Xu *et al.*, 1998*b*). However those advanced methods have to reconstruct the entire control system into a highly complicated control module, which inevitably lose advantages associated with a modularized system, and lose insight to site engineers.

A pre-requisite for the proper functioning of the proposed ILC torque control scheme is the instantaneous torque feedback information. For high-performance

instantaneous torque control, the torque feedback must accurately reflect any instantaneous variations in the developed motor torque. To obtain the torque feedback signal, one way is to directly measure the motor torque by using a torque transducer. However, this direct measurement method is impractical for servo control applications, as torque transducers have disadvantage from either their low bandwidths or high costs. Therefore, alternative means of obtaining the torque feedback information is essential. In this work, a torque estimation module is further added to the ILC module, in which a gain shaped sliding observer is used to achieve the flux estimate first, then the torque estimate. The sliding observer works as a disturbance estimator while the system is in the sliding mode. It should be noted that this module estimates the torque as a lumped quantity, no matter how many harmonic components are involved, hence it is easy to implement in comparison with others work (Low *et al.*, 1994). Different from other adaptive approaches such as (Chung *et al.*, 1998), a promising advantage of the proposed sliding observer is, it can estimate the time varying linkage flux and torque ripples owing to its broad bandwidth. An inherent problem associated with sliding observer is its chattering phenomenon arising from the use of high switching gain. To eliminate the chattering in the estimated signals, a new gain-shaping scheme is employed in the observer. Based on the concept of equivalent control (Utkin, 1978), the "equivalently" estimated signals are extracted using a low pass filter, meanwhile the switching control gain that is responsible for the chattering is also scaled down accordingly as the output of another low pass filter. An interesting feature of the gain shaped sliding observer is that it can be well designed based on the frequency domain knowledge of the system, even though it is originally designed for nonlinear systems.

The chapter is organized as follows. In Section 8.2, the effectiveness and limitations of the existing PMSM control approach are explored through module-based analy-

sis. In Section 8.3, the proposed ILC module is presented with detailed property analysis. In Section 8.4, the construction of the torque estimation module is given. The module consists of a sliding observer and two low pass filters. In Section 8.5, implementation issues are addressed and experimental results are demonstrated.

Nomenclature

θ	Electrical angular motor position.
ω	Electrical angular motor speed.
ω^{ref}	Reference electrical angular motor speed.
J	Inertia angular momentum.
T_m	Motor torque.
T_l	Load torque.
T^{ref}	Reference torque.
B	Damping factor.
i_d, i_q	d-axis and q-axis currents, respectively.
i_d^{ref}, i_q^{ref}	Auxiliary reference d-axis and q-axis currents, respectively.
L_d, L_q	d-axis and q-axis inductances, respectively.
u_d, u_q	d-axis and q-axis currents, respectively.
P	Number of pole pairs.
R	Stator resistance.
ψ_{dm}	d-axis flux linkage.
ψ_{d0}	d-axis average dc of the flux linkage.
ψ_{d6}, ψ_{d12}	$6th$ and $12th$ harmonics terms of the flux linkage.
τ_{cog}	Torque ripples due to cogging .
$\tau_{\triangle I}$	Torque ripples due to current measurement error.

8.2 Problem Formulation and Module-based Analysis

In this section, a module based analysis is conducted for the conventional PMSM speed control system. The analysis result shows that it is inadequate to suppress the torque pulsation influence within the existing control framework.

A. Model of PMSM Control System

A permanent magnet synchronous motor consists of a mechanical subsystem and a electrical subsystem

$$\frac{d\theta}{dt} = \omega \tag{8.1}$$
$$\frac{d\omega}{dt} = \frac{1}{J}(T_m - T_l - B\omega) = \frac{1}{J}(k_t i_q - T_l - B\omega) \tag{8.2}$$
$$\frac{di_d}{dt} = \frac{1}{L_d}(u_d + \omega L_q i_q - R i_d) \tag{8.3}$$
$$\frac{di_q}{dt} = \frac{1}{L_q}(u_q - \omega L_d i_d - R i_q - \omega \psi_{dm}) \tag{8.4}$$

where (8.1) and (8.2) represent the mechanical subsystem; (8.3) and (8.4) represent the electrical subsystem. u_d and u_q are the $d-q$ axes stator voltages which are control inputs. i_d and i_q are the $d-q$ axes stator currents. R is the stator resistance; L_d and L_q are the $d-q$ axes stator self-inductances; J is the inertia angular momentum; B is the damping factor; ψ_{dm} is the d-axis flux-linkage due to permanent magnet and T_l is the load torque. For the above electromechanical model, we assume that the true states (*i.e.* θ, ω, i_d, i_q) are all measurable. T_m is the motor torque, in the ideal case is given by the following

$$T_m = k_{t0} i_q = \frac{3}{2}\frac{P}{2}\psi_{d0} i_q, \tag{8.5}$$

where P is a constant which represents the number of poles in the motor; k_{t0} is the torque constant and ψ_{d0} is a constant d-axis flux linkage. In practice, however, the

motor torque is expressed as below

$$T_m = \frac{3}{2} P_p \psi_{dm} i_q + \tau_{cog} + \tau_{\triangle I} \tag{8.6}$$

where τ_{cog} and $\tau_{\triangle I}$ are periodic torque pulsation due to cogging and current measurement error respectively. τ_{cog} is dominated by the $6th$ harmonics, and $\tau_{\triangle I}$ is dominated by the $1st$ and $2nd$ harmonics. The actual flux linkage ψ_{dm} can be shown as

$$\psi_{dm} \quad = \quad \psi_{d0} + \sum_{j=1}^{\infty} \psi_{d6j} cos(j6\theta), \tag{8.7}$$

where ψ_{d0} and ψ_{d6j} are the average DC and $6j$-th harmonics terms of the flux linkage respectively, while θ is the electrical angle of the rotor. The pulsating flux is due to the distortion of the stator flux linkage distribution and variable magnetic reluctance at the stator slots. Rewrite (8.6) and (8.7) as

$$T_m = k_t i_q + \eta$$

where k_t is the actually torque coefficient, $\eta = \tau_{cog} + \tau_{\triangle I}$ is the additive perturbation and

$$\sum_{j=1}^{\infty} \psi_{d6j} cos(j6\theta).$$

in k_t is the multiplicative perturbation. The block diagram of the conventional PMSM speed control system is shown in $Fig.8.1$. The whole system can be divided into 3 control modules: PI speed control module, reference current generating module, PI current control modules, as well as the plant module, each with a unique function.

The flow of control signals is shown in Fig.8.2, where $W_E(s)$ is the transfer function of the electrical subsystem, $W_M(s)$ is the transfer function of the mechanical subsystem, and $\eta(s)$ is the additive part of torque pulsations. The i_d PI control loop is ignored in subsequent analysis as the task $i_d = 0$ is a much easier regulation problem and well under control in practice.

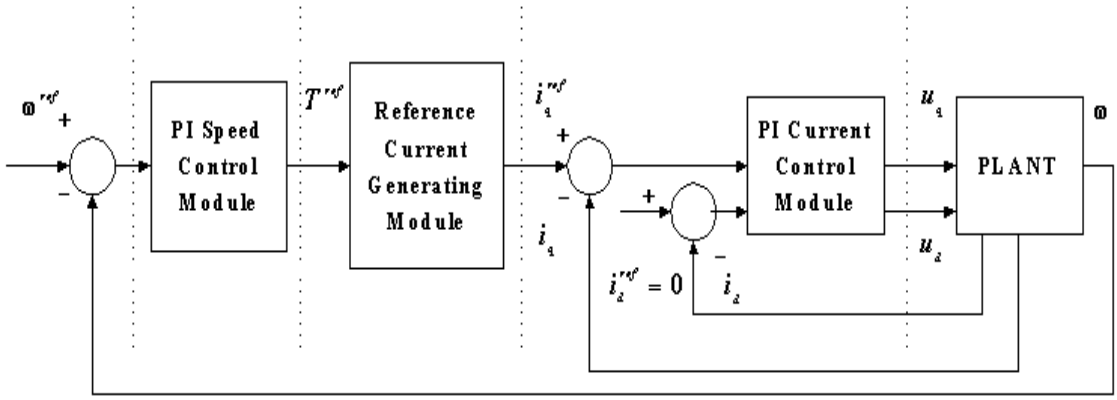

Figure 8.1. Block diagram of conventional PI control scheme

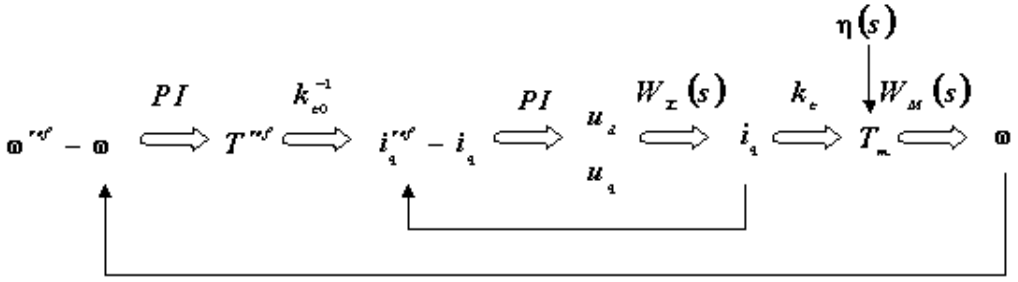

Figure 8.2. Flow of control signals

B. PI Speed Control Module

The objective of the PI speed control module is to generate the following torque reference

$$T^{ref} = K_{p,s}(\omega^{ref} - \omega) + K_{i,s}\int_0^t (\omega^{ref} - \omega)dt = K_{p,s}e + K_{i,s}\int_0^t e d\tau, \qquad (8.8)$$

where $K_{p,s}$ and $K_{i,s}$ are respectively proportional and integral gains of the speed control module, $e = \omega^{ref}(t) - \omega(t)$.

Now let us investigate the capability for the speed control module to track a given reference speed ω_d and to reject any disturbance. To focus on this, we assume the ideal case where two subsequent control modules can work perfectly such that the motor torque can always follow the reference torque. Note the transfer function

between T^{ref} and T_m is 1 in the ideal case. On the other hand from (8.2), we have

$$J\frac{de}{dt} + Be = J\frac{d\omega^{ref}}{dt} + T_l + B\omega^{ref} - T_m. \tag{8.9}$$

Substituting (8.8) into (8.9) the error dynamics is

$$J\frac{de}{dt} + (K_{p,s} + B)e + K_{i,s}\int_0^t e d\tau = J\frac{d\omega^{ref}}{dt} + T_l + B\omega^{ref} \triangleq d(t)$$

where $d(t)$ is the lumped disturbance to the speed control loop. Applying the Laplace transform, we have

$$E(s) = G(s)D(s), \quad G(s) = \frac{s}{Js^2 + (K_{p,s} + B)s + K_{i,s}}. \tag{8.10}$$

The control system can be simplified into Fig.8.3.

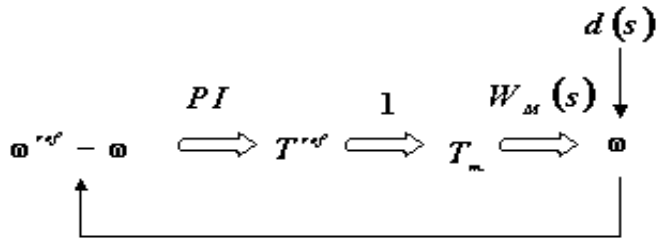

Figure 8.3. Simplified control signal flow

Can the desired speed be strictly followed by the simple PI control (8.8)? From (8.10), it depends on how much of $D(s)$ can be rejected by $G(s)$ which is in fact a band pass filter. Fig.8.4 shows the bode plot of $G(s)$ for a real PMSM system to be detailed later in this chapter.

From the plot we can see that in order to fully attenuate $D(s)$, PI gains should be carefully chosen such that the peak value of $G(s)$ can be kept far away from that of $D(s)$. A constant disturbance can be perfectly rejected, in other words the PI speed control module can well perform when ω^{ref} and T_l are constants or slow time varying. It is clear that the PI speed control module is designed for tracking the constant speed reference, hence is not able to reject the torque pulsations in η and k_t.

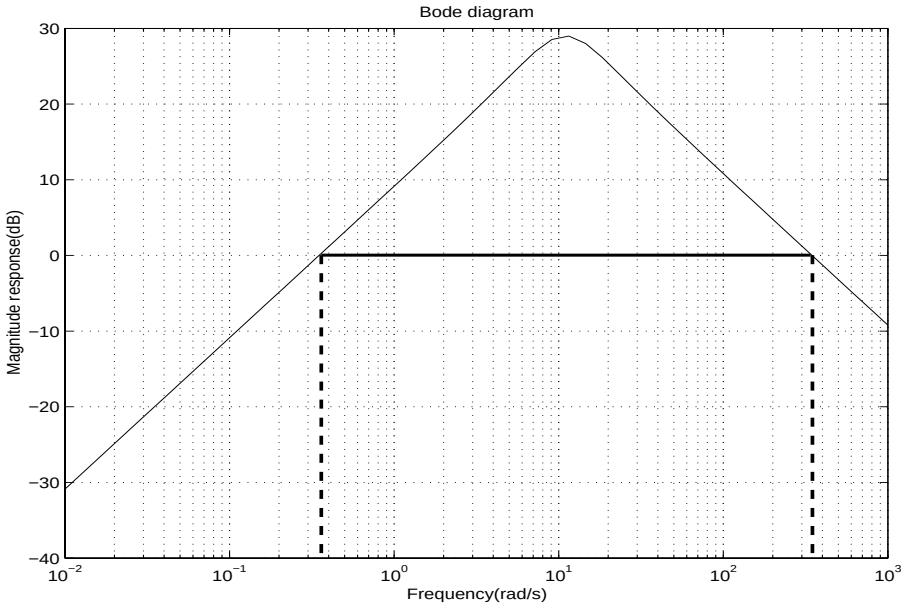

Figure 8.4. Bode plot for the PI speed loop: $J = 0.00289$, $B = 0.0004$, $K_{p,s} = 0.035$, $K_{i,s} = 0.35$

C. PI Current Control Module

The PI current controls are designed to generate the control output voltages as,

$$\begin{aligned} u_d &= K_{p,c}(i_d^{ref} - i_d) + K_{i,c}\int_0^t (i_d^{ref} - i_d)dt \\ u_q &= K_{p,c}(i_q^{ref} - i_q) + K_{i,c}\int_0^t (i_q^{ref} - i_q)dt, \end{aligned}$$

where $K_{p,c}, K_{i,c} > 0$ are current control module proportional and integral gains respectively. Usually i_d^{ref} is set to zero and $i_d \approx 0$ can be easily achieved by PI control. Analogous to the speed control, we can derive the error dynamics below

$$L_q\frac{de}{dt} + (K_{p,c} + R)e + K_{i,c}\int_0^t e d\tau = L_q\frac{i_q^{ref}}{dt} + Ri_q^{ref} - L_d\omega i_d - \omega\psi_{dm} \qquad (8.11)$$

where $e \stackrel{\triangle}{=} i_q^{ref} - i_q$. The major difference between two PI modules is: current control gains can be chosen much higher because the much smaller electrical time constant L_q/R in comparison with the mechanical subsystem. In the sequel, the PI current module can also follow the reference signal i_q^{ref} to certain bandwidth.

This can be easily seen from (8.11) by letting $K_{p,c} \to \infty$, leading to

$$(1 + \frac{R}{K_{p,c}})e + \frac{K_{i,c}}{K_{p,c}} \int_0^t e d\tau \approx 0.$$

Can the PI current module reject the torque pulsations in η and k_t? From Fig.8.2, the sole objective of the current control module is to faithfully track the reference current. In the ideal case when the PI gains are sufficiently high, the transfer function from i_q^{ref} to i_q approaches to unity. Of course, a unity gain in feed-through path cannot do anything to disturbance rejection.

D. Reference Current Generating Module

From Fig.8.2, the role of this module is quite straightforward: cancel out the torque coefficient k_t, so that a unity transfer function from T^{ref} to T_m can be achieved if the PI current module can work perfectly. Unfortunately, k_t is perturbed by harmonics with known order but unknown magnitude as shown in (8.7). In conventional design an estimated value k_{t0} is used. Note that this estimate may not be equal to the average DC component in (8.7), needless to mention the possibility to compensate those harmonics in k_t and η.

E. Alternative Control Methods

Let us reach some conclusions and find alternative ways to solve the problem. First, two PI control modules are able to fulfill their jobs but not for torque pulsation compensation. Second, the reference current generating module is obviously too simple to be of any help. From Fig.8.2, all torque pulsations are reflected in T_m. We can introduce a feedback loop from T_m to T^{ref} as shown in Fig.8.5, and replace k_{t0}^{-1} with an appropriate control module C. However, if C is a pure and smooth error feedback, no matter linear or nonlinear, we still cannot achieve our target. Let us verify this using the concept of internal model. Assume that the PI current control module performs well so that the deviation between i_q^{ref} and i_q is negligible. The output of C should directly cancel out perturbations from k_t and η. Nevertheless

for a pure and smooth error feedback, the output of C is zero whenever the input is zero, i.e. $T_m = T^{ref}$. On the other hand, pulsations in k_t and η are always present. By incorporating integrators in C we can only eliminate constant perturbations.

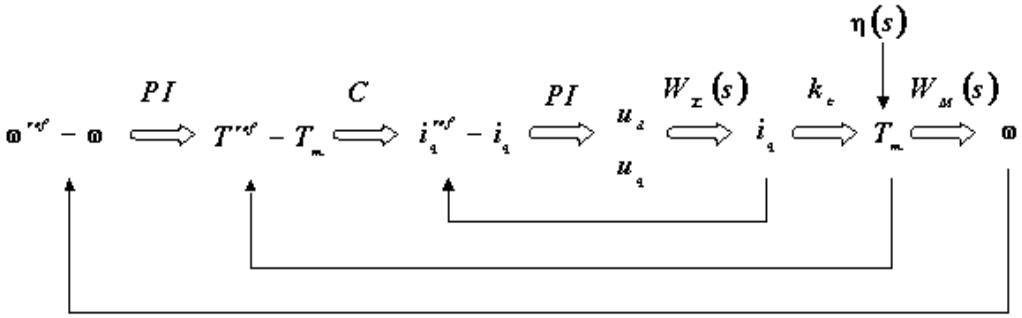

Figure 8.5. Flow of control signals with new control module

Variable structure control (VSC) approach (Chung *et al.*, 1998) can partially overcome the difficulty by introducing a discontinuous control law which possesses infinite gain at the equilibrium $T_m = T^{ref}$. In case perturbations are random or non-periodic, VSC perhaps is the best solution when high performance is required, though it inevitably incurs chattering. Since PMSM torque pulsations are periodic harmonics, a more suitable control approach is to incorporate an internal model in C which constantly provides the necessary signals for compensation, even through the input to C is zero. In Section 3 we show that this task can be easily fulfilled with ILC when a periodic i_q^{ref} is to be learned.

It is worthwhile to point out that there are other alternative control approaches for PMSM control tasks, such as robust adaptive (Dawson *et al.*, 1994), (Xu *et al.*, 1998*b*). This kind of controller design is a highly integrated one, and the whole control system forms a single module which is usually complicated, model based and without insight into the internal structure of PMSM (Fig.8.6). Those methods are more appropriate for more general control tasks such as position servo, speed servo with a fast time varying target trajectory, etc.

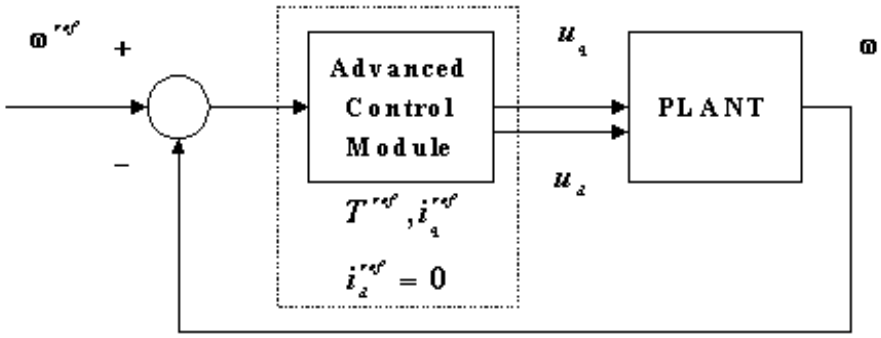

Figure 8.6. Block diagram of advanced control scheme

8.3 The Proposed ILC Control Module

A. ILC Mechanism

The block diagram of the PMSM control system with ILC module is shown in Fig.8.7.

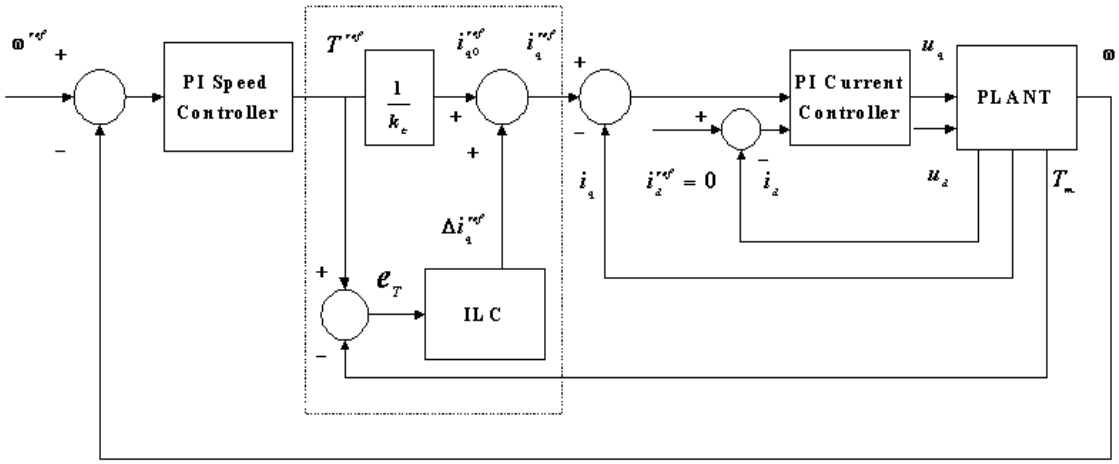

Figure 8.7. Block diagram of the control scheme with ILC

In this section we assume the instantaneous torque is available. First we demonstrate the periodic characteristic of the desired reference current signal i_q^{ref}, which is indispensable for an ILC mechanism to learn and re-produce.

Consider the actual torque (8.6), the desired reference current control is

$$i_q^{ref} = \frac{T^{ref} - \tau_{cog} - \tau_{\triangle I}}{\frac{3}{2}P_p\psi_{dm}}. \tag{8.12}$$

Since the PI current control module can achieve sufficient tracking accuracy, namely $i_q \approx i_q^{ref}$, such a i_q^{ref} ensures $T_m \to T^{ref}$. Based on prior knowledge, i_q^{ref} can be expressed as

$$i_q^{ref} = i_{q0}^{ref} + \triangle i_q^{ref}. \tag{8.13}$$

where i_{q0}^{ref} is the nominal DC component, and $\triangle i_q^{ref}$ represents all the remaining unknown components. The objective of ILC is to learn the unknown $\triangle i_q^{ref}$, for this we need to show that $\triangle i_q^{ref}$ is periodic, which is given the following proposition.

Proposition 8.1. *$\triangle i_q^{ref}$ is a periodic signal.*

Proof: Note that periodicity of i_q^{ref} and $\triangle i_q^{ref}$ is the same, thus we prove i_q^{ref} is a periodic signal. Rewrite i_q^{ref} as below

$$i_q^{ref}(\theta) = \frac{T^{ref} - \eta(\theta)}{k_t(\theta)}$$

Since $\eta(\theta) = \tau_{cog} + \tau_{\triangle I}$ and $k_t = \dfrac{3}{2}P_p\psi_{dm}$ constitute torque harmonics and are essentially the same periodic signals, and T^{ref} is a constant reference torque,

$$i_q^{ref}(\theta + T) = \frac{T^{ref} - \eta(\theta + T)}{k_t(\theta + T)} = \frac{T^{ref} - \eta(\theta)}{k_t(\theta)} = i_q^{ref}(\theta)$$

which is periodic, where T is the period of the fundamental harmonics.

Iterative learning control appears to be a natural approach to achieve the pulsating torque minimization since it uses the repetitive nature of the torque pulsation. The iterative learning torque controller learns and then generates the desired compensating current profile $\triangle i_q^{ref}$ and is added to i_{q0}^{ref} and the process is carried out iteration by iteration, each with a period of one electrical cycle. As learning progresses, the pulsating torque decreases and the motor torque tracks the desired

torque. The iterative learning scheme is

$$\triangle i_{q,i+1}^{ref}(\theta_e) = (1-\alpha)\triangle i_{q,i}^{ref}(\theta_e) + \Gamma e_i(\theta_e) + \Phi e_{i+1}(\theta_e), \tag{8.14}$$

where $e_{i+1}(\theta_e) = T^{ref}(\theta_e) - T_{m,i+1}(\theta_e)$; θ_e is the electrical angle; $T = [0, 2\pi]$ is the fundamental harmonic period for θ_e; $i = 0, 1, 2, \cdots$ represents the ith electrical cycle or the ith "iteration", hence $\triangle i_{q,i+1}^{ref}(\theta_e)$ is equivalent to $\triangle i_{q,i}^{ref}(2\pi + \theta_e)$; Γ and Φ are constant gain matrices; α is a constant in $(0, 1]$. The initial values $\triangle i_{q,0}^{ref}(\theta_e)$ and $e_0(\theta_e)$ $\forall \theta_e \in [0, 2\pi]$ are either zero or generated by the feedback part alone.

In terms of (8.14), the reference current of the present cycle $i_{q,i+1}^{ref}$ $\forall \theta_e \in T$ is updated by using the preceding cycle reference current $\triangle i_{q,i}^{ref}$ and error signal e_i. The learning update is performed according to electrical angle θ_e instead of time t, because torque pulsations are periodic with respect to the electrical angle. Another point in the application of the ILC in the PMSM is that the iterative learning part is essentially an open-loop feedforward control between two electrical cycles, thus it may be sensitive to small perturbations. To overcome this shortcoming, the present error signal $e_{i+1}(\theta_e)$ is included in the learning law to enhance the system robustness.

Fig.8.8 shows the schematic diagram for the proposed learning control scheme, where the LPF is a low pass filter introduced to remove measurement noise. From the figure we can see how is the internal model principle applied. Suppose $\alpha = 0$, and $i_{q,i}^{ref}$ did a perfect job such that $T^{ref} - T_{m,i} = 0$. In such circumstance $e_i(\theta_e) = 0$. By virtue of the memory based learning, $i_{q,i}^{ref}$ is preserved in memory for the entire period T and being used for the new cycle, in the sequel $i_{q,i+1}^{ref} = i_{q,i}^{ref}$ and the perfect compensation repeats. In practice, the error signal e_i may contain certain non-periodic components such as noise. Those components will be accumulated as ILC scheme (8.14) is simply an integrator in iterating domain. Consequently a forgetting factor $1 - \alpha$ is introduced to make a trade off between perfect learning

and robustness.

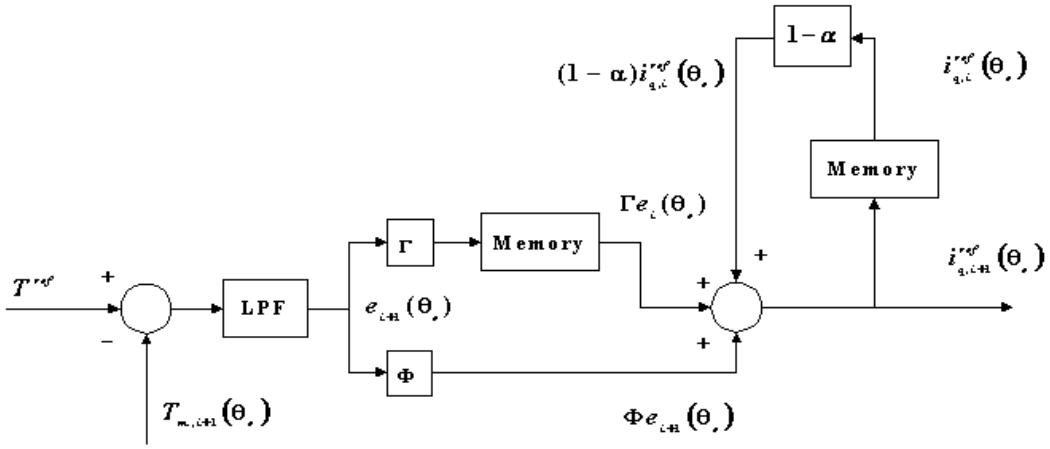

Figure 8.8. Schematic diagram of the proposed ILC module

B. ILC Convergence Analysis

Starting from the relationship $T_m = k_t i_q + \eta$ and $i_q \approx i_q^{ref}$, we have

$$T_{m,i+1} = k_t i_{q,i+1}^{ref} + \eta + d_{i+1} \tag{8.15}$$

where d_{i+1} is a residue term resulting from the replacement of i_q by i_q^{ref}. Recall that the objective of ILC is to make $i_{q,i+1}^{ref}$ converge to the ideal reference torque i_q^{ref} such that $T_{m,i+1} \to T^{ref}$ iteratively. This is summarized in the theorem below.

Theorem 8.1. *The learning scheme (8.14) is convergent by choosing gains to satisfy* $\Phi > 0$ *and* $0 < \alpha + k_t\Gamma < 2$. *The torque tracking error* e_i *will converge to a bound linearly proportional to the forgetting coefficient* α *and the PI current module tracking error.*

Proof: Subtracting (8.15) from $T^{ref} = k_t i_q^{ref} + \eta$, substituting (8.13) and (8.14) we have

$$\begin{aligned} e_{i+1} &= k_t(\triangle i_q^{ref} - \triangle i_{q,i+1}^{ref}) \\ &= k_t\{\triangle i_q^{ref} - \Big[(1-\alpha)\triangle i_{q,i}^{ref} + \Gamma e_i + \Phi e_{i+1} + d_i\Big]\} \\ &= k_t\Big[(1-\alpha)(\triangle i_q^{ref} - \triangle i_{q,i}^{ref}) + \alpha\triangle i_q^{ref} - \Gamma e_i - \Phi e_{i+1} - d_i\Big]. \end{aligned} \tag{8.16}$$

From the first equality in above equation we also have

$$k_t(1-\alpha)(\triangle i_q^{ref} - \triangle i_{q,i}^{ref}) = (1-\alpha)e_i.$$

As a result (8.16) becomes

$$\begin{aligned}(1+k_t\Phi)e_{i+1} &= (1-\alpha-k_t\Gamma)e_i + k_t(\alpha\triangle i_q^{ref} - d_i) \\ e_{i+1} &= \frac{1-\alpha-k_t\Gamma}{1+k_t\Phi}e_i + \frac{k_t(\alpha\triangle i_q^{ref} - d_i)}{1+k_t\Phi}. \end{aligned} \tag{8.17}$$

It is easy to see that the convergence condition is

$$|\rho| = |\frac{1-\alpha-k_t\Gamma}{1+k_t\Phi}| < 1. \tag{8.18}$$

Since $k_t > 0$, the convergence condition is satisfied with $\Phi > 0$ and $|1-\alpha-k_t\Gamma| < 1$ which can also be expressed as $0 < \alpha + k_t\Gamma < 2$.

In the presence of the residue term d_i and the forgetting factor α, the tracking error e_i will not converge to zero but within a bound. Let us calculate the bound. Denote

$$\tilde{d_i} = \frac{k_t(\alpha\triangle i_q^{ref} - d_i)}{1+k_t\Phi}, \tag{8.19}$$

associated with an upperbound $|\tilde{d_i}| \leq d_{max}$. Accordingly,

$$\begin{aligned}|e_{i+1}| &= |\rho e_i + \tilde{d_i}| \\ &\leq |\rho(\rho e_{i-1} + \tilde{d}_{i-1})| + |\tilde{d_i}| \\ &\leq \rho^2|e_{i-1}| + \rho|\tilde{d}_{i-1}| + |\tilde{d_i}| \\ &\leq \cdots\cdots \\ &\leq \rho^{i+1}|e_0| + \rho^i|\tilde{d_0}| + \rho^{i-1}|\tilde{d_1}| + \cdots + \rho|\tilde{d}_{i-1}| + |\tilde{d_i}| \\ &\leq \rho^{i+1}|e_0| + (\rho^i + \rho^{i-1} + \cdots + 1)d_{max} \\ &= \rho^{i+1}|e_0| + \frac{1-|\rho|^{i+1}}{1-|\rho|}d_{max}. \end{aligned} \tag{8.20}$$

As $i \to \infty$, the error is bounded to $\frac{1}{1-|\rho|}d_{max}$.

Remark 8.1. *Since the error bound is linearly proportional to α and d_i, we can choose a small α and design an appropriate PI current module so that the learning error bound is sufficiently small.*

Remark 8.2. *Note that one of the convergence condition is*

$$0 < \Gamma < \frac{2-\alpha}{k_t}.$$

Since k_t is unknown, we need to estimate its upperbound in order to set Γ. A conservative estimate guarantees convergence for a wider range of k_t, but leads to a lower gain and slower convergence speed. Having Φ that is too large will cause oscillatory response when time delay is present. As before, a conservative choice of Φ such that $\Phi \leq \Gamma$ would suffice in producing good results. As for the forgetting factor, the smaller α is, the smaller d_{max} will be. Thus a small value of α ($\alpha = 0.05 \sim 0.1$) would be adequate to ensure robustness of the controller.

8.4 Torque Estimation Module Using a Gain Shaped Sliding Mode Observer

The pre-requisite for the proposed ILC module to properly function is the instantaneous torque feedback information. For high-performance instantaneous torque control, the torque feedback should reflect any instantaneous variations in the developed motor torque accurately. To obtain the torque feedback signal, the direct measurement method is impractical for servo control applications due to either the limited bandwidth or cost. Therefore, alternative means of obtaining the torque feedback information is essential. In this section, the design of an on-line torque estimator that employs the sliding mode flux observer is presented (Fig.8.9).

The concept of sliding mode observer has been proposed (Hashimoto *et al.*, 1990). The main advantage of the sliding mode observer lies in its robustness to unknown

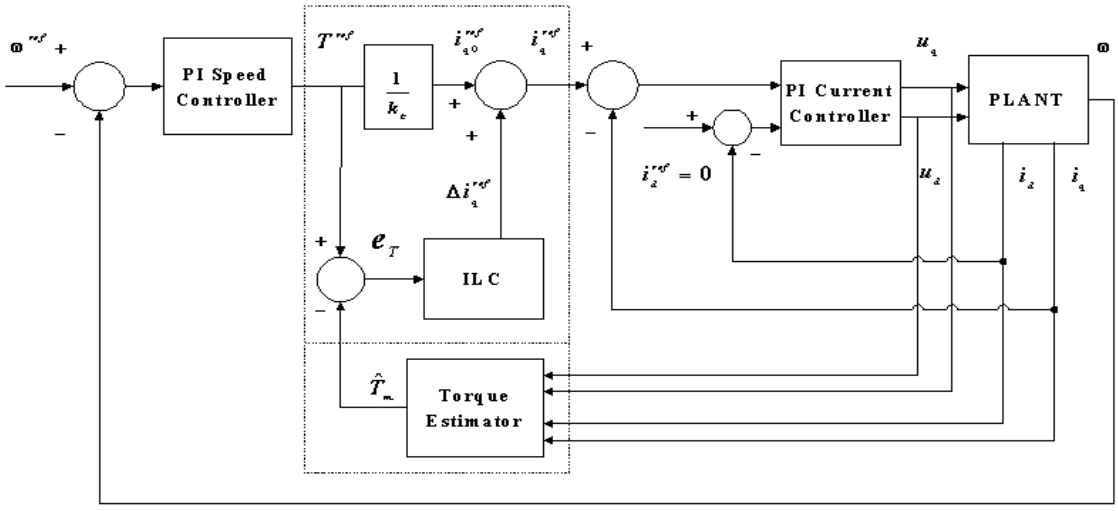

Figure 8.9. Block diagram of the proposed modular-based control scheme with ILC and torque estimation

system disturbances. However, an inherent problem associated with this technique is the chattering of the estimated signals in the sliding mode. To eliminate the chattering in the estimated signals, a gain-scheduled VSC scheme is employed in the observer. When in the sliding mode, from the concept of "equivalent control", the equivalently estimated signals are extracted while the switching control gain that is responsible for the chattering is scaled down accordingly. These are done by means of simple first-order filtering of the control signals.

First rewrite (8.3) and (8.4) in state−space form as below

$$\dot{\mathbf{x}} = A\mathbf{x} + B\mathbf{u} + \mathbf{d}, \tag{8.21}$$

where $\mathbf{x} = [i_d, i_q]^T$, $\mathbf{u} = [u_d, u_q]^T$, $\psi_{qm} = 0$, $A = \begin{bmatrix} -\frac{R}{L_d} & \frac{L_q\omega}{L_d} \\ -\frac{L_d\omega}{L_q} & -\frac{R}{L_q} \end{bmatrix}$, $B = \begin{bmatrix} \frac{1}{L_d} & 0 \\ 0 & \frac{1}{L_q} \end{bmatrix}$, $\mathbf{d} = \begin{bmatrix} 0 \\ -\frac{\omega}{L_q}\psi_{dm} \end{bmatrix}$. Accordingly a standard sliding mode observer can be constructed

$$\dot{\hat{\mathbf{x}}} = A\hat{\mathbf{x}} + B\mathbf{u} + K(\mathbf{x} - \hat{\mathbf{x}}) + \mathbf{k} \tag{8.22}$$

where $\hat{\mathbf{x}} = \left[\hat{i}_d, \hat{i}_q\right]^T$, $K = \begin{bmatrix} k_{1d} & -\frac{L_q\omega}{L_d} \\ \frac{L_d\omega}{L_q} & k_{1q} \end{bmatrix}$, $\mathbf{k} = [k_{2d}sign(e_d), k_{2q}sign(e_q)]^T$, and $[e_d, e_q]^T \triangleq \mathbf{e} = \mathbf{x} - \hat{\mathbf{x}}$.

Remark 8.3. *Without the switching term* $\mathbf{k}$*, (8.22) is in fact the well known Luenberg's observer that achieves asymptotic convergence of the state estimation in the absence of* $\mathbf{d}$*. However, in our problem currents* i_d *and* i_q *are physically measurable. The objective of the above sliding mode observer is not to reconstruct the state variables, but to estimate the disturbance* $\mathbf{d}$*.*

Now let us show how does the sliding mode flux observer work and what is the existing problem. Subtracting (8.22) from (8.21)

$$\dot{\mathbf{e}} = (A - K)\mathbf{e} + \mathbf{d} - \mathbf{k}. \tag{8.23}$$

By choosing appropriate gains k_{1d} and k_{1q} the matrix $\bar{A} = A - K$ can be made Hurwitz (stable), therefore according to Lyapunov equation there exist $P = P^T > 0$ and $Q > 0$ such that $\bar{A}^T P + P\bar{A} = -Q$. Now selecting a Lyapunov function $V = \mathbf{e}^T P\mathbf{e}$, differentiating it yields

$$\begin{aligned} \dot{V} &= \mathbf{e}^T(\bar{A}^T P + P\bar{A})\mathbf{e} - 2\mathbf{e}^T P(\mathbf{k} - \mathbf{d}) \\ &\leq -\mathbf{e}^T Q\mathbf{e} - 2\mathbf{e}^T P\mathbf{k} + 2\|\mathbf{e}^T P\mathbf{d}\| \end{aligned} \tag{8.24}$$

Assume a bound on the disturbance $\|\mathbf{d}\| \leq \rho$, it is easy to design $\mathbf{k}$ to guarantee $\mathbf{e}^T P\mathbf{k} \geq \|\mathbf{e}^T P\mathbf{d}\| + \epsilon\|\mathbf{e}\|$ with $\epsilon > 0$, such that in a finite time interval e_q reaches zero. For instance, a possible choice of the switching gains in $\mathbf{k}$ is

$$k_{2d} = k_{2q} = \rho\frac{\lambda_{max}(P)}{\lambda_{min}(P)} + \epsilon$$

where $\lambda_{min}(P)$ and $\lambda_{max}(P)$ indicate the minimum and maximum eigenvalues of P.

When the observer is in the sliding mode, it is straightforward to derive the relationship $\mathbf{k} = \mathbf{d}$. This can be readily seen from (8.23), because in the sliding mode $\mathbf{e} = \dot{\mathbf{e}} = 0$. Since $\mathbf{k}$ contains fast switching functions, a low pass filter can be applied to extract the average of $\mathbf{k}$, which is $\mathbf{d}$ according the equivalent control (Utkin, 1978). The main difficulty in applying the above sliding mode observer lies in the last step extracting the average profile from highly chattering signals. A low pass filter with a small time constant is not able to acquire a smooth estimate. A low pass filter with a large time constant will incur unacceptable phase lag. Chattering in sliding mode arises mainly due to two factors: extremely high gain around the equilibrium and limited switching frequency. For practical system it is hardly possible to increase the Nyquist frequency, the only way is to shape the switching gain. Numerous smoothing schemes have been proposed, but none of them can retain the tracking accuracy because the feedback gain around the equilibrium is scaled down. To overcome this dilemma, once again we need to introduce feedforward to work concurrently with feedback. Gain shaped sliding mode control with filtering technology (Xu *et al.*, 2000*d*) is developed exactly for this purpose. Briefly speaking, two low pass filters are used. The first filter LPF1 is

$$\tau_1 \dot{k}_v + k_v = \gamma_1 sign(e_q) \tag{8.25}$$

which is to extract the average signal. The second filter LPF2 is

$$\tau_2 \dot{k}_l + k_l = \gamma_2 g(e_q) \tag{8.26}$$

which is to shape the switching gain k_{2q} as below

$$k_{2q}(t) \;=\; \begin{cases} \rho + \epsilon & 0 \le\ t \le\ t_r \\ k_l(t) & t > t_r. \end{cases} \tag{8.27}$$

Here τ_1, τ_2, γ_1 and γ_2 are filter parameters appropriately chosen to meet certain convergence conditions (Xu *et al.*, 2000*d*). $g(e_q)$ is a continuous and even function of e_q. t_r is the reaching time of the sliding mode, which can be calculated in

terms of (8.24). The original switching control $k_{2q}sign(e_q)$ in **k** is now replaced by $k_{2q}(t)sign(e_q)+k_v(t)$. As long as the observer remains in the sliding mode, $e_d \to 0$, $e_q \to 0$ and $\dot{e}_q \to 0$. Note that $k_l(t)$, thereafter $k_{2q}(t)$ will also go to zero when in the sliding mode $e_q(t) = 0$. According to (8.23),

$$k_v \to -\frac{\omega}{L_q}\psi_{dm}.$$

Thus the flux linkage ψ_{dm} can be estimated as

$$\hat{\psi}_{dm} = -\frac{L_q}{\omega}k_v.$$

The estimated instantaneous motor torque is

$$\hat{T}_m = \frac{3}{2}P_p\hat{\psi}_{dm}i_q.$$

The block diagram of the gain shaped SMC torque estimator is as shown in *Fig.*8.10.

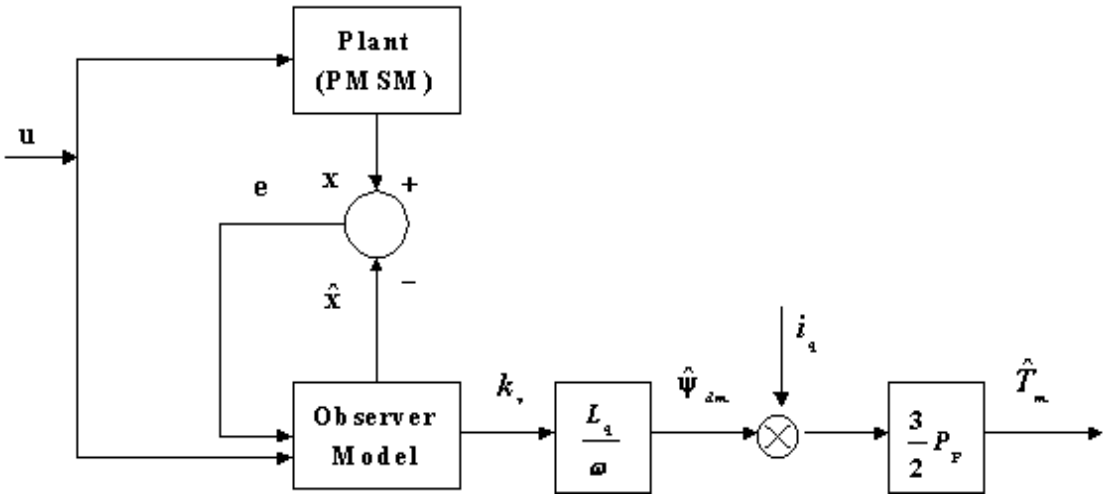

Figure 8.10. Gain shaped sliding mode torque estimator

Remark 8.4. *Estimator works only at steady state $\omega = const \neq 0$. It would be meaningless to cancel torque pulsation during transient period as fast response is the sole objective.*

8.5 Implementation and Experimental Results

A. Low-order Harmonics estimate in Practical Implementation

During the actual operation of the PMSM, it was observed that the motor speed consists of not only the sixth and twelfth harmonic ripples, but also the first and second harmonic ripples as well. The source of those low-order harmonic speed ripples is very likely due to current measurement error that produces the first and second-order harmonic torque pulsations (Chung *et al.*, 1998). However, those torque pulsations are not reflected in the estimated torque signal using the sliding mode observer technique. The sliding mode flux observer only estimate the 6th and higher harmonics in k_t. From $T_m = k_t i_q + \eta$, the additive unknown part η is left to be further estimated and compensated. An additional torque pulsation estimator is employed (Zhao *et al.*, 1997), and it essentially uses the speed pulsation information to determine the magnitude of the low torque harmonics.

From equation (8.2), the following can be expressed:

$$T_m = k_t i_q + \eta = J\frac{d\omega}{dt} + B\omega + T_l. \tag{8.28}$$

All dominant frequencies in torque pulsations can be divided into three bands: DC component, 1st/2nd harmonics, and 6th harmonics and above. At steady−state operation, the average motor torque equals the sum of the load torque and the frictional torque. As the higher frequency pulsations are naturally attenuated more by the system inertia, the motor speed ω should be predominated by DC component ω_0, as well as the 1st and 2nd harmonics, i.e. $\triangle\omega$. In practice a low-pass filter $F[\star]$ with cutoff set at the second-order harmonic frequency is used to further attenuate any sixth and higher harmonics in ω. By applying the low pass filter F to (8.28),

$$F[k_t i_q] \approx DC\ torque \tag{8.29}$$

because of the attenuation of 6th and higher harmonics;

$$F[\eta] \approx \eta, \tag{8.30}$$

because η consists mainly of 1st and 2nd harmonics; and

$$\begin{aligned} F[J\frac{d\omega}{dt} + B\omega + T_l] &\approx J\frac{dF[\omega_0 + \triangle\omega]}{dt} + F[B(\omega_0 + \triangle\omega) + T_l] \\ &\approx J\frac{dF[\triangle\omega]}{dt} + BF[\triangle\omega] + DC\ torque. \end{aligned} \tag{8.31}$$

As far as the 1st harmonics is not extremely low, say above 1 Hz,

$$J\frac{dF[\triangle\omega]}{dt} \gg BF[\triangle\omega]. \tag{8.32}$$

From the above relationships and (8.28) we finally reach

$$\hat{\eta} \approx J\frac{dF[\triangle\omega]}{dt},$$

and

$$\hat{T}_m \approx \hat{k}_t i_q + \hat{\eta} \tag{8.33}$$

Therefore, the total estimated torque consists of the DC torque from $\hat{k}_t i_q$, the 1st and 2nd harmonics from $\hat{\eta}$, 6th and higher harmonics from $\hat{k}_t i_q$, that are due to the combined effect of current measurement error and non-ideal back-emf waveform. Note that the cogging torque, characterized by 6th and higher harmonics, is left out in the process of the torque estimation. Since much of it is absorbed by the motor inertia, the speed performance is less affected with this torque residue.

B. Sampled ILC Scheme

In practice, implementation of the learning control is in digital form. Hence, the learning law in discrete form can be expressed as follows

$$\begin{aligned} \triangle i^{ref}_{q,i+1}(\theta_e) &= \triangle i^{ref}_{q,i+1}(n\triangle\theta), \qquad n\triangle\theta \leq\ \theta_e \leq\ (n+1)\triangle\theta \\ \triangle i^{ref}_{q,i+1}(n\triangle\theta) &= (1-\alpha)\triangle i^{ref}_{q,i}(n\triangle\theta) + \Gamma e_i((n+n_{step})\triangle\theta) + \Phi e_{i+1}((n-1)\triangle\theta), \end{aligned}$$

where $\triangle\theta$ is the sampling period, n is the sample index, $n \in \{0, 1, 2, \cdots, N-1\}$ and N equals the sample size (number of samples per learning cycle) with $N\triangle\theta = 2\pi(elec.)$. n_{step} is the number of steps-ahead compensation in the past tracking error signal to compensate for any delay originated from the sampled-data system and error signal filtering. The n-step ahead compensation is an inherent advantage of the ILC, since both $\triangle i_{q,i}^{ref}(\theta_e)$ and $e_i(\theta_e)$ are stored in memory components and hence can be manipulated arbitrarily in the present $(i+1)$th cycle. Typically, $n_{steps} = 1$ is chosen to make up for the one-step sampling delay encountered in the conversion of the learning control law from continuous to discrete time. The present cycle error term e_{i+1} has an index of $(n-1)$ because at the instant of the nth sample, $e_{i+1}((n-1)\triangle\theta)$ is the latest available error signal, since $e_{i+1}(n\triangle\theta)$ cannot be practically obtained before $T_{m,i+1}(n\triangle\theta)$ is produced by the physical system.

It is worthwhile to note that ILC only provides the reference compensation current $\triangle i_{q,i}^{ref}$ that adds to the constant reference current i_{q0}^{ref}, as shown in equation (8.13). During the first trial, *i.e.* at the 0th iteration $(i = 0)$, the initial value of $\triangle i_{q,i}^{ref}$ is set to zero. As the iteration progresses, $\triangle i_{q,i}^{ref}$ will approach the optimal value that cancels out the pulsating torque. However, it is not vital to set $\triangle i_{q,i}^{ref}$ to zero at the first trial. Using sufficiently accurate pre-determined values of $\triangle i_{q,i}^{ref}$ at the first trial would greatly increase the rate at which the torque pulsations are minimized. Nevertheless, one of the primary advantages of the ILC is that it does not require any a priori off-line computation. Numerical pre-determination of the initial values of $\triangle i_{q,i}^{ref}$ is not performed in this work so as to preserve the advantage of the ILC over the pre-programmed stator current excitation scheme.

C. System Set-up

As shown in Fig.8.9, the pulsating torque minimization is approached by well incorporating ILC and gain shaped sliding mode observer. During the transient state,

the ILC is turned off and $i_{q,i}^{ref}$ is provided only by the PI speed controller output. When steady-state is reached, the ILC is applied and it provides the additional compensation term $\triangle i_{q,i}^{ref}$ to the reference current signal $i_{q,i}^{ref}$ so as to minimize the torque pulsations by generating the desired current control signal.

The performance of the drive system using the ILC scheme is compared with the scheme using only the PI controller. The ratio of the peak-to-peak torque pulsation to the average torque is called the torque pulsation factor, $TRF = T_{pp}/T_{ave}$. The TRF is used as a performance criterion to evaluate the effectiveness of the proposed scheme for torque pulsation minimization. Similarly, a $SRF = S_{pp}/S_{ave}$ reflects the ratio of peak-to-peak speed to average speed is also used. The sampling times for the controllers are: ILC controller and torque estimator 500 μs, current controller 250 μs and PI speed controller 2 ms. The gains of the PI speed controller are: $K_{p,s} = 0.035$, $K_{i,s} = 0.35$, while the gains of the PI current controller: $K_{p,c} = 40$, $K_{i,c} = 600$. Notice that the current control gains are much higher than the speed control gains. The learning gains are: $\Phi = 0.04$, $\Gamma = 0.02$. The forgetting factor is $\alpha = 0.10$. The parameters of the gain shaped sliding mode observer are: $\tau_1 = 0.1$ s, $\gamma_1 = 500$, $\tau_2 = 0.5$ s, $\gamma_2 = 100$, $k_{1d} = k_{2d} = 0$, $k_{2d} = 150$, $k_{2q}(0) = 1000$, and $g(\star) = |\star|$.

In the experiment, the motor parameters of the surface-mounted PMSM are given in $Table$.8.1. The configuration of the experimental setup is shown in Fig.8.11 and the photograph of the experimental setup is shown in Fig.8.12. A DC generator provides the loading. The proposed control is realized in the DSP-based control system using the floating point DSP $TMS320C31$ with an instruction cycle of 60 MHz. The proposed algorithm is implemented using C-program and compiled using a $TMS320C31$ compiler. The position of the rotor is detected by using an incremental encoder, and the speed is then estimated using a FIR filter. Currents of two phases are measured using Hall-effect devices and the measured voltage

signal is converted into digital value using the 16−bit resolution A/D converter. All the internal data of the DSP can be displayed on an oscilloscope via a 12-bit D/A converter.

Table 8.1. Specifications of the surface mounted test PMSM

Rated power	1.64 kW	Rated speed	2000 rpm
Rated torque	7.8 Nm	Stator resistance	2.125 Ω
Stator inductance	11.6 mH	Magnet flux	0.387 Wb
Number of poles	6	Inertia	0.00289 kgm^2

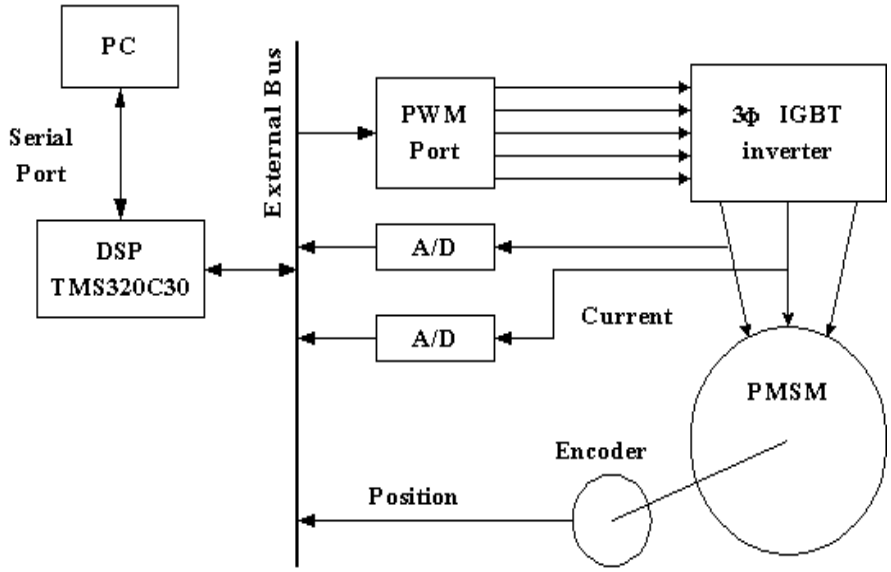

Figure 8.11. Configuration of DSP-based experimental setup

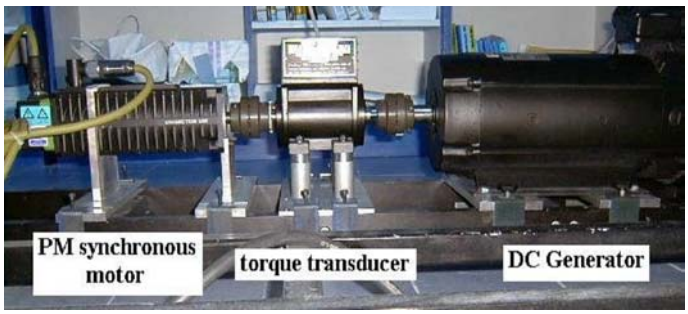

Figure 8.12. Photograph of the motor experimental setup

D. Experimental Results

In order to verify the effectiveness of the proposed scheme, experiments are carried out using the DSP-based PMSM drive system described in the previous sections. The experiment was conducted for three different motor speeds with different applied load torques: (1) $\omega^{ref} = 0.005\ p.u.\ (10rpm)$, $T_l = 0.045\ p.u.\ (0.35Nm)$; (2) $\omega^{ref} = 0.025\ p.u.\ (50rpm)$, $T_l = 0.154\ p.u.\ (1.2Nm)$; (3) $\omega^{ref} = 0.026\ p.u.\ (51.5rpm)$, $T_l = 0.051\ p.u.\ (0.4Nm)$.

As shown in Fig.8.13, Fig.8.14 and Fig.8.15, after ILC compensation the toque ripples are minimized significantly with the TRF varied from 36.1% to 5.6%, from 9.7% to 1.9% and from 27.5% to 7.5% respectively. The frequency spectrums of all the cases are also shown in the figures. The reference speeds and the load torques from Fig.8.16 to Fig.8.18 belong to case (3) as discussed above. In Fig.8.16, the SRF is evaluated which varied from 9% to 3% before and after ILC compensation. This shows that speed pulsations are also minimized as the torque pulsations minimized. From Fig.8.17, we can observe that the current canceling the flux harmonics are added to the sinusoidal current so that the phase current contains the high order harmonics as such as $5th$, $7th$, $11th$, $13th$ and so on. It is noted in Fig.8.18(b) that the reference q-axis current contains the high order harmonics $\triangle i_{q,i}^{ref}$ after ILC compensation whereas $Fig.8.18(a)$ shows i_q^{ref} the DC component only. The estimated flux is shown in Fig.8.19. Fig.8.20 verifies validity of the implementation considerations in frequency domain described in subsection A. The total estimated torque is quite consistent with the measured speed waveform both in lower and higher order harmonics. In Fig.8.21, the transient responses of the estimated torque and the real torque are uniformly same. In a whole, the presence of the 1st, 2nd and 6th harmonics in the speed, as well as the reduction of these harmonics with compensation are evident from the figures shown above. The new scheme significantly minimizes most of the torque pulsations.

8.6 Conclusion

A new modular control approach is proposed and applied to the speed control of PMSM drive system. Two new modules, the ILC module and torque estimation module based on gain shaped sliding mode observer, are incorporated to work consistently with the exisitng PI speed and current control modules. The iterative learning control module guarantees convergence of the motor torque to the desired value, at the same time minimizes torque pulsations and only requires minimal knowledge of the machine parameters. The torque estimation module effectively reconstructs the pulsating flux and the low harmonics. Experiments have been carried out to evaluate the performance of the proposed conttrol approach, which validate the expected effectiveness in minimizing torque and speed pulsations.

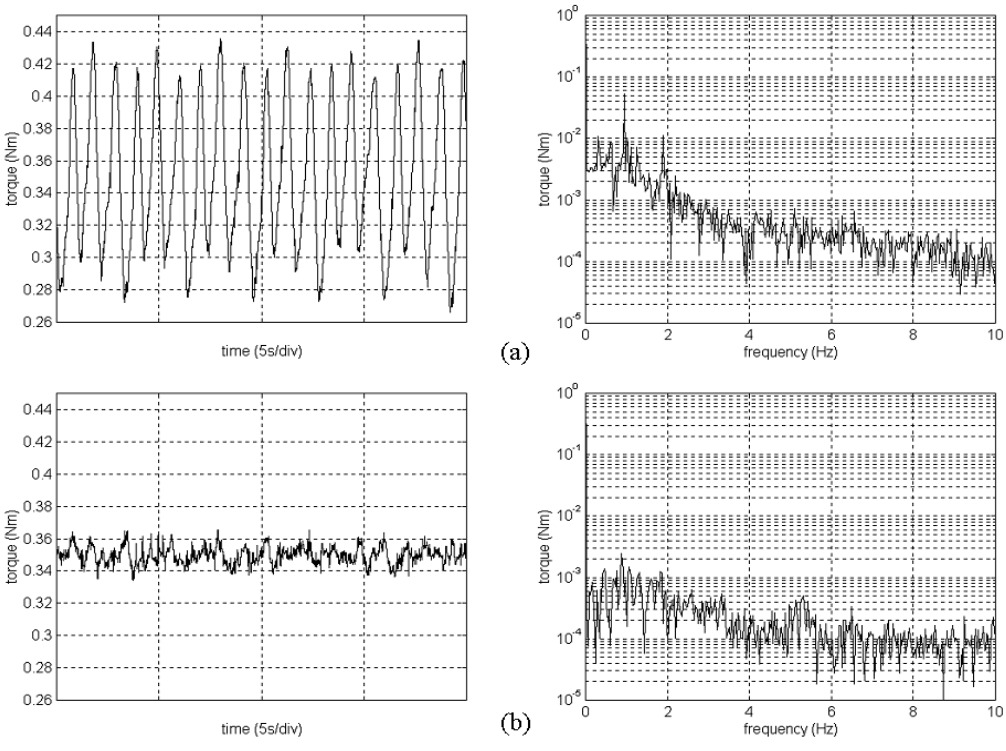

Figure 8.13. Steady-state motor estimated torque response under load of $T_l = 0.045$ $p.u.$ $(0.35Nm)$ at $\omega^{ref} = 0.005$ $p.u.$ $(10rpm)$. (a) Without ILC compensation $(TRF = 36.1\%)$. (b) With ILC compensation $(TRF = 5.6\%)$.

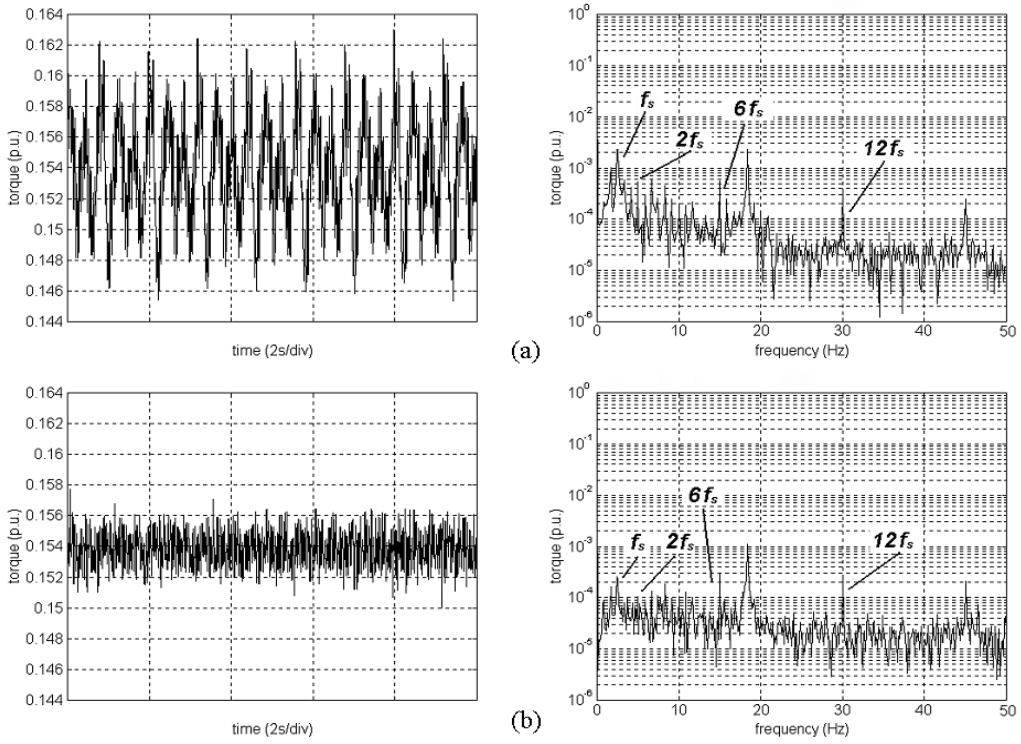

Figure 8.14. Steady-state motor estimated torque response under load of $T_l = 0.154\ p.u.\ (1.2Nm)$ at $\omega^{ref} = 0.025\ p.u.\ (50rpm)$. (a) Without ILC compensation $(TRF = 9.7\%)$. (b) With ILC compensation $(TRF = 1.9\%)$.

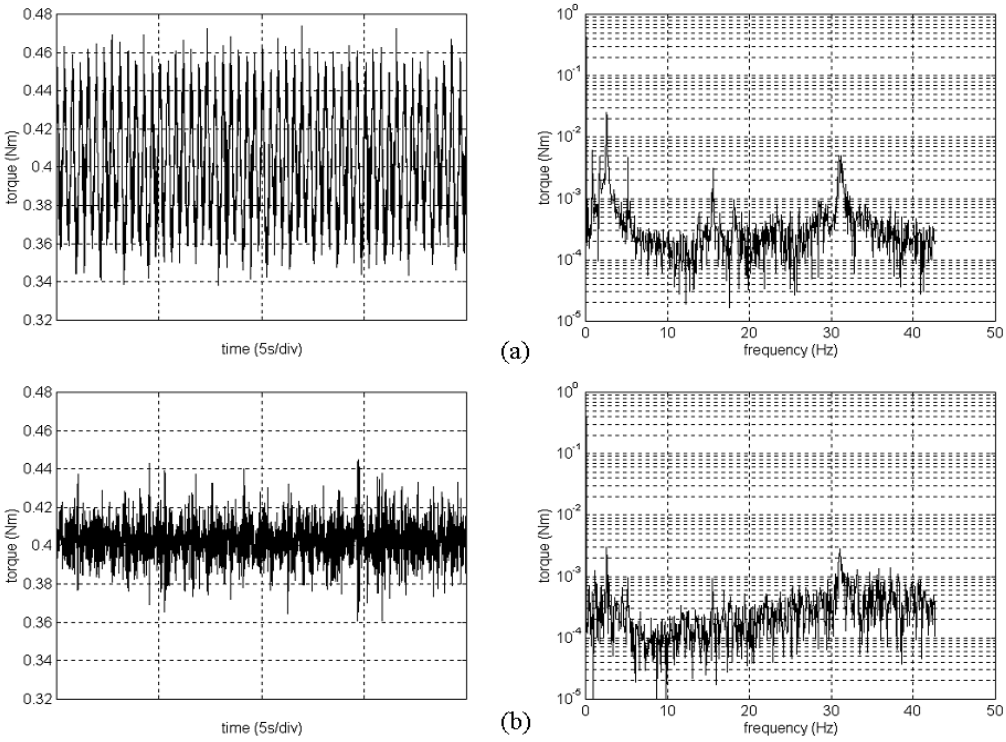

Figure 8.15. Steady-state motor estimated torque response under load of $T_l = 0.051$ $p.u.$ $(0.4Nm)$ at $\omega^{ref} = 0.026$ $p.u.$ $(51.5rpm)$. (a) Without ILC compensation $(TRF = 27.5\%)$. (b) With ILC compensation $(TRF = 7.5\%)$.

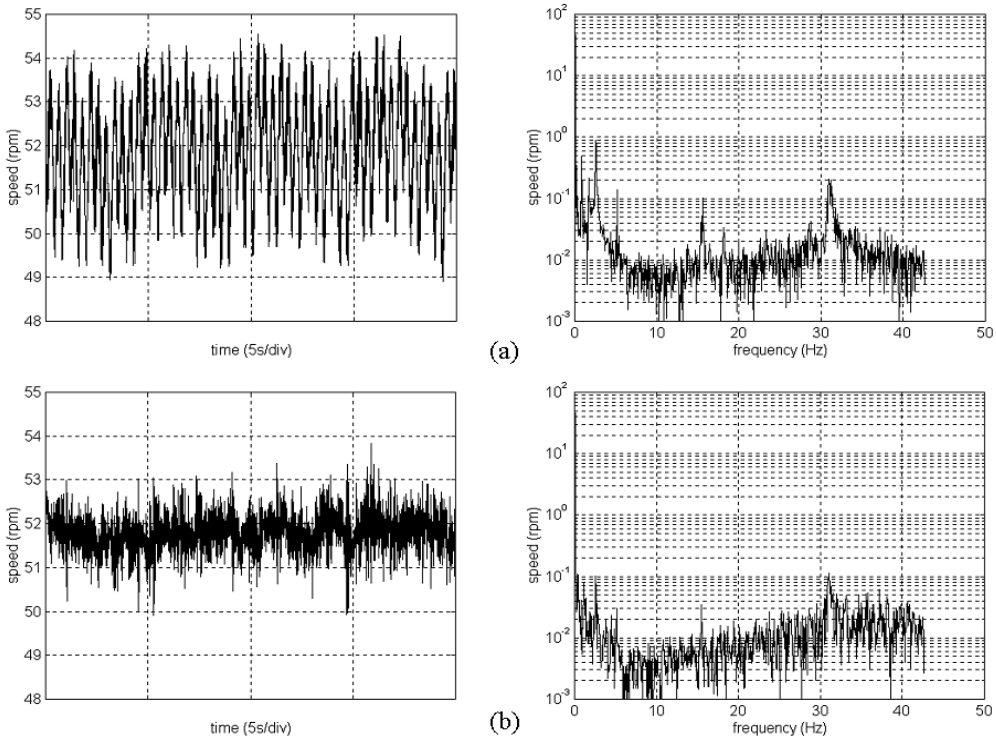

Figure 8.16. Steady-state motor speed response under load of $T_l = 0.051$ $p.u.$ $(0.4Nm)$ at $\omega^{ref} = 0.026$ $p.u.$ $(51.5rpm)$. (a) Without ILC compensation $(SRF = 9\%)$. (b) With ILC compensation $(SRF = 3\%)$.

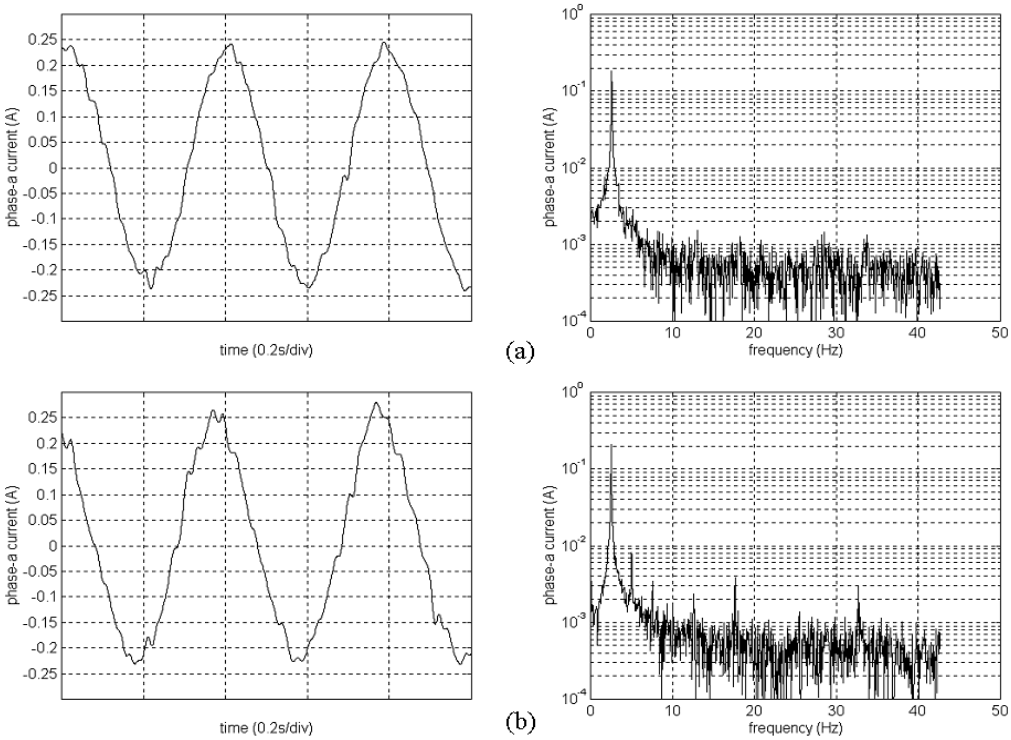

Figure 8.17. Configuration of the steady-state motor phase current with $T_l = 0.051$ $p.u.$ $(0.4Nm)$ and $\omega^{ref} = 0.026$ $p.u.$ $(51.5rpm)$. (a) Without ILC compensation. (b) With ILC compensation.

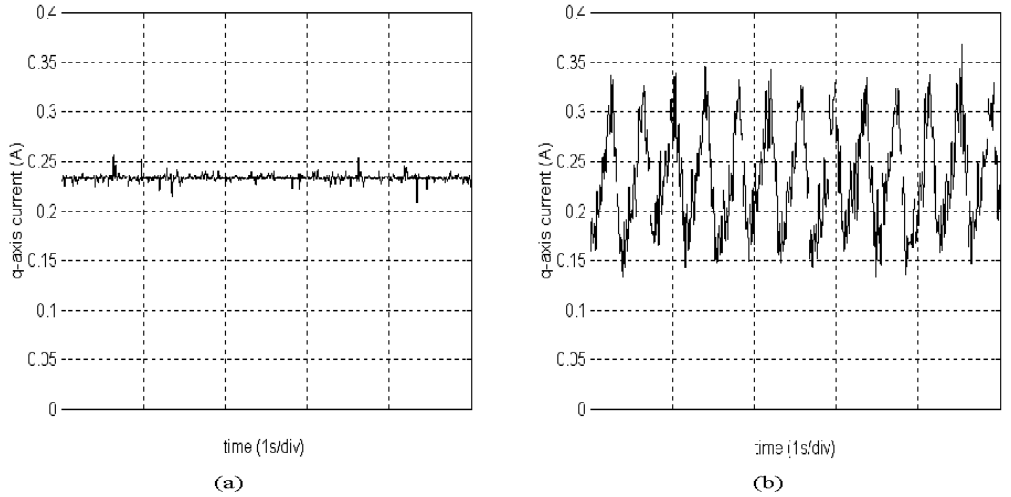

Figure 8.18. Comparison of reference q-axis current with $T_l = 0.051$ $p.u.$ $(0.4Nm)$ and $\omega^{ref} = 0.026$ $p.u.$ $(51.5rpm)$. (a) Without ILC compensation. (b) With ILC compensation.

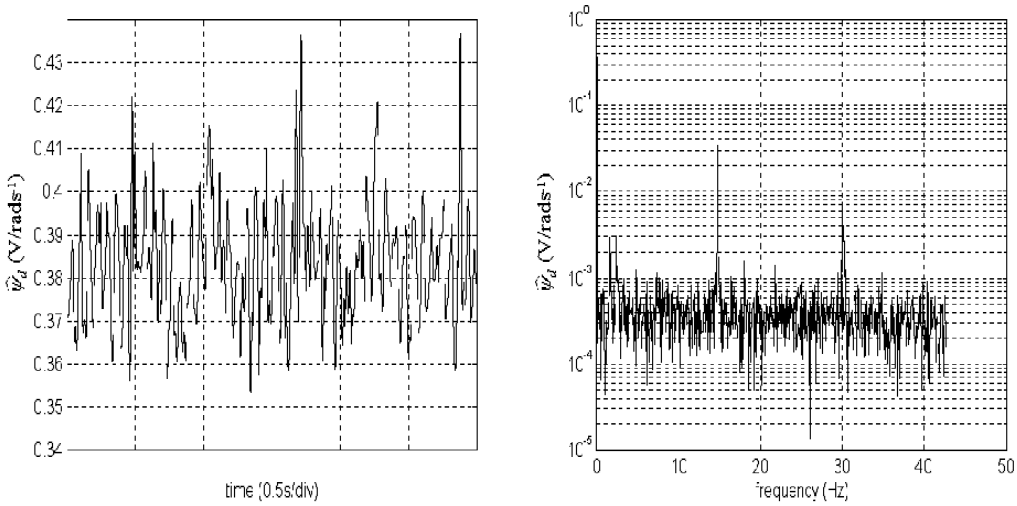

Figure 8.19. (a) Estimated flux. (b) Frequency spectrum ($6f_s = 15\ Hz$ and $12f_s = 30\ Hz$ where $f_s = 2.5\ Hz$).

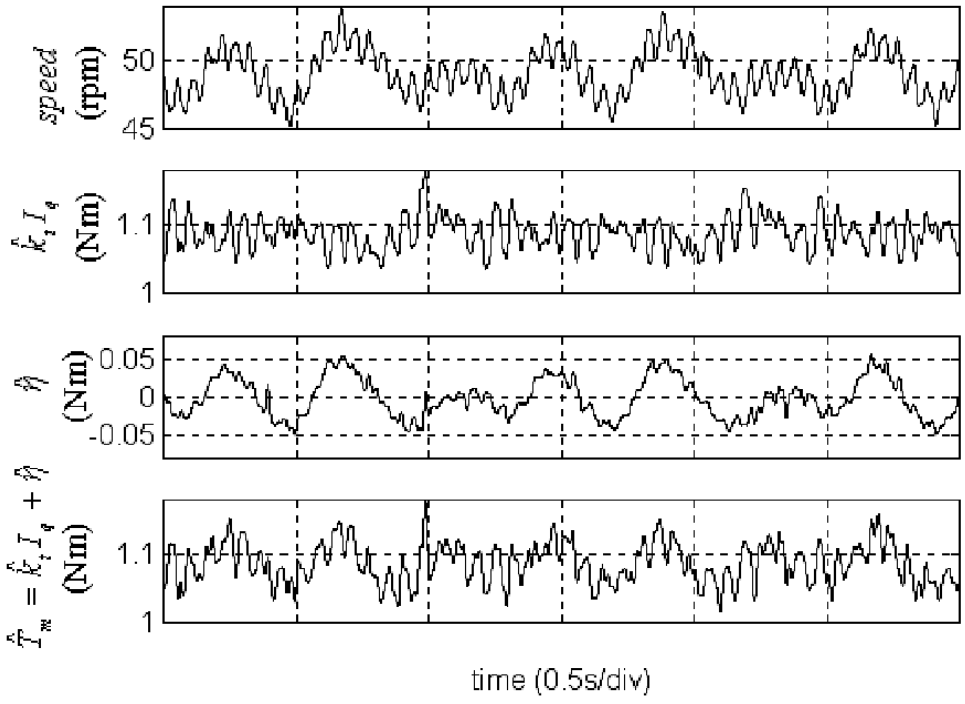

Figure 8.20. Comparison of estimated torque with speed oscillations

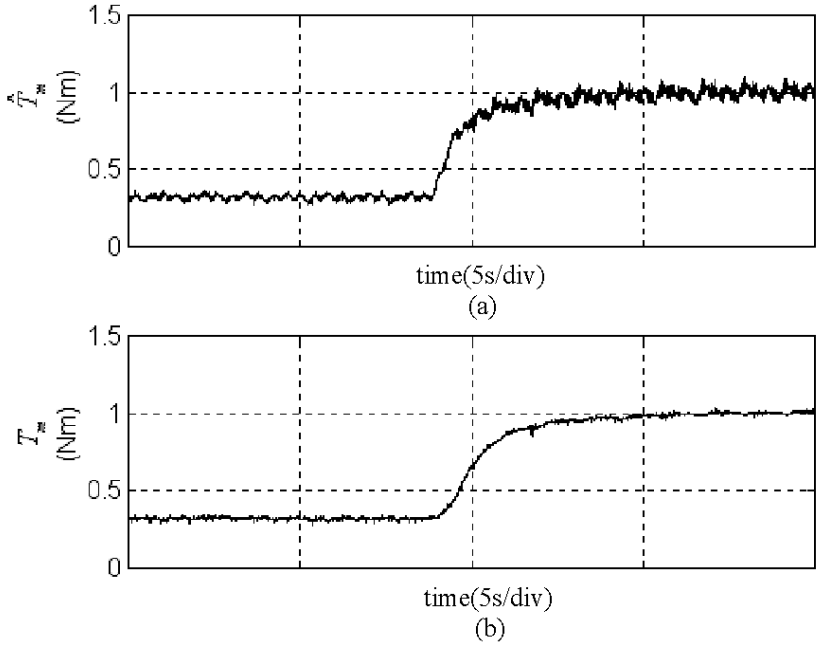

Figure 8.21. (a) Transient response of the estimated torque. (b) Transient response of the real torque.

Chapter 9

On the Sliding Mode Control for DC Servo Mechanisms in the Presence of Unmodeled Dynamics

9.1 Introduction

It is well known that a typical Sliding Mode Control (SMC) with switching mechanism has superior robustness to matched system uncertainties (Utkin, 1992) (Xu *et al.*, 1997) (Man and Yu, 1997) (Xu *et al.*, 2000*a*) (Su and Tsai, 2001) (Shin and Choi, 2001). However, such a SMC may lose its robustness when unmodeled system dynamics exist, as the discontinuous switching will lead to limit cycles – the chattering phenomenon.

There are two factors jointly generating a limit cycle: a relative degree above two and an overly high control gain around the equilibrium. According to classical control theory, a higher relative degree implies the possibility of a large phase lag beyond -180°. Meanwhile a higher gain means less phase margin. Unfortunately,

a typical discontinuous switching control in SMC processes has an infinite gain in the equilibrium. When the system is strictly positive real (relative degree one), a phase margin of 90° is guaranteed. Limit cycles occur mainly in two circumstances: either in the presence of a sampling delay or an unmodeled dynamics of relative degree above two.

Let us first look at the sampling delay. Since a sampling mechanism generates a pure time delay, the corresponding Nyquist curve will move spirally towards the origin and cut cross the negative real axis infinitely many times. Thus at certain phase cross frequency the phase reaches $-180°$ and limit cycles occur. As far as a servo system is concerned, with a perfect switching mechanism (infinite switching frequency available or equivalently the sampling delay is infinitesimal), phase crossover frequency is also infinity and the limit cycle magnitude is zero owing to the low pass filter nature of the servo. In practice when the sampling frequency is limited, a common way to eliminate chattering is to incorporate a smoothing control scheme to reduce the gain around the equilibrium.

In the presence of unmodeled dynamics, the chattering problem will worsen due to the extra phase lag, thereafter a rather lower phase crossover frequency and a larger chattering magnitude will occur. In particular when the unmodeled part has a relative degree of two or more, limit cycles are inevitable even with a perfect switching mechanism. Most SMC designs for servomechanism ignore two kinds of dynamic factors in the motor stator circuit and sensor devices (encoder and tachogenerator). They will present at least two first order low pass filters cascaded to the mechanical part of the servomechanism.

Here a question is, can we take those dynamic factors into consideration in SMC design? The first difficulty we have is the unavailability of internal state variables corresponding to those unmodeled dynamics. The second difficulty is the presence

of unknown parameters in unmodeled dynamics, which hinders state estimation. Third, by taking stator dynamics, encoder and tachogenerator dynamics into account, the system is of fifth order (likely higher with state estimation), and the sliding mode controller would be over complicated for practical servo applications. On the other hand, the unmodeled dynamics are stable and usually less influential to matched disturbance rejection. Thus we can extend the widely adopted chattering elimination approach – smoothing the control input. Note that this way leads to a lower control gain in servo mechanisms, consequently to certain extent sacrifices control precision. However this will be rewarded by the elimination of limit cycles that usually generate a larger tracking error and lead to fast wear and tear of torque transmission device. Moreover, the SMC can be designed solely based on the reduced order servo system, i.e. the mechanical part without concerning the unmodeled dynamics.

In this chapter, a new fractional interpolation based smoothing scheme is proposed to eliminate the limit cycle in DC servo mechanisms. Because of the nonlinear switching control in SMC, the describing function method, an extended version of the frequency response method for linear systems (Slotine and Li, 1991) (Chung and Lin, 1998), is used to analyze and predict the limit cycle approximately. Through both theoretical analysis and simulation of a typical DC servo mechanism, it is verified that the limit cycle occurs if a conventional SMC with signum function is applied, and disappears when the SMC is revised with an appropriate smoothing scheme. Many chattering reduction methods have been proposed (Kachroo and Tomizuka, 1996) (Bartolini *et al.*, 1998) (Krupp and Shtessel, 1999), which are effective when the process structure, in particular the relative degree, is known and fixed. However, these methods are not applicable to our cases because either the unmodeled dynamics may change the process structure, or relative degree is not available in the controller design.

The chapter is organized as follows. Section 9.2 gives the descriptions of the DC servo motor and the unmodeled dynamics. In Section 9.3, via describing function techniques, the limit cycle problem associated with SMC is first analyzed, then a new smoothing function is introduced to eliminate limit cycles. Section 9.4 considers a DC servo motor and shows the validity of the analysis and the effectiveness of the proposed control scheme.

9.2 Problem Formulation

A. Mechanical Dynamics of DC Servo

A typical DC servo motor can be expressed as below

$$J\ddot{\theta} + b_s\dot{\theta} + k_s\theta = \tau + \tau_l \tag{9.1}$$

where θ is the motor angular displacement, τ and τ_l are the motor torque and load torque respectively, J is the total inertia, b_s is the viscous friction coefficient and k_s is the spring constant. Defining $x_1(t) = \theta$ and $x_2(t) = \dot{\theta}$, the state space form of (9.1) is

$$\begin{cases} \dot{x}_1(t) = x_2(t), \\ \dot{x}_2(t) = -\frac{1}{J}(k_s x_1 + b_s x_2) + \frac{1}{J}(\tau + \tau_l) \end{cases} \tag{9.2}$$

where $x_1(0) = \theta(0)$ and $x_2(0) = \dot{\theta}(0)$. Note that (9.1) or (9.2) represents the mechanical subsystem of the DC servo. Often the sliding surface is designed by taking this mechanical subsystem into account, which is $\sigma = e_2 + c_1 e_1$ where $e_1 = x_1 - x_{d,1}$, $e_2 = x_2$ and $x_{d,1}$ is a set point. The simplest switching control is $\tau = -k\ sign(\sigma)$, where the gain k is designed appropriately by taking all servo system uncertainties into account. A convenient design tool is the Lyapunov's direct method with the Lyapunov function candidate $V = \frac{1}{2}\sigma^2$. It is worthy to

point out that the relative degree from the system input τ to the extended output σ is one. Hence the process may have a phase margin of 90°.

B. Unmodeled Dynamics

In practice the DC servo motor has a first order stator electrical dynamics

$$\begin{aligned} \dot{I}_q &= \frac{1}{L_q}(u - RI_q), \\ \tau &= k_t I_q, \end{aligned} \tag{9.3}$$

where I_q is the q-axis current, L_q is the q-axis inductance, R is the stator resistance, u is the control input voltage and k_t is the torque constant. Define a new state $x_3(t) = I_q$, (9.3) becomes

$$\dot{x}_3 = \frac{1}{L_q}(u - Rx_3), \tag{9.4}$$

and its transfer function is

$$D_1(s) = \frac{\tau(s)}{u(s)} = \frac{\frac{k_t}{L_q}}{s + \frac{R}{L_q}}. \tag{9.5}$$

Another source of unmodeled dynamics is related to sensing devices. A sensor is truly a dynamic system and the general dynamic structure of a sensor is (Bernstein, 2001)

$$\dot{z} = f(z, x), \qquad \hat{x} = \phi(z, x), \tag{9.6}$$

where z is the internal sensor state, x is the physical input to the sensor, and $\hat{x}$ is the sensor output. In the DC servo motor, the angular displacement x_1 is measured by encoder and the angular velocity x_2 by tachogenerator. By considering the sensor dynamics, we have the following relationship

$$\tau_1\dot{\hat{x}}_1 + \hat{x}_1 = k_1 x_1, \qquad \tau_2\dot{\hat{x}}_2 + \hat{x}_2 = k_2 x_2,$$

where $\hat{x}_1$ and $\hat{x}_2$ are the acquired state variables through sensor dynamics. In practice the sensor DC gains k_1 and k_2 can be easily calibrated through static

tests. However it is not an easy task to accurately measure time constants τ_1 and τ_2.

The transfer function from the applied switching surface $\hat{\sigma}$ to the theoretical one is

$$\begin{aligned} D_2(s) &= \frac{\hat{\sigma}(s)}{\sigma(s)} = \frac{\hat{x}_2 + c_1(\hat{x}_1 - x_{d,1})}{x_2 + c_1(x_1 - x_{d,1})} = \frac{\frac{k_2 s}{\tau_2 s+1} + \frac{c_1 k_1}{\tau_1 s+1}}{s + c_1} \\ &= \frac{\tau_1 k_2 s^2 + (k_2 + c_1 k_1 \tau_2)s + c_1 k_1}{[\tau_1 \tau_2 s^2 + (\tau_1 + \tau_2)s + 1](s + c_1)}. \end{aligned} \tag{9.7}$$

Remark 9.1. *It is a common practice to use low pass filters to get rid of measurement noise. In such case τ_1 and τ_2 should include these filter time constants. In addition, there often exist a variety of parasitic dynamics in practical systems and they also account for the existence of unmodeled dynamics.*

Due to the existence of above two classes of unmodeled dynamics, the system may not work properly under a conventional sliding mode scheme with signum function, or even under a smoothing control scheme. This can be shown in the analysis of the subsequent sections via describing function techniques.

9.3 Describing Function Techniques Based Analysis

A. Limit Cycle Problem with Signum Function

The system in (9.1) can be rewritten as an extended error dynamics

$$\begin{cases} \dot{e}_1(t) = e_2(t), \\ \dot{e}_2(t) = -a_0 e_1 - a_1 e_2 - a_0 e_3 + b\tau \\ \dot{e}_3(t) = 0 \end{cases} \tag{9.8}$$

where $a_0 = k_s/J$, $a_1 = b_s/J$, $b = 1/J$ and $e_3(t) = x_{d,1}$ is a constant. The switching control with signum function is $\tau = -k\ sign(\sigma)$. The block diagram of the system is shown in $Fig.9.1$, where $G(s)$ can be regarded as a low pass filter without poles at the origin

$$G(s) = \frac{\sigma(s)}{\tau(s)} = \frac{b(s + c_1)}{s^2 + a_1 s + a_0}. \tag{9.9}$$

Define $G_d(s) = D_1(s)G(s)D_2(s)$ which is the transfer function of the plant linear part.

Assume there exists a self-sustained oscillation (limit cycle) of amplitude A_c and frequency ω_c. When ω_c is sufficiently high in comparison with the cut-off frequency of $G_d(j\omega_c)$, according to the describing function analysis method the switching surface can be approximately written as $\sigma = A_c sin(\omega_c t)$. Limit cycles exist if the Nyquist curve of the linear plant $G_d(j\omega_c)$ intersects with $H(A, \omega) = -1/N(A, \omega)$, where $N(A, \omega)$ is the describing function of the system nonlinear part. The describing function of the signum function is $N(A) = 4k/\pi A$. Thus $H(A, \omega) = -1/N(A)$ is the whole negative real axis with the initial point $(0, 0)$ corresponding to $A = 0$.

There will be three possible classes of system motions in terms of the intersection points as shown in $Fig.9.2$. In the absence of unmodeled dynamics D_1 and D_2, since the relative degree of $G(s)$ in (9.9) is one, there is an intersection at $(A_c = 0 \cup \omega_c = \infty)$. This is exactly the ideal sliding motion which has infinite switching frequency and zero off-set. Owing to the theoretically larger phase margin (90°), any extra small phase lag practically existing, such as sampling delay, will produce a limit cycle with very small magnitude. Next when the system linear part has relative degree two, i.e. either GD_1 or GD_2 is under consideration, the intersection point is still at $(A_c = 0 \cup \omega_c = \infty)$. However, the phase margin in this case could be zero, which implies that the system may not be robust at all. Hence the extra small phase lag may produce limit cycle with relatively large magnitude. Finally,

if a second order unmodeled dynamics $D_1 D_2$ is present, there definitely exists one intersection at $(A_c > 0 \cup \omega_c < \infty)$, thereby limit cycle motion exists even without considering any extra phase lag factors.

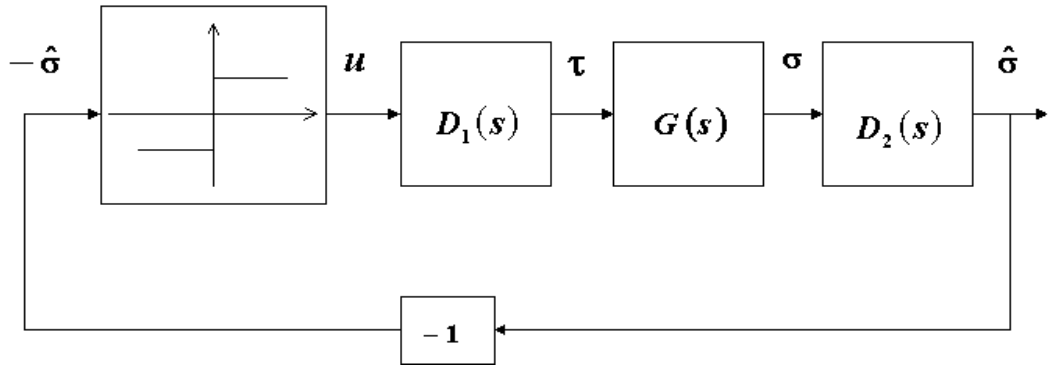

Figure 9.1. Block diagram of the DC servo motor with signum function.

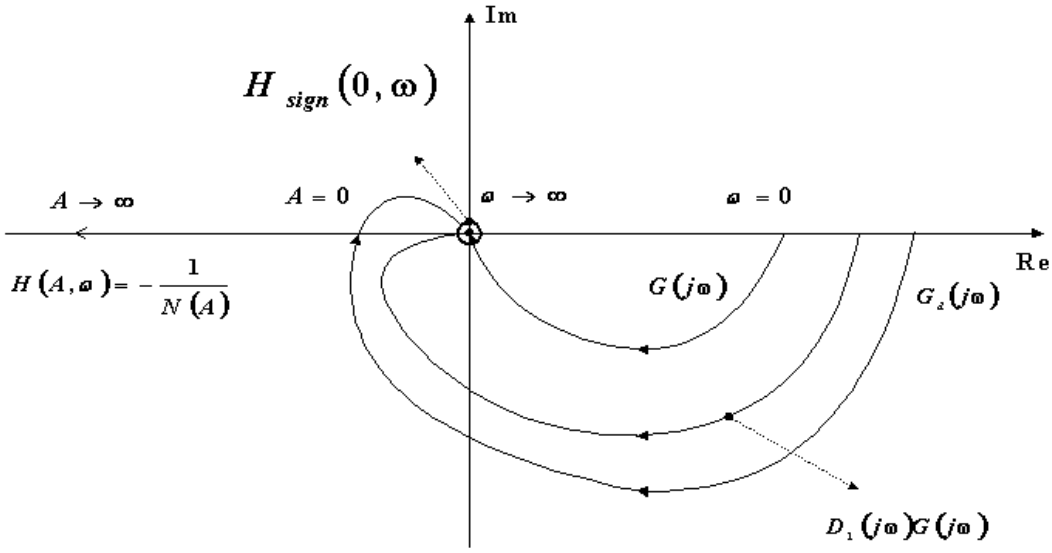

Figure 9.2. Detections of the limit cycle in the DC servo motor.

B. Limit Cycle Elimination with a New Fractional Interpolation Smoothing Control Scheme

In order to eliminate the limit cycle problem described above, a new fractional interpolation smoothing control scheme (as in (6.7) in the subsection 6.3.1 in Chapter

6) is proposed to replace the signum function

$$u = -k\ \frac{(|\sigma| + \delta_1)\sigma}{(|\sigma| + \delta)^2} = -k_e\ sign(\sigma), \tag{9.10}$$

where the equivalent switching gain is

$$k_e = k\ \frac{(|\sigma| + \delta_1)|\sigma|}{(|\sigma| + \delta)^2}, \tag{9.11}$$

and δ and $\delta_1 = 2\delta + \dfrac{\delta^2}{\alpha}$ are two design parameters. As shown in the subsection 6.3.2, the new smoothing scheme does possess the highly preferred three properties and has a smoother shape and an adjustable gain within the precision bound in comparison with the saturation scheme.

Now let us show that the new fractional interpolation smoothing scheme is able to eliminate limit cycles, as given in the following theorem.

Theorem 9.1. *The Nyquist plot of* $H(A,\omega) = -\dfrac{1}{N(A)}$, *where* $N(A)$ *is the describing function of the proposed controller, will be a line on the negative real axis from the initial point* $\left(-\dfrac{\delta\alpha}{k(2\alpha+\delta)}, 0\right)$ *to the end point* $(-\infty, 0)$.

Proof: The input of the control function in (9.10) is σ. When only the fundamental is being considered, we have $-\sigma = Asin(\omega t)$. Accordingly the output is

$$u(t) = -\frac{k[|Asin(\omega t)| + \delta_1]\,[-Asin(\omega t)]}{[|Asin(\omega t)| + \delta]^2} = \frac{k[|Asin(\omega t)| + \delta_1]Asin(\omega t)}{[|Asin(\omega t)| + \delta]^2}. \tag{9.12}$$

Define $r = Asin(\omega t)$ for simplicity. In the case $A \leq\ \delta$ which is the condition for the following series expansion, (9.12) can be expressed by

$$\begin{aligned} u(t) &= \frac{k(|r| + \delta_1)r}{(|r| + \delta)^2} = -\frac{k(|r| + \delta_1)r}{\delta}\frac{d}{d|r|}\left(\frac{1}{1 + \frac{|r|}{\delta}}\right) \\ &= -\frac{k(|r| + \delta_1)r}{\delta}\frac{d}{d|r|}\left[1 - \frac{|r|}{\delta} + \left(\frac{|r|}{\delta}\right)^2 + \cdots + (-1)^n\left(\frac{|r|}{\delta}\right)^n + \cdots\right] \\ &= -\frac{k(|r| + \delta_1)r}{\delta}\left[-\frac{1}{\delta} + 2\left(\frac{|r|}{\delta^2}\right) + \cdots + (-1)^n n\left(\frac{|r|^{n-1}}{\delta^n}\right) + \cdots\right] \end{aligned}$$

$$
\begin{aligned}
&= \frac{kr}{\delta^2}\left\{\delta_1 - (2\delta_1-\delta)\frac{|r|}{\delta} + \cdots + (-1)^{n+2}\left[(n+1)\delta_1 - n\delta\right]\left(\frac{|r|}{\delta}\right)^n + \cdots\right\} \\
&= \sum_{i=1}^{i=\infty}(-1)^{i+1}\frac{\left[i\delta_1-(i-1)\delta\right]kr|r|^{i-1}}{\delta^{i+1}} \\
&= \sum_{i=1}^{i=\infty} h_i, \qquad (9.13)
\end{aligned}
$$

where $h_i = (-1)^{i+1}\frac{\left[i\delta_1-(i-1)\delta\right]kr|r|^{i-1}}{\delta^{i+1}}$. The output $u(t)$ in (9.12) can be expanded as a Fourier series, with the fundamental being as

$$u = \bar{a}_1 cos(\omega t) + \bar{b}_1 sin(\omega t).$$

Because $u(t)$ is an odd function with respect to σ, $\bar{a}_1 = 0$. The coefficient $\bar{b}_1$ is

$$
\begin{aligned}
\bar{b}_1 &= \frac{1}{\pi}\int_{-\pi}^{\pi} u(t)sin(\omega t)d\omega t = \frac{1}{\pi}\int_{-\pi}^{\pi}\frac{k[|Asin(\omega t)|+\delta_1]Asin(\omega t)}{\left[|Asin(\omega t)|+\delta\right]^2}sin(\omega t)d\omega t \\
&= \frac{1}{\pi}\int_{-\pi}^{\pi}\sum_{j=1}^{j=\infty} h_j sin(\omega t)d\omega t = \sum_{j=1}^{j=\infty} b_j. \qquad (9.14)
\end{aligned}
$$

The integrations of the first three parts are $b_1 = \frac{Ak\delta_1}{\delta^2}$, $b_2 = -\frac{2A^2k(2\delta_1-\delta)}{\pi\delta^3}$ and $b_3 = \frac{A^3k(3\delta_1-2\delta)}{4\delta^4}$. From (9.13), it is clear that the jth ($j > 3$) component b_j is proportional to A^j, thus

$$\bar{b}_1 = \frac{Ak\delta_1}{\delta^2} - \frac{2A^2k(2\delta_1-\delta)}{\pi\delta^3} + \frac{A^3k(3\delta_1-2\delta)}{4\delta^4} + \sum_{j=4}^{\infty} A^j d_j,$$

where d_j is the coefficient composed of the parameters k, δ_1 and δ. Therefore, when $A \leq \delta$ is satisfied, the describing function of the proposed control scheme is

$$N(A) = \frac{\bar{b}_1}{A} = \frac{k\delta_1}{\delta^2} - \frac{2Ak(2\delta_1-\delta)}{\pi\delta^3} + \frac{A^2k(3\delta_1-2\delta)}{4\delta^4} + \sum_{j=4}^{\infty} A^{j-1}d_j, \qquad (9.15)$$

and the initial point is r

$$H(A,\omega)\,|_{A=0} = -\frac{1}{N(A)}\,|_{A=0} = -\frac{\delta\alpha}{k(2\alpha+\delta)}.$$

From (9.14) and (9.12), $H(A,\omega)$ can also be expressed as

$$H(A,\omega) = -\frac{1}{N(A)} = -\frac{A}{\bar{b}_1} = -\frac{\pi}{4k\int_0^{\frac{\pi}{2}} v(A,\omega t)d\omega t},$$

where $v(A,\omega t) = \dfrac{[|Asin(\omega t)| + \delta_1]sin^2(\omega t)}{[|Asin(\omega t)| + \delta]^2}$. $\forall A > 0$, $v(A,\omega t) < v(0,\omega)$ because

$$\begin{aligned} v(A,\omega t) - v(0,\omega t) &= -\frac{sin(\omega t)^2|Asin(\omega t)|}{\delta^2\left[|Asin(\omega t)| + \delta^2\right]^2}\left[(2\delta + \frac{\delta^2}{\alpha})|Asin(\omega t)| + (3\delta^2 + \frac{2\delta^3}{\alpha})\right] \\ &< 0. \end{aligned}$$

Then

$$\forall A \in (0,\infty), \quad H(A,\omega) < H(0,\omega) = -\frac{\delta\alpha}{k(2\alpha+\delta)} < 0.$$

Let γ be the maximum value of the magnitude of $|G_d(j\omega)|$ at the phase crossover frequency ω_{pc}, i.e. the leftmost point m in $Fig.9.3$, while the unmodeled dynamics D_1 and D_2 take all possible values. By properly selecting the parameters δ and α such that $\delta\alpha/\left[k(2\alpha+\delta)\right] > \gamma$, we can achieve the sliding mode without any limit cycle. It should be noted that in most robust control systems designed in frequency domain, such as H^∞ control, the uncertainty bound γ is known *a prior*.

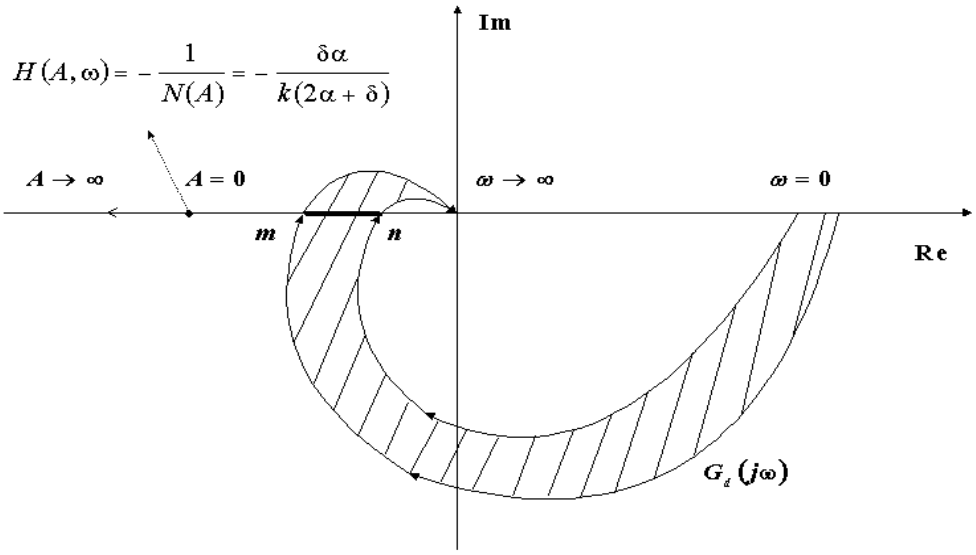

Figure 9.3. Detection of a limit cycle in the case of a second order unmodeled dynamics.

Remark 9.2. *Since the limit cycle is definitely an undesirable phenomenon in SMC, in order to thoroughly eliminate limit cycle the product of $\delta\alpha$ should not be*

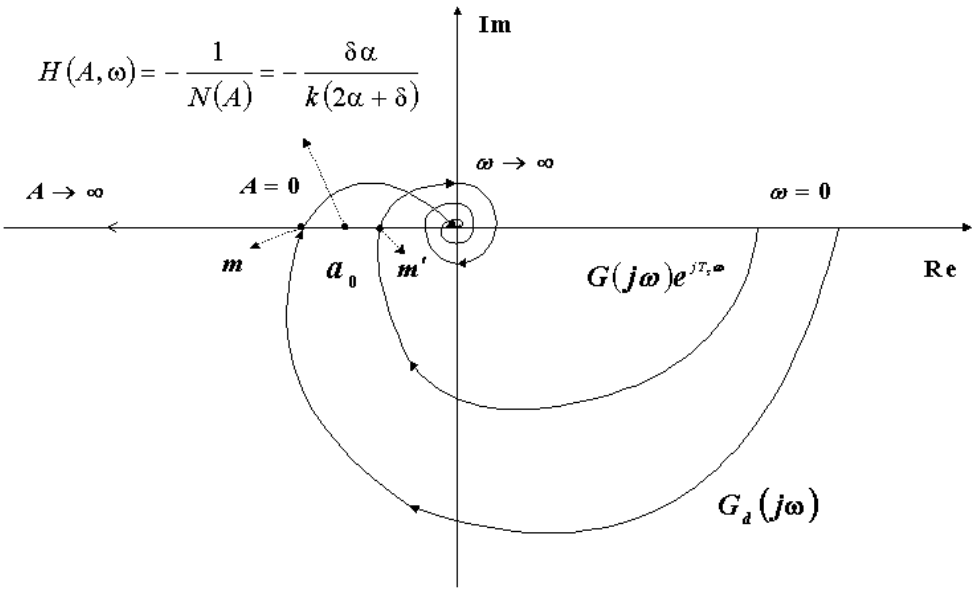

Figure 9.4. Detection of a limit cycle in the case of a second order unmodeled dynamics and sampling delay.

too small, such that H can be kept to the left of the point m which represents the worst case. This implies that a trade-off has to be made in SMC design between two contradict objectives: smoothness and accuracy. This underlying idea essentially applies to all smoothing schemes in SMC.

Remark 9.3. *A sampled-data system with limited sampling frequency will inevitably incur a pure time delay e^{-sT_s} with the sampling period T_s. Fig.9.4 shows that the Nyquist plot of system $G(s)e^{-sT_s}$ approaches the origin in a spiral manner, hence there are theoretically infinite intersections with the negative real axis, therefore infinite number of limite cycles. Usually in practical systems the sampling period is sufficiently small, thus the m' point, which corresponds to the limit cycle with the maximum magnitude, will be very near to the origin. This implies that limit cycles due to sampling delay can be easily avoided by introducing a smoothing function which moves the rightmost point of $H(0,\omega)$ from origin to the position a_0. Note that a small α can achieve this if a_0 is small. As a consequence, a small T_s allows a higher precision bound. It can also be seen from Fig.9.4 that, to avoid*

the point m we have to further move a_0 leftwards, leading to a rather larger α – a lower tracking precision.

9.4 An Illustrative Example with DC Servo Motor

Consider the DC servo motor dynamics described by (9.1), (9.3) and (9.7) jointly. The parameters are $J = 6.0 \times 10^{-2}\ Kg \cdot m$, $k_s = 0.255\ N \cdot m/rad$, $b_s = 0.075\ N \cdot m \cdot sec/rad$, $L_q = 11.6 \times 10^{-3}\ H$, $R = 2.215\ \Omega$, $k_t = 1$, $\tau_1 = 0.01$, $\tau_2 = 0.008\ sec$ and $k_1 = k_2 = 1$. The set point is $\theta_d = 2\ rad$. The sampling interval is $T_s = 0.001\ sec$. The sliding surface is $\sigma = e_2 + 6e_1$. The initial values of the states are $x_1(0) = 1$ and $x_2(0) = -1$. The initial values of unmodeled dynamics are assumed to be zero. The switching control gain can be calculated as $k = 5.3$. $G(s)$ in (9.9) is

$$G(s) = \frac{\sigma(s)}{\tau(s)} = \frac{16.67(s+6)}{s^2 + 1.25s + 4.25} \tag{9.16}$$

and

$$D_1(s) = \frac{86.2}{s + 190.93}, \qquad D_2(s) = \frac{125s^2 + 12585s + 75000}{(s^2 + 225s + 12500)(s+6)}.$$

The prior knowledge of the unmodeled dynamics is that the parameters L_q, R, k_t, τ_1 and τ_2 vary $\pm 20\%$ from their rated values.

Case 1: No Unmodeled Dynamics

First look at the SMC with signum function. As shown in *Fig.*9.5, there exists a very small limit cycle in the absence of unmodeled dynamics. This limit cycle is due to sampling delay and can be easily eliminated by the smoothing scheme (9.10) with the tracking precision bound $\alpha = 0.08$ ($\delta = 1$), see *Fig.*9.6.

Case 2: With Unmodeled Dynamics

Now still using the same smoothing control parameters $\alpha = 0.08$ ($\delta = 1$), we can see from $Fig.9.7$ that limit cycle occurs again. By drawing Nyquist plot of $G_d = GD_1D_2$ and taking the $\pm 20\%$ parametric variations into account, we can see that the two extreme points are at m (-0.034) and n (-0.0176) as shown in $Fig.9.8$. On the other hand, $H(0,\infty) = -\dfrac{\delta\alpha}{k(2\alpha+\delta)} = -0.013$ falls even right to the n point, thus the limit cycle is inevitable, and incurs rather larger tracking error $\sigma \approx 0.8$.

Finally to eliminate limit cycle we have to further reduce the control gain with $\alpha = 0.3$, $\delta = 1.5$. Now $H(0,\omega) = -\dfrac{\delta\alpha}{k(2\alpha+\delta)} = -0.04$ which is again left to m. We are able to produce very smooth control responses and smooth control input profiles shown in $Fig.9.9$. The actual error at steady state is 0.049, which is far lower than the preceding circumstance.

9.5 Conclusions

In this chapter, describing function techniques are applied to analyze the sliding mode control of the DC servo mechanisms. In the presence of unmodeled dynamics, especially when the unmodeled part has a relative degree of two or more, the limit cycle problem will occur when using conventional SMC scheme with switching mechanism. The proposed new fractional interpolation smoothing scheme, which is used to avoid high switching chattering, effectively eliminates the limit cycle. Moreover, the new smoothing scheme can be easily designed based on the reduced order servo mechanical system. An illustrative example shows the effectiveness of the proposed new scheme.

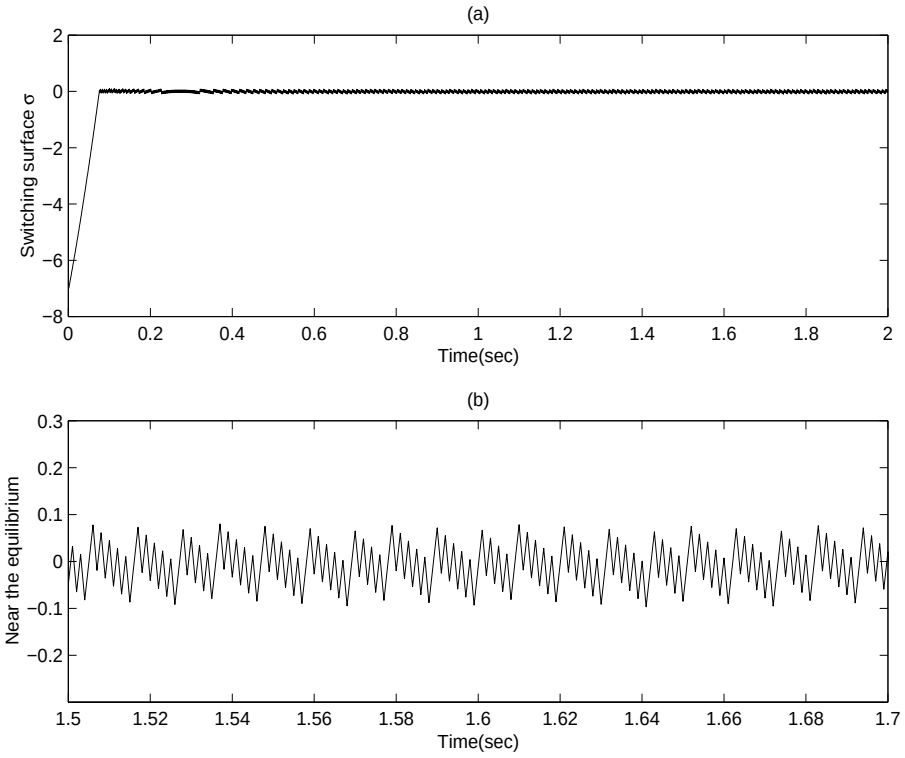

Figure 9.5. System performance under conventional signum controller without unmodeled dynamics: (a) Switching surface; (b) Near the equilibrium.

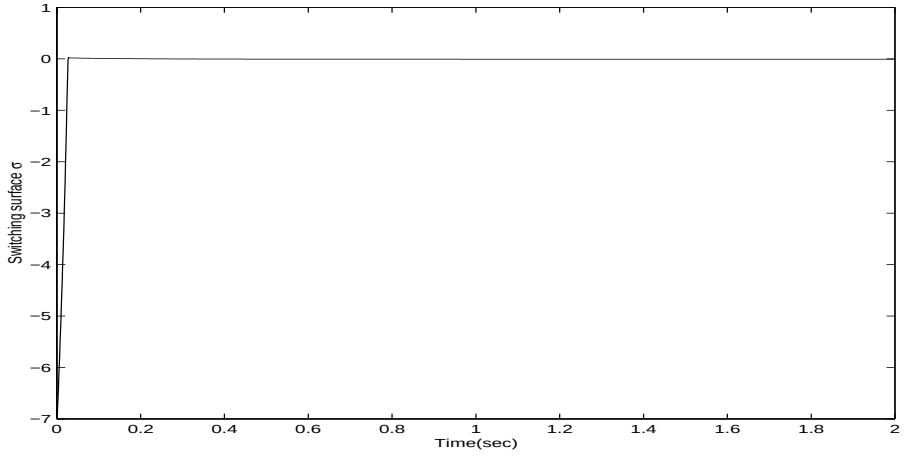

Figure 9.6. The evolution of the switching surface under the proposed fractional interpolation scheme ($\alpha = 0.08$ and $\delta = 1$).

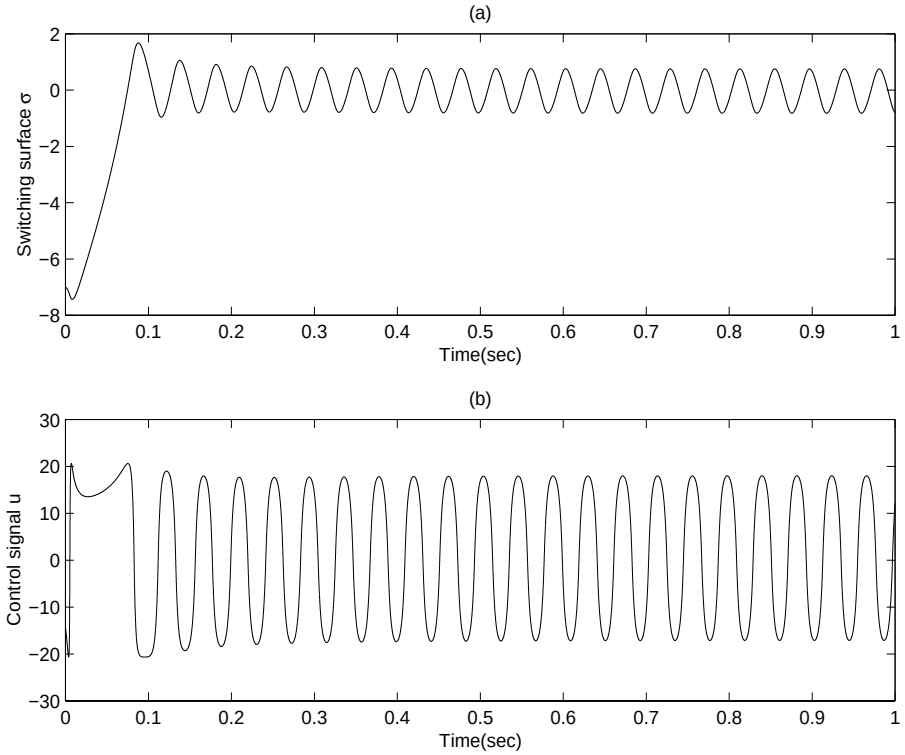

Figure 9.7. System performance under the proposed fractional interpolation control scheme ($\alpha = 0.08$ and $\delta = 1$) with the second order stable unmodeled dynamics $D_1(s)D_2(s)$: (a) Switching surface; (b) Control profile.

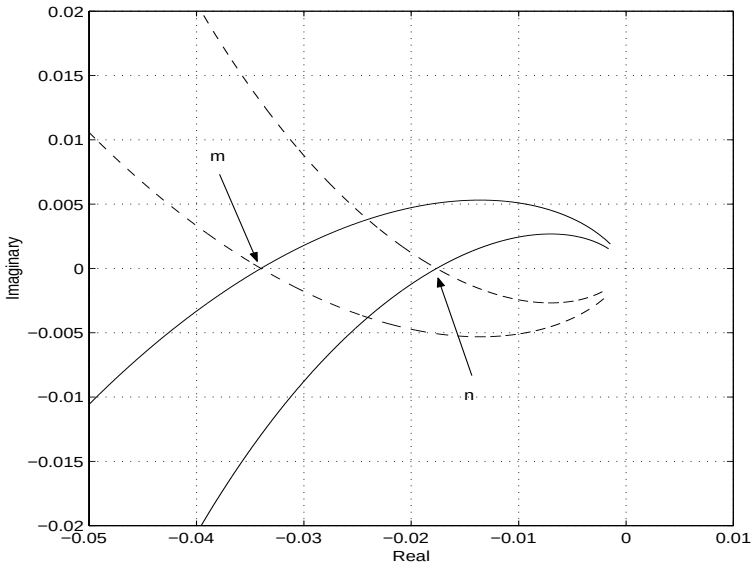

Figure 9.8. The nyquist plot of the system $G_d(s) = D_1(s)G(s)D_2(s)$. Solid line - Nyquist plot of $G_d(j\omega)$; Dashed line - The auxiliary line to identify m and n which is the profile of $G_d(j\omega)$ when $\omega \in (-\infty, 0]$.

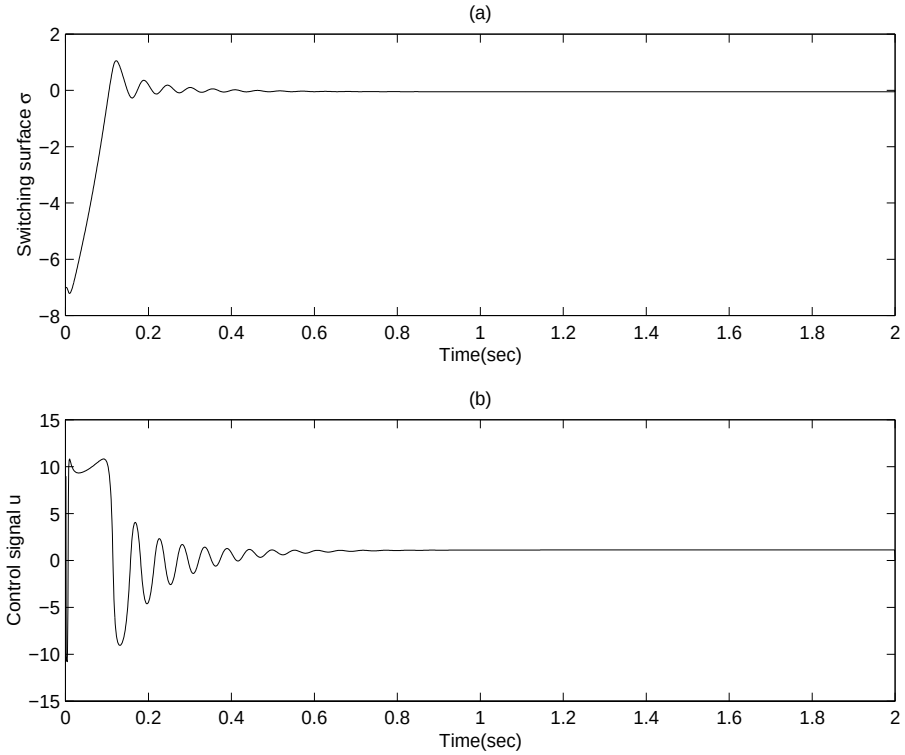

Figure 9.9. System performance with proposed controller ($\alpha = 0.3$ and $\delta = 1.5$) in the case of the second order stable unmodeled dynamics: (a) Switching surface; (b) Control profile.

Chapter 10

A VSS Identification Scheme for Time-Varying Parameters

10.1 Introduction

Over the past few decades, system identification has become a quite matured field with comprehensive results, such as documented by (Ljung, 1987) (Soderstrom, 1989) (Robert, 1999) (Bontayeb, 2000) *et al*. Numerous results are now available addressing fundamental issues in system identification. When the system is open-loop unstable, closed-loop approaches have been developed, e.g. (Van den Hof and Schrama, 1995) (Hjalmarsson *et al.*, 1996) (Ljung and Forssell, 1999) *et al*. When the unknown parameters are slowly time varying, several methods with forgetting factor have been proposed, e.g. (Bittanti and Campi, 1994) (Lindoff and Holst, 1996) (De Mathelin and Lozano, 1999) (Dimogianopoulos and Lozano, 2001) *et al*. When the system is nonlinear in the parametric space, perhaps one of the most difficult problems in system identification, specific algorithms based on the system dynamics have been suggested, e.g. (Xu and Hashimoto, 1996) (Robert, 1999) *et*

al.

While most identification methods are effective respectively in dealing with one of the fundamental issues, it would be a challenging task where all above three key issues are involved simultaneously, and in addition the parameters may be of fast time varying. Clearly, it would be hard to find a universal approach to handle such a problem, and in this work we focus on a kind of systems, which are rational nonlinear in the parametric space. This kind of systems can be widely found in various areas of engineering, a typical class is a mechatronic system such as industrial robotics. In (Xu and Hashimoto, 1993) and (Xu and Hashimoto, 1996), a VSS-theory based parameter identification scheme has been proposed to address this kind of nonlinearity when the unknown parameters are constants. In this work we extend the scheme to the time varying case.

The first reason for us to close the loop with variable structure control (VSC), is the outstanding robustness property of VSC in stabilizing highly nonlinear and uncertain processes (Utkin, 1992) (Zinober, 1994) (Man and Yu, 1997) (Young *et al.*, 1999) (Furuta and Pan, 2000*a*) (Fridman, 2000) (Thein and Misawa, 2000) (Chen and Hiroyuki, 2000). The second and the most important reason for us to employ VSC, is the generation of sliding mode, which allows us to approximate the derivative signals of the system states, in the sequel renders the system dynamics into a structure that is linear in parameters. In a sense, this scheme is similar to the indirect identification using prediction error (Van den Hof and Schrama, 1995).

The chapter is organized as follows. In Section 10.2, we present the underlying idea of the VSS-based identification scheme, discuss the role of sliding mode and equivalent control, and compare with the numerical approach. In order to clearly demonstrate the nature of the problem and the feature of the identification scheme, we concentrate on a single-input-single-output (SISO) system with one unknown

time varying parameter. In section 10.3, the VSS-based identification scheme is extended to a class of multi-input-multi-output (MIMO) systems with multiple unknown time varying parameters. In Section 10.4, a two-linkage robotic manipulator with unknown time varying load and torque disturbance and a numerical example are used to verify the proposed identification scheme. Finally, Section 10.5 draws the conclusions.

10.2 The VSS-based Identification Scheme

Consider the SISO nonlinear system

$$\dot{x}(t) = \frac{f(x,t)}{g_0(x,t) + p(t)g(x,t)} + b(x,t)u(t) \tag{10.1}$$

where $x \in \mathcal{R}$ is the physically measurable state, $u \in \mathcal{R}$ is the control input, $p(t) \in L_\infty[0,\infty)$ is an unknown time-varying parameter in the parameter space $\mathcal{P}$. Functions f, g_0, g and b are known and smooth, and in general highly nonlinear, e.g. $\frac{e^x sin(x^2)}{1+x^2}$, etc. The system is required to track a reference trajectory $x_r \in C^1[0,\infty)$. Because the unknown parameter is in the denominator, the dynamics (10.1) is *rational nonlinear in parameters*. For notational simplicity, the arguments x and t will be omitted wherever no confusion arises.

Here the time varying parameter is assumed bounded as

Assumption 10.1. *$\forall p \in \mathcal{P}, p_{min} \leq\ p(t) \leq\ p_{max}$, where p_{max} and p_{min} are known constant bounds.*

Since the nonlinear system may be open-loop unstable, we need the closed-loop identification and thus the following assumption is needed.

Assumption 10.2. *$\forall x \in \mathcal{X}$ and $\forall p \in \mathcal{P}$, $|g_0(x,t) + pg(x,t)| \geq\ r$, where r is a known positive constant.*

Note that the system (10.1), whether in open-loop or closed-loop, can be treated as linear in parameters if the derivative signal of the state, i.e. $\dot{x}$, is available. However, $\dot{x}$ is not available for most real engineering problems. An alternative approach, from the practical point of view with sampled-data mechanism, is to approximate $\dot{x}$ using numerical difference. We will come back to this important issue after introducing the VSS-based scheme.

Our idea here is to construct a controller that forces the system state $x(t)$ to follow a given reference trajectory $x_r(t)$. If we are able to let $x(t) \equiv x_r(t)$, $t \geq t_0$ for some t_0, then we have $\dot{x}(t) = \dot{x}_r(t)$, $\forall t \geq t_0$. Obviously, it requires that the system state reaches the reference trajectory in a *finite time interval* $[0, t_0]$, regardless of the presence of the high nonlinearities in f, g_0, g and b, and regardless of the system parametric interval uncertainty $p(t)$. VSC is most suitable for this kind of control task.

The first step is to select a switching surface $\sigma(e)$ where $e(t) = x_r(t) - x(t)$ is the state tracking error, and $D_e\sigma = \dfrac{\partial \sigma}{\partial e} \neq 0$. If $\sigma \to 0$, then $e \to 0$ and thereafter $x(t) \to x_r(t)$. The ultimate objective of VSC is to ensure that the system (10.1) enters the sliding mode $\sigma = 0$ in finite time.

The second step is to design a VSC mechanism as follows

$$u(t) = u_c(t) + u_v(t) \tag{10.2}$$

where u_c is a compensation part and u_v is a switching part. Define $\hat{p}$ as the parameter estimate, and $\bar{p}$ as its projection

$$\bar{p}(t) = \begin{cases} p_{min} & if \ \ \hat{p} < p_{min}, \\ \hat{p}(t) & if \ \ \hat{p} \in [p_{min}, p_{max}] \\ p_{max} & if \ \ \hat{p} > p_{max}. \end{cases}$$

The compensation part is constructed as below

$$u_c(t) = b^{-1}\left(\dot{x}_r - \frac{f}{g_0 + \bar{p}g}\right). \tag{10.3}$$

The switching control input is designed as

$$u_v = \begin{cases} \rho(x,t) sign\left[b\sigma(D_e\sigma)\right] & if \ \ \sigma \neq 0 \\ 0 & if \ \ \sigma = 0, \end{cases} \tag{10.4}$$

where $\rho(x,t) = \left|\dfrac{fg}{b(g_0+\bar{p}g)}\right| \dfrac{d}{r} + \varepsilon$, $d = p_{max} - p_{min}$ and $\varepsilon > 0$ is a positive constant.

In the third step we show that the above VSC does force the system to enter sliding mode in finite time, as summarized in the following theorem.

Theorem 10.1. *Sliding mode can be reached in a finite time interval under the VSC law (10.2) (10.3) and (10.4).*

Proof: Choose a Lyapunov function $V = \dfrac{1}{2}\sigma^2 > 0$. Using (10.1), (10.2), (10.3) and (10.4), the derivative of V is

$$\begin{aligned} \dot{V} &= \sigma\dot{\sigma} = \sigma\frac{\partial\sigma}{\partial e}(\dot{x}_r - \dot{x}) = \sigma(D_e\sigma)\left(\dot{x}_r - \frac{f}{g_0+pg} - bu\right) \\ &= \sigma(D_e\sigma)\left[\dot{x}_r - \frac{f}{g_0+\bar{p}g} + \left(\frac{f}{g_0+\bar{p}g} - \frac{f}{g_0+pg}\right) - bu\right] \\ &= \sigma(D_e\sigma)\left[\frac{fg(p-\bar{p})}{(g_0+\bar{p}g)(g_0+pg)} - bu_v\right] \\ &\leq \left|\sigma(D_e\sigma)\frac{fg}{(g_0+\bar{p}g)}\right|\frac{d}{r} - \sigma(D_e\sigma)bu_v \leq \ -\varepsilon\|b\sigma(D_e\sigma)\|. \end{aligned}$$

Since $b(D_e\sigma) \neq 0$, the sliding mode is reached in a finite time interval $[0, t_0]$. The negative definiteness of $\dot{V}$ implies that $\sigma(t) \equiv 0 \ \forall t \geq t_0$. In the sequel $\dot{\sigma}(t) = \dot{x}_r(t) - \dot{x}(t) = 0 \ \forall t \geq t_0$.

Now we are in a position to enter the fourth step: identify the time varying parameter $p(t)$. When the system is in the sliding mode, $u = u_{eq}$ is the equivalent control, $\sigma = 0 \Rightarrow x = x_r$ and $\dot{\sigma} = 0 \Rightarrow \dot{x} = \dot{x}_r$, we have

$$\begin{aligned} &\dot{\sigma}(u = u_{eq}) = D_e\sigma\left[\dot{x}_r - \left(\frac{f_r}{g_{0,r}+pg_r} - b_r u_{eq}\right)\right] = 0 \\ &\Rightarrow (g_{0,r}+pg_r)(\dot{x}_r - b_r u_{eq}) = f_r \end{aligned}$$

where $f_r = f(x_r, t)$, $g_{0,r} = g_0(x_r, t)$, $g_r = g(x_r, t)$, and $b_r = b(x_r, t)$. It is straightforward to derive

$$\hat{p}(t) = \phi^{-1}(t)\omega(t), \tag{10.5}$$

where $\phi = g_r(\dot{x}_r - b_r u_{eq})$ is the regressor, and $\omega = f_r - g_{0,r}(\dot{x}_r - b_r u_{eq})$, provided ϕ is nonsingular $\forall t \geq t_0$.

Now let us discuss two important issues related to PE condition and measurement noise.

PE Condition

First, we can observe one of the advantages of closed-loop identification – enhance the PE condition. We can choose the appropriate reference trajectory to avoid any potential singularities in ϕ. For instance, if $g(0, t) = 0$, then it is necessary to choose $x_r \neq 0$ $\forall t$.

Second we can observe that the identification mechanism (10.5) works in an instantaneous manner. This is necessary when $p(t)$ is fast time varying in nature. Indeed, if $p(t)$ is fast time varying, $p(t)$ and $p(t-\tau)$ should be considered irrelevant for any non-infinitesimal $\tau > 0$. In such circumstance, the past measurements up to $t - \tau$ do not reflect the influence from the present $p(t)$ to the system state. Only the present measurement can capture the relationship between $p(t)$ and $x(t)$. On the other hand, when $p(t)$ is time invariant, it produces a constant influence to the system behavior. Hence the past measurements can be used to enhance the PE condition, as can be clearly seen from the definition of a traditional PE condition: for any $t \in [0\ \infty)$, there exists a strictly positive constant τ such that $\int_t^{t+\tau} \phi^2(t)dt > 0$.

A question associated with the PE condition is: can we estimate multiple unknown time varying parameters in a single state dynamics such as (10.1)? Suppose there are two unknown time varying parameters $p_1(t)$ and $p_2(t)$. Applying an appropriate

VSC and following the preceding four steps will yield a relationship

$$\phi_1(t)p_1(t) + \phi_2(t)p_2(t) = \omega(t).$$

The regressors $\phi_1(t)$ and $\phi_2(t)$, at a fixed time instant t, is obviously linearly dependent. Consequently, an instantaneous identification scheme requires the dimensions of the parametric space not exceeding that of the state space.

Measurement Noise

It can be seen that one of the main objectives of introducing VSC is to acquire the derivative signal of the state, $\dot{x} \to \dot{x}_r$. Note that in sampled data systems the term $\dot{x}$ can also be achieved using numerical difference. From the system (10.1), if the derivative signal $\dot{x}$ is available, then the unknown parameter $p(t)$ can be estimated simply by the formula $\hat{p}(t) = \dfrac{f - g_0(\dot{x} - bu)}{g(\dot{x} - bu)}$.

Let $w(t)$ be a white zero mean measurement noise, the actual state is $x(t) + w(t)$. The numerical difference of the state yields the approximation $\dot{x} = \dfrac{x(t) - x(t - T_s)}{T_s}$, with T_s the sampling period. When the system parameters are of fast time varying, a fast sampling mechanism is imperative, or $T_s \ll 1$. However, the noise $w(t)$ may be amplified by $\dfrac{2}{T_s}$ times. For instance, a small $T_s = 0.1$ ms leads to a noise amplification of 2×10^4 in the worst case! Obviously such an approximation is not practical, even after adding filters.

Can the VSS-based identification outperforms the numerical approximation in this aspect? Rewrite and compare the VSS-based identification scheme

$$\hat{p} = \frac{f_r - g_{0,r}(\dot{x}_r - b_r u_{eq})}{g_r(\dot{x}_r - b_r u_{eq})},$$

with the numerical approximate based scheme

$$\hat{p} = \frac{f - g_0(\dot{x} - bu)}{g(\dot{x} - bu)}.$$

In the first place, the VSS-based is smoother because x_r and $\dot{x}_r$ are used. The difference between $\dot{x}_r$ and $\dot{x}$ could reach the scale of $\dfrac{2}{T_s}$ because of the presence of

measurement noise. Next u must be a robust stabilizing control for the dynamics (10.1), and designed using the same *a priori* bounding knowledge as incorporated in VSC design. Thus u and u_{eq} should in general be of the same order of amplitude. Moreover, numerous smoothing algorithms have been developed in VSC to replace the signum function in (10.4), which will further scale down the VSC gain. Hence the conclusion is, that it is a easier job to make the VSS-based identification scheme less sensitive to the measurement noise compared with the numerical approximatic methods.

Remark 10.1. *The availability of the system derivatives in the sliding mode is a natural consequence or by-product of the closed-loop variable structure control. We do not need additional or sophisticated mechanisms to generate the derivative signals in particular. This is a "hidden" advantage over filtering based numerical approaches.*

Remark 10.2. *If the system* (10.1) *is* $\dot{x} = f + \dfrac{b}{g_0 + pg}u$, $p(t)$ *can be identified the same way as in* (10.5) *with* $\phi = g_r(\dot{x}_r - f_r)$ *and* $\omega = b_r u_{eq} - g_{0,r}(\dot{x}_r - f_r)$.

10.3 Extension to a Class of Nonlinear MIMO Systems

Consider the following nonlinear system, which is the extension of (10.1) to MIMO

$$G(\mathbf{x}, \mathbf{p}, t)\dot{\mathbf{x}}(t) = \mathbf{f}(\mathbf{x}, \mathbf{p}, t) + B(\mathbf{x}, \mathbf{p}, t)\mathbf{u} \tag{10.6}$$

where $\mathbf{x} \in \mathcal{R}^n$ is the physically measurable state vector, $\mathbf{u} \in \mathcal{R}^n$ is the input vector, $\mathbf{p}(t)$ is an unknown time-varying parameter vector in the parameter space $L_\infty^{n_p}[0, \infty)$. This class of systems includes many real engineering systems as a subset, for instance the industrial robot which has a symmetric G and a unity B.

Here functions G, $\mathbf{f}$ and B are linear in parameters, in particular,

$$\begin{aligned} G(\mathbf{x},\mathbf{p},t)\dot{\mathbf{x}} &= \mathbf{g}(\dot{\mathbf{x}},\mathbf{x},t)+\Phi_1(\dot{\mathbf{x}},\mathbf{x},t)\mathbf{p}(t) \\ \mathbf{f}(\mathbf{x},\mathbf{p},t) &= \mathbf{f}_0(\mathbf{x},t)+\Phi_2(\mathbf{x},t)\mathbf{p}(t) \\ B(\mathbf{x},\mathbf{p},t)\mathbf{u} &= \mathbf{b}(\mathbf{x},\mathbf{u},t)+\Phi_3(\mathbf{x},\mathbf{u},t)\mathbf{p}(t). \end{aligned} \tag{10.7}$$

In addition, $B(\mathbf{x},\mathbf{p},t)=B_0(\mathbf{x},t)[I+E(\mathbf{x},\mathbf{p},t)]$, where B_0 is full rank and $e_{ij}(\mathbf{x},\mathbf{p},t)=\mathbf{e}_{ij}(\mathbf{x},t)\mathbf{p}$. Note that the control gain matrix is $H=G^{-1}B$. In order to stabilize (10.6) so that the closed-loop identification can be carried out, the following assumptions are needed.

Assumption 10.3. *$\forall\mathbf{p}\in\mathcal{P}$, $p_{i,min}\le\ p_i\le\ p_{i,max}$, $i=1,\cdots,n_p$, where $p_{i,max}$ and $p_{i,min}$ are known bounds.*

Assumption 10.4. *$\forall(\mathbf{x},\mathbf{p},t)\in\mathcal{R}^n\times\mathcal{P}\times\mathcal{R}^+$, $\|G^{-1}\|\le\ \beta(\mathbf{x},t)$, and $\forall\mathbf{y}\in\mathcal{R}^n$, $\mathbf{y}^THy\ge\ q\|\mathbf{y}\|^2>0$, where $\beta(\mathbf{x},t)$ is a known positive bounding function, and q is a positive constant.*

The VSC law is designed as

$$\mathbf{u}=\mathbf{u}_c+\mathbf{u}_v, \tag{10.8}$$

where $\mathbf{u}_c$ is the compensation part and $\mathbf{u}_v$ is the switching part. The switching surface $\boldsymbol{\sigma}(\mathbf{e})$ is chosen to be a function of the tracking error $\mathbf{e}=\mathbf{x}_r-\mathbf{x}$ and $C(\mathbf{e})=\partial\boldsymbol{\sigma}/\partial\mathbf{e}$ is of full rank. Define $\hat{\mathbf{p}}$ as the parametric estimate, and $\bar{\mathbf{p}}$ the projection

$$\bar{p}_i(t)=\begin{cases} p_{i,min} & if\ \ \hat{p}_i<p_{i,min}, \\ \hat{p}_i(t) & if\ \ \hat{p}_i\in[p_{i,min},p_{i,max}] \\ p_{i,max} & if\ \ \hat{p}_i>p_{i,max}. \end{cases} \tag{10.9}$$

The compensation part is designed to be

$$\mathbf{u}_c=[B_0(I+\bar{E})]^{-1}[\dot{\mathbf{x}}_r-\mathbf{f}_0+\mathbf{g}-(\Phi_2-\Phi_1)\bar{\mathbf{p}}], \tag{10.10}$$

where $\bar{E} = E(\mathbf{x}, \bar{\mathbf{p}}, t)$, $\mathbf{g} = \mathbf{g}(\dot{\mathbf{x}}_r, \mathbf{x}, t)$ and $\Phi_1 = \Phi_1(\dot{\mathbf{x}}_r, \mathbf{x}, t)$.

The switching control input is designed to be

$$\mathbf{u}_v = \begin{cases} \rho\boldsymbol{\alpha} & if \ \boldsymbol{\sigma} \neq 0 \\ 0 & if \ \boldsymbol{\sigma} = 0, \end{cases} \tag{10.11}$$

where

$$\begin{aligned} \rho &= \frac{(\beta\|\Phi\|\|\mathbf{d}\| + \varepsilon)\|\boldsymbol{\alpha}\|}{q\boldsymbol{\alpha}^T\boldsymbol{\alpha}}, \qquad \Phi = \Phi_2 + \Phi_3 - \Phi_1, \\ \boldsymbol{\alpha} &= C^T\boldsymbol{\sigma}, \ \ \mathbf{d} = [(p_{1,max} - p_{1,min}), \cdots, (p_{n_p,max} - p_{n_p,min})]^T, \end{aligned}$$

where $\varepsilon > 0$ is a constant.

Now we are ready to show the existence of sliding mode under the VSC law.

Theorem 10.2. *Sliding mode can be reached in a finite time interval under the control law (10.8), (10.10) and (10.11).*

Proof: The Lyapunov function candidate is chosen as $V = \frac{1}{2}\boldsymbol{\sigma}^T\boldsymbol{\sigma} > 0$. When $\boldsymbol{\sigma} \neq 0$, substituting (10.6) and (10.8), the derivative of V is

$$\begin{aligned} \dot{V} &= \boldsymbol{\sigma}^T\dot{\boldsymbol{\sigma}} = \boldsymbol{\sigma}^T C(\dot{\mathbf{x}}_r - \dot{\mathbf{x}}) = \boldsymbol{\sigma}^T C(\dot{\mathbf{x}}_r - G^{-1}\mathbf{f} - G^{-1}B\mathbf{u}) \\ &= \boldsymbol{\alpha}^T G^{-1}[\mathbf{g}(\dot{\mathbf{x}}_r, \mathbf{x}, t) + \Phi_1(\dot{\mathbf{x}}_r, \mathbf{x}, t)\mathbf{p} - \mathbf{f}_0 - \Phi_2\mathbf{p} - B_0(I + E)\mathbf{u}_c] \\ &\quad -\boldsymbol{\alpha}^T G^{-1}B\mathbf{u}_v \\ &= \boldsymbol{\alpha}^T G^{-1}[\mathbf{g} - \mathbf{f}_0 + (\Phi_1 - \Phi_2)\mathbf{p} - B_0(I + \bar{E})\mathbf{u}_c + B_0(\bar{E} - E)\mathbf{u}_c] - \boldsymbol{\alpha}^T H\mathbf{u}_v \\ &= \boldsymbol{\alpha}^T G^{-1}[\Phi_2 + \Phi_3 - \Phi_1](\bar{\mathbf{p}} - \mathbf{p}) - \rho\boldsymbol{\alpha}^T H\boldsymbol{\alpha} \\ &\leq \beta\|\boldsymbol{\alpha}\|\|\Phi\|\|\mathbf{d}\| - (\beta\|\Phi\|\|\mathbf{d}\| + \varepsilon)\|\boldsymbol{\alpha}\|\frac{\boldsymbol{\alpha}^T H\boldsymbol{\alpha}}{q\boldsymbol{\alpha}^T\boldsymbol{\alpha}} \leq \ -\varepsilon\|\boldsymbol{\alpha}\|. \end{aligned}$$

The negative definiteness of $\dot{V}$ warrants the existence of the sliding mode, and $\boldsymbol{\sigma} = 0$ can be reached in finite time.

Now we can proceed to identification. When the system is in the sliding mode, $\mathbf{u} = \mathbf{u}_{eq}$, $\mathbf{x} = \mathbf{x}_r$ and $\dot{\mathbf{x}} = \dot{\mathbf{x}}_r$, therefore from (10.7) we have

$$\mathbf{g}_r + \Phi_{1,r}\mathbf{p} = \mathbf{f}_{0,r} + \Phi_{2,r}\mathbf{p} + \mathbf{b}_r + \Phi_{3,r}\mathbf{p}, \quad \Rightarrow \Phi_r(t)\mathbf{p}(t) = \boldsymbol{\omega}(t),$$

where $\mathbf{g}_r = \mathbf{g}(\dot{\mathbf{x}}_r, \mathbf{x}_r, t)$, $\mathbf{f}_{0,r} = \mathbf{f}_0(\mathbf{x}_r, t)$, $\mathbf{b}_r = \mathbf{b}(\mathbf{x}_r, \mathbf{u}_{eq}, t)$, $\Phi_{1,r} = \Phi_1(\dot{\mathbf{x}}_r, \mathbf{x}_r, t)$, $\Phi_{2,r} = \Phi_2(\mathbf{x}_r, t)$, $\Phi_{3,r} = \Phi_3(\mathbf{x}_r, \mathbf{u}_{eq}, t)$, $\Phi_r = \Phi_{2,r} + \Phi_{3,r} - \Phi_{1,r}$, and $\boldsymbol{\omega} = \mathbf{g}_r - \mathbf{f}_{0,r} - \mathbf{b}_r$. Thus if the matrix $\Phi_r^T\Phi_r$ is nonsingular, then we can directly derive

$$\hat{\mathbf{p}} = (\Phi_r^T\Phi_r)^{-1}\Phi_r^T\boldsymbol{\omega}. \tag{10.12}$$

Remark 10.3. *Analogous to the SISO, we can choose appropriate* $\mathbf{x}_r$ *to avoid singularity in the regressor* Φ_r*.*

Remark 10.4. *Note that* $\Phi_r \in \mathcal{R}^{n\times n_p}$*. Hence a necessary condition for a nonsingular* $\Phi_r^T\Phi_r$ *is that the dimensions of the vector* $\mathbf{p}$ *should not exceed the dimensions of the system states, i.e.* $n_p \leq n$*.*

Remark 10.5. *It can be seen that instantaneous identification is rather restrictive due to PE condition. Can we relax this condition by incorporating previous data, as we do for time invariant and slow time varying cases? When parameters are of fast time varying nature, previous data are in general not reliable. In order to use previous data, we need to explore the relationship (correlation) between the measured system output and time varying parameters, that is, how faithfully those old data can capture the dynamic varying nature of unknown parameters. In other words, we need a quantitative analysis so as to avoid potential misleading from using previous data. Though such analysis could be extremely difficult due to the high nonlinearity and uncertainty, it is an interesting topic and worthy for more exploitation in future.*

10.4 Illustrative Examples

A. Example 1

Consider a planar, two-link, articulated robotic manipulator in the vertical plane. The dynamics can be written as

$$\begin{bmatrix} h_{11} & h_{12} \\ h_{21} & h_{22} \end{bmatrix} \begin{bmatrix} \ddot{x}_1 \\ \ddot{x}_2 \end{bmatrix} + \begin{bmatrix} -h\dot{x}_2 & -h(\dot{x}_1 + \dot{x}_2) \\ -h\ \dot{x}_1 & 0 \end{bmatrix} \begin{bmatrix} \dot{x}_1 \\ \dot{x}_2 \end{bmatrix} + \begin{bmatrix} g_1 \\ g_2 \end{bmatrix} = \begin{bmatrix} u_1 \\ u_2 \end{bmatrix} + \begin{bmatrix} 0 \\ \tau_l \end{bmatrix}.$$

with $\mathbf{x} = [x_1, x_2]^T$ the two joint angular displacements, $\mathbf{u} = [u_1, u_2]^T$ the joint torque inputs, and

$$\begin{aligned} h_{11} &= I_1 + m_1 l_{c1}^2 + I_2 + m_2 l_{c2}^2 + m_2 l_1^2 + m_p(l_1^2 + l_2^2) + (2m_2 l_1 l_{c2} + 2m_p l_1 l_2)cos(q_2) \\ h_{12} &= h_{21} = I_2 + m_2 l_{c2}^2 + m_p l_2^2 + (m_2 l_1 l_{c2} + m_p l_1 l_2)cos(q_2) \\ h_{22} &= I_2 + m_2 l_{c2}^2 + m_p l_2^2 \\ h &= (m_2 l_1 l_{c2} + m_p l_1 l_2)sin(q_2) \\ g_1 &= (m_1 l_{c1} g + m_p l_1 g)cos(q_1) + m_2 g\,[l_{c2} cos(q_1 + q_2) + l_1 cos(q_1)] \\ &\quad + m_p l_2 g cos(q_1 + q_2) \\ g_2 &= (m_2 l_{c2} g + m_p l_2 g)cos(q_1 + q_2). \end{aligned}$$

The pairs $\{m_1, m_2\}$, $\{I_1, I_2\}$, $\{l_1, l_2\}$, $\{l_{c1}, l_{c2}\}$ are the masses, moments of inertia, lengths, center of gravity coordinates of the two robotic arms respectively. In the simulation, the parameters are: $m_1 = 4kg$, $m_2 = 3kg$, $l_1 = 0.5m$, $l_2 = 0.5m$, $l_{c1} = 0.3m$, $l_{c2} = 0.25m$, $I_1 = 0.4kg \cdot m^2$, $I_2 = 0.25kg \cdot m^2$, $g = 9.8N/kg$. The sampling period is $T_s = 0.1\ ms$. The robot initially resets at $x_1(0) = 30°$; $x_2(0) = 15°$, is commanded a reference trajectory $x_{1r}(t) = 0.5 + 0.2e^{-1.2t}$ and $x_{2r}(t) = 0.2 + 0.3e^{-1.5t}$. The value of the unknown payload is a time varying one $m_p(t) = 1 + (0.8t^2 + 1.2t + 1)/(0.1t^3 + t^2 + 1.2t + 1)$, for example the robotic manipulator

is carrying a metal load and moving in a magnetic field, or is carrying a tank and watering. τ_l can be any external disturbance, in this example $\tau_l(t) = 1+0.5sin(10t)$ is a time varying load torque.

The switching surface is chosen to be $\boldsymbol{\sigma} = \dot{\mathbf{e}} + 5\mathbf{e}$ and $\mathbf{e} = \mathbf{x}_r - \mathbf{x}$. In practice, the existence of a discontinuity in control input together with the limited sampling rate will deteriorate the quality of the equivalent control signals, such as causing chattering. Here a smoothing scheme using a fractional interpolation is employed for the switching control part

$$\mathbf{u}_v = \rho \left[\frac{(|\sigma_1| + \delta_1^*)\sigma_1}{(|\sigma_1| + \delta_1)^2}, \frac{(|\sigma_2| + \delta_2^*)\sigma_2}{(|\sigma_2| + \delta_2)^2} \right]^T,$$

where $\delta_i^* = 2\delta_i + \delta_i^2/\alpha_i$, $i = 1, 2$, and δ_1, δ_2, α_1 and α_2 are constants. This smoothing scheme guarantees the tracking precision bounds $|\sigma_1| \leq \alpha_1$ and $|\sigma_2| \leq \alpha_2$.

The identification results of the time-varying parameters $m_p(t)$ and $\tau_l(t)$ are shown in $Fig.10.1$ and $Fig.10.2$ in case that there is no measurement noise in the system. In the identification process we choose $\delta_1 = 0.01$, $\delta_2 = 0.5$, $\alpha_1 = 0.005$ and $\alpha_2 = 0.1$. It is shown that the estimated parameter takes some time to approach the their true value. This is because during the reaching phase, the sliding mode does not exist, hence the identification mechanism cannot work properly. Note that the gain ρ in $\mathbf{u}_v$ can influence the reaching time of the reaching phase. Especially, a larger ε can lead to a shorter reaching time.

When a zero mean white noise with variance 0.01, is added to the measurement of states x_1, x_2, $\dot{x}_1$ and $\dot{x}_2$. The identification results of the time-varying parameters $m_p(t)$ and $\tau_l(t)$ are shown in $Fig.10.3$ and $Fig.10.4$ respectively. In the identification process we choose $\delta_1 = 0.1$, $\delta_2 = 0.5$, $\alpha_1 = 0.005$ and $\alpha_2 = 0.15$. It is observed that there is some fluctuation in the parameter estimates. This is due to the effect of the noise on the acquisition of the equivalent control signal, which cannot be reduced because the instantaneous identification formula prohibits the

use of filtering or moving average operation.

For comparison purpose we also conducted identification using the first order numerical difference of $\ddot{\mathbf{x}}$. Since the result is really bad, some filtering must be used to mitigate the measurement noise influence. However, a low pass filter will inevitably introduces a phase lag, therefore lead to rather large identification error especially when the parameters are fast time varying. In order to achieve a smoother $\ddot{\mathbf{x}}$ signal without phase lag, we use a moving average noncausal filter which is the arithmetic average of in total 21 samples, with 10 samples before and 10 samples after the current instant t. Note that in this way the identification can only be done off-line, whereas the VSS-based one is on-line. The identification results are shown in $Fig.10.5$ and $Fig.10.6$ respectively. It is observed that the identification errors of the parameters $\hat{m}_p$ and $\hat{\tau}_l$ are at least twice as larger as the VSS-based ones.

B. Example 2

Consider the following system which is a nonlinear MIMO system

$$G(\mathbf{x},\mathbf{p},t)\dot{\mathbf{x}} = \mathbf{f}(\mathbf{x},\mathbf{p},t) + B(\mathbf{x},\mathbf{p},t)\mathbf{u}$$

where $\mathbf{x} = [x_1 \quad x_2]^T$ is the measurable state vector, $x_1(0) = -2$, $x_2(0) = 2$, $\mathbf{u} = [u_1 \quad u_2]^T$ is the measurable input vector, $\mathbf{p} = [a_1(t) \quad a_2(t)]^T$ is the unknown time-varying parameter vector,

$$\begin{aligned} G(\mathbf{x},\mathbf{p},t) &= \begin{bmatrix} 3 & 1 \\ 0 & 1+a_1(t)|sin(x_1)| \end{bmatrix}, \\ \mathbf{f}(\mathbf{x},\mathbf{p},t) &= \begin{bmatrix} a_2(t)x_1^2 \\ -2x_1^2 - x_1x_2 \end{bmatrix}, \\ B(\mathbf{x},\mathbf{p},t) &= \begin{bmatrix} 3 & \frac{1}{2}cos(x_1) \\ a_1(t) & 3 \end{bmatrix}. \end{aligned}$$

The unknown parameters are $a_1(t) = 2 + sin(5\pi t)$, $a_2(t) = 2 - 0.5cos(5\pi t) + 0.5sin(10\pi t)$, and their bounds are given by $a_{1,max} = a_{2,max} = 4$, $a_{1,min} = a_{2,min} =$

1. The switching surface are $\sigma_1 = x_{1r} - x_1$, $\sigma_2 = x_{2r} - x_2$, where the desired trajectory are

$$\begin{aligned} x_{1r} &= 0.5cos(\pi t) + 0.5cos(2\pi t) + 0.3sin(3\pi t) - 5, \\ x_{2r} &= 0.3sin(3\pi t) + 0.2cos(5\pi t) + 0.15sin(6\pi t) + 2. \end{aligned}$$

The identification mechanism is constructed according to (10.12). A smoothing scheme using fractional interpolation is employed for the switching control part which may cause chattering

$$\mathbf{u}_v = \frac{\beta \|\Phi\| \|\mathbf{d}\| \|\boldsymbol{\alpha}\| (\boldsymbol{\alpha}^T \boldsymbol{\alpha} + \delta^*) \boldsymbol{\alpha}}{q(\boldsymbol{\alpha}^T \boldsymbol{\alpha} + \delta)^2},$$

where δ is a small positive constant, $\delta^* = 2\delta + \dfrac{\delta^2}{\alpha}$. It ensures that the equivalent control signal can be approximated to any degree of accuracy by choosing the precision bound $\|\boldsymbol{\alpha}\|^2 \leq \alpha$ sufficiently small. The sampling period is selected as $T_s = 0.1 \ \ ms$. For simplicity in all subsequent simulations we only demonstrate identification results of $a_1(t)$. The proposed schemes nevertheless work equally well for $a_2(t)$.

$Fig.$10.7 shows the identification result for the time-varying parameters $a_1(t)$ when there is no measurement noise added. In this case, $\alpha = 0.01$, $\delta = 0.003$. $Fig.$10.8 shows that $\|\boldsymbol{\alpha}\|^2 < \alpha = 0.01$ is always satisfied.

In second case, a measurement white noise with zero mean and variance 0.01, is added to both states x_1 and x_2. In consideration of noise influence, $\alpha = 0.5$ and $\delta = 0.5$ is selected. A smoothing algorithm is able to reduce the noise impact. The trade-off is to sacrifice the precision to certain extent. The identification results of the time-varying parameter $a_1(t)$ is shown in $Fig.$10.9. It is observed that there is chattering in the identified parameter. This is due to the effect of the noise on the acquisition of the equivalent control signal, and the use of the instantaneous LSE formula which does not have moving average operation. Generally speaking,

identification schemes for time-varying parameters possess a higher gain for the latest measurement, and a weaker averaging operation over the measured data set up to date because of the "forgetting" nature. Thus these identification schemes could be more sensitive to the measurement noise.

In the third case, for comparison purpose, the integration based indirect identification scheme (Xu and Hashimoto, 1996) is applied to time-varying parameters. In this case, there is no measurement noise, the equivalent control signal is acquired by the same smoothing mechanism with $\alpha = 0.01$ and $\delta = 0.003$. The identification results of the time-varying parameter $a_1(t)$ is shown in $Fig.10.10$. It is observed that $\hat{a}_1(t)$ fails to follow the real $a_1(t)$, though the same scheme was shown to work satisfactory for constant parameters in (Xu and Hashimoto, 1996).

To explore the capability of the integral type identification scheme, a number of simulations are conducted where the magnitude and frequency of the time varying part in $a_1(t)$ are kept decreasing. They show that the profile of $\hat{a}_1(t)$ is able to approach the real $a_1(t)$ ($Fig.10.11$) only when the magnitude is reduced from 1 to 0.1, and frequency from 5π to 0.3π, i.e. $a_1(t) = 2 + 0.1sin(0.3\pi t)$.

10.5 Conclusion

In this chapter, an instantaneous identification scheme based on the variable structure control theory, has been developed to identify fast time-varying parameters. The system, originally rational nonlinear in parameters, becomes linear in parameters after entering the sliding mode. The new scheme shows lower sensitivity to the measurement noise, in comparison with the numerical difference based approach. The VSS-based identification scheme was applied to a two-link robotic manipulator with time varying payload and torque disturbance and a numerical example. The

results confirmed the effectiveness of the proposed scheme.

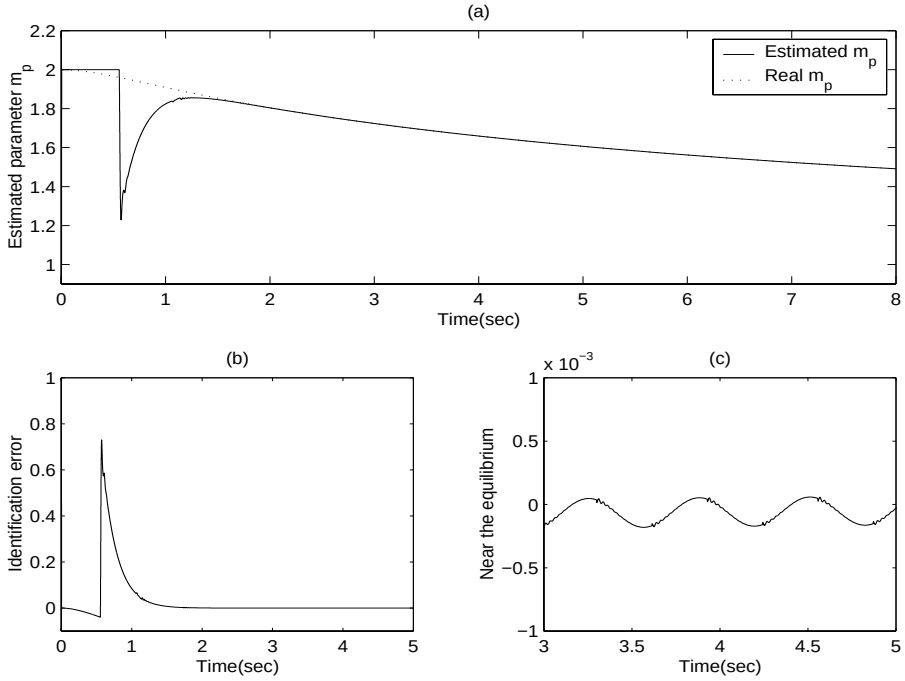

Figure 10.1. VSS-based estimate without noise (a) Solid line: evolution of $\hat{m}_p$; Dashed line: real m_p; (b) Identification error of m_p; (c) Identification error near the equilibrium.

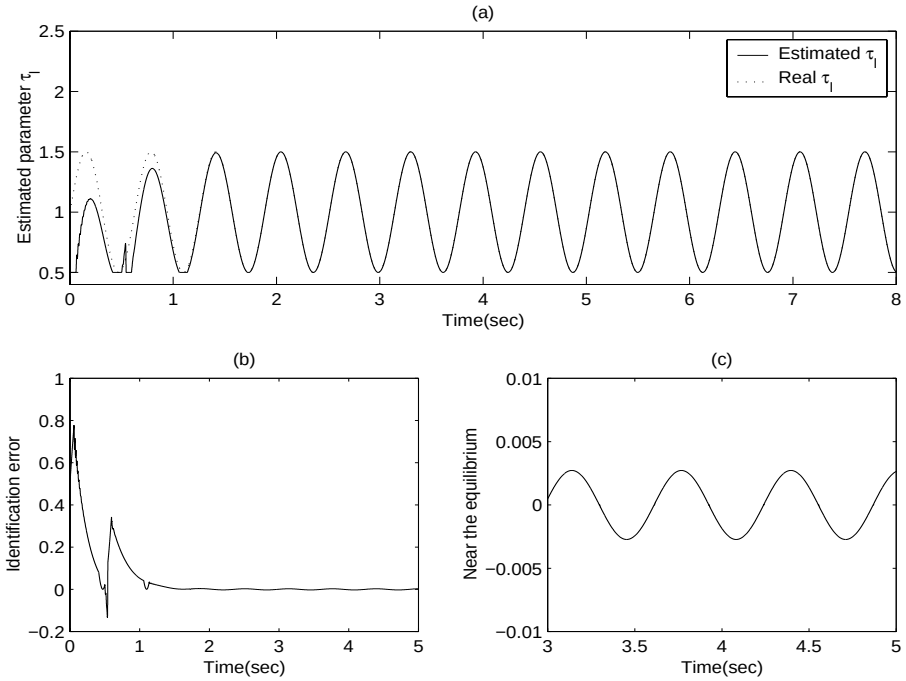

Figure 10.2. VSS-based estimate without noise (a) Solid line: evolution of $\hat{\tau}_l$; Dashed line: real τ_l; (b) Identification error of τ_l; (c) Identification error near the equilibrium.

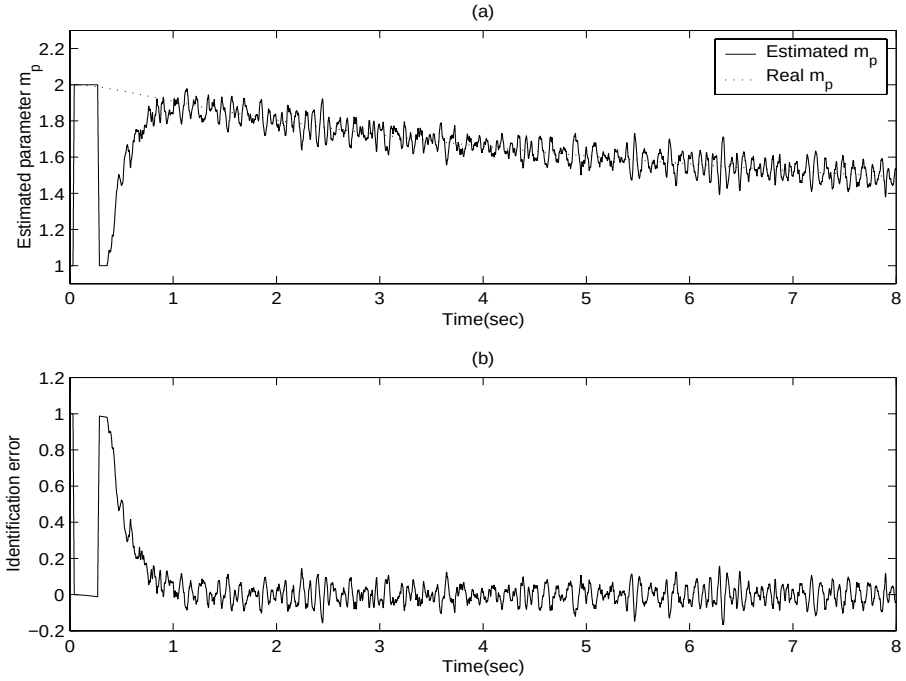

Figure 10.3. VSS-based estimate (a) Solid line: evolution of $\hat{m}_p$; Dashed line: real m_p; (b) Identification error of m_p.

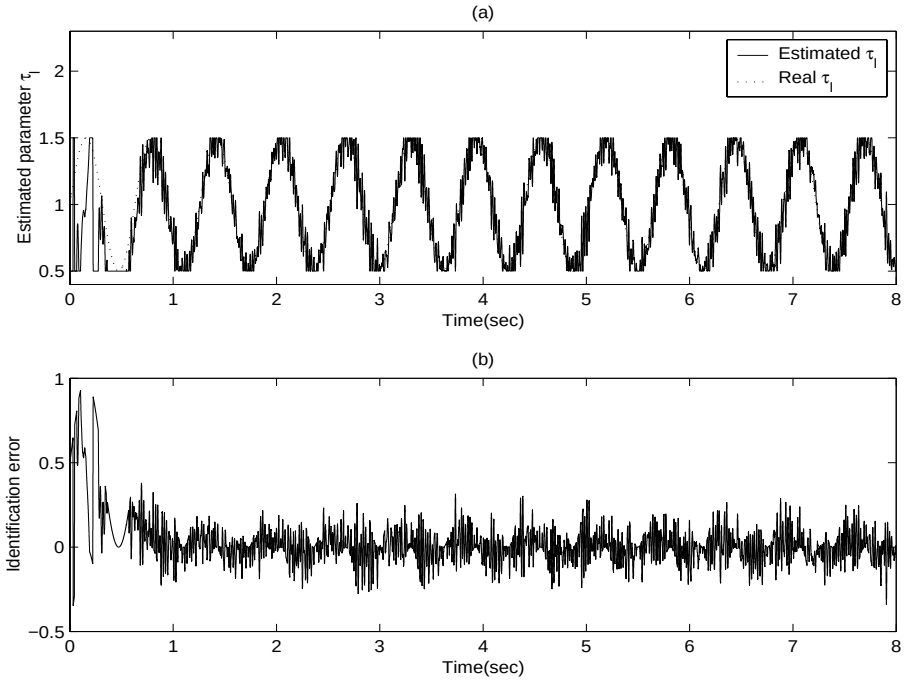

Figure 10.4. VSS-based estimate (a) Solid line: evolution of $\hat{\tau}_l$; Dashed line: real τ_l; (b) Identification error of τ_l.

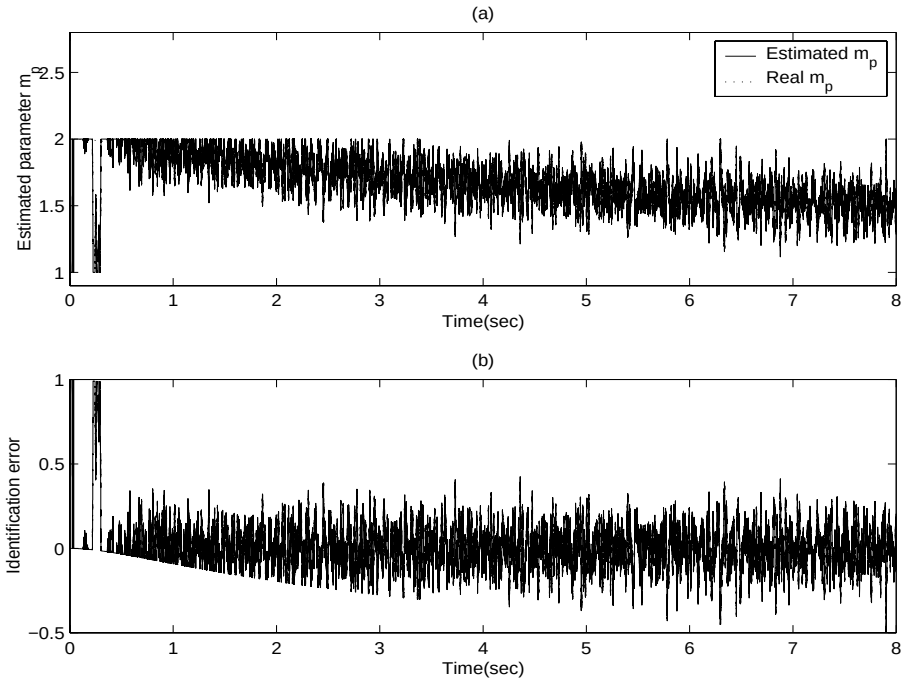

Figure 10.5. Numerical difference based estimate (a) Solid line: evolution of $\hat{m}_p$; Dashed line: real m_p; (b) Identification error of m_p.

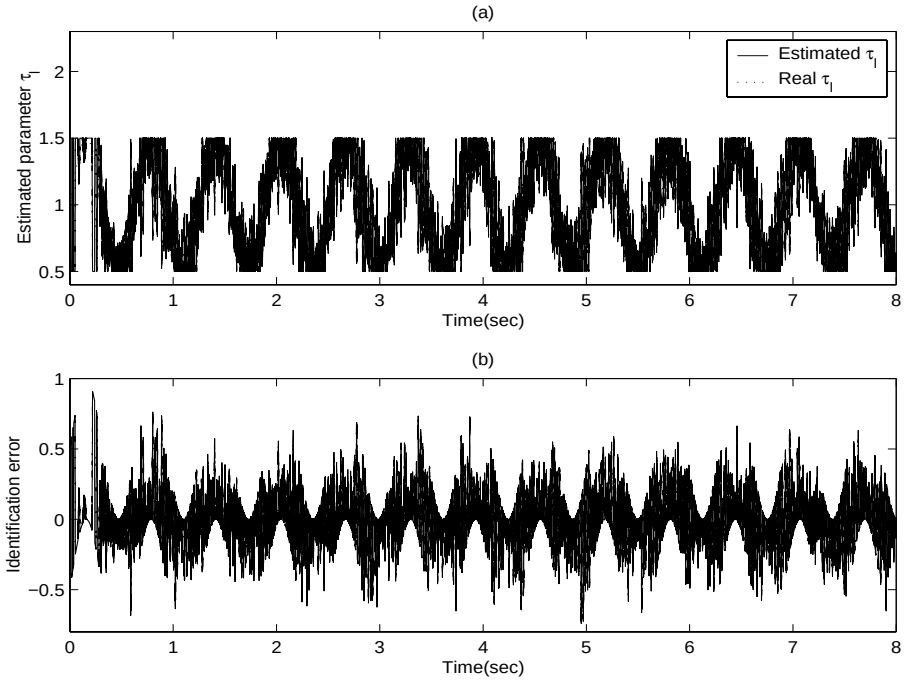

Figure 10.6. Numerical difference based estimate (a) Solid line: evolution of $\hat{\tau}_l$; Dashed line: real τ_l; (b) Identification error of τ_l.

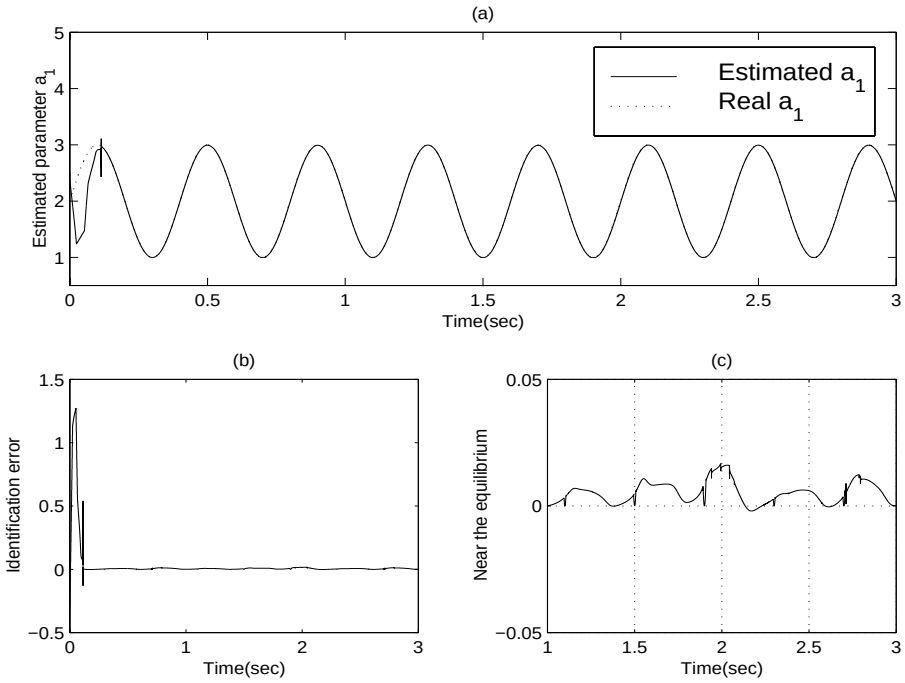

Figure 10.7. VSS-based estimate without noise (a) Solid line: evolution of $\hat{a}_1(t)$; Dashed line: real $a_1(t)$; (b) Identification error of $a_1(t)$; (c) Identification error near the equilibrium.

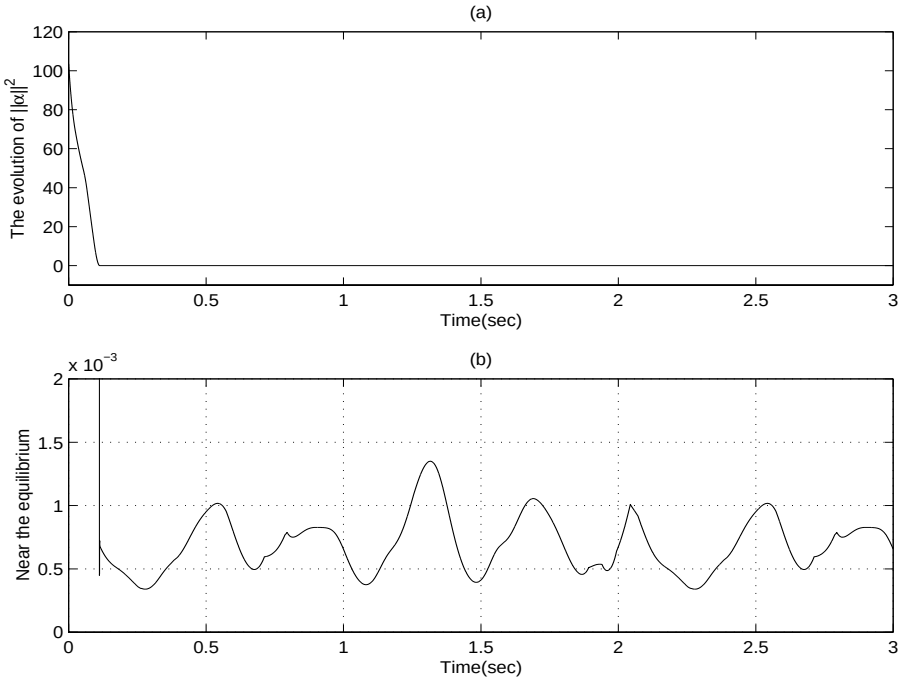

Figure 10.8. (a) The evolution of the term $\|\boldsymbol{\alpha}\|^2$; (b) The term $\|\boldsymbol{\alpha}\|^2$ near the equilibrium.

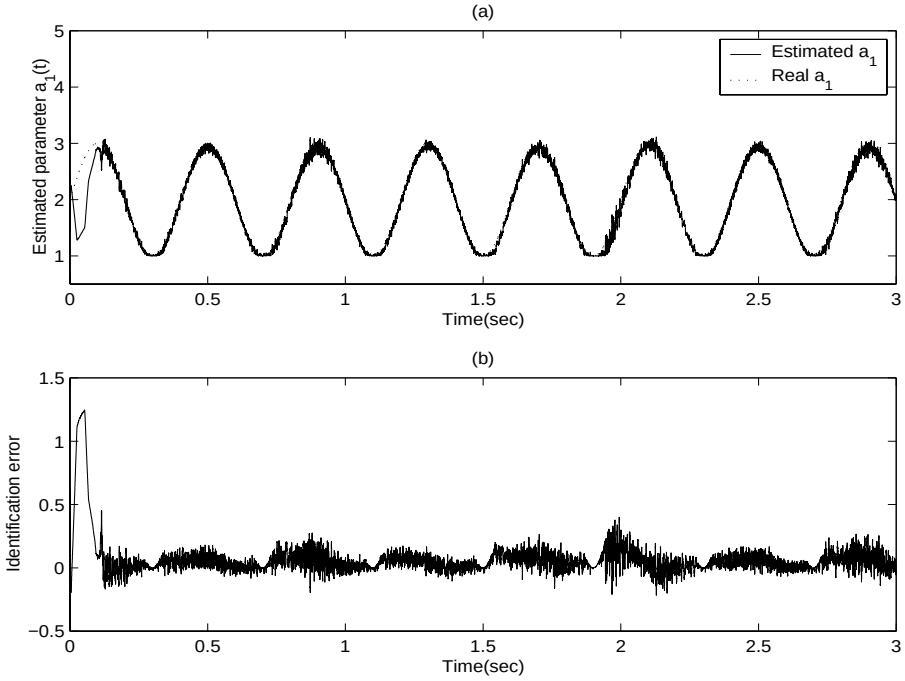

Figure 10.9. VSS-baded estimate (a) Solid line: evolution of $\hat{a}_1(t)$; Dashed line: real $a_1(t)$; (b) Identification error of $a_1(t)$.

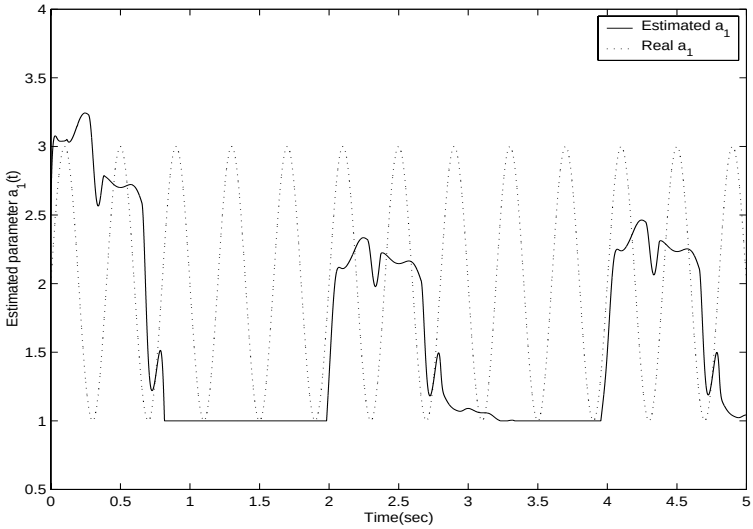

Figure 10.10. Estimated time-varying parameter $\hat{a}_1(t)$ (Solid-line: $\hat{a}_1(t)$; Dashed line: real $a_1(t)$).

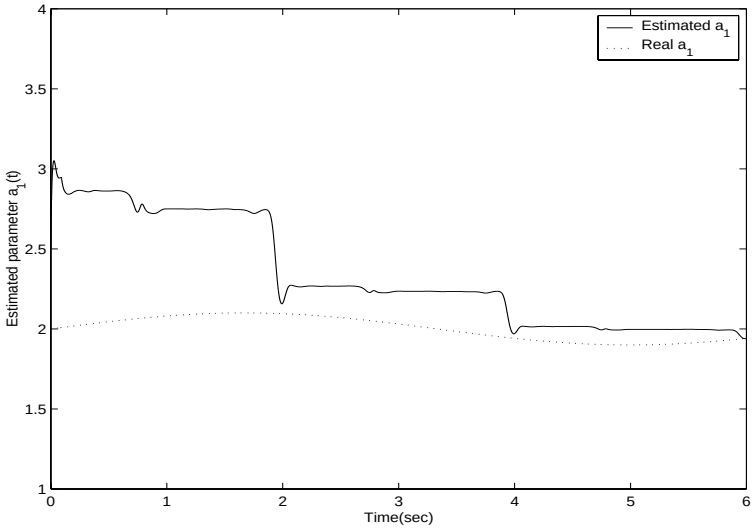

Figure 10.11. Estimated time-varying parameter $\hat{a}_1(t)$ (Solid-line: $\hat{a}_1(t)$; Dashed line: real $a_1(t)$).

Chapter 11

Conclusions and Future Research

11.1 Conclusions

In this thesis, new developments in several different aspects of SMC are presented to enhance the performance of control systems and to facilitate the applications of SMC to the real systems such as robotic manipulators, servo mechanisms, etc.

In SMC, if the equivalent control profile can be acquired directly, perfect system performance such as tracking issue, system identification and disturbance estimation will be surely achievable. However, the equivalent control is not easily available due to the existence of the uncertainties in the plant. But nevertheless, to acquire the equivalent control is the most straightforward and appropriate idea for perfect system performance. In Chapter 2, closed-loop filtering techniques are incorporated into sliding mode control to acquire equivalent control and shape the switching control gain in the presence of bounded system uncertainties for a class of nonlinear systems. In this new control scheme, the system disturbance can be compensated accurately by the equivalent control approach and the magnitude of the switching gain can be scaled to the minimum level while retaining the system

in sliding mode. In the filter design, both time domain and frequency domain knowledge can be used, hence achieving excellent tracking performance. Another virtue of the new controller scheme is that it is easy to be implemented as only two simple first-order filters are employed.

In Chapter 3, through synthesizing sliding mode control and nonlinear H^∞ techniques, a novel nonlinear H^∞ sliding mode control scheme has been developed for tracking control problems of a class of nonlinear cascaded systems. In this work, by means of the nonlinear H^∞ method, a nonlinear switching surface is constructed firstly, which ensures a stable sliding manifold even in the presence of unmatched L_2 type uncertainties. Furthermore, a new reaching control law in conjunction with a Lyapunov function is proposed to obtain the L_2 gain property for the entire tracking period. Hence the system behavior in the reaching phase can be guaranteed.

In Chapter 4, the feature of the proposed integral SMC was first highlighted and compared with conventional SMC. A nonlinear integral-type sliding surface is used to yield a sliding manifold specified in the entire state space and the ISMC leads to a sliding manifold that spans the whole state space. Using Lyapunov's direct method, it is easy to design a nonlinear nominal control law to stabilizing the sliding manifold. When the system is particularly with L_∞ or $L_2 \cap L_\infty$ type unmatched uncertainties, the ISMC can achieve both uniform boundedness and asymptotic stability.

In Chapter 5, by incorporating a Nussbaum-type function, a new adaptive VSC law is proposed for nonlinear systems without a prior knowledge of control directions and the asymptotic convergence of the tracking error in the existence of non-parametric uncertainties can be ensured.

A new fractional interpolation based smoothing scheme for variable structure con-

trol in dealing with the chattering problem has been proposed in Chapter 6. The new properties of the proposed scheme have been analyzed and well presented. This newly developed smoothing scheme can also be applied to eliminate the limit cycles which can be caused by sampling delay or the existence of unmodeled dynamics.

The newly developed gain shaped SMC scheme is succesfully applied for the tracking control task of the multi-link robotic manipulators (as in Chapter 7). A gain shaped SMC disturbance estimator is integrated with the PI speed control module, the ILC module and the PI current control module for the PMSM speed control with pulsating torque minimization (as in Chapter 8). In Chapter 9, it is shown that in the presence of unmodeled dynamics, especially when the unmodeled part has a relative degree of two or more, the limit cycle problem will happen when using conventional SMC scheme with switching mechanism. Fortunately, based on the describing function techniques, the sliding mode control of the DC servo mechanisms can be analyzed and the limit cycle problem can be effectively eliminated by applying the proposed new fractional interpolation smoothing scheme. In order to identify fast time-varying parameters, an instantaneous identification scheme based on the variable structure control theory has been developed in Chapter 10. Once entering the sliding mode, the system which is originally rational nonlinear in parameters, becomes linear in parameters. Hence the unknown time varying parameters can be identified in an instantaneous manner. The new scheme shows lower sensitivity to the measurement noise, in comparison with the numerical difference based approach.

11.2 Suggestions for Future Research

Based on the work in this thesis, there are some possibilities for future research and investigations. Specifically, the following aspects are suggested:

1. Chapter 2 presents a closed-loop filtering architecture to acquire the equivalent control profile. The sliding motion will be ensured by selecting the two low-pass filter parameters which should satisfy Theorem 2.1. However, there is no specific rules or conditions. This means that for different filter parameters which satisfy Theorem 2.1, the system performance will be a little different. Moreover for the designer, it is difficult to select the parameters. Hence, more investigations can be on the filter design. For example, instead of the first-order low-pass filter, more complicated filter can be applied to achieve a better system performance. Further research can also focus on how to give the optimal filter parameters in filter design.

2. In Chapter 3, the nonlinear H^∞ SMC scheme is proposed for the tracking control tasks of a class of nonlinear cascaded systems. Note that in this class of nonlinear cascaded systems, there are no unmatched uncertainties in the range space subdynamics. More investigations can be given to extend the proposed nonlinear H^∞ SMC scheme to a more general case, e.g., a classes of cascaded systems in which both matched and unmatched uncertainties exist in the range space subdynamics.

3. Chapter 7 proposes a gain shaped sliding mode control for multi-link robotic manipulators. Note that a robotic manipulator (7.1) is a multi-input multi-output plant with some special attributes such as $\dot{M}-2C$ is a skew-symmetric matrix. Further investigation can be on establishing the gain shaped sliding mode control scheme for more general case of the multi-input multi-output plant.

4. It is noted that the controller designs presented in this report are mainly based on the continuous-time systems. It will be nice to further these results into the discrete-time systems.

5. In order to achieve perfect system performance, it will be a challenging piece of work to find more new equivalent control schemes and their corresponding applications. Another interesting research area is how to acquire the equivalent control signal in frequency domain by appropriate signal processing techniques.

Bibliography

Ackermann, J. and V. I. Utkin (1998). Sliding mode control design based on ackermann's formula. *IEEE Transactions on Automatic Control* **43**(2), 234–237.

Ball, J. A., I. W. Helton and M. L. Walker (1993). H^{∞} control for nonlinear systems with output feedback. *IEEE Transactions on Automatic Control* **38**(4), 546–559.

Barbosa, L. L. S., P. L. D. Peres and R. H. C. Takahashi (1999). A sliding mode controlled sinusoidal voltage source with ellipsoidal switching surface. *IEEE Transactions on Circuits and Systems I: Fundamental Theory and Applications* **46**(6), 714–721.

Bartolini, G., A. Ferrara and A. Stotsky (1999). Robustness and performance of an indirect adaptive control scheme in presence of bounded disturbances. *IEEE Transactions on Automatic Control* **44**(4), 789–793.

Bartolini, G., A. Ferrara and E. Usai (1998). Chattering avoidance by second-order sliding mode control. *IEEE Transactions on Automatic Control* **43**(2), 241–246.

Bartolini, G. and A Ferrara (1999). On the parameter convergence properties of a combined VS/adaptive control scheme during sliding motion. *IEEE Transactions on Automatic Control* **44**(1), 70–76.

Bartolini, G. and P. Pydynowski (1996). An improved, chattering free, VSC scheme for uncertain dynamical systems. *IEEE Transactions on Automatic Control* **41**(8), 1220–1226.

Basar, T. and P. Berhard (1990). *H^∞ control for nonlinear systems with output feedback*. Birkhauser. Berlin, Germany.

Bernstein, D. S. (2001). Sensor performance specifications. *IEEE Control Systems Magazine* **21**(4), 9–18.

Bittanti, S. and M. Campi (1994). Bounded error identification of time-varying parameters by RLS techniques. *IEEE Transactions on Automatic Control* **39**(5), 1106–1110.

Bontayeb, M. (2000). Identification of nonlinear systems in the presence of unknown but bounded disturbances. *IEEE Transactions on Automatic Control* **45**(8), 1503–1507.

Brogliato, B. and R. Lozano (1992). Adaptive control of a simple nonlinear system without a priori information on the plant parameters. *IEEE Transactions on Automatic Control* **37**, 30–37.

Brogliato, B. and R. Lozano (1994). Adaptive control of first-order nonlinear systems with reduced knowledge of the plant parameters. *IEEE Transactions Automatic Control* **39**, 1764–1768.

Burton, J. A. and A. S. I. Zinober (1986). Continuous approximation of variable structure control. *International Journal of Systems Science* **17**(6), 876–885.

Byrnes, C. I. and A. Isidori (2000). Output regulation for nonlinear systems: an overview. *International Journal of Robust and Nonlinear Control* **10**, 323–337.

Carrasco, J.M., L.G. Franquelo, M.A. Perales, J.M. Quero and F.P. Ridao (1997). Sliding mode control of a DC/DC PWM converter with PFC implemented by

neural networks. *IEEE Transactions on Circuits and Systems I: Fundamental Theory and Applications* **44**(8), 743–749.

Chan, S. P. (1995). Robust sliding mode control of robot manipulators using internal model. *International Journal of Robotics and Automation* **10**(2), 63–69.

Chan, S. P. (1996). An approach to perturbation compensation for variable structure systems. *Automatica* **32**(3), 469–473.

Chang, J. L. and Y. P. Chen (2000). Sliding vector design based on pole-assignment method. *Asian Journal of Control* **2**, 10–15.

Chen, L. W. and G.P. Papavassilopoulos (1994). Robust variable structure and switching-σ adaptive control of single-arm dynamics. *IEEE Transactions on Automatic Control* **39**(8), 1621 –1626.

Chen, X. K. and K. Hiroyuki (2000). Robust output tracking control for a class of uncertain systems. In: *Proceedings of the 6th IEEE international workshop on Variable Structure Systems (VSS'2K)*. Vol. 36. Boston. pp. 179–188.

Chern, T. L. and Y. C. Wu (1992). Integral variable structure control approach for robot manipulators. *IEE Proceedings-Control Theory and Applications* **139**(2), 161–166.

Chern, T. L., Y. C. Wu and R. L. Jiang (1996). Design of discrete integral variable structure control systems and application to a brushless DC motor control. *Automatica* **32**(5), 773–779.

Chien, C. J. and L. C. Fu (1999). Adaptive variable structure control. In: *Variable Structure Control for Robotics and Aerospace Applications* (G. Feng and R. Lozano, Eds.). pp. 41–62. Newnes. Oxford.

Chung, C. Y. and C. L. Lin (1998). A general class of sliding surface for sliding mode control. *IEEE Transactions on Automatic Control* **43**(1), 115–119.

Chung, C. Y. S.; Lin, C. L. (1999). A transformed lure problem for sliding mode control and chattering reduction. *IEEE Transactions on Automatic Control* **44**(3), 563–568.

Chung, S. K., H. S. Kim, C. G. Kim and You (1998). A new instantaneous torque control of pm synchronous motor for high-performance direct-drive application. *IEEE Transactions on Power Electronics* **13**(3), 388–400.

Dawson, D. M., J. J. Carroll and M. Schneider (1994). Integrator backstepping control of a brush DC motor turning a robotic load. *IEEE Transactions on Control Systems Technology* **2**(2), 233–244.

De Mathelin, M. and R. Lozano (1999). Robust adaptive identification of slowly time-varying parameters with bounded disturbances. *Automatica* **35**(7), 1291–1305.

Dimogianopoulos, D. and R. Lozano (2001). Adaptive control for linear slowly time-varying systems using direct least-squares estimation. *Automatica* **37**(2), 251–256.

Edwards, C. and S. K. Spurgeon (1998). *Sliding mode control: theory and applications*. Vol. 7. Taylor and Francis. London.

Edwards, C., S. K. Spurgeon and R. J. Patton (2000). Sliding mode observers for fault detection and isolation. *Automatica* **36**(4), 541–553.

Emelyanov, S. V. (1967). *Variable Structure Control Systems*. Nauka. Moscowin (in Russian).

Favre, E., L. Cardoletti and M. Jufer (1993). Permanent-magnet synchronous motors: A comprehensive approach to cogging torque suppression. *IEEE Transactions on Industry Applications* **29**(6), 1141–1149.

Filippov, A. F. (1964). Differential equations with discontinuous right-hand sides (translated in english). *Transactions of the American Mathematical Society* **62**(11), 199–231.

Filippov, A. F. (1988). *Differential equations with discontinuous right hand sides*. Vol. 1. Dordrecht: Kluwer Academic Publishers. London.

Filippov, A.F. (1960). Differential equations with discontinuous right-hand side. *Matemat. Sbornik.* **51**(60), 99–128.(In Russian).

Fridman, L. (2000). Periodic motions in VSS and singular perturbations. In: *Proceedings of the 6th IEEE international workshop on Variable Structure Systems (VSS'2K)*. Vol. 36. Boston. pp. 365–374.

Fridman, L. and A. Levant (1996). Sliding modes of higher order as a natural phenomenon in control theory. In: *Robust control via variable structure and Lyapunov techniques, Lecture notes in control and information sciences 217* (F. Garofalo and L. Glielmo, Eds.). pp. 107–133. Springer Verlag.

Fu, L.-C. (1992). Robust adaptive decentralized control of robot manipulators. *IEEE Transactions on Automatic Control* **37**(1), 106–110.

Fu, L.-C. and T.-L. Liao (1990). Globally stable robust tracking of nonlinear systems using variable structure control and with an application to a robotic manipulator. *IEEE Transactions on Automatic Control* **35**(12), 1345–1350.

Fujimoto, Y. and A. Kawamura (1995). Robust servo-system based on two-edge-of-freedom control with sliding mode. *IEEE Transactions on Industrial Electronics* **42**(2), 272–280.

Furuta, K. and Y. Pan (2000*a*). Sliding sectors for VS controller. *Automatica* **36**(2), 211–228.

Furuta, K. and Y. Pan (2000*b*). Variable structure control with sliding sector. *Automatica* **36**(2), 211–228.

Giral, R., R. Leyva, J. Maixe and L. Martinez-Salamero (1997). Sliding mode control of interleaved boost converters. *IEEE Transactions on Circuits and Systems I: Fundamental Theory and Applications* **47**(9), 1330–1339.

Habibi, S. R. (1999). Sliding mode control of a hydraulic industrial robot. *Transactions of the ASME-Journal of Dynamic Systems, Measurement, and Control* **121**(2), 312–318.

Habibi, S. R. and R. J. Richards (1992). Sliding mode control of an electrically powered industrial robot. *IEE Proceedings-Control Theory and Applications* **139**(2), 207–225.

Hanselman, D. C. (1994). Minimum torque ripple, maximum efficiency excitation of brushless permanent magnet motors. *IEEE Transactions on Industrial Electronics* **41**(3), 292–300.

Hashimoto, H., J. J. E. Slotine, J. X. Xu, Arai and F. Harashima (1987). Implementation of VSS control to robotic manipulations – smoothing modification. In: *In Proceedings of 1987 IEEE International Conference on Robotics and Automation*. North Carolina, United States. pp. 2039–2046.

Hashimoto, H., V. I. Utkin, J. X. Xu, H. Suzuki and F. Harashima (1990). VSS observer for time varying systems. In: *In Proceedings of 16th Annual Conference of the IEEE Industrial Electronic Society*. pp. 34–39.

Hjalmarsson, H., M. Gevers and F. De Bruyne (1996). For model-based control design, closed loop identification gives better performance. *Automatica* **32**, 1659–1673.

Hung, J. and Z. Ding (1993). Design of current to reduce torque ripple in brushless permanent magnet motors. *IEE Proceedings-Control Theory and Applications* **140**(4), 260–266.

Ioannou, P. A. (2002). Robust switching adaptive control of multi-input nonlinear systems. *IEEE Transactions on Automatic Control* **47**(4), 610–624.

Ioannou, P. A. and J. Sun (1996). *Robust adaptive control*. Prentice Hall. Upper Saddle River, New Jersey.

Itkis, Y. (1976). *Control systems of variable structure*. Wiley. New York.

Jahns, T. M. and W. L. Soong (1996). Pulsating torque minimization techniques for permanent-magnet ac motor drives - a review. *IEEE Transactions on Industrial Electronics* **43**(2), 321–330.

Kachroo, P. and M. Tomizuka (1996). Chattering reduction and error convergence in the sliding mode control of a class of nonlinear systems. *IEEE Transactions on Automatic Control* **41**(7), 1063–1068.

Kaloust, J. and Z. Qu (1995). Continuous robust control design for nonlinear uncertain systems without a priori knowledge of control direction. *IEEE Transactions on Automatic Control* **40**(2), 276–282.

Karakasoglu, A. and M. K. Sundareshan (1995). A recurrent neural-network-based adaptive variable-structure model-following control of robotic manipulators. *Automatica* **31**(10), 1495–1507.

Khalil, H. K. (1996). *Nonlinear Systems*. Second Edition. Prentice-Hall. Upper Saddle River, New Jersy.

Krstic, M. and P. Tsiotras (1999). Inverse optimal stabilization of a rigid spacecraft. *IEEE Transactions on Automatic Control* **44**(5), 1042–1049.

Krupp, D. and Y. B. Shtessel (1999). Chattering-free sliding mode control with unmodeled dynamics. In: *Proceedings of the 18th American Control Conference*. San Diego, California. pp. 530–534.

Kuc, T. Y., J. S. Lee and K. Nam (1992). Iterative learning control theory for a class of nonlinear dynamic systems. *Automatica* **28**(6), 1215–1221.

Lam, B. H., S. K. Panda and J. X. Xu (1999). Torque ripple minimization in PM synchronous motors using interactive learning control. In: *Proc. of the IEEE 1999 Inter. Conf. on Power Electronics & Drive Systems*. The Hong Kong Polytechnic University, Hong Kong. pp. 144–149.

Lee, T. H., J. X. Xu and M. Wang (2000). An adaptive variable structure output controller with improved transient performance. *International Journal of Systems Science* **31**(1), 35–45.

Liao, T. L., L. C. Fu and C. F. Hsu (1990). Adaptive robust tracking of nonlinear systems and with an application to a robotic manipulator. *Systems and Control Letters* **15**(4), 339–348.

Lin, F. J. and S. L. Chiu (1998). Adaptive fuzzy sliding-mode control for PM synchronous servo motor drives. *IEE Proceedings-Control Theory and Applications* **145**(1), 63–72.

Lindoff, B. and J. Holst (1996). Exact distribution and moments for the RLS estimate in a time-varying AR(1) process. *Automatica* **32**(3), 429–433.

Ljung, L. (1987). *System identification: theorey for the user*. Vol. 7. Prentice-Hall. Englewood Cliffs, NJ.

Ljung, L. and U. Forssell (1999). An alternative motivation for the indirect approach to closed-loop identification. *IEEE Transactions on Automatic Control* **44**(11), 2206–2209.

Low, T. S., K. J. Tseng, T. H. Lee and Lim (1990). Strategy for the instantaneous torque control of permanent magnet brushless DC drives. *IEE Proceedings-Control Theory and Applications* **137**(6), 355–363.

Low, T. S., T. H. Lee, K. J. Tseng and Loc (1994). Servo performance of a BLDC drive with instantaneous torque control. *IEEE Transactions on Industry Applications* **28**(2), 455–462.

Luenberger, D. G. (1969). *Optimization by vector space methods*. Vol. 36. John Wiley. New York.

Lusternik, L.A. and V.J. Sobolev (1961). *Elements of functional analysis*. Gordon and Breach Science. New York.

Man, Z., A. P. Paplinkski and H. R. Wu (1994). A robust MIMO terminal sliding mode control scheme for rigid robotics manipulators. *IEEE Transactions on Automatic Control* **39**(12), 2464–2469.

Man, Z. and X. H. Yu (1997). Terminal sliding mode control of MIMO linear systems. *IEEE Transactions on Circuits and Systems I: Fundamental Theory and Applications* **41**(1), 1065–1070.

Man, Z. and X. H. Yu (2002). Fast terminal sliding-mode control design for nonlinear dynamical systems. *IEEE Transactions on Circuits and Systems I: Fundamental Theory and Applications* **49**(2), 261–264.

Marchand, C. and A. Razek (1993). Optimal torque operation of digitally controlled permanent magnet synchronous motor drives. *IEE Proceedings-Control Theory and Applications* **140**(3), 232–240.

Moore, K. L. and J. X. Xu (2000). Editorial – special issue on iterative learning control. *International Journal of Control* **73**(10), 819–823.

Mudgett, D. R. and A. S. Morse (1985). Adaptive stabilizing of systems with unknown high frequence gain. *International Journal of Control* **30**, 549–554.

Narendra, K. S. and A. M. Annaswamy (1989). *Stable adaptive systems*. Vol. 3. Prentice-Hall. Englewood Cliffs, New Jersey.

Nussbaum, R.D. (1983). Some remarks on the conjecture in parameter adaptive control. *Systems and Control Letters* **3**, 243–246.

Oh, S. R., Z. Bien and I. H. Suh (1988). An iterative learning control method with application to robot manipulators. *IEEE Transactions on Robotics and Automation* **4**(5), 508–514.

Ozguner, U. and S. Yurkovich (1987). Decentralized variable structure control of a two-arm robotic system. *Journal of Robotic Systems* **4**(3), 377–395.

Pandian, S. R. and M. Hanmandlu (1995). Model-based sliding mode controller for robot manipulators. *International Journal of Robotics and Automation* **10**(1), 29–34.

Park, K. B. and J. J. Lee (1996). A robust MIMO terminal sliding mode control scheme for rigid robotic manipulators - comments. *IEEE Transactions on Automatic Control* **41**(5), 761–762.

Parra-Vega, V. and S. Arimoto (1995). Exponentially convergent adaptive sliding mode control of robot manipulators. *International Journal of Systems Science* **26**(12), 2263–2276.

Qu, Z. H. (1998). *Robust control of nonlinear uncertain systems*. Wiley Interscience. New York.

Robert, H. (1999). *Nonlinear system identification: input-output modeling approach*. Vol. 109. Kluwer Academic Publishers. Boston.

Ryan, E. P. (1991). A universal adaptive stabilizer for a class of nonlinear systems. *Systems and Control Letters* **16**, 209–218.

Sadegh, N. and R. Horowitz (1990). Stability and robustness analysis of a class of adaptive controllers for robotic manipulators. *International Journal of Robotics Research* **9**(3), 74–92.

Sahoo, N. C., J. X. Xu and S. K. Panda (1999). Determination of current waveforms for torque ripple minimization in switched reluctunce motors using terative learning–an investigation. *IEE Proceedings on Electric Power Applications* **146**(4), 369–377.

Shen, T. and K. Tamura (1995). Robust H^{∞} control of uncertain nonlinear system via state feedback. *IEEE Transactions on Automatic Control* **40**(4), 766–768.

Shin, H. C. and S. B. Choi (2001). Position control of a two-link flexible manipulator featuring piezoelectric actuators and sensors. *Mechatronics* **11**(6), 709–729.

Shyu, K. K., Y. W. Tasi and C. F. Yung (1992). A modified variable structure controller. *Automatica* **28**(6), 1209–1213.

Sinha, N. K. (1998). *Control Systems*. New Age International Publishers. New Delhi.

Sira-Ramirez, H. (1993). On the dynamical sliding mode control of nonlinear systems. *International Journal of Control* **57**(5), 1039–1061.

Slotine, J. J. E. (1984). Sliding controller design for nonlinear systems. *International Journal of Control* **40**(4), 421–434.

Slotine, J. J. E. and S. S. Sastry (1983). Tracking control of nonlinear systems using sliding surfaces with applications to robot manipulators. *International Journal of Control* **39**(2), 106–110.

Slotine, J. J. E. and W. P. Li (1991). *Applied nonlinear control*. Vol. 34. Prentice-Hall. Englewood Cliffs, New Jersey.

Soderstrom, T. (1989). *System identification*. Prentice Hall. Englewood Cliffs, New Jersey.

Su, W. C. and C. C. Tsai (2001). Discrete-time VSS temperature control for a plastic extrusion process with water cooling systems. *IEEE Transactions on Control Systems Technology* **9**(4), 618–623.

Sundareshan, M. K. and C. Askew (1997). Neural network-assisted variable structure control scheme for control of a flexible manipulator arm. *Automatica* **33**(9), 1699–1710.

Thein, M. L. and E. A. Misawa (2000). A discrete time sliding mode observer with attractive boundary layer. In: *Proceedings of the 6th IEEE international workshop on Variable Structure Systems (VSS'2K)*. Vol. 36. Boston. pp. 74–83.

Tsaprounis, C. J. and N. A. Aspragathos (1999). Sliding mode with adaptive estimation force control of robot manipulators interacting with an unknown passive environment. *Robotica* **17**(4), 447–458.

Tzafestas, S., M. Raibert and C. Tzafestas (1996). Robust sliding-mode control applied to a 5-link biped robot. *JIRS* **15**(1), 67–133.

Utkin, V. I. (1965). On compensation of the forced term of motion in variable structure control systems. *Tekhinicheskaya Kibernetika (in Russian)* (4), 169–173.

Utkin, V. I. (1977). Variable structure systems with sliding modes. *IEEE Transactions on Automatic Control* **22**(2), 212–222.

Utkin, V. I. (1978). *Sliding modes and their application in variable structure systems*. MIR. Moscow.

Utkin, V. I. (1992). *Sliding Modes in Control and Optimization*. Vol. 34. Springer-Verlag. Berlin.

Utkin, V. I. and J. X. Shi (1996). Integral sliding mode in systems operating under uncertainty conditions. In: *Proceedings of the 35th IEEE Conference on Decision and Control*. Kobe, Japan.

Van den Hof, P.M.J. and R.J.P. Schrama (1995). Identification and control – closed-loop issues. *Automatica* **31**, 1751–1770.

Van der Schaft, A. J. (1991). A state space approach to nonlinear H^∞ control. *Systems and Control Letters* **16**(1), 1–8.

Van der Schaft, A. J. (1992). L_2 gain analysis of nonlinear systems and nonlinear state feedback H^∞ control. *IEEE Transactions on Automatic Control* **37**(6), 770–784.

Vidyasagar, M. (1993). *Nonlinear Systems Analysis*. Vol. 3. Prentice Hall. Englewood Cliffs, NJ, 2nd edition.

Wang, J. D., Lee T. L. and Y. T. Juang (1996). New methods to design an integral variable structure controller. *IEEE Transactions on Automatic Control* **41**(1), 140–143.

Wu, Y. and X. Yu (1999). Variable structure control design for uncertain dynamic systems with disturbances in input and output channels. *Automatica* **35**(2), 311–319.

Xu, J. X. and H. Hashimoto (1993). Parameter identification methodologies based on variable structure control. *International Journal of Control* **57**(5), 1202–1220.

Xu, J. X. and H Hashimoto (1996). VSS theory-based parameter identification scheme for MIMO systems. *Automatica* **32**(2), 279–284.

Xu, J. X. and J. Zhang (2000). A suboptimal variable structure control approach for nonlinear uncertain MIMO systems. In: *In Proceedings of 6th IEEE Variable Structure System Workshop: Advances in Variable Structure Control – Analysis, integration and applications*. Queensland, Australia. pp. 303–312.

Xu, J. X. and J. Zhang (2001). On the optimal and suboptimal VSC apporaches for nonlinear uncertain systems. In: *In Proceedings of IEEE 2001 American Control Conference*. Arlington, VA, USA. pp. 4992–4997.

Xu, J. X. and J. Zhang (2002). On quasi-optimal variable structure control approaches. In: *Variable Structure Systems: Towards the 21st Century* (X. H. Yu and J. X. Xu, Eds.). pp. 175–200. Springer-Verlag. Berlin, Germany. ISBN 3–540–42965–4.

Xu, J. X. and W. J. Cao (2000). Synthesized sliding mode control of a single-link flexible robot. *International Journal of Control* **73**(3), 197–209.

Xu, J. X. and W. J. Cao (2001*a*). Direct tip regulation of a single-link flexible manipulator by adaptive variable structure control. *International Journal of System Science* **31**(1), 121–135.

Xu, J. X. and W. J. Cao (2001*b*). Learning variable structure control approaches for repeatable tracking control tasks. *Automatica* **37**(7), 997–1006.

Xu, J. X. and Z. H. Qu (1998). Robust iterative learning control for a class of nonlinear systems. *Automatica* **34**(8), 983–988.

Xu, J. X., H Hashimoto, J J E slotine, Y Arai and F Harashima (1989). Implementation of VSS control to robotic manipulations – smoothing modification. *IEEE Transactions on Industrial Electronics* **36**(3), 321–329.

Xu, J. X., Q. W. Jia and T. H. Lee (2000*a*). Adaptive robust control scheme for a class of nonlinear uncertain descriptor systems. *IEEE Transactions on Circuits and Systems, Part I: Fundamental Theory and Applications* **47**(6), 957–962.

Xu, J. X., S. K. Panda, Y. J. Pan, T. H. Lee and B. H. Lam (2000*b*). Improved PMSM pulsating torque minimization with iterative learning and sliding mode observer. In: *In Proceedings of 2000 IEEE International Conference on Industrial Electronics, Control and Instrumentation*. Nagoya, Japan. pp. 1931–1936.

Xu, J. X., S. K. Panda, Y. J. Pan, T. H. Lee and B. H. Lam (2001*a*). A modular control scheme for PMSM speed control with pulsating torque minimization (submitted). *IEEE Transactions on Industrial Electronics*.

Xu, J. X., T. H. Lee and C. He (1997). Controller design for a class of nonlinear multi-input systems using modified sliding mode. *International Journal of System Science* **28**(8), 777–789.

Xu, J. X., T. H. Lee and M. Wang (1998*a*). Self-tuning type variable structure control method for nonlinear systems. *International Journal of Robust and Nonlinear Control* **8**(8), 1133–1153.

Xu, J. X., T. H. Lee and Q. W. Jia (1998*b*). On adaptive robust backstepping control schemes suitable for PM synchronous motors. *International Journal of Control* **70**(6), 893–920.

Xu, J. X., T. H. Lee and Y. J. Pan (2003*a*). On the sliding mode control for DC servo mechanisms in the presence of unmodeled dynamics (in press). *Mechatronics*.

Xu, J. X., T. H. Lee, M. Wang and X. H. Yu (1996). Design of variable structure control with continuous switching control. *International Journal of Control* **65**(3), 409–431.

Xu, J. X., V. Badrinath and Z. H. Qu (2000*c*). Robust learning control for robotic manipulators with an extension to a class of non–linear systems. *International Journal of Control* **73**(10), 858–870.

Xu, J. X., Y. J. Pan and T. H. Lee (2000*d*). A gain scheduled sliding mode control scheme using filtering techniques with applications to multi–link robotic manipulators. *ASME Journal of Dynamic Systems, instrument and Control* **122**(4), 624–631.

Xu, J. X., Y. J. Pan and T. H. Lee (2000*e*). A new gain scheduled sliding mode control scheme using filtering techniques. In: *In Proceedings of 6th IEEE Variable Structure System Workshop: Advances in Variable Structure Systems – Analysis, integration and applications*. Queensland, Australia. pp. 345–354.

Xu, J. X., Y. J. Pan and T. H. Lee (2001*b*). A gain shaped sliding mode control scheme using filtering techinques with application to multi–link robotic manipulators. In: *In Proceedings of IEEE 2001 American Control Conference*. Arlington, VA, USA. pp. 4363–4368.

Xu, J. X., Y. J. Pan and T. H. Lee (2002*a*). Adaptive variable structure control design without a priori knowledge of control directions (submitted). *Automatica*.

Xu, J. X., Y. J. Pan and T. H. Lee (2002*b*). Analysis and design of integral sliding mode control based on Lyapunov's direct method (submitted). *Automatica*.

Xu, J. X., Y. J. Pan and T. H. Lee (2002*c*). A new fractional interpolation based smoothing scheme for variable structure control. In: *In Proceedings of the 4th Asian Control Conference*. Singapore. pp. 602–607.

Xu, J. X., Y. J. Pan and T. H. Lee (2002*d*). On nonlinear H^∞ sliding mode control for a class of nonlinear cascaded systems. In: *In Proceedings of the 7th*

IEEE Variable Structure System Workshop. Sarajevo, Bosnia and Herzegovina. pp. 95–104.

Xu, J. X., Y. J. Pan and T. H. Lee (2002*e*). On nonlinear H^{∞} sliding mode control for a class of nonlinear cascaded systems (submitted). *Systems and Control Letters*.

Xu, J. X., Y. J. Pan and T. H. Lee (2002*f*). On the sliding mode control for DC servo mechanism in the presence of unmodeled dynamics. In: *In Proceedings of the 15th IFAC World Congress on Automatic Control*. Barcelona, Spain.

Xu, J. X., Y. J. Pan and T. H. Lee (2002*g*). Sliding mode control with closed-loop filtering architecture for a class of nonlinear systems (revised). *IEEE Transactions on Circuits and Systems - I: Fundamental Theory and Applications*.

Xu, J. X., Y. J. Pan and T. H. Lee (2002*h*). VSS identification schemes for time-varying parameters. In: *In Proceedings of the 15th IFAC World Congress on Automatic Control*. Barcelona, Spain.

Xu, J. X., Y. J. Pan and T. H. Lee (2003*b*). Adaptive variable structure control design without a priori knowledge of control directions (accepted). In: *the Fourth International Conference on Control and Automation*. Montreal, Canada.

Xu, J. X., Y. J. Pan and T. H. Lee (2003*c*). Analysis and design of integral sliding mode control based on Lyapunov's direct method (submitted). In: *IEEE 2003 American Control Conference*. Denver, Colorado, USA.

Xu, J. X., Y. J. Pan and T. H. Lee (2003*d*). A new fractional interpolation based smoothing scheme for variable structure control (revised). *Asian Journal of Control*.

Xu, J. X., Y. J. Pan and T. H. Lee (2003*e*). A VSS identification scheme for time-varying parameters (in press). *Automatica*.

Yao, B., S P. Chan and D. Wang (1994). Variable structure adaptive motion and force control of robot manipulators. *Automatica* **30**(9), 1473–1477.

Ye, X. D. and J.P. Jiang (1998). Adaptive nonlinear design without a priori knowledge of control directions. *IEEE Transaction on Automatic Control* **43**(11), 1617–1621.

Yeung, K.S. and Y.P. Chen (1988). A new controller design for manipulators using the theory of variable structure systems. *IEEE Transactions on Automatic Control* **33**(2), 200 –206.

Yoo, D. S. and M. J. Chung (1992). A variable structure control with simple adaptation laws for upper bounds on the norm of the uncertainties. *IEEE Transactions on Automatic Control* **37**(6), 860–864.

Young, K. D. (1993). *Variable structure control for robotics and aerospace applications*. Vol. 57. Elsevier, The Netherlands. Boston, USA.

Young, K. D. and U. Ozguner (1999). *Lecture notes in control and information sciences 247, Variable structure systems, sliding mode and nonlinear control*. Vol. 51. Springer-Verlag. London.

Young, K. D., V. I. Utkin and U. Ozguner (1999). A control engineer's guide to sliding mode control. *IEEE Transactions on Control Systems Technology* **7**(3), 328–342.

Young, K.-K. D. (1977). Asymptotic stability of model reference systems with variable structure control. *IEEE Transactions on Automatic Control* **22**(4), 279–281.

Young, K.-K. D., P. V. Kokotovic and V. Utkin (1977). A singular perturbation analysis of high-gain feedback systems. *IEEE Transactions on Automatic Control* **22**(6), 931–938.

Young, K.D. (1978). Design of variable structure model following control systems. *IEEE Trans. Auto. Control* **AC–23**(4), 1079–1085.

Young, K.D. and U. Ozguner (1997). Sliding-mode design for robust linear optimal control. *Automatica* **33**(7), 1313–1323.

Yu, X. and Z. Man (1998). Multi-input uncertain linear systems with terminal sliding-mode control. *Automatica* **34**(3), 389–392.

Yu, X. H. (1999). Tracking inherent periodic orbits in chaotic dynamic systems via adaptive variable structure time-delayed self control. *IEEE Transactions on Circuits and Systems I: Fundamental Theory and Applications* **46**(11), 1408–1411.

Yu, X. H. and J. X. Xu (2000). *Advances in Variable Structure Systems – Analysis, Integration and Applications*. World Scientific. Singapore. ISBN 981–02–4464–9, (Hardcover).

Zhao, J., M. J. Kemper and F. S Van der Merwe (1997). On-line control method to reduce mechanical vibration and torque ripple in reluctance synchronous machine drives. In: *Proceedings of IEEE International Conference on Industrial Electronics, Control and Instrumentation*. Vol. 1. London. pp. 126–131.

Zhihong, M., M. O'Day and X. Yu (1999). Robust adaptive terminal sliding mode control for rigid robotic manipulators. *JIRS* **24**(1), 23–41.

Zinober, A. S. I. (1994). *Lecture Notes in Control and Information sciences, variable structure and Lyapunov control*. Vol. 64. Springer-Verlag. London.

Appendix A

Mathematical Background

A.1 Norms

The notion of norm is a generalization of distance or length. In a Banach space, a norm is defined by a scalar, positive definite function that satisfies the triangular inequality and is linear with respect to a real, positive multiplier. The following is a brief summary of norms used in this thesis (Lusternik and Sobolev, 1961), (Luenberger, 1969), (Vidyasagar, 1993).

Vector norms For a vector $\mathbf{x} \in \mathcal{R}^n$, the corresponding $p-$norm ($p \geq 1$) and $\infty-$norm are defined by

$$\|\mathbf{x}\|_p = \left[\sum_{i=1}^{n} |x_i|^p\right]^{\frac{1}{p}}, \qquad \|\mathbf{x}\|_\infty = \max_i |x_i|$$

respectively, where x_i denotes the i-th element of $\mathbf{x}$.

Induced matrix norms For a matrix $X \in \mathcal{R}^{n\times m}$, the $1-$ and $\infty-$ norm of its induced norms are

$$\|X\|_1 = \max_j \sum_i |x_{ij}|, \quad \|X\|_\infty = \max_i \sum_j |x_{ij}|$$

respectively, where x_{ij} denotes the element of X at the intersection of the ith row and the jth column. Moreover, $\|\cdot\|$ is used to denote Euclidean norm (2-norm) of a vector, and induced 2-norm or spectral norm of a matrix.

Function norms For a Lebesgue measurable function $g(t)$, then $p-$norm ($1 \leq p < \infty$) and $\infty-$norm of the function $g(t)$ are

$$\|g\|_p \triangleq \left(\int_0^\infty |g(t)|^p d\tau\right)^{\frac{1}{p}}, \quad \|g\|_\infty \triangleq \sup_{0\leq t<\infty} |g(t)|.$$

Function $g(t)$ is said to belong to L_p space if $\|g(t)\|_p < \infty$ and to L_∞ space if $\|g(t)\|_\infty < \infty$.

A.2 Singular Values

For any matrix $X \in \mathcal{R}^{n\times m}$, there exists a unique transformation such that $X = U\Lambda V^T$, where $U \in \mathcal{R}^{n\times n}$, $V \in \mathcal{R}^{m\times m}$ and Λ is a diagonal matrix with non-negative elements as $\Lambda = [\Lambda_1 \ \mathbf{0}]^T$, if $n \geq m$; $\Lambda = [\Lambda_1 \ \mathbf{0}]$, if $n \leq m$, where $\Lambda_1 = \text{diag}(\sigma_1, \ \cdots, \ \sigma_k)$ and $k = \min(m, n)$. The σ_i, $i = 1, \cdots, k$, are called the singular values of X. The singular values have the following properties

$$\sigma_i(X) = \sqrt{\lambda_i(XX^T)} = \sqrt{\lambda_i(X^TX)}.$$

$\sigma_i(X) = 0$ implies $det(X) = 0$ when X is square, where $det(\star)$ denotes the determinant. A square X has the following properties

$$\prod_{i=1}^{n} \sigma_i(X) = \prod_{i=1}^{n} |\lambda_i(X)|, \quad \bar{\sigma}(X) \geq \max_i |\lambda_i(X)|, \quad \underline{\sigma}(X) \leq \min_i |\lambda_i(X)|,$$

where $\bar{\sigma}(\star)$ and $\underline{\sigma}(\star)$ denote the maximal and minimal singular values of X respectively.

A.3 Symmetric

X is symmetric if $X^T = X$. Eigenvalues of symmetrical matrices are always real. X is normal if $X^T X = XX^T$. For any normal matrix X, $\sigma_i(X) = |\lambda_i(X)|$.

A.4 Positive-Definiteness

Let $P \in \mathcal{R}^{n\times n}$ be a symmetric matrix. Matrix P is said to be positive semidefinite if $\mathbf{x}^T P\mathbf{x} \geq \ 0, \forall \mathbf{x} \in \mathcal{R}^n$. If in addition $\mathbf{x}^T P\mathbf{x} \neq 0, \forall \mathbf{x} \neq 0$, matrix P is said to be positive definite. Matrix P is negative (semi)-definite if $-P$ is positive (semi)-definite. If matrix P is neither positive semidefinite nor negative semidefinite, it is indefinite. Matrix P is positive-(semi) definite if and only if

(i) all its eigenvalues are (nonnegative) positive;

(ii) all its leading principal minors are (nonnegative) positive;

(iii) $P = YY^T$ for (some) invertible matrix Y.

A.5 Quadratic Functions

A quadratic function g: $\mathcal{R}^n \to \mathcal{R}$ is in the form of $g(\mathbf{x}) = \mathbf{x}^T P\mathbf{x}$ for some symmetric matrix P. If P is a time-varying matrix, the quadratic function g becomes $g(\mathbf{x}, t)$, in which case its definiteness should be defined not simply pointwise but uniformly. The quadratic function g is positive definite, then it can be used as Lyapunov function candidates. In stability analysis, the following *Rayleigh-Ritz Inequality* is always be used

$$\lambda_{min}(P)\|\mathbf{x}\|^2 \leq \mathbf{x}^T P\mathbf{x} \leq \lambda_{max}(P)\|\mathbf{x}\|^2,$$

where P is symmetric, $\lambda_{min}(P)$ and $\lambda_{max}(P)$ are the minimum and maximum eigenvalues of the matrix P respectively.

A.6 Vector and Matrix Derivatives

The derivative of a scalar function $g(\mathbf{x}, t)$, where $\mathbf{x} \in \mathcal{R}^n$, with respect to the vector $\mathbf{x}$, is denoted by $D_{\mathbf{x}}g(\mathbf{x}, t) = \dfrac{\partial g}{\partial \mathbf{x}} \in \mathcal{R}^n$. $D_{\mathbf{x}}g(\mathbf{x}, t)$ is defined to be a row vector as

$$D_{\mathbf{x}}g = \frac{\partial g}{\partial \mathbf{x}} \triangleq \begin{bmatrix} \frac{\partial h}{\partial x_1} & \cdots & \frac{\partial h}{\partial x_n} \end{bmatrix},$$

where x_i is the ith element of $\mathbf{x}$.

The Jacobian matrix of vector function $\mathbf{g}(\mathbf{x})$ where $\mathbf{x} \in \mathcal{R}^n$ and $\mathbf{g} \in \mathcal{R}^m$, denoted by $D_{\mathbf{x}}\mathbf{g} = \dfrac{\partial \mathbf{g}}{\partial \mathbf{x}} \in \mathcal{R}^{m \times n}$, is defined as

$$D_{\mathbf{x}}\mathbf{g} = \frac{\partial \mathbf{g}}{\partial \mathbf{x}} \triangleq \begin{bmatrix} \frac{\partial g_1}{\partial x_1} & \cdots & \frac{\partial g_1}{\partial x_n} \\ \cdot & \cdots & \cdot \\ \frac{\partial g_m}{\partial x_1} & \cdots & \frac{\partial g_m}{\partial x_n} \end{bmatrix} = \begin{bmatrix} D_{x_1}g_1 & \cdots & D_{x_n}g_1 \\ \cdot & \cdots & \cdot \\ D_{x_1}g_m & \cdots & D_{x_n}g_m \end{bmatrix},$$

where g_i is the ith element of $\mathbf{g}$.

A.7 Useful Definitions, Inequalities and Lemmas

Class $\mathcal{K}$ and class $\mathcal{K}_\infty$ function: (Khalil, 1996) A continuous function g: $[0, a) \to [0, \infty)$ is said to belong to class $\mathcal{K}$ if it is strictly increasing and $g(0) = 0$. It is said to belong to class $\mathcal{K}_\infty$ if $a = \infty$ and $g(r) \to \infty$ as $r \to \infty$.

Class $\mathcal{KL}$ function: (Khalil, 1996) A continuous function g: $[0, a) \to [0, \infty)$ is said to belong to class $\mathcal{KL}$ if, for each fixed s, the mapping $g(r, s)$ belongs to class $\mathcal{K}$ with respect to r and, for each fixed r, the mapping $g(r, s)$ is decreasing with respect to s and $g(r, s) \to 0$ as $s \to \infty$.

Hölder inequality (Ioannou and Sun, 1996) If $p, q \in [1, \infty]$ and $p^{-1} + q^{-1} = 1$, then $f \in \mathcal{L}_p, g \in \mathcal{L}_q$ imply that $fg \in \mathcal{L}_1$ and $\|fg\|_1 \leq \|f\|_p \|g\|_q$. When $p = q = 2$, the *Hölder inequality* becomes the *Schwartz inequality*, i.e., $\|fg\|_1 \leq \|f\|_2 \|g\|_2$.

Barbalat's Lemma (Narendra and Annaswamy, 1989) Let g: $\mathcal{R} \to \mathcal{R}$ be a uniformly continuous function on $[0, \infty)$. Suppose that $lim_{t\to\infty} \int_0^t g(\tau)d\tau$ exists and is finite. Then,

$$g(t) \to 0 \quad \text{as} \quad t \to \infty.$$

Appendix B

Author's Publications

The author has contributed to the following publications:

Journal Publications

1. Jian-Xin Xu, Ya-Jun Pan and Tong-Heng Lee (2000), "A Gain Scheduled Sliding Mode Control Scheme Using Filtering Techniques with Applications to Multi-link Robotic Manipulators", *Transactions of the ASME: Journal of Dynamic Systems, Measurement and Control*, vol. 122, no. 4, pp. 641-649.

2. Jian-Xin Xu, Ya-Jun Pan and Tong-Heng Lee (2003), "VSS Identification Schemes for Time-Varying Parameters," In press, *Automatica*, vol. 39, no. 4, pp. 727-734.

3. Jian-Xin Xu, Tong-Heng Lee and Ya-Jun Pan (2003), "On the Sliding Mode Control for DC Servo Mechanisms in the Presence of Unmodeled Dynamics", *Mechatronics*, vol. 13, no. 7, pp. 755-770.

4. Jian-Xin Xu, Ya-Jun Pan and Tong-Heng Lee (2003), "Sliding Mode Control with Closed-Loop Filtering Architecture for a Class of Nonlinear Systems", Accepted by *IEEE Transactions on Circuits and Systems - I: Fundamental Theory*

and Applications.

5. Jian-Xin Xu, Ya-Jun Pan and Tong-Heng Lee (2003), "A New Fractional Interpolation Based Smoothing Scheme for Variable Structure Control", Revised for *Asian Journal of Control*.

6. Jian-Xin Xu, Sanjib-Kumar Panda, Ya-Jun Pan, Tong-Heng Lee and Boon-Hor Lam (2001), "A Modular Control Scheme for PMSM Speed Control with Pulsating Torque Minimization", Submitted to *IEEE Transactions on Industrial Electronics*.

7. Jian-Xin Xu, Ya-Jun Pan and Tong-Heng Lee (2002), "On Nonlinear H^{∞} Sliding Mode Control for a Class of Nonlinear Cascaded Systems", Submitted to *International Journal of Robust and Nonlinear Control*.

8. Jian-Xin Xu, Ya-Jun Pan and Tong-Heng Lee (2002), "Adaptive Variable Structure Control Design Without a Priori Knowledge of Control Directions", Submitted to *Automatica*.

9. Jian-Xin Xu, Ya-Jun Pan and Tong-Heng Lee (2002), "Analysis and Design of Integral Sliding Mode Control Based on Lyapunov's Direct Method", Submitted to *Automatica*.

Conference Publications

1. Jian-Xin Xu, Sanjib-Kumar Panda, Ya-Jun Pan, Tong-Heng Lee and Boon-Hor Lam (2000), "Improved PMSM Pulsating Torque Minimization with Iterative Learning and Sliding Mode Observer", in *Proceedings of the 2000 IEEE International Conference on Industrial Electronics, Control and Instrumentation* (IECON'2K), pp. 1931-1936, Nagoya, Japan.

2. Jian-Xin Xu, Ya-Jun Pan and Tong-Heng Lee (2000), "A New Gain Scheduled Sliding Mode Control Scheme Using Filtering Techniques", in *Proceedings of the 6th IEEE International Workshop on Variable Structure Systems* (VSS'2K), pp. 345-354, Gold coast, Australia.

3. Jian-Xin Xu, Ya-Jun Pan and Tong-Heng Lee (2001), "A Gain Shaped Sliding Mode Control Scheme Using Filtering Techniques with Applications to Multi-link Robotic Manipulators", in *Proceedings of the 2001 American Control Conference* (ACC'01), pp. 4363-4368, Arlington, VA, USA.

4. Jian-Xin Xu and Ya-Jun Pan (2001), "Nonlinear Sliding Mode Design with Optimality", in *Proceedings of the 3rd International Conference on Control Theory and Applications* (TA'01), pp. 345-349, Pretoria, South Africa.

5. Jian-Xin Xu, Ya-Jun Pan and Tong-Heng Lee (2002), "On the Sliding Mode Control for DC Servo Mechanism in the Presence of Unmodeled Dynamics", to be appeared in *Proceedings of the 15th IFAC World Congress on Automatic Control* (IFAC'02), Barcelona, Spain.

6. Jian-Xin Xu, Ya-Jun Pan and Tong-Heng Lee (2002), "VSS Identification Schemes for Time-varying Parameters", in *Proceedings of the 15th IFAC World Congress on Automatic Control* (IFAC'02), Barcelona, Spain.

7. Jian-Xin Xu, Ya-Jun Pan and Tong-Heng Lee (2002), "On Nonlinear H^∞ Sliding Mode Control for a Class of Nonlinear Cascaded Systems", in *Proceedings of the 7th IEEE Variable Structure System Workshop* (VSS'02), pp. 95-104, Sarajevo, Bosnia and Herzegovina.

8. Jian-Xin Xu, Ya-Jun Pan and Tong-Heng Lee (2002), "A New Fractional Interpolation Based Smoothing Scheme for Variable Structure Control", in *Proceedings of the 4th Asian Control Conference* (ASCC'02), pp. 602-607, Singapore.

9. Jian-Xin Xu, Ya-Jun Pan and Tong-Heng Lee (2003), "Adaptive Variable Structure Control Design Without a Priori Knowledge of Control Directions", in *Proceedings of the 2003 Fourth International Conference on Control and Automation* (ICCA'03), Montreal, Canada.

10. Jian-Xin Xu, Ya-Jun Pan and Tong-Heng Lee (2003), "Analysis and Design of Integral Sliding Mode Control Based on Lyapunov's Direct Method", in *Proceedings of the 2003 American Control Conference* (ACC'03), Denver, Colorado, USA.